Investigations of the role of colloids in radionuclide migration

Thesis

Investigations Of The Role Of Colloids In Radionuclide Migration

By Silvia Antón Gascón

SUBMITTED IN PARTIAL FULFILMENT OF THE
REQUIREMENTS FOR THE
AWARD OF
DOCTOR OF PHILOSOPHY

Loughborough University

September 2011

Research Supervisor Professor Peter Warwick

ABSTRACT

Intermediate and low level radioactive waste is planned to be disposed of in deep underground repositories where the waste packages will be surrounded by layers of engineered and geological barriers. In the event of leakage and mobilisation of radionuclides from the canisters, radionuclides may be transported by groundwaters into the Geosphere, where radionuclide mobility may be retarded by sorption to the geological host rock. However, colloidal particles, which provide large surface area per mass, may potentially enhance the transport of radionuclides.

The mobility of radionuclides through the Geosphere depends greatly on the sorption and desorption of radionuclides with the host rock. However, the presence of colloidal particles may influence the transport of radionuclides. Given a stable and mobile colloidal suspension which sorbs radionuclides onto its surface in a reversible manner, the radionuclide may be transported along with the colloidal suspension. The work presented in this thesis aims to contribute to understanding the role of inorganic colloids in contaminant transport through the Geosphere.

Colloids are small and metastable particles which can be transported long distances with groundwater. This mobility is determined mainly by the stability of colloids, as unstable colloids tend to coagulate, thus reducing significantly colloidal transport.

Stable colloids present in groundwater may sorb radionuclides onto them. Given an irreversible interaction, where a strong sorption is followed by a weak or no desorption, radionuclides may be transported until the colloids flocculate, becoming immobilised. On the contrary, a reversible interaction, where a weak sorption is followed by desorption, may lead to a scenario where the radionuclide is immobilised by sorption to the host rock.

Given the importance of the reversibility of the sorption of radionuclides to inorganic colloids on the fate of contaminant transport through the Geosphere, the interactions of three metals (Cs^{+}, Ni^{2+} and Eu^{3+}) with boehmite and montmorillonite colloids has been investigated by means of sorption and desorption batch experiments.

Data on the sorption of metals onto colloids (and solid surfaces) is generally expressed in terms of distribution ratio, R_d. The results showed that the R_d, and hence, the sorption, generally increased with the ionic charge of the metal. The R_d value, however, depends on the specific experimental conditions of the experiment, making comparison with existing literature difficult. Moreover, in the case of sorption onto colloidal particles, the distribution ratio also depends strongly on the size distribution of the colloids, as the surface provided by colloids for sorption may vary with the size of the colloids.

The number of investigations carried out in the literature on contaminant sorption onto solid surfaces is much greater than those carried out on colloidal surfaces. As a result, the data available on distribution ratios for metal sorption onto solid surfaces is greater than that available onto colloidal surfaces. Assuming that the main difference between a solid surface and a colloidal surface is the difference in surface area, one could assume that the distribution ratios of a metal on a colloid and a solid are related by the specific surface area. An attempt was made to test a mathematical model whereby the R_d values were related by the ionic charge of the metal and the specific surface areas of boehmite colloidal and solid particles. Other surface properties, like proton exchange capacity, were tested for the same model.

Desorption experiments help understand the extent of the reversibility of the sorption. The sorption of metals onto both boehmite and montmorillonite was found to be reversible, except in the case of Eu^{3+} sorption onto montmorillonite, which desorbed from the colloids in an amount less than a 5% of that which would be expected for a reversible system.

Organic colloids, such as humic acids, are present in natural groundwaters. Although their structure is not yet clear, the large number of functional groups make humic acids organic complexing ligands which may influence the interaction of metals with inorganic colloids or surfaces, and may, therefore, influence the mobility of radionuclides through the Geosphere. In this work, the influence of humic acid on the sorption of Cs^{+}, Ni^{2+} and Eu^{3+} on boehmite colloids was studied, observing a decrease in the sorption of metals onto the colloids. The interaction of humic acids

with boehmite colloids was also assessed, as the net negative charge of humic acids tended to neutralise the net positive charge of boehmite colloids and thus led to the flocculation of the colloids.

Ternary systems, constituted by metals, solid surfaces and humic acids has been generally modelled with the linear additive model. Its applicability on colloids has not been tested as much as on solid surfaces, but generally, a slight modification has been needed for success. In this work, the linear additive model was tested on the experimental results.

The transport of radionuclides associated to inorganic colloids has been assessed by means of column experiments. A radiometric technique consisting of radiolabelling inorganic silica colloids with ^{152}Eu spike was used to detect and quantify the migration of silica colloids through a sand column. Furthermore, the same method was used to investigate the migration of ^{137}Cs associated to silica colloids through a sand column. The mobility of the radionuclide through the sand column was found to be enhanced by the silica colloids.

Overall, the investigations carried out in this thesis demonstrate that inorganic colloids may influence the mobility of radionuclides in the Geosphere by enhancing their transport and should thus be considered in the performance assessments of deep underground repositories.

Acknowledgements

Fistly, I would like to acknowledge my supervisor, Prof. Peter Warwick for giving me the chance to initiate my career into research. I would like to thank him for all his support, encouragement, guidance and all his efforts to make this PhD possible.

I would like to thank Feralco Ltd. (UK) and Nabaltech (Germany) for kindly providing the boehmite used in this work. I would like to thank Dr. Sneh Jain for taking the time and dedication to carry out the SEM and SSA measurements at BGS.

During my three years, the help of Mrs. Linda Sands, both professionally and personally, has been extraodinary, thank you for your words of wisdom and comfort, and for all your encouragement and support. All my collegues in the lab have made my time so enjoyable, thank you to Anumaija for her friendship, to Ricky for putting up with our “friday afternoon” music, to Larry, Adam and Ebong for making me laugh so many times, to Amy, Kirsty and Katie for all our moments in (and outside) the lab, and also thank you to Sneh for our long conversations in the “micro-lab” and to Mónica for all your efforts and time on my project. Thanks to Sneh for being my post-doc; your experience has been very helpful in the past two years.

Thank you to my dear “spanish crew”, Jesús, Arancha, Adela and Noelia, for making my arrival in Loughborough so easy. You made my week-ends and lunches some of the best moments, and thank you for your friendship, which will last for very long.

To my french housemates, Eric and Julien, thanks for welcoming into Loughborough and for your friendship, thanks for being my mates and for being so involved in my personal adventure in this town.

About a year after I started this PhD, new friends appeared, Anumaija, who arrived from Finland by train, Jasón, who flew from Barcelona and perhaps had too many cheeseburgers in his first week of PhD, and Hayley, who was my housemate for over a year and with whom I hosted very good parties.

In the completion of this thesis, I would like to thank the help Mónica and Sneh for proof-reading, and to Sneh for the SEM and SSA measurements. A special mention to my uncle, Vicente. Thank you for all your interest shown during the years of experimental work. But most importantly, your support, interest, excitement and joy have been my main encouragement and reference to keep going. Your trust and confidence on this project and on me helped me believe in it.

I would like to thank my mother, Pilar, for all her support during the whole time I was in Loughborough. Thank you for listening to me in the rough times, thank you for sharing with me the good moments, thank you because your love and your confidence helped me hang on. Thank you for being strong for me when I was lacking strength.

To Iván, my love, thank you for being next to me all the way, thank you for not letting the distance be an inconvenience, thank you for spending your free time with me and for sharing part of my time in Loughborough. Thank you for your support and for believing in me, I know it has been hard some times, thank you for being there all along.

I would like to thank my collegues, Elena, Mar and Rosa for their friendship, as well as for the interest shown in the progress of this thesis.

Finally, I would like to dedicate this thesis to those in my family who unfortunately are no longer here to see it accomplished.

Table of Contents

Table of Figures

List of tables

List of abbreviations

HA	Humic acid
MES	Buffering agent, 2-(N-morpholino)ethanesulfonic acid
TEOS	Tetraethyl orthosilicate
DI water	Deionised water
DPSO	Diphenyl sulfoxide
4-NBA	4-nitrobenzylalcohol
3-NP	3-nitrophenol
IS	Ionic strength
DLVO theory	Deryajin-Landau-Verwey-Overbeek
DLS	Dynamic light scattering
XRD	X-ray diffraction analysis
UV-Vis	Ultraviolet Visible spectroscopy
a.u.	Arbitrary units
CE	Cation exchange
PE	Proton exchange
JChess	Chemical speciation modelling program
LAM	Linear additive model

ORGANISATION OF THIS REPORT

This report is divided into chapters concerning the influence of colloids on the sorption and transport of radionuclides through the Geosphere.

Chapter 1 introduces the need to consider colloids when considering risk assessment. A short introduction to colloids and their stability is followed by a description of the inclusion of colloids in radionuclide transport. Examples given demonstrate the need to fully understand the interactions of colloids and radionuclides.

Chapter 2 describes the binary interaction between metals and colloidal mineral phases. By modelling the sorption isotherms, distribution ratios are collected. Desorption experiments provide quantitative measurements of the reversible behaviour of the metals under examination. Futhermore, a modelling approach was used in an attempt to predict the distribution ratios of metals on the colloidal phase by extrapolating from those distribution ratios found on the solid phase.

Ternary systems including humic acids were investigated in Chapter 3, where the influence of humic acids on the sorption of the binary metal colloid system was measured. The linear additive model was applied to the experimental results.

The mobility of colloids through a column was investigated in Chapter 4, as well as the effect of colloids in the migration of radionuclides through the column. The colloids were radiolabelled with ^{152}Eu from early stages of the synthesis process, allowing the colloids to be detected radiometrically along the column.

Chapter 5 concludes with a summary of the most relevant findings of the thesis.

Chapter 1. INTRODUCTION

Long term disposal of low level and intermediate level radioactive waste includes interim storage and then disposal in deep underground repositories. Due to the long half-life of the radioactive waste, the underground facilities should be designed to ensure isolation of the waste packages even after hundreds of thousands of years. However, because of the long time scales involved, radionuclides may eventually be released to the Geosphere by mobilisation and transport in groundwater [1].

Performance assessment of potential nuclear waste repositories requires a thorough understanding of physico-chemical and engineering aspects of the waste packaging, the geological disposal facility as well as the geological environment surrounding the facility. To prevent radionuclides from being released into the environment, both engineered and geological barriers are considered. The former is constituted by backfill or buffer material which can act as a retardant for radionuclides. The latter consists of the host rock geology, which provides a long groundwater travel time for dispersion and retention of radionuclides by sorption to the surrounding solid matrix [2].

Retention or retardation may occur mainly by sorption onto the surface of the host rock. Nonetheless, the presence of mobile, sorbent particles may reduce the effectiveness of retardation of radionuclides [2]. These small particles released from the host rock may have the same sorptive capacity as the host, but may provide a large surface which contaminants may sorb to. The mobility of these colloidal particles may lead to an enhancement of the transport of the contaminants.

1.1. Basics of colloid chemistry

1.1.1. Definition and stability of colloids

Colloids are particles which size range 1 to 1000 nm, being generally smaller than the pores in permeable and fractured media. These particles, are sufficiently stable to form another phase to the aqueous phase and sufficiently “small” to undergo

Brownian motion [3]. Colloids possess a large surface area to volume ratio [4] and can thus act as a sorbent of contaminants.

The stability of a colloidal system depends on the net energy balance of two forces: the Van der Waals attractive forces, and the repulsive, electrostatic forces which prevent the particles from colliding [4]. The DLVO (Deryajin-Landau-Verwey-Overbeek) theory is a quantitative model for predicting the stability of colloidal systems based on the summatory of both attractive and repulsive forces and the distance between the particles [4]. When particles undergoing Brownian motion collide with sufficient energy to overcome the long range repulsive forces, then the attractive forces will lead to a minimum in the potential and thus aggregation may occur [5]. A secondary minimum in the energy potential, which leads to a reversible flocculation of the particles, may be found in colloidal systems. Hence, stability of a colloidal system is attained by generating enough repulsion between colloidal particles to prevent the particles from flocculating.

The background electrolyte in solution plays a key role on the stability of the colloidal system. An increase of the concentration of the electrolyte leads to a descrease in the repulsion forces due to screening of the double layer interaction. Consequently, the colloidal particles coagulate [5]. Other parameters which influence the stability of colloids are hydration forces [6], which involve the organisation of water molecules around the surface by polarisation induced by the dipole moments of the ion pairs [5], or sterical stability, which may be attained by coating the particles with an absorbed polymeric layer on the surface of the colloid [7].

Stability of colloidal suspensions is often studied by measurements of zeta potential [8,9], where the general trend observed is an increase of the stability with the net surface charge [10].

1.1.2. Types of Colloids

Groundwater colloids may be inorganic particles, organic molecules, or microorganisms [11,12,13]. Colloids can be formed by weathering of rocks, plants and soils, as well as by dissolution of minerals, leading to the formation of secondary

minerals [14]. Actinide oxides and hydroxides present in the near field of a repository may undergo hydrolysis and polymerisation processes leading to the formation of actinide colloids [10].

1.1.2.1. Biocolloids

Biocolloids are those microorganisms, such as bacteria or viruses, which are colloidal in size and naturally exist in the subsurface. Bacteria generally possess net negative charge in natural environments [11], although the cell surface and other properties depend on environmental conditions [13]. Microbes may alter, by enhancing the kinetics, processes in groundwater chemistry which would be slow otherwise [2]. Recent investigations have reported adsorption of metals, such as Ni(II), Cu(II), Zn(II) or Cr(VI) on fungus under different pH and temperature conditions [15]. The sorption of Co(II) and Sr(II) onto moss was maximum at pH 5 – 6. The sorption isotherms were modelled satisfactorily by the Langmuir model and spectroscopic techniques revealed ion exchange was the main mechanism for the sorption of metals [16]. The transport of Cd(II) through gravel aquifer media by bacteria spores [17] was assessed, leading to the development of a computer code to model the transport of Cd(II). Bioremediation by the chitosan biopolymer has been widely studied; Muzzarelli [18] and Wan Nhag *et al.* [19] reviewed the findings of the investigations.

1.1.2.2. Organic substances

Humic acids (HA) are the fraction of organic substances which are soluble in solution at pH above 2 [20]. HA are ubiquitous in groundwater systems [2], as they originate from decomposition of plants and animal matter [20]. A large number of functional groups are found in HA molecules, including carboxylic groups and phenolic groups. Due to the complexity of HA, a structure has not yet been found, although many have been proposed. From the different spectroscopic studies, properties like flexibility have been attributed to HA [21]. This property allows the structure to contract or expand depending on the pH and ionic strength conditions. In this manner, an increase on the ionic strength will cause the molecules to shrink due to screening of the charges. On the contrary, an increase in the pH leads to the

formation of negative charges that will cause repulsive interactions, thus leading to expansion.

HA present in groundwater systems can act as a sorbent for contaminants [21], thereby potentially enhancing the transport of these contaminants, and can also promote colloidal transport by preventing their coagulation and consequent deposition on the solid matrix [20].

The effect of HA on minerals and contaminants has been addressed from different approaches:

- Coating of minerals by HA. These investigations generally study the sorption of HA on minerals and clays under a variety of chemical conditions. For example, Liu *et al.* [22] found that the sorption of HA on montmorillonite decreased with an increase of pH. Yoshida *et al.* [23] reported an increase in the migration of alumina through a sand column when coated by HA.
- Influence of HA on the sorption of metals onto minerals and clays. Investigations of the sorption of metals in the ternary system include the sorption of U(IV) onto kaolin in the presence of HA [24]. The effect that HA has in a ternary system has been the object of study to understand the mechanisms of sorption and modelling attempts have been made. Examples include the quantification of the blocking effect of HA on the sorption sites of latex colloids, studied by Yang et al. [20]
- Sorption of metals onto HA. For example, the enhancement in the transport of Eu(III) by HA through a sand column was reported by Warwick et al. [25]. More examples can be found in Chapter 3.

A number of investigations have been carried out to understand the mechanisms of sorption in ternary systems. Anirudhan *et al.* [26] reported that the sorption of Cu(II), Zn(II) and Co(II) onto bentonite occurred through ion exchange and complexation mechanisms. Bivalent metal sorption onto montmorillonite was reported to take place by bridging of the metals. A bridged corundum-HA-Pb(II) complex was reported by Boily and Fein [27] at low to neutral pH. An increase in the pH was found to introduce competition for the metal by the surface sites (adsorbed metal) and by

the HA (formation of aqueous Pb-humate complexes), leading to the decrease of Pb sorption on the corundum surface.

1.2. Migration of colloids

The presence of colloids in the subsurface is ubiquitous and has been recorded by several investigators [13]. Tipping et al. [3] reported data on colloidal speciation in several field sampling points. Special attention has been paid to the presence of colloids at the Grimsel test site in Switzerland, where several groups have investigated not only the release of colloids and their transport but also their role in facilitating the transport of radionuclides [35, 36, 37].

A clear understanding of the mobility of colloids is essential in order to assess the influence of colloids on contaminant migration through the subsurface. The mobility of colloidal particles includes transport, release from and retention on the solid geological material.

1.2.1. Release of colloids

This process depends on particle-surface interactions and is governed by the hydrodynamics of the flow field [28]. In this context, colloidal particles may be released by sliding or rolling of particles due to the flow forces. Dettachment of colloidal particles occur mainly due to changes in solution chemistry, like ionic strength or pH [29, 30]. Sen *et al.* [29] suggested that a favourable chemical environment for the release of colloidal particles is that saturated in Na^+ ions, with high pH and low ionic strength. Under these conditions, an expansion of the electric double layer would lead to mobilisation of the particle due to repulsion of like-charged particle and matrix.

The release of colloids has been investigated at laboratory scale by means of column experiments with subsurface materials [28]. Grolimund and Bokovec [28] reported an increase in particle release with decreasing ionic strength and presence of monovalent counterions. Another factor which influenced the release of colloidal particles was aging the subsurface materials. This caused the release of colloidal particles to decrease as the time of aging increased.

Reviews on the release of colloids can be found in Ryan *et al.* [30] and more recently in Sen *et al.* [29].

1.2.2. Transport of colloids

Colloid transport has been experimentally observed through fractured materials, like carbonate rocks or glacial tills [13].

Transport of colloids can be described by two phenomena: size exclusion mechanism and hydrodynamic chromatography. The former is based on the fact that colloids are excluded from fine pores. The latter is based on the chromatographic effect that the velocity profile through a cylinder is parabolic, being maximum at the center and decreasing towards the walls. Due to the size, particles will be excluded from the slowest regions and thus migrate at higher velocity than the average water [31].

1.2.3. Retention of colloids

Transport of colloids may be reduced by immobilising the colloids on the solid surface. Colloid stability can be achieved by maintaining the repulsive forces between colloids and solid surface [13]. Thus, colloid retention can be achieved by minimising those repulsive forces, leading to the coagulation of colloids, and hence the deposition of colloids on the surface. Retention of colloids may be enhanced by increasing the ionic strength of the solute suspension [32]. Multivalent cations in the solute may also contribute to a higher retention of colloids [13].

For example, the retention of alumina colloids on mica was studied by Spalla *et al.* [33] who reported no desorption of colloids when the sample was aged in salt ($NaNO_3$) water, but observed desorption of the colloids when aging the sample with citrate (> 5 mmol dm^{-3}), due to the change in the charge in the alumina surface introduced by the citrate.

1.3. Colloid-facilitated transport of contaminants

Transport of contaminants due to association with colloids was suggested in the early 1980s [13]. It is widely accepted that colloidal particles may play a key role in determining the fate of contaminants in the subsurface. For colloids to have a fundamental influence on the transport of contaminants, three criteria must be met [30,2]: First, colloids need to be present in a significant amount to have a significant probability of interaction between contaminants and colloids. In this case, release of colloidal particles from the solid matrix must occur. Secondly, colloids must adsorb contaminants on their surface; interactions between the surface of the colloids and the radionuclides must take place so that the radionuclide attaches to the colloidal particle. Finally, colloids have to migrate through the groundwater in order to co-transport contaminants along with them. The interactions between contaminants and colloids are represented in Figure 1:

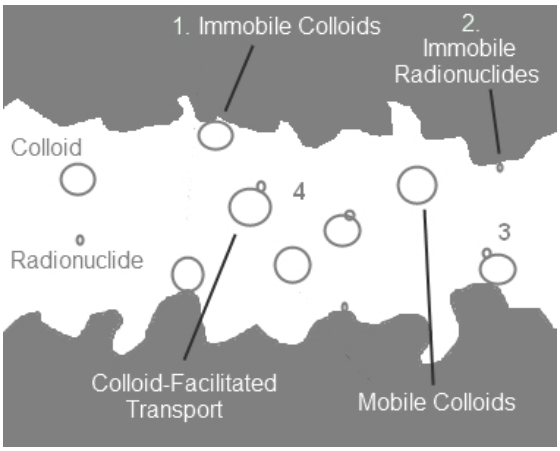

Figure 1. Possible interaction between colloids and radionuclide particles in the subsurface.

Figure 1 presents the scenario in which a mobile colloid may interact with a radionuclide. For ease of interpretation, a simple diagram has been shown where only one colloidal particle and one radionuclide particle are shown. The following interactions may occur:

1. Interaction of the mobile colloid with the solid matrix, leading to its retention;
2. Interaction of the mobile radionuclide with the solid matrix, leading to its immobilisation;

3. Irreversible interaction of the mobile radionuclide with an immobile colloid. In this case, the transport of the radionuclide will depend on the rate of release of the colloid.
4. Interaction of the mobile colloid with the mobile radionuclide, leading to an enhancement of the transport of the radionuclide. However, depending on the reversibility of the interaction, the radionuclide can be transported long distances, until deposition of the colloid (irreversible sorption) or can be transported until the radionuclide desorbs from the colloidal particle (reversible sorption).

The transport of contaminants and colloidal particles through the subsurface can be generally described by four terms: diffusion, dispersion, advection and a chemical term which takes into account deposition and release of the transported particle [12]. Migration of radionuclides is generally diminished by sorption onto the solid matrix. However, the presence of colloids can significantly enhance the migration of contaminants, as seen by the scheme in Figure 1. Hence, an understanding of the sorption of contaminants onto colloidal particles is fundamental [34].

Examples of experimental observations of enhanced mobility of contaminants due to co-transportation with colloidal particles are given below.

The breakthrough of ^{241}Am and ^{244}Pu [35] and ^{131}I, ^{85}Sr, ^{137}Cs, ^{99}Tc, ^{232}Th, ^{233}U, ^{237}Np, ^{238,244}Pu, and ^{241}Am [36] associated with Febex bentonite colloids through Grimsel groundwater was studied by means of column experiments. The radionuclides were found to be co-transported with the bentonite colloids. Furthermore, the sorption of Am on bentonite colloids was reversible, but slow. Sr transport through a crystalline structure was slightly enhanced by the presence of bentonite colloids [37]. However, the transport was less than expected due to partly the retention of the colloids in the structure and partly due to, perhaps, desorption of Sr from the colloids. Grolimund *et al.* [38] reported the outbreak of Pb through a non-calcareous soil; Nagasaki *et al.* [39] observed enhanced transport of Am and Np by montmorillonite colloids; Cs migration through a granite fracture was enhanced by clay colloids [40] and by silica colloids when passed through glass bead columns [41]. Natural organic colloids

enhanced slightly the transport of ^{241}Am through a fracture in granite, but did not influence greatly the transport of ^{85}Sr, as reported by Vilks *et al.* [42].

1.4. Modelling

The classic approach describes transport of contaminants as a function of diffusion, advection and deposition/release on the porous matrix. Inclusion of colloids in the transport equation has been approached by adding sorptive terms in the original transport equation (see section 1.4.3). Modelling the effects of bacteria on contaminant transport has also been addressed, simply by adding sorption and desorption interactions to the classic approach [11].

The inclusion of colloids in the solute transport equation needs the complete knowledge and understanding of the interaction between radionuclides and colloids. The study of both the sorption and migration of colloidal particles and contaminants have led to the development of computer codes.

1.4.1. Modelling solute transport

The transport of solute depends of three terms: a dispersive / diffusive term, an advective term and a chemical term. The transport equation can be defined as [28,12,11]:

$$\frac{\partial c_i}{\partial t} = D\frac{\partial^2 c_i}{\partial x^2} - v\frac{\partial c_i}{\partial x} - \rho\frac{\partial q_i}{\partial t} \qquad \textbf{Equation 1.1}$$

$$\frac{\partial q_i}{\partial t} = -j_i^{des} + j_i^{ads} \qquad \textbf{Equation 1.2}$$

Where c_i is the concentration of a given solute i, D is the dispersion coefficient, v is the flow velocity, ρ is the solid mass per unit pore volume, q_i is the concentration of adsorbed solute, j_i^{des} and j_i^{ads} are the kinetic fluxes due to desorption and adsorption reactions, respectively.

1.4.2. Inclusion of colloids in modelling solute transport

The transport of colloids through the subsurface may be described similarly to the transport of solutes (Equation 1.1). Considering deposition of colloids as linear and reversible, the mass balance equation for colloidal transport would result [11]:

$$\frac{\partial(\theta c_j)}{\partial t} = D_j \frac{\partial^2(\theta c_j)}{\partial x^2} - \upsilon_j \frac{\partial(\theta c_j)}{\partial x} - \theta k_j^{dep} c_j + \theta k_j^{ads} c_m \qquad \textbf{Equation 1.3}$$

Where c_j describes the concentration of suspended colloidal particles (mobile colloids), k_j^{dep} and k_j^{ads} are the deposition and release rate coefficients, respectively, θ is the porosity and c_m is the concentration of deposited colloids (immobile colloids).

The transport equation for a contaminant migrating through the subsurface in the presence of colloids would result in the following equation, which includes the diffusion and advection term, as well as the sorption and desorption terms of the radionuclide from the solid matrix, from mobile colloids and from immobile colloids [11]:

$$\frac{\partial c_i}{\partial t} = D_i \frac{\partial^2 c_i}{\partial x^2} - \upsilon \frac{\partial c_i}{\partial x} - \rho \frac{\partial q_i}{\partial t} - k_{ij}^{ads} \theta c_i - k_{im}^{ads} \theta c_i + k_{im}^{des} c_m \sigma_m + k_{ij}^{des} c_j \sigma_j \qquad \textbf{Equation 1.4}$$

Where the term $\frac{\partial q_i}{\partial t}$ includes the sorption and desorption of the contaminant on the solid matrix, θ is the porosity, σ is the mass fraction of the contaminant sorbed on the mobile (j) and immobile (m) colloids and $k_{ij}^{ads}, k_{im}^{ads}.k_{im}^{des}, k_{ij}^{des}$ are the adsorption rate coefficients onto the mobile and immobile colloids, respectively; and the desorption rate coefficients from the immobile and mobile colloids, respectively.

Other models have been developed based on the classic approach described above. For example, Irina *et al.* [12] defined a pseudo-two-phase approach where two types of clusters of pores were taken into account: one in which only pure water could be found (colloids were excluded due to the small size of the pores) and another where the colloid suspension occupied larger pores.

1.4.3. Modelling contaminant sorption to colloids

Successful modelling of the transport of radionuclides through the subsurface in the presence of colloids needs a full understanding of the processes which govern the sorption of radionuclides onto the colloids. Sorption of contaminants on colloids has been widely studied and different models have been used to model such sorption. Some of the simpler models are based on empirical equations, like the Langmuir or the Freundlich isotherms.

Thermodynamic interpretations are based on the assumption that equilibrium is reached when measurements are taken to enable the construction of sorption isotherms. This however, may not be true as kinetics of the sorption may be slow and equilibrium may not be attained on the period of time of the experiment [43].

From the study of the sorption and desorption of contaminants from colloids, or, in general, from solid surfaces, a mechanistic interpretation can be derived. Once the contaminant has sorbed onto the surface, given the necessary time to reach a new equilibrium, the adsorbate can (a) diffuse slowly into the matrix, (b) form inner-sphere surface complexation, or (c) crystallise in the form of a new solid phase [43]. The mechanisms of sorption are modelled using surface complexation models (refer to Goldberg *et al.* [44] for more details) by testing the ability of the models to reproduce the data satisfactorily [45].

Many models have been used to describe the mechanisms of sorption of metals onto colloids. Based on surface complexation and cation exchange, models and computer codes have been developed. For example, Missana *et al.* [45] interpreted the sorption of U(VI) onto goethite colloids using the double difuse layer model, Kraepiel *et al.* [46] used potentiometric data and combined it with surface complexation and cation exchange models to develop a computer code for the modelling of sorption of metals onto Na-montmorillonite.

Although mechanistic interpretations of metal-colloid interactions were not an aim in this thesis, interpretations found in the literature are used to interpret some of the experimental results.

Chapter 2. COLLOID BINARY SYSTEMS

2.1. Introduction

Understanding the migration of metals through the Geosphere may start by evaluating the interactions of contaminants with the host rock. Due to various factors, such as friction, the host rock might release smaller, metastable particles called colloids. Because of their small size, colloids may be excluded from pores while migrating along the Geosphere following the flows of groundwater.

Having the same properties as the host rock, colloids might interact with contaminants in the same way as the original minerals, with the addition that they may be transported along with the colloids. Therefore, colloids can be considered potential transporters of contaminants, i.e. radionuclides, through the Geosphere.

The knowledge of the extent of sorption of metals onto colloids present in the environment is therefore important in evaluating the possible migration of radionuclides through the Geosphere. In this matter, not only sorption, but also desorption of the metals from the colloids is of great relevance [36,45], as an irreversible sorption would lead to transport of the contaminant; whereas a reversible sorption could limit the enhancement of the transport of the contaminant. In any case, the assessment of the interactions of radionuclides with colloids is fundamental in understanding the fate of radionuclides in the Geosphere.

This chapter aims to extend the knowledge of the interactions between three metals: caesium (Cs), nickel (Ni) and europium (Eu), chosen because they are mono, di and trivalent; with two different colloids that are abundant in the environment: boehmite and montmorillonite. Sorption of the metals onto the colloids was studied under fixed conditions of pH and ionic strength, followed by an investigation of the desorption of the metals, carried out in three consecutive steps, in order to gain a better understanding of the reversibility of the sorptive process.

Colloids can be considered to have the same sorptive properties as the minerals they originated from, but their smaller dimensions provide colloids with a larger surface area per mass which metals might sorb to, thereby enhancing the sorptive properties. In this investigation, special attention is paid to the sorption of metals onto colloids and the solid phase of the corresponding mineral in order to compare the extent of sorption onto colloids and to bulk surfaces of the same material. To facilitate comparisons, the surface areas of both colloid and solid phase were measured, along with other surface properties like proton or cation exchange capacities.

The sorption of a metal onto a solid is generally expressed by a distribution ratio, which is the ratio of surface-bound metal to dissolved metal in solution. Databases of these distribution ratios exist [44] and a large number of sorption studies are found in the literature. However, the distribution ratio is a parameter specific to the conditions in which the sorption was carried out. Furthermore, most of the distribution ratios determined are so for the systems consisting of metals and solid phases. The number of investigations where sorption of metals is carried out on colloids is more limited. Considering the only differences between colloidal and solid phases might be related to the surface area, this investigation suggests that the distribution ratio for the sorption of a metal onto a colloid might be proportional to the distribution ratio of the metal and the ratios of surface areas. This idea was introduced by Wieland *et al.* [14], who suggested that a "scaling factor" between the distribution ratios could be the ratios between surfaces areas. This idea has been extended, although, due to the limited knowledge in modelling, only a robust approach is presented herein, needing further insight to produce a mathematical expression that could relate both distribution ratios.

2.2. Experimental

The experimental procedure was based mainly on batch experiments measuring the sorption and desorption of metals onto colloidal and solid phases using two different minerals. In addition to batch experiments, other measurements were needed in order to characterise the colloids, i.e. measurement of average size, zeta potential and surface area.

2.2.1. Method development

2.2.1.1. Materials used

Two different colloids were used in this investigation: boehmite and montmorillonite. The structures and main properties of both are summarised below. Three metals were used to study the sorption onto the mineral phases, Cs, Ni and Eu. The solutions were prepared from the chloride salts of each metal. The details are described in section 2.2.1.1.3.

2.2.1.1.1. Boehmite

Boehmite is an aluminum oxyhydroxide of formula AlO(OH). Its structure consists of double layers of octahedra held together by hydrogen bondings of the OH groups (Figure 2) [47]. Two different types of oxygen can be distinguished according to their location within the octahedra (red and blue in Figure 2): (1) the oxygens in red are those in the middle of the octahedra and are shared by four other octahedra. (2) the oxygens in blue are the hydrogen-bonded to the oxygens in the neighbouring double layers. The ratio between oxygen and hydroxyl groups is expected to be one to one. [48].

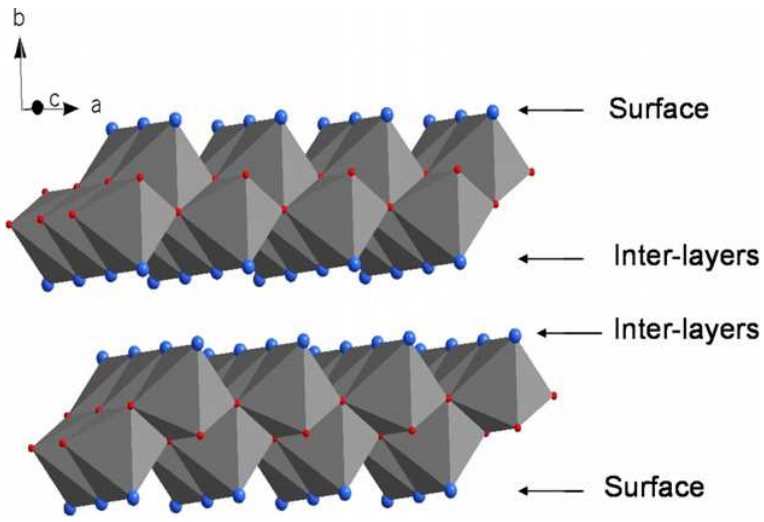

Figure 2. Structure of boehmite [47].

Boehmite can be found in the environment in bauxites and laterites, as it constitutes a main component of these minerals, together with gibbsite/bayerite($Al(OH)_3$) and diaspore (α-AlOOH). Boehmite is used in industry as a source of aluminum [48,49].

The morphology, size and surface area of the synthesised boehmite depend on the conditions of processing, *i.e.* acidic/alkaline conditions, temperature of furnace, time of processing and precursor used [50,51]. Boehmite can be synthesised by hydrothermal processing of aluminum alkoxide [47], aluminum salts, such as chloride [52,51,53] or nitrate [54,55,56], aluminum acetate powder [57], aluminum sulphate and urea [58], aluminum isopropoxide / isopropanol [59] or aluminum hydroxides [60].

Two phases of boehmite were used in the work presented herein: colloidal and solid phase. Boehmite colloids were provided by FERALCO Ltd. (UK) as CERASOL. The solid phase was provided by Nabaltec (Germany), as APYRAL AOH20. Both products were used without further treatment.

2.2.1.1.2. Montmorillonite

Montmorillonite was purchased from Aldrich (UK) as Montmorillonite K10. A proposed structural formula of montmorillonite is:

$Na_{0.05}Ca_{0.15}Mg_{0.03}(Al_{1.5}Fe(III)_{0.1}Mg_{0.4})(Si_4)O_{10}(OH)_2 \cdot n\ H_2O$ [61]

Montmorillonite is a clay mineral belonging to the phyllosilicates. The structure of montmorillonite consists of two silicon tetrahedra layers separated by an aluminum octahedra layer (see Figure 3) [62].

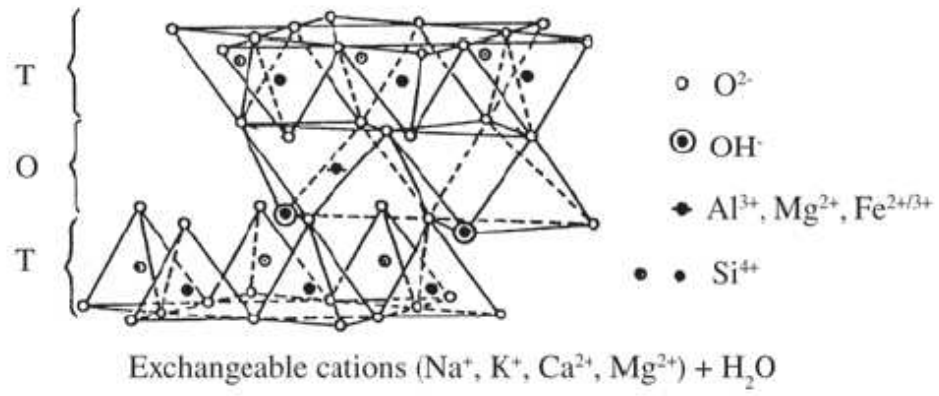

Figure 3. Structure of montmorillonite [62].

The surface of montmorillonite carries a net negative charge due to isomorphous substitution of lattice cations by cations of lower valence. Charge neutrality is

achieved by the formation of electrostatic interactions with nearby cations in solution, which can undergo ion exchange processes with other cations in solution [63].

Together with kaolinite, illite or chlorite, montmorillonite is a major component of bentonite, used as backfill material for radioactive waste repositories [63]. Upon a release of radionuclides, the first barrier encountered would be the backfill material. Hence, understanding the interactions of radionuclides with montmorillonite is essential towards assessing the mobility and fate of radionuclides in the Geosphere.

2.2.1.1.3. Metal solutions

Metal solutions were prepared by diluting a known amount of solid with deionised (DI) water to the desired volume. The solids used for each metal were: CsCl (BDH Laboratories AnalaR®), $NiCl_2$ (Fisher Scientific) and $EuCl_3$ (Sigma-Aldrich). NaCl and KCl, from Sigma-Aldrich chemicals, were used to adjust the ionic strength. In some cases 2-(N-morpholino)ethanesulfonic acid (MES) (Sigma-Aldrich) was used as a buffering agent and was chosen for its non-complexing properties.

Radioactive stock solutions, obtained from Amersham International Plc., were prepared by diluting a known volume of radioactive stock into the desired volume of DI water. Generally, 10 – 20 x 10^{-3} cm^3 would be taken from the stock solution provided from the manufacturers and diluted into 10 – 20 cm^3 DI water. The isotopes used are shown below.

Table 1. Isotopes and radioactive parameters.

Isotope	Inorganic Salt	Radiation measured	Half life (years)
^{137}Cs	CsCl	Gamma	30.2
^{63}Ni	$NiCl_2$	Beta	100
^{152}Eu	$EuCl_3$	Gamma	13.5

The metal concentration of the active metal stock solution can be calculated from the exponential decay law:

$$-\frac{dN}{dt} = \lambda N$$ **Equation 2.1**

$$t_{1/2} = \frac{\ln 2}{\lambda}$$ **Equation 2.2**

Where λ is the decay constant, related to the half-time of the isotope by Equation 2.2, and N is the number of atoms involved. The metal concentration may be calculated dividing N by the avogadro number (N_A = 6.022 x 10^{23}). Table 2 shows the metal concentration of the active metal stock solution, given that the specific activity was approximately 8.33 x 10^6 Bq dm^{-3}.

Table 2. Metal concentration in active metal stock solution.

Metal	$t_{1/2}$ (seconds)	[M] (mol dm^{-3})
^{137}Cs	952387200	1.89 x 10^{-8}
^{63}Ni	3153600000	6.29 x 10^{-8}
^{152}Eu	425736000	8.49 x 10^{-9}

The study of these three metals was carried out due to the following importance of the metals:

- ^{137}Cs is present in the environment due to nuclear activities and accidents [64].
- Ni is a toxic heavy metal [65], which can be found in wastewater due to its use in industry [66]. Ni is an analogue for other heavy metal and radionuclide contaminants, i.e. Pb (II) [65].
- ^{152}Eu is a well-known analogue for transuranic metals and other lanthanides [67].

2.2.1.2. Preparation for measurements

Average sizes and zeta potentials of colloids were measured using a Zeta Master S (Malvern Instruments). Ten recordings were measured and the average and standard deviations are reported.

pH measurements were carried out using a Jenway 350 pH meter. The instrument was calibrated prior to its use with three standard solutions (pHs 4, 7 and 10).

Samples were centrifuged in a Hermle Z206A centrifuge at 6000 rpm for 30 minutes. When necessary, samples were mixed using a Labnet VX100 Vortex mixer. The filters used in all sorption and desorption experiments were supplied by Elkay (0.45 and 0.22 μm in pore size) or Anachem (PES Syr-filter 0.2 μm filters) and the plastic syringes used (5 cm^3) were provided by BD Plastipak. When used, the plastic syringes were filled with sample, the filter fitted to the end and the first 5 cm^3 of the filtered sample were discarded, collecting the following 2 cm^3 for radiometric measurement. Control experiments showed that no sorption of activity to the syringe filters or to the centrifuge tubes took place.

Radionuclide assays (to an error of two sigma or better) were performed using either a Tricarb 1900TR Liquid Scintillation Analyzer (Packard Ltd) or a Cobra II Auto-Gamma Counter (Packard). The activities measured were converted by calculation into concentrations.

Powder X-ray measurements were performed using Cu-Kα radiation (λ = 1.5418 Å) on a Bruker D8 diffractometer in reflection geometry and a Braun position sensitive detector. The sample was loaded onto a silicon zero background substrate and data were collected in the range $5 < 2\theta < 90°$ with a step time of 1 second and step width of 0.014°.

2.2.1.3. Speciation

The JChess speciation programme was used to predict the metal species for each of the systems studied in batch sorption experiments. These were constituted by the MCl_x (M = Cs, Ni, Eu), the colloid (boehmite or Na-montmorillonite), 0.05 mol dm^{-3} NaCl as background electrolyte and pH 7.

2.2.1.4. Data processing

Sorption isotherms were constructed from data obtained from the batch experiments. The results were fitted to three different models: the Langmuir, the Freundlich and the Dubinin-Radushkevich equations. The three models are briefly described in this

section. In addition to this, the distribution ratios were determined from the sorption isotherms.

2.2.1.4.1. Distribution ratio

The simplest type of sorption isotherm is the linear isotherm (n = 1 in the Freundlich isotherm -Section 2.2.1.4.2-), where the concentration of sorbed metal on the solid (mol kg^{-1}) is directly proportional to the concentration of dissolved metal in solution (mol dm^{-3}). The proportionality factor is defined as the distribution ratio, R_d (dm^3 kg^{-1}) (Equation 2.4) [68,69]. It can be determined from radiometric measurements as:

$$Q = R_d C \qquad \textbf{Equation 2.3}$$

$$R_d = \frac{A_0 - A_{eq}}{A_{eq}} \frac{V}{m} \qquad \textbf{Equation 2.4}$$

Where Q is the concentration of metal bound to the solid surface (mol kg^{-1}), C is the concentration of dissolved metal in solution (mol dm^{-3}), R_d is the distribution coefficient (dm^3 kg^{-1}), A_0 is the activity of the blank active sample (no sorption took place), referring to the initial concentration, A_{eq} is the activity of the sample after sorption, referring to the equilibrium concentration, V is the volume of the sample, in dm^3 and m is the mass of colloid, or solid, in kg.

The distribution coefficient can therefore be derived from the slope of the linear range in the sorption isotherm of a given radionuclide to a given surface. Due to the empirical nature of the distribution coefficient, it is subject to the specific conditions under which the experiment was developed, *i.e.* pH, ionic strength or complexing ligands [68]. Thus, the value of the R_d for the sorption of metals on solids may vary depending on the chemical conditions of the experimental process (discussed in section 4).

The distribution ratios presented herein were calculated by linear regression of the linear sorption isotherm of metals. Whenever the sorption isotherm was non-linear, data used to determine the R_d value were those which would exhibit a linear behaviour. Data were presented as the mean value of the distribution ratio ± the

standard deviation. The minimum number of samples used to calculate the R_d value was, where possible, five replicates for ten different concentrations. These were the cases where the sorption isotherm showed a linear response for the whole range of concentrations studied. In the cases where the isotherm curved, suggesting saturation, the number of samples used to calculate the R_d value decreased.

2.2.1.4.2. Freundlich isotherm

The Freundlich model is an empirical isotherm which describes a non-linear sorption of the adsorbate to the solid surface. The equation and the linearised form for the Freundlich isotherm are shown below [68,43]:

$$Q = FC^n \qquad \textbf{Equation 2.5}$$

$$\log Q = \log F + n \log C \qquad \textbf{Equation 2.6}$$

Where Q and C are the concentration of metal bound to the surface and free in solution, in mol kg^{-1} and mol dm^{-3}, respectively. F and n are characteristic parameters of the Freundlich model, related to the adsorption capacity and the adsorption intensity, respectively [70]. A value of unity for n indicates linear sorption. Values of F and n are reported herein and discussions are made based on n values obtained.

2.2.1.4.3. Langmuir isotherm

The Langmuir model is based on the assumption that an electric double layer exists between the adsorbent surface and the adsorbate. Further assumptions include: (1) no interactions take place between the adsorbed species; (2) no migration of species occur in the plane of the surface; (3) only a monolayer of metal is adsorbed to the surface; and (4) all adsorption sites are homogeneous. The Langmuir sorption isotherm introduced the idea that sorption to the surface is limited, whereas the linear and Freundlich isotherms assumed infinite sorption of the adsorbate [70].

The Langmuir equation, as well as the derivation to the linearised form of the equation are shown below [68,70]:

$$Q = Q_{\max} \frac{LC}{1+LC}$$ **Equation 2.7**

Rearranging and reversing the equation,

$$\frac{Q_{\max}}{Q} = \frac{1+LC}{LC} = \frac{1}{LC} + 1$$ **Equation 2.8**

Dividing by Q_{max},

$$\frac{1}{Q} = \frac{1}{Q_{\max}} + \frac{1}{L \cdot Q_{\max}} \frac{1}{C}$$ **Equation 2.9**

Where Q and C are the concentration of metal bound to the surface and free in solution, in mol kg^{-1} and mol dm^{-3}, respectively. Q_{max} is the maximum concentration of metal that can adsorb to the surface; in other words, the sorption capacity of the mineral; and L is an equilibrium constant related to the energy of adsorption.

2.2.1.4.4. D-R isotherm

The linearised Dubinin-Radushkevich (D-R) equation can be described as [204]:

$$\ln Q = \ln Q_{\max} - k\varepsilon^2$$ **Equation 2.10**

$$\varepsilon = RT \ln\left(1 + 1/C\right)$$ **Equation 2.11**

$$E = \left(-2k\right)^{-1/2}$$ **Equation 2.12**

Where Q and C are the concentration of bound to surface and dissolved in solution metal, in mol kg^{-1} and mol dm^{-3}, respectively. Q_{max} is the sorption capacity of the mineral, in mol kg^{-1}, k is a constant related to the adsorption energy, E is the mean free energy, in kJ mol^{-1}, ε is the Polanyi potential, R the gas constant (8.314 $JK^{-1}mol^{-1}$) and T the temperature, in K.

2.2.1.4.5. Statistics

Batch experiments were carried out to measure the sorption of metals onto minerals. A minimum of five replicates were used for each metal concentration. In some cases,

up to eight replicates were used. The radioactivity of the samples was measured to a 2σ error.

The concentrations of dissolved metal in solution and surface-bound metal were determined mathematically from the measured activity values. The mean and standard deviation of these concentrations were determined from the number of replicates used in the batch experiment.

The R_d values presented are shown as $\overline{R_d} \pm SD$ where $\overline{R_d}$ is the mean value obtained for the distribution ratio and *SD* is the standard deviation. Both values were determined by applying the linear regression method. The same method was applied to determine the standard deviation of characteristic parameters of the Freundlich, Langmuir and D-R isotherms.

2.2.2. Generation and stability of colloids

2.2.2.1. Boehmite

Boehmite colloids were used as provided with no treatment prior to their use, except dilution. Initial measurements of average size and particle counts per second were carried out to find the concentration of boehmite colloids to be used in sorption experiments.

Characterisation and stability of boehmite colloids was carried out by measuring the average size, particle counts and zeta potential. This last parameter was measured as a function of pH in a wide range of pHs and ionic strengths.

Separation of colloids from solution was achieved by centrifugation of samples at 6000 rpm. An experiment was carried out whereby samples of boehmite colloids were centrifuged for different times, ranging from 0 to 50 minutes and recording the average size after the test.

2.2.2.2. Montmorillonite

Montmorillonite colloids were extracted by repeatedly washing Montmorillonite K-10 (Aldrich) with 25 cm^3 aliquots of 0.05 mol dm^{-3} NaCl, combined with filtration and centrifugation. The filtrate was measured with dynamic light scattering (DLS) for average size and particle counts.

Montmorillonite colloids were characterised by DLS and zeta potential. The stability of the obtained colloids was measured as a function of pH and ionic strength.

2.2.3. Sorption and desorption experiments

The study of the interactions between metals and minerals was performed by investigating the sorption and later desorption of metals from colloidal and solid surfaces by using batch experiments. The experimental procedure and the results are shown first for the colloidal phase of each mineral and then for the solid phase. The desorption experiments are then detailed.

2.2.3.1. Sorption experiments

The sorption of metals onto colloids was studied using three different metals, Cs, Ni and Eu, which are mono-, di- and trivalent, respectively; and two different colloids, boehmite and montmorillonite.

The experimental procedure for sorption onto colloids and solids was slightly different.

Sorption onto colloids

10 cm^3 of colloid suspension were pipetted into 15 cm^3 polypropylene centrifuge tubes, along with 1 cm^3 of metal solution, buffer and background electrolyte. The pH was adjusted to 7 by adding small volumes of NaOH or HCl. The suspensions were then spiked with 100 μL of a radioactive tracer (approximately 0.83 KBq) and left to equilibrate for 24 hours. After the equilibrating period, the samples were centrifuged in a Hermle Z206A for 30 minutes at 6000 rpm. Control experiments showed that this time was sufficient for the colloids to be separated from the bulk. To further ensure this separation, prior to the radiometric measurement of the solution, the

samples were filtered using 0.45 μm Elkay filters. The 24 hour contact time was chosen following previous experiments carried out at Loughborough University [71].

Sorption onto solids

The procedure was the same as that used for colloids except that the solid was weighed into the centrifuge tubes. To keep the solid to liquid ratio similar to the adsorption carried out on colloids, aproximately 30 mg of solid were weighed into the vessels. In several sets, the influence of the amount of solid on the sorption of metals was tested.

Experimental conditions

pH and ionic strength were kept constant in all batch experiments. However, the influence of other parameters was assessed:

- The influence of the solid to liquid ratio was studied by changing the colloid concentration in suspension: it varied from 15 to 54 mg of colloid present in the 10 cm^3, in different batch experiments to study the influence of the colloidal concentration. This concentration was measured gravimetrically. The colloid concentration will be clearly stated in the results for ease of interpretation.
- The influence of background electrolyte on the sorption of Cs and Ni onto boehmite colloids was studied by batch experiments, using the same procedure as the one described previously.

Control experiments

The pH of the samples was adjusted to 7.0 ± 0.1 prior to leaving the samples to equilibrate, followed by monitoring of the pH after the equilibration period. As an example, the sorption of Ni onto solid montmorillonite was tested in the presence and in the absence of MES, noting the evolution of the pH.

On conclusion of the equilibration period, separation of the colloidal phase from the solution took place by centrifugation and later filtration. The filters were tested for radioactivity retention. Furthermore, filters of 0.45 and 0.22 μm pores were used. A separate test was carried out to study any differences on the sorption.

2.2.3.2. Desorption experiments

Reversibility of the sorption of metals onto colloids and solids was studied by performing three consecutive desorptions after the sorption experiments. The procedure was carried out equally on the experiments for colloidal and solid surfaces.

At the end of the sorption experiments, an aliquot of background electrolyte containing buffer solution was added to the centrifuge tubes in order to restore the initial solid to liquid ratio. The colloids were resuspended by briefly sonicating and then left to equilibrate for 24 hours. After the equilibration period, the samples were subjected to the separation process as explained in the adsorption section. The desorption experiments were carried out carefully to reproduce the same conditions as the sorption experiments, to minimise the effect of experimental differences between sorption and desorption.

2.2.4. Surface area measurements

An extensive study of the surface of boehmite, both colloids and solid, was carried out by measuring the surface area, proton and cation exchange capacities.

Spectroscopic techniques were used on both phases of boehmite, aiming to see differences on the surface of the colloid and the solid. With this purpose, both SEM and X-ray Powder Diffraction (XRD) techniques were used on both phases of the mineral.

2.2.4.1. Specific surface area

The specific surface area (SSA) can be defined as the ratio of the surface area of a solid surface and its mass; the former accounts for all sites accesible for cations in the inner surfaces [72]. The units of the SSA are $m^2 g^{-1}$.

The most common method used to measure the SSA of solids is the BET method [73], which consists of the measurement of the amount of adsorbed nitrogen gas required to cover the solid surface with a complete monolayer. The surface area is determined

from this measurement, together with the cross-sectional area of the adsorbed gas [74,72].

The BET method is generally used to measure the SSA of solids; however, it can also be used to determine the SSA of colloids [75,76,77] by previously drying the colloidal suspension. This can be done by evaporation, although during this process the colloidal suspension might undergo aggregation, in which case some of the interfaces might become inaccesible to the adsorbate gas, leading to an underprediction of the surface area of the particle [78]. Other methods have been proposed for the determination of SSA of colloidal particles involving the adsorption of polyvinylpirrolydone (PVP) [78], organic dyes [79], or the titration of hydroxyl groups on the surface of the colloid with a standard solution of NaOH in a saturated NaCl solution [80].

Two different methods were used experimentally to determine the SSA of boehmite colloids:

- The BET method

The SSA was determined by the BET method at BGS [74] using a Micromeritics Gemini VI 2385C series physisorption system.

- Dye adsorption method

This method was first tried on solid boehmite, and then, upon success, on boehmite colloids. The experimental procedure followed that described by Avena *et al.* [79] to measure the surface area of kaolinite colloids by measuring the sorption capacity of the surface with methylene blue. Briefly, the method consisted on adding a known amount of dye solution to a known amount of boehmite. The samples were placed on a shaker for 15 minutes. After this time, the samples were centrifuged for 5 minutes to separate the phases and UV measurement was performed to measure the concentration of remaining dye in solution. The supernatant was discarded and a new aliquot of dye solution was added to the boehmite. The procedure was repeated until the concentration of dye solution in the centrifuged sample was equal to the concentration of dye solution added.

Since the surface of boehmite is positively charged in the pH range 2 to 8, the appropiate dyes for the application of this method on boehmite would be negatively

charged. The following dyes were tried: diphenylsulfoxide (DPSO), 4-nitrobenzylalcohol (4NBA), 3-nitrophenol (3NP) and ponceau S (structures shown in Figure 4).

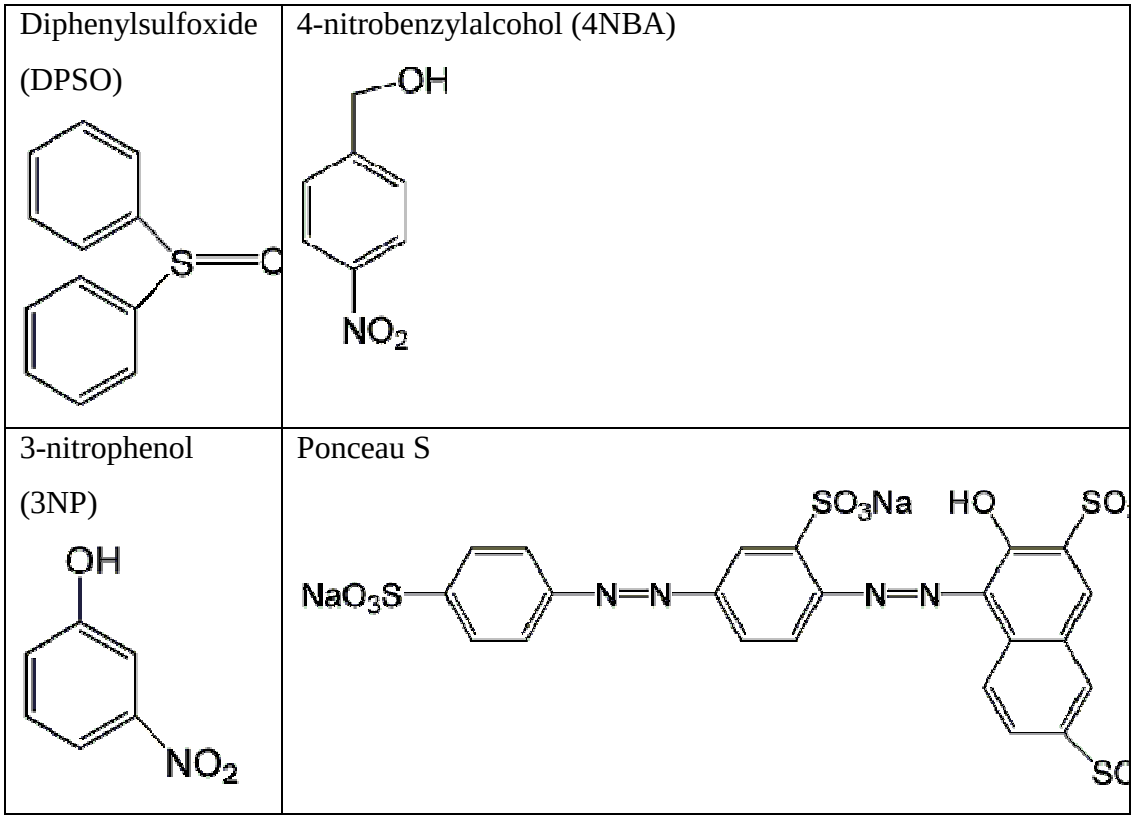

Figure 4. Organic dyes used in the surface area measurement of boehmite colloids.

2.2.4.2. Exchange capacity measurements

Other parameters indicative of the surface area of the colloids are the proton and cation exchange capacities, PEC and CEC, respectively. Both properties were measured for boehmite using the methods described in detail below.

2.2.4.2.1. Proton exchange capacity

The PEC method used in this investigation was modified from that described by He *et al.* [81] in order to prevent the colloids from flocculating. The method developed consisted of the titration of boehmite in 0.05 mol dm^{-3} NaCl. The pH of the suspension was taken to 3 with 0.01 mol dm^{-3} HCl and then titrated to pH 8 with 0.01 mol dm^{-3} NaOH. The pH was not increased above pH 8 so as to avoid flocculation of boehmite colloids. Once the suspension was at pH 8, it was back-titrated to pH 3.5

with 0.01 mol dm^{-3} HCl. The system tended to buffer at pH 3.5. The moles used to titrate (n_{OH}) and backtitrate (n_H) could be calculated from the volume used. The PEC was calculated as [81]:

$$PEC = \frac{molH^+ sites}{g_{boehmite}} \quad \textbf{Equation 2.13}$$

$$molH^+ sites = n_{OH} - n_H \quad \textbf{Equation 2.14}$$

In the case of the solid, 1.5 g were used in the experiment. In the case of the colloids, the gravimetric analysis of the sample showed that 0.496 g were titrated.

2.2.4.2.2. Cation exchange capacity

The CEC is defined as the capacity of a mineral, clay or soil to sorb cations which can later be exchanged by other cations in solution [82]. Many methods have been proposed for the measurement of this fundamental property of clays [83,84]. The cobaltihexamine chloride method was chosen to measure the CEC of the minerals used herein.

The method is based on spectrometrically measuring the concentration of $Co(NH_3)_6^{3+}$ before and after it was contacted with the mineral. UV absorbance was measured at 472 nm. In detail, 40 cm^3 of 0.0167 mol dm^{-3} $Co(NH_3)_6Cl_3$ were added to 2 g of mineral. The resulting suspension was shaken for one hour, after which centrifugation at 6000 rpm took place for 10 minutes. An aliquot of the supernatant was filtered through 0.22 μm filters and the absorbance measured. The CEC was calculated as [85]:

$$CEC = \left(\frac{A_0 - A_i}{A_0} \right) \times 50 \times \frac{V}{m} \times 100 \quad \textbf{Equation 2.15}$$

Where A_0 is the absorbance of the $Co(NH_3)_6Cl_3$ sample, A_i is the absorbance of the sample after shaking for one hour, V is the volume of sample, in cm^3, and m is the mass of boehmite, in g. The CEC was calculated in units of meq g^{-1}.

2.2.4.2.3. SEM and XRD powder diffraction

Part of this investigation included assessing the differences in surfaces between the colloidal and the solid phase of boehmite. For this purpose, SEM images were taken aiming to observe physical differences in the surface of the colloidal and solid phases of boehmite.

XRD diffraction patterns were taken after the sorption processes of either metals or HA had taken place, aiming to find alterations in the surface of boehmite due to the sorption of metals or HA.

Sorption of metals on boehmite colloids was studied by radiometric batch experiments. However, a batch of sorption experiments was carried out radiotracer-free to measure any changes in the surface due to the presence of metals. These changes were assessed by measuring XRD diffraction patterns and SEM images.

SEM measurements were carried out at BGS (Keyworth, UK) using a LEO (Zeiss) 435VP Variable Pressure Digital Scanning Electron Microscope (SEM). Powder diffraction measurements were taken using Cu-Kα radiation (λ = 1.5418 Å) on a Bruker D8 diffractometer in reflection geometry and a Braun position sensitive detector. The sample was loaded onto a silicon zero background substrate and data were collected in the range $5 < 2\theta < 90°$ with a step time of 1 second and step width of 0.014°.

2.3. Results

This section presents the results of the experiments detailed in section 2.2. The characterisation of colloids, along with the analysis of the stability are presented. An understanding of the conditions in which colloids were stable was fundamental for the batch sorption and desorption study. Those sorption experiments were performed always at the same pH and ionic strength. However, other factors influencing the sorption of metals on colloids were investigated, e.g. the solid to liquid ratio or the background electrolyte.

Desorption of metals from minerals and soils plays an important role on the mobility of radionuclides. The results for these experimental tests are shown following those of sorption.

The study of the surface area concentrated on the boehmite colloids. The results of the surface area, PEC and CEC of the colloid and the solid phase of boehmite are compared to extend the comprehension of the difference in sorption of metals on boehmite.

2.3.1. Characterisation and stability of colloids

2.3.1.1. Boehmite

Boehmite colloids were used for sorption experiments by diluting aliquots of the Cerasol suspension in 1000 cm^3 DI water. Prior to the sorption experiments and due to the high concentration of colloids of the Cerasol suspension, dilution was necessary for further experiments. Different dilutions were carried out and characterisation of those samples took place to select the optimum concentration of colloids. Table 3 shows the characterisation of the dilutions.

Table 3. Average size of boehmite colloids as determined using a Zeta Master S. 1 cm^3 boehmite colloids diluted into x cm^3 deionised water.

Dilution (cm^3)	Average Size (nm)	Kcounts per second	pH
50	125.0 ± 1.8	121.9 ± 0.2	4.05
80	127.8 ± 1.7	92.0 ± 0.5	4.07
100	123.9 ± 1.3	81.4 ± 0.2	4.11
120	118.6 ± 2.6	52.9 ± 0.3	4.16
150	128.4 ± 5.7	43.0 ± 0.2	4.41

Table 3 shows the average size and particle counts for sols containing 1 cm^3 of boehmite colloids diluted into DI water. The volume of water is indicated in the first column, in cm^3. The results indicated that as the volume of DI water increased, the average size remained constant and the particle counts decreased, the latter being due to the lower amount of colloids in suspension. A constant value of average size

suggested colloidal stability. Only a slight increase in pH was observed for the most diluted sample. Further monitoring of pH, measured daily, showed constant pH of the sols with time, suggesting stability of the diluted colloids.

As the average size was not influenced by the dilution factor, the only parameter relevant for choosing the dilution to use in further sorption experiments was the particle counts per second. Dilution of 1 cm^3 of boehmite colloids into 100 cm^3 DI was chosen as it yielded a reasonable amount of particle counts. Hence, the boehmite sols used for the sorption experiments were prepared by diluting 10 cm^3 of Cerasol colloids into 1000 cm^3 of DI water, yielding approximately 30 mg of boehmite in suspension per 10 cm^3, as determined gravimetrically.

Stability of boehmite colloids

Centrifugation of colloids took place for different time periods at 6000 rpm. The average size of the remaining suspension was recorded.

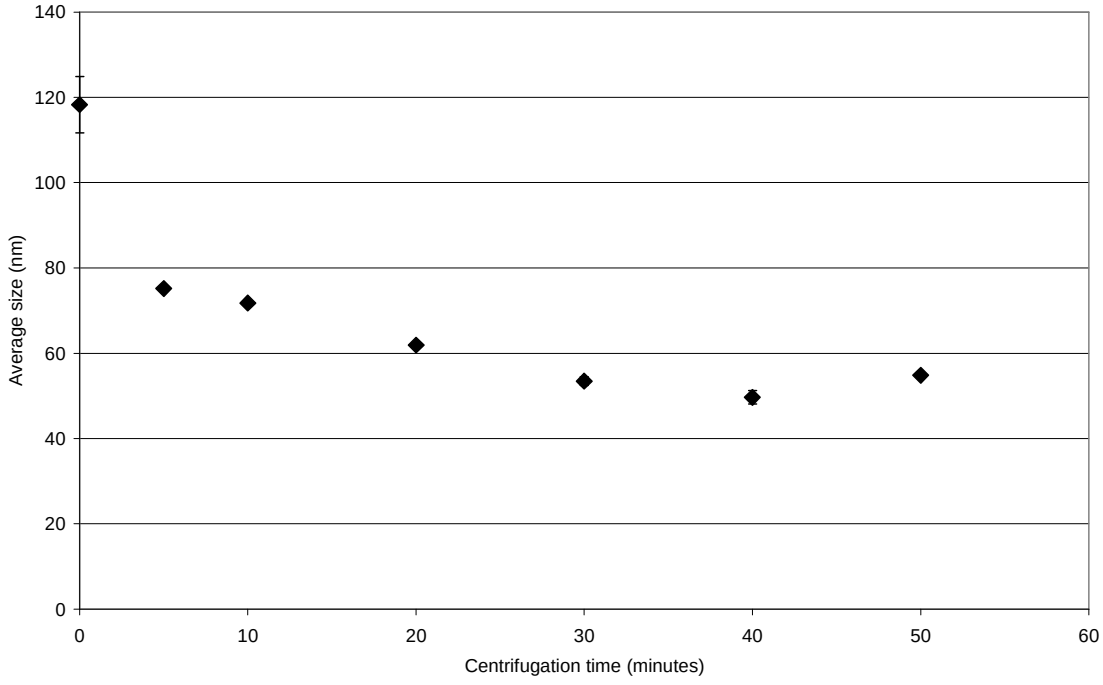

Figure 5. Average size and kcounts per second of boehmite colloids after different centrifugation periods.

Figure 5 shows the decrease in the average size and of boehmite before and after being centrifuged for different periods of time. The initial size of the colloids, of almost 120 nm decreased to approximately 50 nm after centrifuging for 30 minutes. Furthermore, this value remained constant when centrifugation was carried out for longer times. This experiment showed that the centrifugation time of 40 minutes chosen for the sorption and desorption experiments ensured the separation of boehmite colloids from solution.

The stability of boehmite colloids was measured by DLS as a function of pH and time. Kinetic measurements were carried out by recording the average size of boehmite colloids during 60 minutes at different pHs. The results are shown in Figure 6.

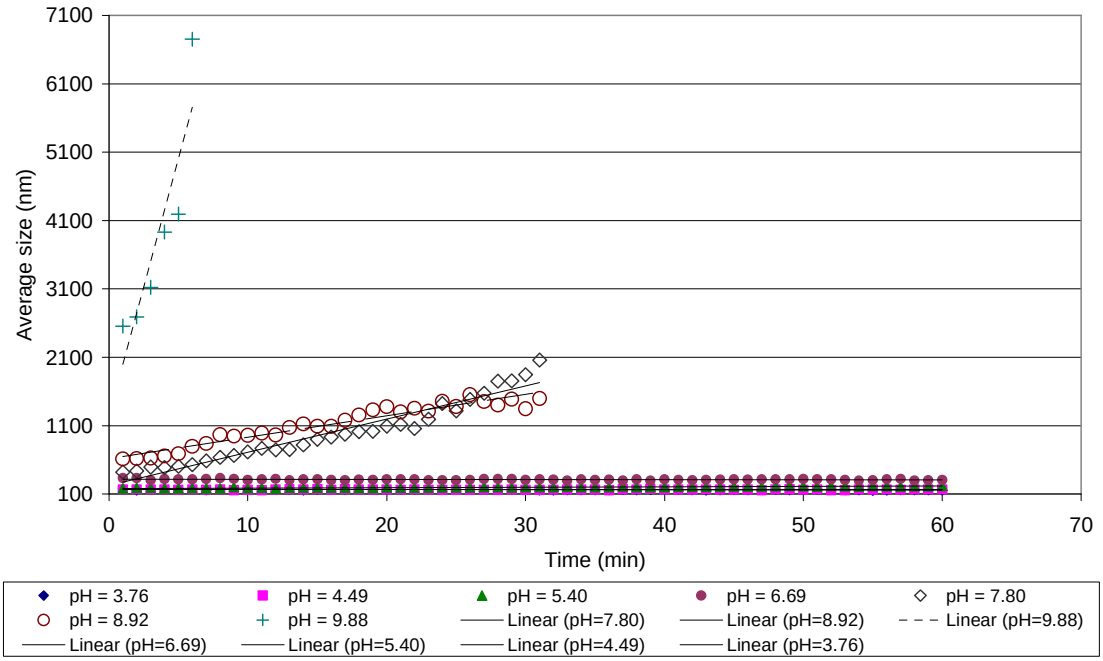

Figure 6. Average size of boehmite colloids as a function of pH and time.

Figure 6 shows the kinetic behaviour of boehmite colloids as a function of pH. Three different groups can be observed. The first one, in the bottom part of Figure 6 shown by the fully coloured data points, shows constant values throughout the time of the experiment. These results suggested stability of the colloids during this time at pHs 3.7 to 6.7. Increasing the pH, from 7.8 to 8.9, led to an increase of the average size of

the colloids with time, suggesting that boehmite colloids were no longer stable, but particles were slowly flocculating. A further increase of the pH, to pH 10, showed a rapid increase of average size with time, indicating almost immediate flocculation of the colloids.

Summarising, Figure 6 indicated that stability of the colloids was ensured at acidic to neutral pHs, but colloids were no longer stable at alkaline pHs. This pattern was also shown by the zeta potential, shown in Figure 7.

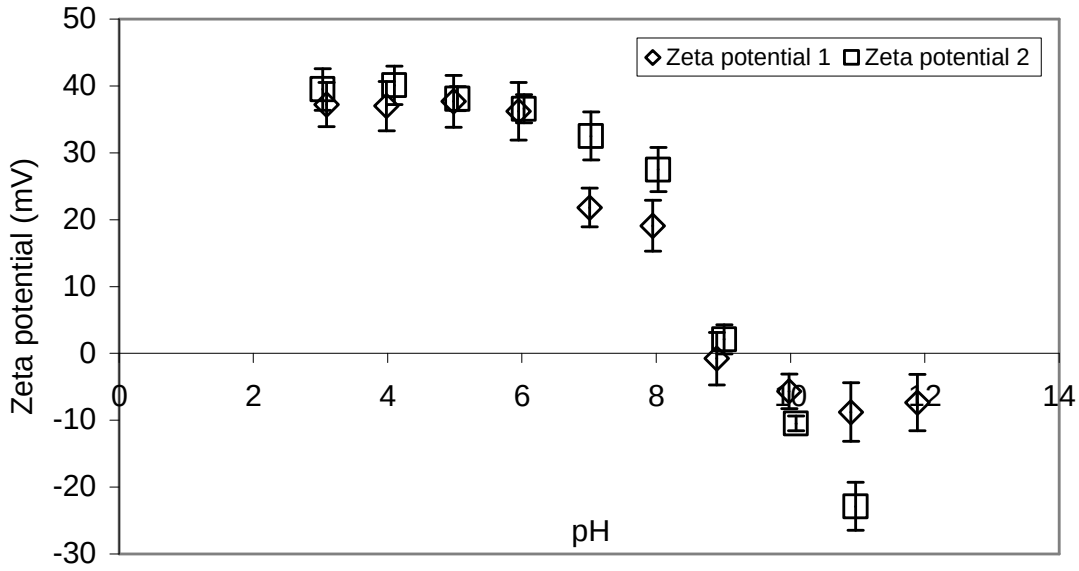

Figure 7. Zeta potential of boehmite colloids as a function of pH, for two samples of boehmite colloids.

Figure 7 shows the zeta potential of two samples of boehmite colloids across a wide range of pHs. The zeta potential was positive in the acidic and neutral range, becoming negative at pHs above approximately 8.5 (isoelectric point), in agreement with previous literature [86,87,88].

As the sorption experiments investigated were those where Cs, Ni and Eu were added to boehmite colloids at different concentrations, the measurement of the zeta potential of boehmite colloids in the presence of metals was carried out at pH 7 (Figure 8).

Figure 8 shows the effect of increasing metal concentration on the zeta potential of boehmite colloids at pH 7. The average zeta potential of boehmite colloids at the same pH is delimited by the shaded area in the graph. The zeta potential measured for the metal-colloid suspensions for most of the metal concentrations was within the limits of the boehmite colloids alone. Thus, the presence of metal ions in suspension did not result in a decrease of the stability of boehmite colloids.

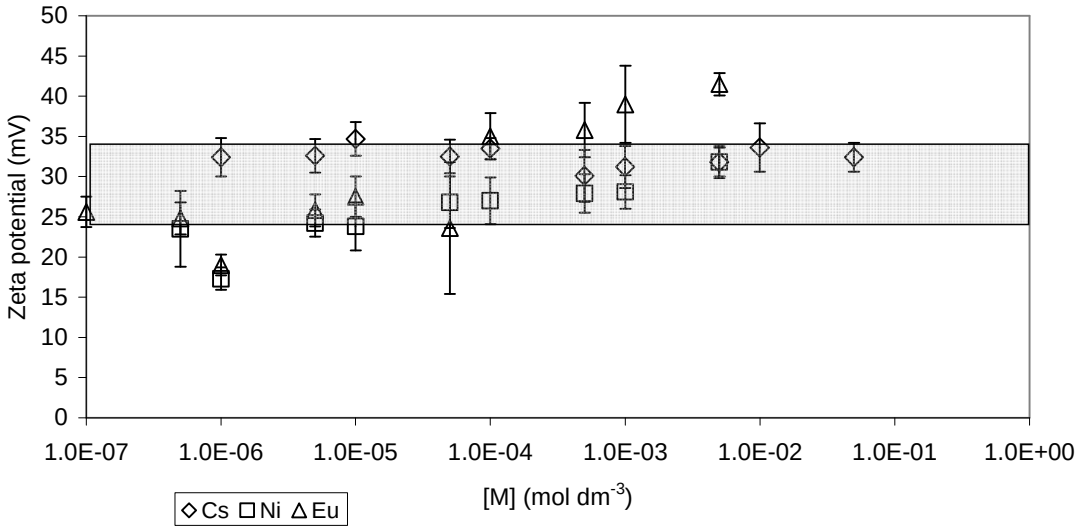

Figure 8. Zeta potential of boehmite colloids as a function of metal concentration (Cs, Ni and Eu) at pH 7.

2.3.1.2. Montmorillonite

Montmorillonite colloids were extracted from Montmorillonite K-10 by washing repeatedly with NaCl 0.05 mol dm^{-3}, followed by filtering and centrifuging. Approximately, 0.4 dm^3 of NaCl 0.05 mol dm^{-3} were used in order to extract colloids from the solid.

Two different batches of extracted montmorillonite colloids were characterised prior to their use in sorption experiments for characterisation tests. The results are shown in Table 4.

Table 4. Characterisation of montmorillonite colloids.

Batch number	Average Size (nm)	Kcounts per second	Zeta potential
1	426.8 ± 16.1	58.2 ± 0.7	-30.1 ± 2.6
2	440.0 ± 19.1	43.1 ± 0.5	-33.1 ± 0.5

Stability of montmorillonite colloids

The stability of colloids with pH was studied by measuring the average size and the zeta potential across the range of pH 3 to 12. The results are shown in Figure 9.

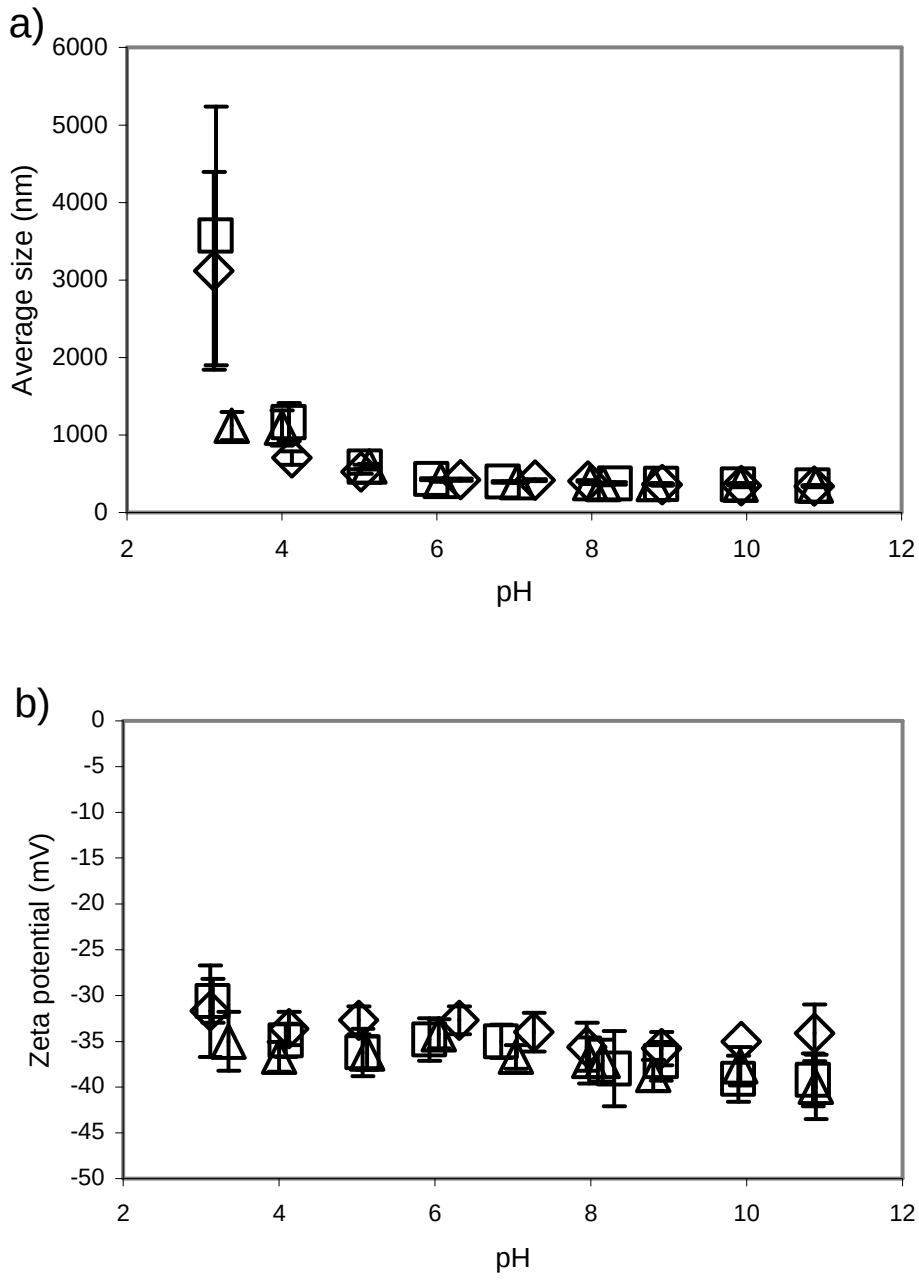

Figure 9. Average size (a) and zeta potential (b) of montmorillonite colloids as a function of pH.

The average size measured at low pH was noticeably higher than that measured in the neutral and alkaline range, as well as the standard deviation in each of the measurements. The results suggested that montmorillonite colloids were not stable at low pHs, gaining stability as the pH increased.

The zeta potential of montmorillonite colloids was negative in the whole range of pHs studied, in agreement with Kaya *et al.* [89].

The stability of montmorillonite colloids with ionic strength was studied by recording the values of average size, particle size and zeta potential at various ionic strengths, adjusted using NaCl. The results are shown in Figure 10.

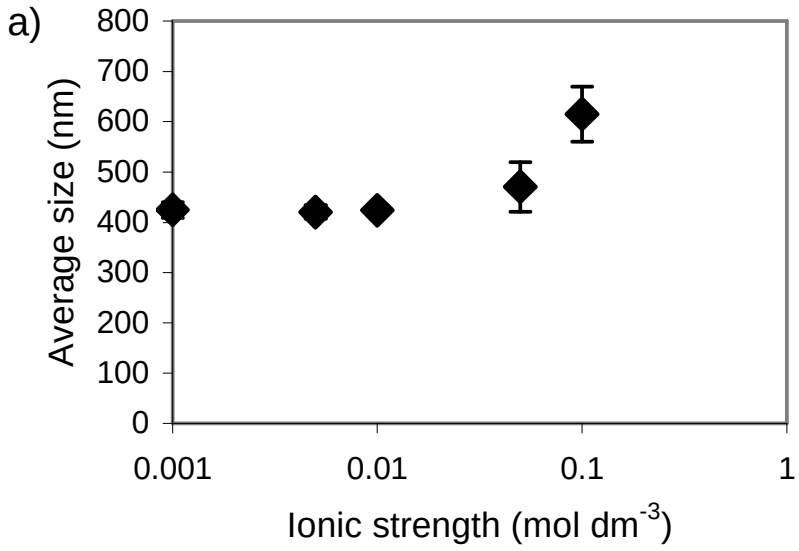

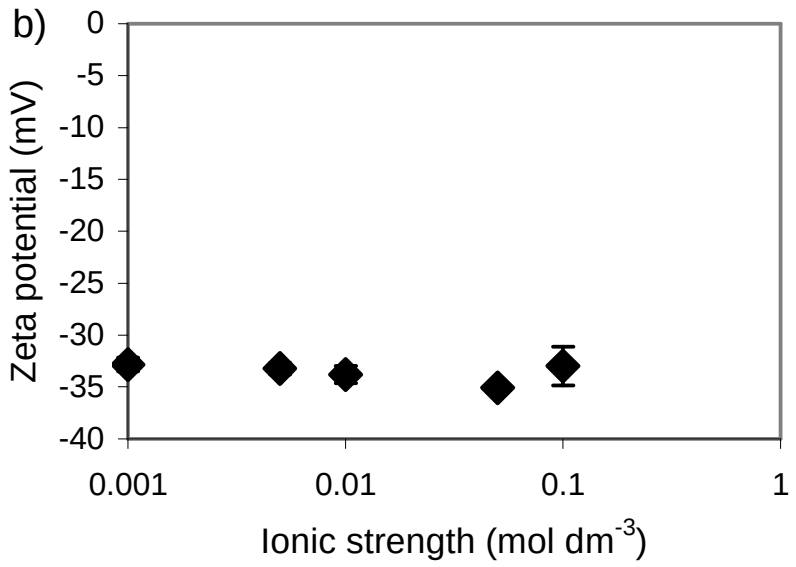

Figure 10. (a) Average size and (b) zeta potential of montmorillonite colloids as a function of ionic strength.

Figure 10 shows the effect of increasing ionic strength on the average size and zeta potential of montmorillonite colloids. The average size increased slightly with increasing values of ionic strength, suggesting a trend to destabilisation as the ionic strength increased. The zeta potential values, however, remained constant as the ionic strength increased.

The stability experiments carried out indicated that both boehmite and montmorillonite colloids were stable at pH 7 and ionic strength 0.05 mol dm^{-3}. Zeta potential and DLS measurements suggested that an increase in pH would lead to flocculation of boehmite colloids, whereas stability of montmorillonite colloids would be ensured at neutral to alkaline pHs. These differences are due to the overall positive charge of boehmite and negative charge of montmorillonite. Applied to natural media, where pH can be considered near-neutral, the results suggest that at low ionic strength values of groundwater flows, both colloids studied would be stable. However, in the near-field of a repository, for example, where the pH is expected to be high due to dissolution of hydroxides [2], the results suggest that only montmorillonite colloids would be mobile, due to coagulation of boehmite colloids.

2.3.2. Sorption and desorption experiments

This section shows the results for the sorption and desorption of metals on both boehmite and montmorillonite, in both the colloidal and solid forms of the minerals. The section starts with the sorption results on boehmite, followed by the results on sorption on montmorillonite. Thereafter, desorption results are shown, first for boehmite, then for montmorillonite. Modelling of the sorption of metals on minerals is summarised along with the sorption isotherms.

The results of the modelling are shown in the form of graphs and tables listing the characteristic parameters of each isotherm. For ease of interpretation desorption results are shown in the form of desorption percentages, as the desorption isotherms were linear for the range of concentrations studied.

2.3.2.1. Sorption experiments

2.3.2.1.1. Speciation

Results for JChess speciation modelling predicted the predominant ionic species for the metals and also the ionic species on the surface of the colloids.

Table 5 shows the concentrations of the possible ionic species present in the systems under evaluation. The JChess speciation programme predicted that the cationic form of Cs, Cs^+, would be predominant over the aqueous, non-dissociated form, CsCl. A number of hydroxide species were predicted for Ni in the system. However, the concentrations of these forms of Ni complexes were orders of magnitude lower than the free metal concentration. Even more numerous hydroxide and chloride forms were predicted for Eu. In the case of Eu, it was not the free metal the one to dominate in solution, but instead a dimeric hydroxide.

Species for boehmite were also predicted, the most dominant species being AlO_2^-. The neutral and cationic form of boehmite were predicted to be present in a lower concentration, by one and two orders of magnitude, respectively (Table 5).

When applied to the binary systems with montmorillonite colloids, the speciation programme yielded similar predictions (Table 7).

Once again the speciation programme predicted higher concentrations of free cationic Cs and Ni above the chloride or hydroxide species. In the case of Eu, the tetravalent dimer was the predominant species in solution. The concentrations of Ni and Eu neutral species (hydroxides or chlorides) were in concentrations below 10^{-10} mol dm^{-3} and thus could be considered negligible. From these results, one can assume that the metal was dissolved in solution and was available for sorption onto the colloidal surfaces.

Data produced from JChess speciation provided a large number of ionic species resulting from the dissociation of montmorillonite. The concentration of Na^{+} ions present in solution, facilitated by montmorillonite was orders of magnitude higher than any other species in solution. Moreover, montmorillonite also produced Mg^{2+} ions, which were present in concentrations higher than those of free Ni^{2+} or Eu^{3+}. Figure 3, in section 2.2.1.1.2, shows the structure of montmorillonite, where the exchangeable cations are Na^{+}, Mg^{2+} and Ca^{2+}. Data provided by the speciation programme showed large concentrations of Na^{+} and Mg^{2+} ions, which can be assumed to undergo ion exchange with the metals introduced into suspension (Cs^{+}, Ni^{2+} or Eu^{3+}), playing a key role o
in the sorption of the latter onto the colloidal surfaces.

Speciation prediction for boehmite showed that $AlOO^{-}$ was the dominant anionic species present. Due to the more complex nature of montmorillonite, the speciation programme provided many more anionic species, some related to the silicates and some from the aluminates.

Both neutral and anionic species would be available for metal sorption. Surface complexation could take place at these sites by deprotonation or complexation with the amphoteric groups [90].

Table 5. Metal speciation for system constituted by 10^{-3} mol dm^{-3} MCl_x and 30 mg boehmite colloids at pH 7 and ionic strength 0.05 mol dm^{-3}.

Ionic Species	[Cs] (mol dm^{-3})	Ionic Species	[Ni] (mol dm^{-3})	Ionic Species	[Eu] (mol dm^{-3})
Cs^+	9.75×10^{-4}	Ni^{2+}	9.98×10^{-4}	$Eu_2(OH)_2^{4+}$	4.96×10^{-4}
CsCl	2.47×10^{-5}	$NiCl^+$	2.38×10^{-6}	Eu^{3+}	7.78×10^{-6}
		$Ni(OH)_2$	4.56×10^{-10}	$EuOH^{2+}$	3.45×10^{-7}
		Ni_2OH^{3+}	2.49×10^{-10}	$EuCl^{2+}$	2.50×10^{-7}
		$Ni_4(OH)_4^{4+}$	2.21×10^{-12}	$Eu(OH)_2^+$	2.08×10^{-7}
		$Ni(OH)_3^-$	5.64×10^{-14}	EuO^+	6.95×10^{-9}
	[Al] (mol dm^{-3})			$EuCl_2^+$	2.64×10^{-9}
AlO_2^-	2.26×10^{-9}			$Eu(OH)_3$	9.22×10^{-10}
$HAlO_2$	5.22×10^{-10}			EuO_2H	4.71×10^{-10}
$Al(OH)_2^+$	4.39×10^{-11}			$EuCl_3$	3.56×10^{-11}
$NaAlO_2$	1.39×10^{-11}			$EuCl_4^-$	7.22×10^{-13}
$AlOH^{2+}$	3.46×10^{-12}			EuO_2^-	4.70×10^{-13}
Al^{3+}	8.46×10^{-12}			$Eu(OH)_4^-$	3.83×10^{-15}
$Al_2(OH)_2^{4+}$	1.00×10^{-20}				

Table 6. Speciation for montmorillonite in the presence of 10^{-3} MCl_x, 0.05 mol dm^{-3} NaCl and pH 7. Concentrations in mol dm^{-3}.

Ionic species	Concentration (mol dm^{-3})	Ionic species	Concentration (mol dm^{-3})
SiO_2	9.79×10^{-5}	$NaAlO_2$	1.34×10^{-9}
$NaHSiO_3$	1.95×10^{-5}	$Al(OH)_2^+$	4.90×10^{-11}
$HSiO_3^-$	1.49×10^{-7}	$AlOH^{2+}$	5.37×10^{-12}
AlO_2^-	2.52×10^{-9}	$H_2SiO_4^{2-}$	3.69×10^{-13}

Table 7. Metal speciation for system constituted by 10^{-3} mol dm^{-3} MCl_x and 30 mg montmorillonite colloids at pH 7 and ionic strength 0.05 mol dm^{-3}.

Ionic Species	[Cs] (mol dm^{-3})	Ionic Species	[Ni] (mol dm^{-3})	Ionic Species	[Eu] (mol dm^{-3})
Cs^+	9.87×10^{-4}	Ni^{2+}	4.98×10^{-5}	$Eu_2(OH)_2^{4+}$	2.17×10^{-4}
CsCl	1.35×10^{-5}	$NiCl^+$	5.18×10^{-8}	Eu^{3+}	5.70×10^{-6}
		$Ni(OH)_2$	1.48×10^{-11}	$EuOH^{2+}$	1.51×10^{-7}
		Ni_2OH^{3+}	6.88×10^{-13}	$Eu(OH)_2^+$	6.65×10^{-8}
		$Ni(OH)_3^-$	2.04×10^{-15}	$EuCl^{2+}$	6.58×10^{-8}
		$Ni_4(OH)_4^{4+}$	1.37×10^{-17}	EuO^+	2.22×10^{-9}
				$EuCl_2^+$	3.09×10^{-10}
				$Eu(OH)_3$	2.65×10^{-10}
				EuO_2H	1.35×10^{-11}
				$EuCl_3$	2.27×10^{-12}
				EuO_2^-	1.50×10^{-13}
				$EuCl_4^-$	3.08×10^{-14}
				$Eu(OH)_4^-$	1.22×10^{-15}

2.3.2.1.2. Control experiments

Two control experiments constituted the study of the sorption of Ni onto solid montmorillonite when the pH was buffered and when it was allowed to drift, and when the supernatant resulting from separating the colloidal phase from solution after the sorption process was filtered through 0.45 or 0.22 μm pore filters.

By measuring the pH of the samples after the equilibration period, a drift in the pH towards lower pHs was observed. For example, the pH of the samples for the sorption of Cs onto boehmite colloids drifted from 6.96 ± 0.14 to 5.48 ± 0.02. In another batch of Cs sorption onto solid montmorillonite, the pH drifted from 6.93 ± 0.08 to 3.81 ± 0.05. The pH drift was also observed for Ni sorption onto solid montmorillonite, where a decrease in 1.30 ± 0.47 units could be observed. From these results, the pH of the samples used to investigate the sorption of metals onto boehmite and montmorillonite was buffered using MES.

After the separation of the colloidal phase from solution by centrifugation, filtering of the sample solutions were carried out with syringe filters. The two pore sizes tested were 0.45 and 0.22 μm. The differences in the sorption isotherms are shown in Figure 11. The sorption isotherms were almost identical, suggesting that colloids above 0.22 μm were not present in solution after centrifuging.

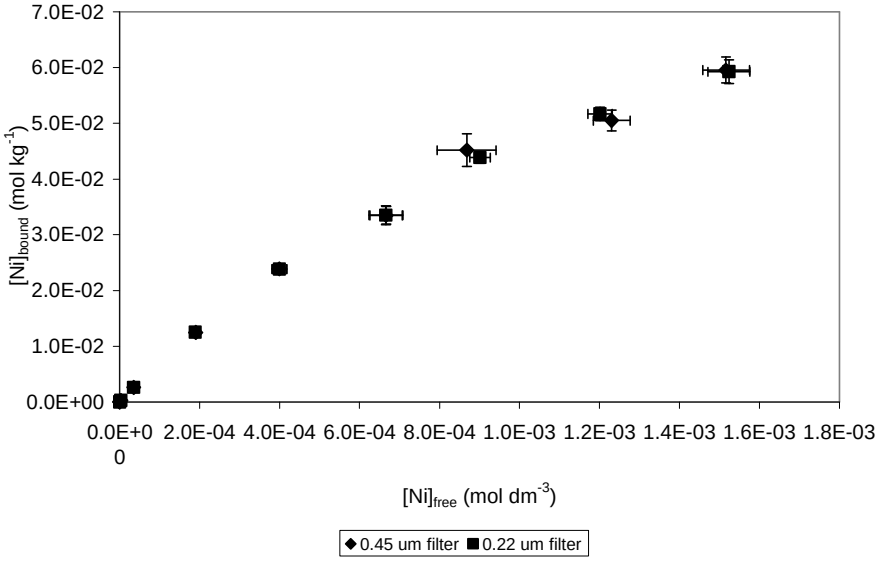

Figure 11. Ni sorption onto solid montmorillonite at pH 7 and ionic strength 0.05 mol dm^{-3}. Filtration through 0.45 and 0.22 μm filters.

2.3.2.1.3. Sorption of metals onto boehmite colloids

The sorption of Cs, Ni and Eu onto boehmite colloids was studied at different boehmite concentrations. Figure 12 shows the sorption of the three metals onto a similar concentration of boehmite, approximately 30 mg in 10 cm^3. The masses of boehmite colloid measured gravimetrically for each set of experiments are shown in Table 8.

Table 8. Mass of boehmite colloids in 10 cm^3 measured gravimetrically.

Metal	Cs	Ni	Eu
Mass boehmite colloids (mg)	29	33.5	28

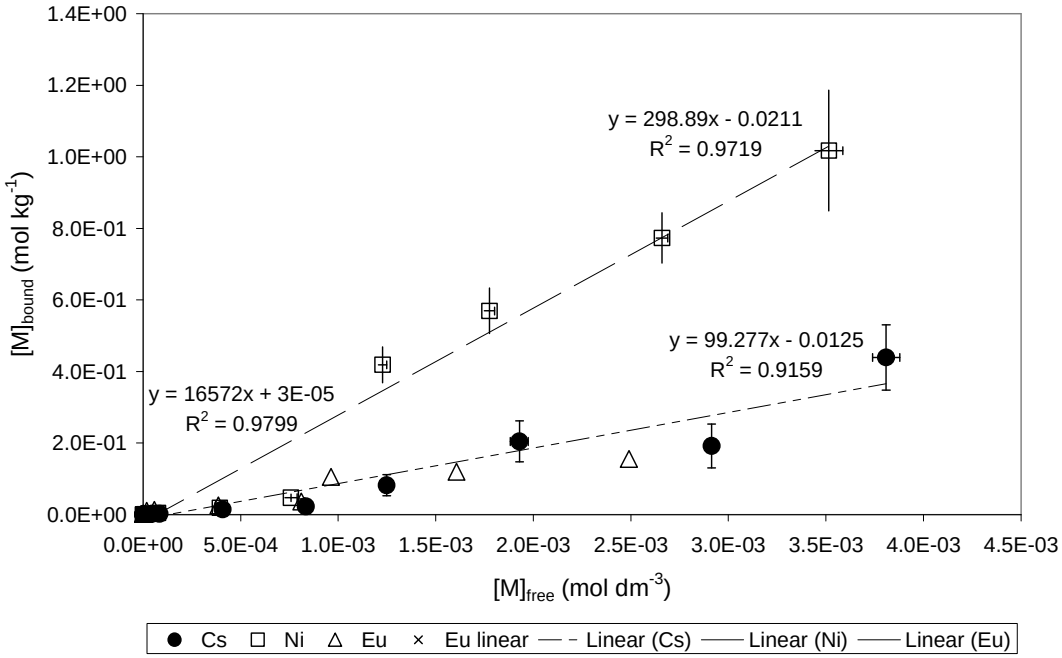

Figure 12. Sorption isotherm for the sorption of Cs, Ni and Eu onto boehmite colloids (30 mg) at pH 7 and ionic strength 0.05 mol dm^{-3}.

Sorption of Cs (black circles) and Ni (white squares) was found to be linear in the whole range of concentrations studied, with R^2 values for the linear fit above 0.9. However, Eu (triangles) sorption on colloidal boehmite exhibited a non-linear behaviour from low values of Eu in solution. For this reason, the sorption of Eu (in Figure 12) is presented as two series, one in which the linear region allowed the determination of the distribution ratio; and another in which the whole isotherm is shown. Note that these two series overlap each other; consequently, the "Eu linear" series can not be appreciated.

Due to the early saturation of the surface by Eu^{3+} ions, the calculation of a distribution coefficient (R_d) in a linear range was confined to the first three data points. The following figure shows the R_d values calculated for Eu, reflecting the non-linear sorption to boehmite colloids.

Figure 13 shows the distribution ratio values calculated for Eu sorption on colloidal boehmite. A clear trend can be seen in which the R_d values decrease as the initial metal concentration increased. The R_d is the ratio of bound to dissolved metal; the results suggested that the concentration of dissolved metal increased faster than the

bound metal as the initial concentration in solution increased. The results indicated that at low Eu concentrations, most of the Eu sorbed on the surface, but as the Eu concentration increased, Eu ions saturated the surface, causing more Eu to remain in solution and hence decreasing the ratio of bound to dissolved Eu. These results are also reflected in the percentages of sorption, which also decreased as the concentration of Eu increased (Figure 13).

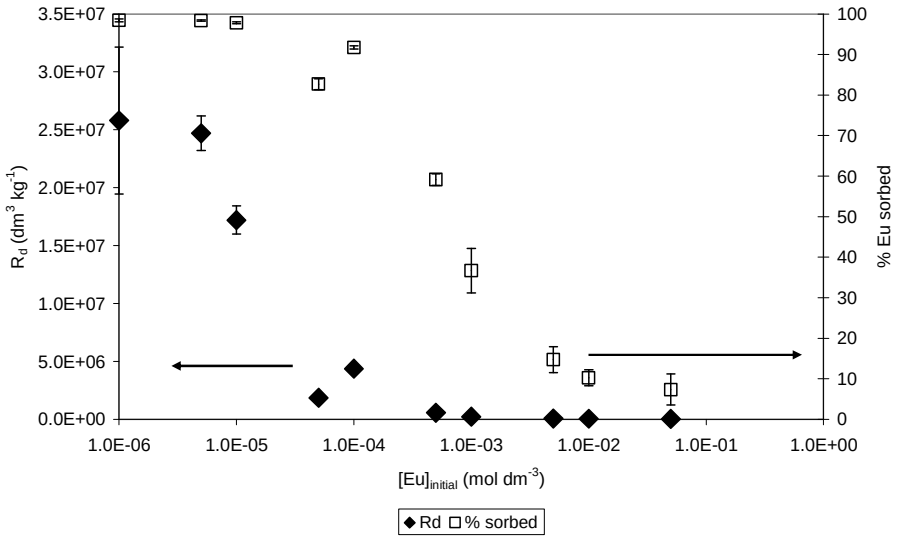

Figure 13. Distribution ratios and percentages of sorbed Eu on colloidal boehmite at pH 7 and ionic strength 0.05 mol dm^{-3}.

The slope of the linear fit corresponds to the R_d value of the sorption of the metal onto the colloid. It is clear from the results that the R_d values, and hence sorption, increased as the valency of the metal increased. The R_d values for Cs, Ni and Eu were measured as 99.3 ± 9.1, 298.9 ± 15.3 and 16572 dm^3 kg^{-1}, respectively. From these values, sorption of metals onto boehmite colloids increased in the order Cs < Ni < Eu. The trend agrees with general observation for ion exchange equilibria of increasing affinity with increasing ionic charge [91].

Modelling

The results were modelled using Langmuir, Freundlich and D-R equations. As observed in Figure 14, the Langmuir model did not fit the experimental results, whereas the Freundlich and D-R models were able to fit the data. The most relevant parameters from modelling is shown in Table 9.

a) Langmuir fit for Cs sorption on boehmite colloids

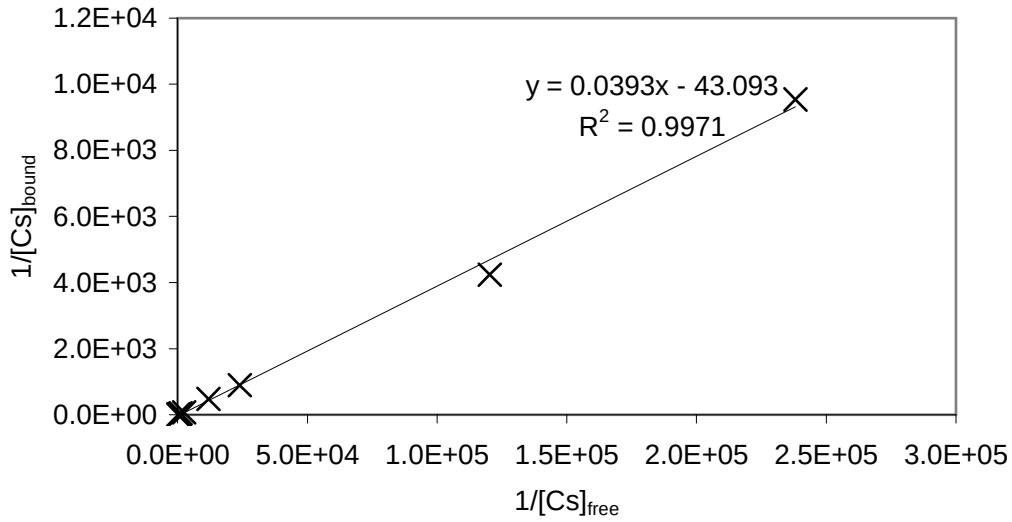

b) Langmuir fit for Ni sorption on boehmite colloids

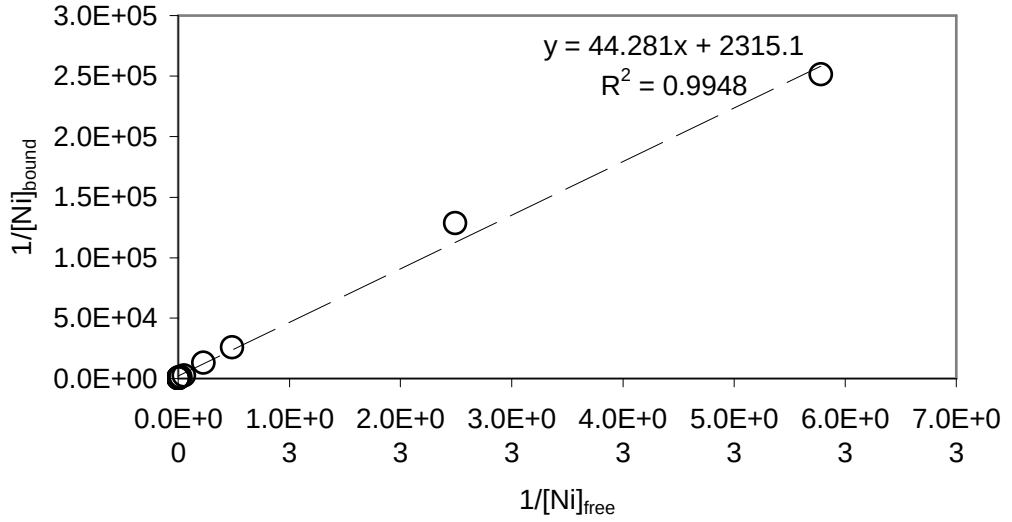

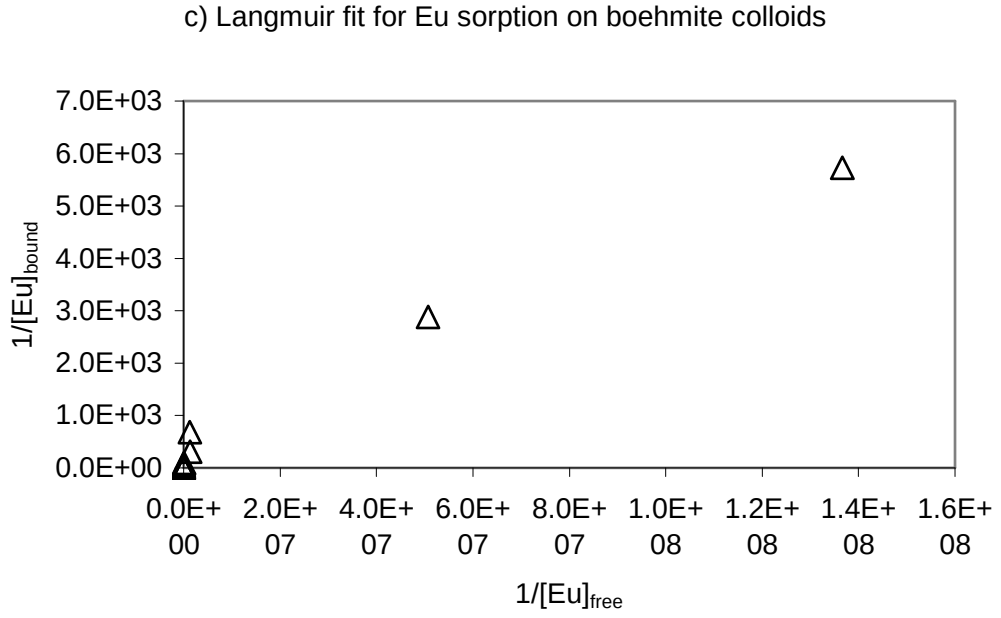

Figure 14. Langmuir fits for (a) Cs, (b) Ni and (c) Eu sorption on boehmite colloids (approximately 30 mg) at pH 7 and ionic strength 0.05 mol dm^{-3}.

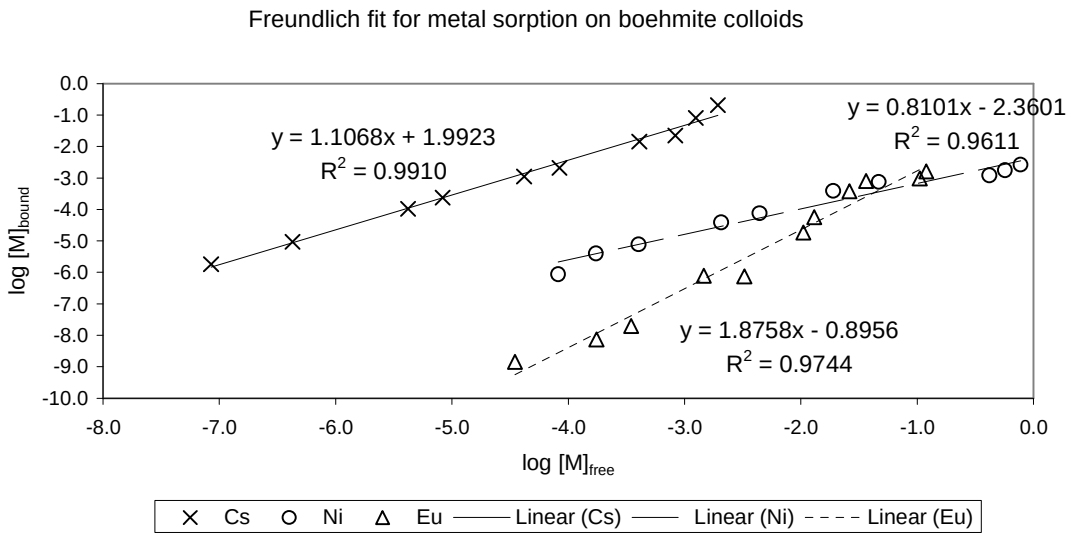

Figure 15. Freundlich fit for metal sorption on boehmite colloids (approximately 30 mg) at pH 7 and ionic strength 0.05 mol dm^{-3}.

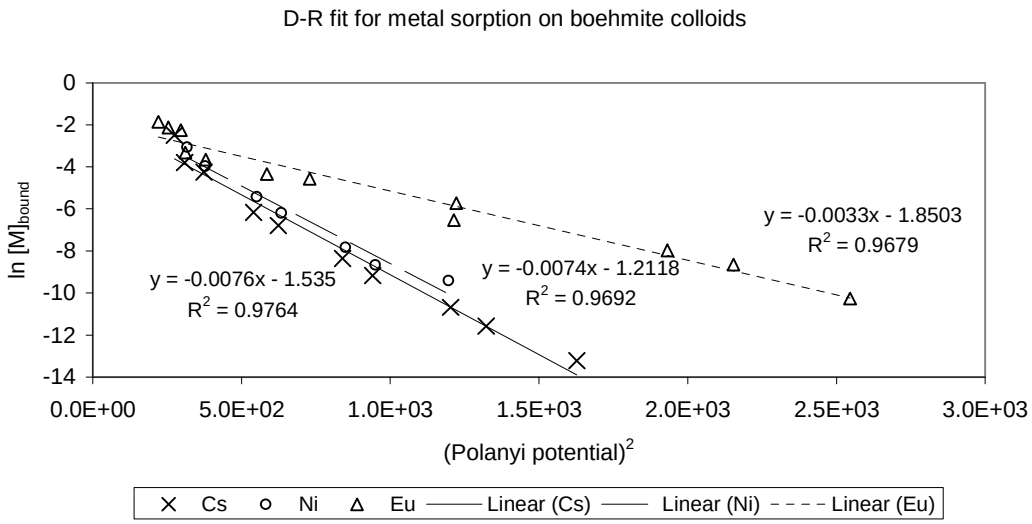

Figure 16. D-R fit for metal sorption on boehmite colloids (approximately 30 mg) at pH 7 and ionic strength 0.05 mol dm^{-3}.

Table 9. Modelling parameters for metal sorption onto boehmite colloids.

	Langmuir		Freundlich		D-R		
	R^2	Q_{max} mol kg^{-1}	R^2	n	R^2	Q_{max} mol kg^{-1}	E kJ mol^{-1}
Cs	0.9971	< 0	0.9910	1.11 ± 0.04	0.9764	0.215	8.11
Ni	0.9350	NA	0.9611	0.81 ± 0.06	0.9692	0.298	8.22
Eu		NA	0.9769	1.87 ± 0.10	0.9888	0.070	13.02

NA = not applicable

Table 9 shows the significant parameters obtained from modelling the sorption of metals onto boehmite colloids. None of the three metals studied was modelled satisfactorily by the Langmuir model, shown by the non-linear behaviour of the plotted data. Both the Freundlich and the D-R models fitted the experimental data, with the following remarks:

From the results Cs showed high values of the Freundlich constant, *n*, near unity, in agreement with the linear sorption isotherm. Both Cs and Ni exhibited similar values of free energy of sorption; those values, between 8 and 11 kJ mol^{-1} suggested an ion exchange mechanism [95].

The saturation values predicted by the D-R model are below the observed values in the sorption isotherm (Figure 12). Eu saturated the surface of boehmite at early stages of sorption, with a maximum uptake of approximately 0.1 mol kg^{-1}. The predicted saturation values for Ni and Cs were below the experimental value, as the predicted values fell in the linear range of sorption.

2.3.2.1.1.1. Influence of colloid concentration

The sorption behaviours of Cs, Ni and Eu were studied by using different amounts of boehmite present in suspension, i.e. changing the solid to liquid ratios. The following table shows the mass of boehmite colloids present in 10 cm^3 of suspension for each metal, measured gravimetrically prior to the sorption experiment.

Table 10. Mass of boehmite colloids in 10 cm^3 of suspension measured gravimetrically.

Metal	Mass of boehmite colloid (mg)	
Cs	14	29
Ni	33.5	54
Eu	14	28

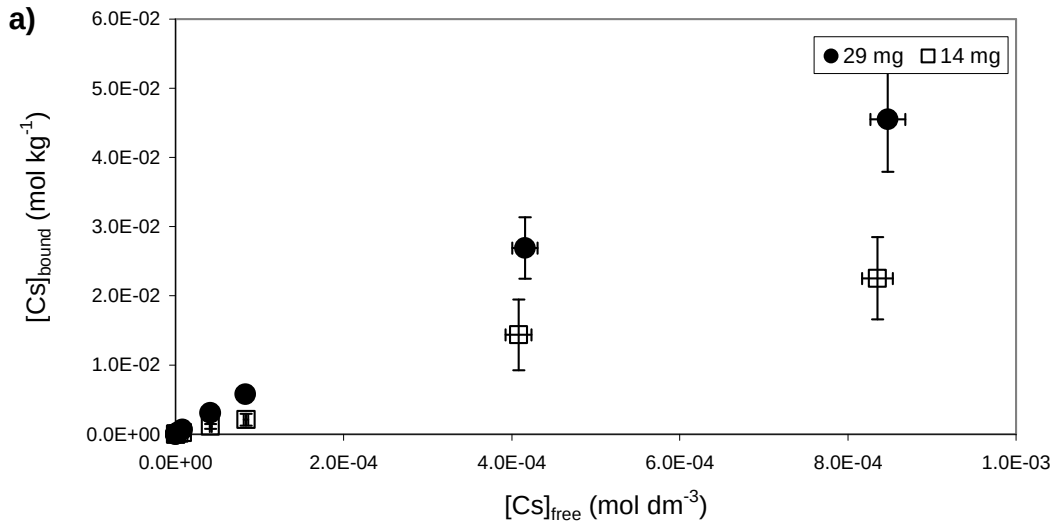

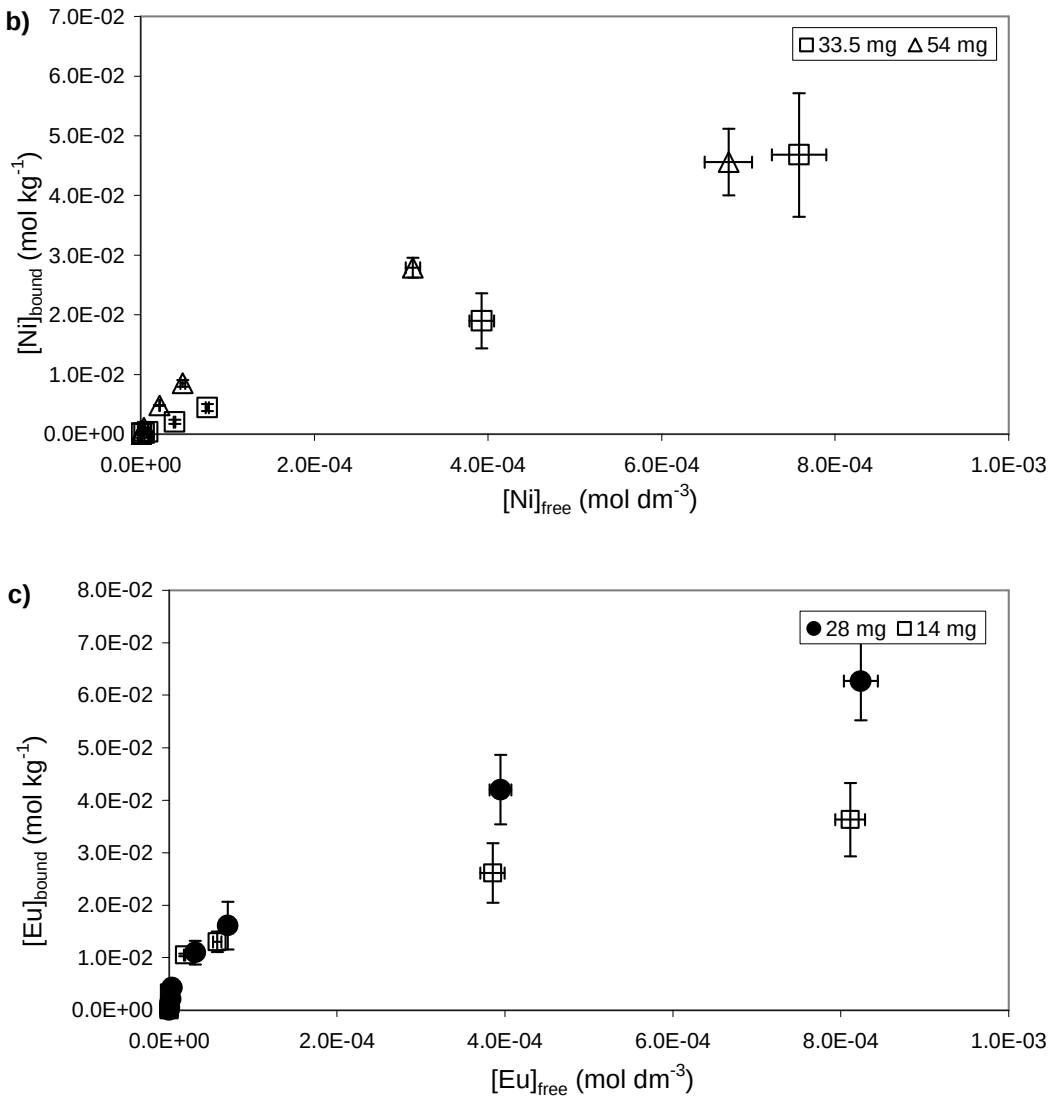

Figure 17. Effect of the solid to liquid ratio on the sorption of (a) Cs, (b) Ni and (c) Eu onto boehmite colloids at pH 7 and ionic strength 0.05 mol dm^{-3}.

In the case of Cs and Eu, Figure 17(a) and (c), the sorption of metal onto the colloids increased as the amount of boehmite increased, as indicated by the R_d values, summarised in Table 11. In the case of Ni, Figure 17(b), the sorption of metal onto colloids showed no significant difference.

As the amount of boehmite colloids present in suspension increased, so did the R_d values. Logically, the more surface available in suspension, the higher the metal sorption. However, this did not apply to Ni, which exhibited lower R_d values at higher boehmite concentrations. Zhang *et al.* [92] suggested particle aggregation could

lead to these results, although colloidal stability was observed throughout the experiment.

Table 11. R_d values for metal sorption onto varying amounts of boehmite colloids.

	R_d (dm^3 kg^{-1})		
mg boehmite	14	30	54
Cs	76.7 ± 1.7	99.3 ± 9.1	
Ni		298.9 ± 15.3	220.9 ± 6.2
Eu	1135.1 ± 54.6	13851.0	

2.3.2.1.1.2. Influence of background electrolyte

Parallel sorption experiments were carried out to study the influence of the background electrolyte on the sorption of Cs onto boehmite colloids. The pH and ionic strength conditions were the same as those described in the experimental section, only the ionic strength varied and this was adjusted using KCl or NaCl. The amount of colloids present in 10 cm^3 was approximately 33.5 mg. For ease of interpretation of results both the sorption and desorption isotherms are shown (Figure 18).

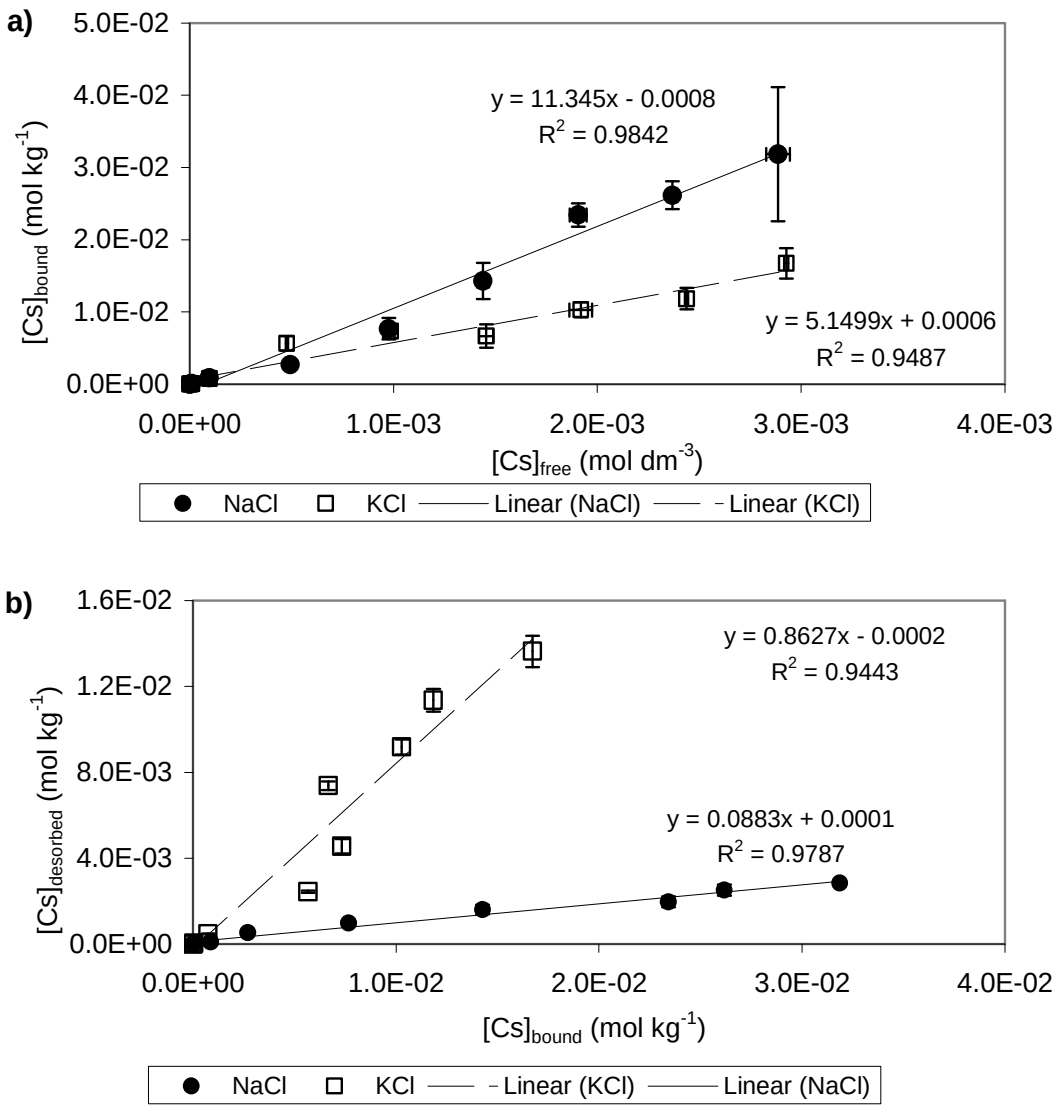

Figure 18. Effect of the background electrolyte on the (a) sorption and (b) desorption of Cs onto boehmite colloids at pH 7 and ionic strength 0.05 mol dm^{-3}.

The sorption isotherm in Figure 18 (a) shows a higher R_d value for the sorption of Cs in the presence of NaCl (11.35 ± 0.51 dm^3 kg^{-1}) than in the presence of KCl (5.15 ± 0.42 dm^3 kg^{-1}), indicating that higher sorption of Cs onto boehmite colloids took place when NaCl was the background electrolyte. Furthermore, the desorption isotherms in Figure 18 (b) showed a significant desorption from boehmite colloids in the presence of KCl (86.27 ± 7.41%), as opposed to a low desorption in the presence of NaCl (8.83 ± 0.46%).

The R_d value obtained for the sorption in the presence of NaCl from Figure 18 (a) was lower than that observed in Figure 12, due to the use of a different batch of

colloids for these sorption experiments. The latter, which were in the form of powder rather than suspended, were used exclusively to study the sorption and desorption of different background electrolytes. Although reproducibility could not be proven with this batch, the aim was to analyse the influence of background electrolyte.

The presence of the background electrolyte introduced a competition of sorption between the Cs^+ ions and the electrolyte ions, the latter being present in higher concentrations. The results indicated that sorption of Cs was higher and desorption was lower in the presence of NaCl, suggesting that NaCl hindered less the sorption of Cs to the colloids. Moreover, the results suggest that the competition introduced by K^+ ions was stronger than that introduced by Na^+ ions, which is attributable to the greater similarity in both ionic size and electronegativity of K^+ ions with Cs^+ ions [93]. These results suggested that the background electrolyte strongly influences the interaction of metals with boehmite.

2.3.2.1.4. Sorption on solid boehmite

Sorption of the three metals studied previously on boehmite colloids was also assessed for the solid phase of boehmite, where the size was substantially greater than for the colloid phase. Section 2.3.3. will show the difference in surface area between the colloidal and the solid phases, which was higher for the colloids. The solid to liquid ratio was kept similar to that used in the adsorption to colloidal boehmite (30 mg to 10 cm^3 suspension) experiments.

Figure 19 shows the sorption isotherms for the sorption of Cs, Ni and Eu onto solid boehmite. Two different series were used for the sorption of Eu, one in which the linear range of the isotherm is fitted to the linear regression, and another where the isotherm is shown for the whole range of concentrations studied.

In general, the sorption increased with the valency of the metal, i.e. the R_d values increased from 26.4 ± 0.3 $dm^3\ kg^{-1}$ for Cs, to 47.7 ± 1.09 $dm^3\ kg^{-1}$ for Ni and 448.4 ± 8.6 $dm^3\ kg^{-1}$ for Eu. Both Cs and Ni showed a linear sorption in the range of metal concentrations studied. On the contrary, the non-linear sorption of Eu indicated saturation of the solid surface.

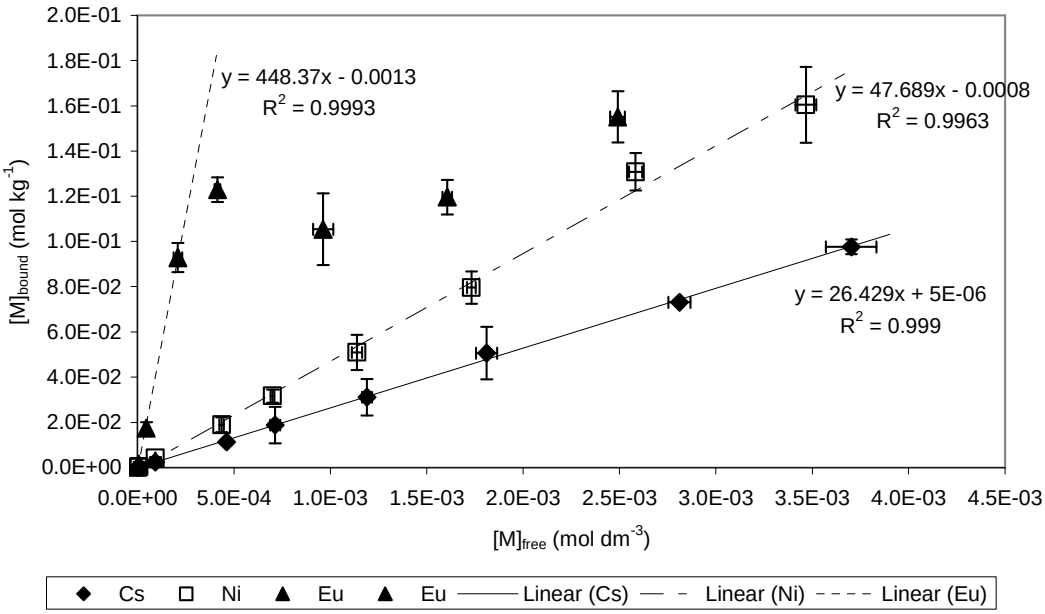

Figure 19. Sorption isotherm for Cs, Ni and Eu onto solid boehmite at pH 7 and ionic strength 0.05 mol dm^{-3}.

Solid vs colloid

All metals showed a greater R_d value for the colloidal phase than for the solid phase, consistent with a higher surface area of colloids; moreover, the difference was increased with the ionic charge of the metal. In this manner, the R_d for Cs increased by 4 times when the surface phase was colloidal. The increase for Ni and Eu was 6 and 30 fold, respectively (see Table 12 for summarised R_d values). These results suggest a direct relation between the R_d, the ionic charge and the surface phase. This relationship will be discussed in section 2.4.

Table 12. Distributio ratios for metal sorption on boehmite (colloidal and solid phase).

		solid to liquid ratio (mg : cm^3)	R_d (dm^3 kg^{-1})
Cs	Colloid	29 : 10	99.3 ± 9.1
	Solid	100 : 30	26.4 ± 0.3
Ni	Colloid	33.5 : 10	298.9 ± 15.3
	Solid	100 : 30	47.7 ± 1.09
Eu	Colloid	28 : 10	13851
	Solid	100 : 30	448.4 ± 8.6

The sorption behaviour of metals on solid boehmite was modelled (Figure 20) and compared to that on colloidal boehmite. Table 13 summarises the results, where, for ease of interpretation, the modelling parameters for both solid and colloid are shown together. Although the Langmuir model yielded good fits in terms of R^2 value, the interpretation of the model failed to explain the experimental observations. The units for Q_{max} are mol kg^{-1} and for the free energy of sorption kJ mol^{-1}.

a) Langmuir fit for metal sorption onto solid boehmite

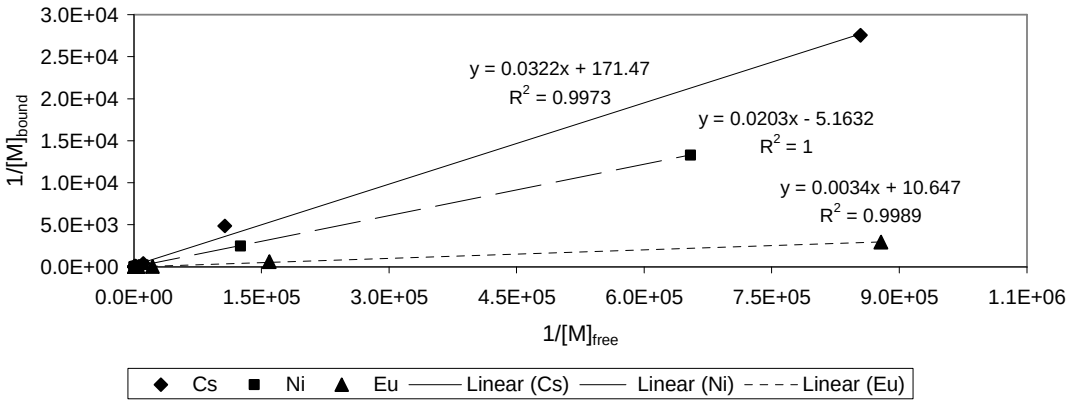

b) Freundlich fit for metal sorption onto solid boehmite

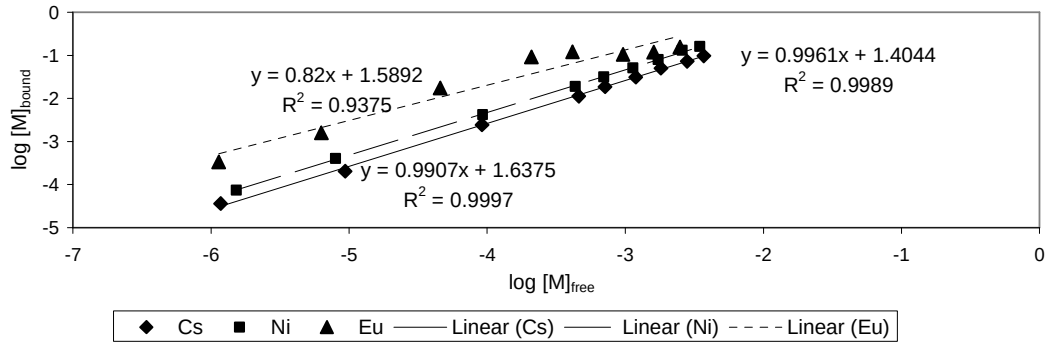

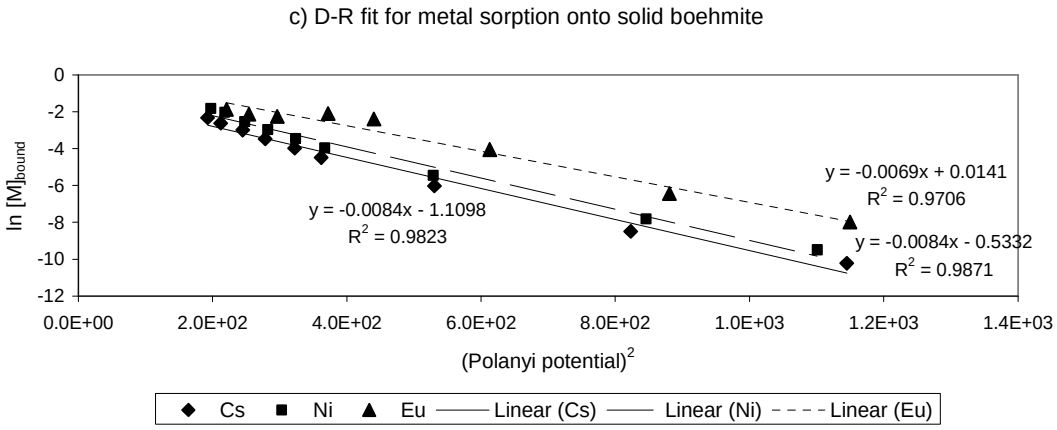

Figure 20. Modelling of metal sorption onto solid boehmite at pH 7 and ionic strength 0.05 mol dm^{-3}.

Table 13. Modelling parameters for metal sorption onto solid and colloidal boehmite.

		Langmuir		Freundlich		D-R		
		R^2	Q_{max}	R^2	n	R^2	Q_{max}	E
Cs	Colloid	0.9996	1.71×10^{-2}	0.9910	1.11 ± 0.04	0.9602	0.595	7.67
	Solid	0.9973	5.83×10^{-3}	0.9989	0.99 ± 0.01	0.9823	0.329	7.72
Ni	Colloid	0.9948	< 0	0.9611	0.81 ± 0.06	0.9692	0.298	8.22
	Solid	1	< 0	0.9997	0.99 ± 0.01	0.9871	0.587	7.70
Eu	Colloid	0.9781	curve	0.9769	1.87 ± 0.10	0.9608	0.145	12.31
	Solid	0.9989	9.39×10^{-2}	0.9375	0.82 ± 0.09	0.9706	1.014	8.51

Table 13 shows some of the modelling parameters for the sorption of metals onto solid and colloidal boehmite. The following conclusions can be made from the results:

- The values for Q_{max} predicted by the Langmuir model were lower than those observed experimentally in the sorption isotherm. The D-R model predicted Q_{max} values similar to those observed experimentally for Ni and Cs, but overpredicted the value for Eu.
- The Langmuir model failed to predict the sorption of Ni onto boehmite, both in the colloid and the solid phase.
- The Freundlich model predicted high values of *n* for Cs and Ni, consistent with the linear sorption observed in the isotherms. The values predicted for

Eu sorption on colloids were lower, as well consistent with the saturation of boehmite by the cations.

- Cs and Ni sorption onto boehmite, both colloids and solid, was best described by the Freundlich isotherm, as better values of R^2 were obtained.
-

2.3.2.1.5. Sorption onto montmorillonite colloids

The sorption of Cs, Ni and Eu onto montmorillonite colloids was studied. The sorption isotherm of the three metals is shown in Figure 21. Different batches of montmorillonite colloids were used to measure the sorption experiments. The mass of montmorillonite colloids in the vials, measured by gravimetric analysis, as well as the average size are shown in Table 14.

Table 14. Characteristic parameters of montmorillonite colloids used in sorption batch experiments.

Metal	Mass (mg)	Average size (nm)
Cs	60	583.6 ± 33.8
Ni	11	559.3 ± 156.5
Eu	16	775.7 ± 168.8

Table 14 shows a significant variability in the mass of colloids present in each set of adsorption experiments. This reflects the difficulty in preparing the montmorillonite colloids. The size of the colloids was in all cases above 500 nm and therefore still in the colloidal region.

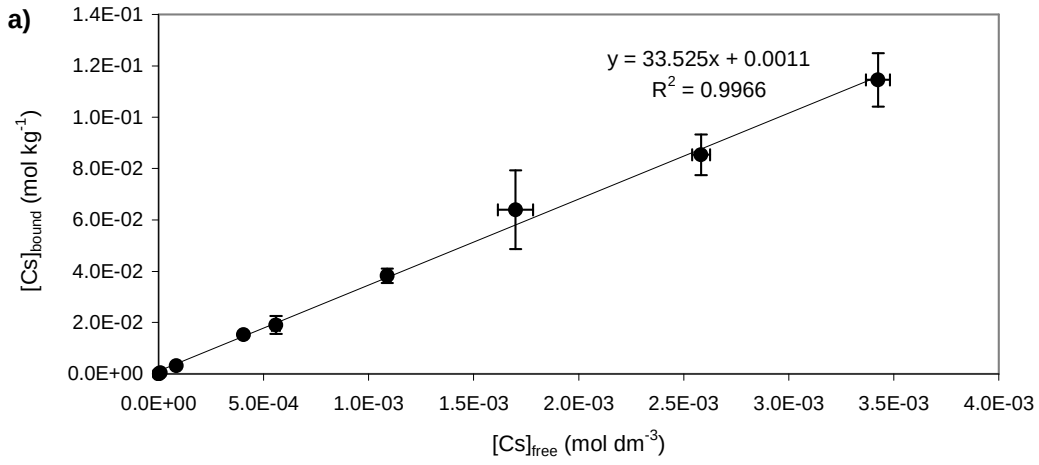

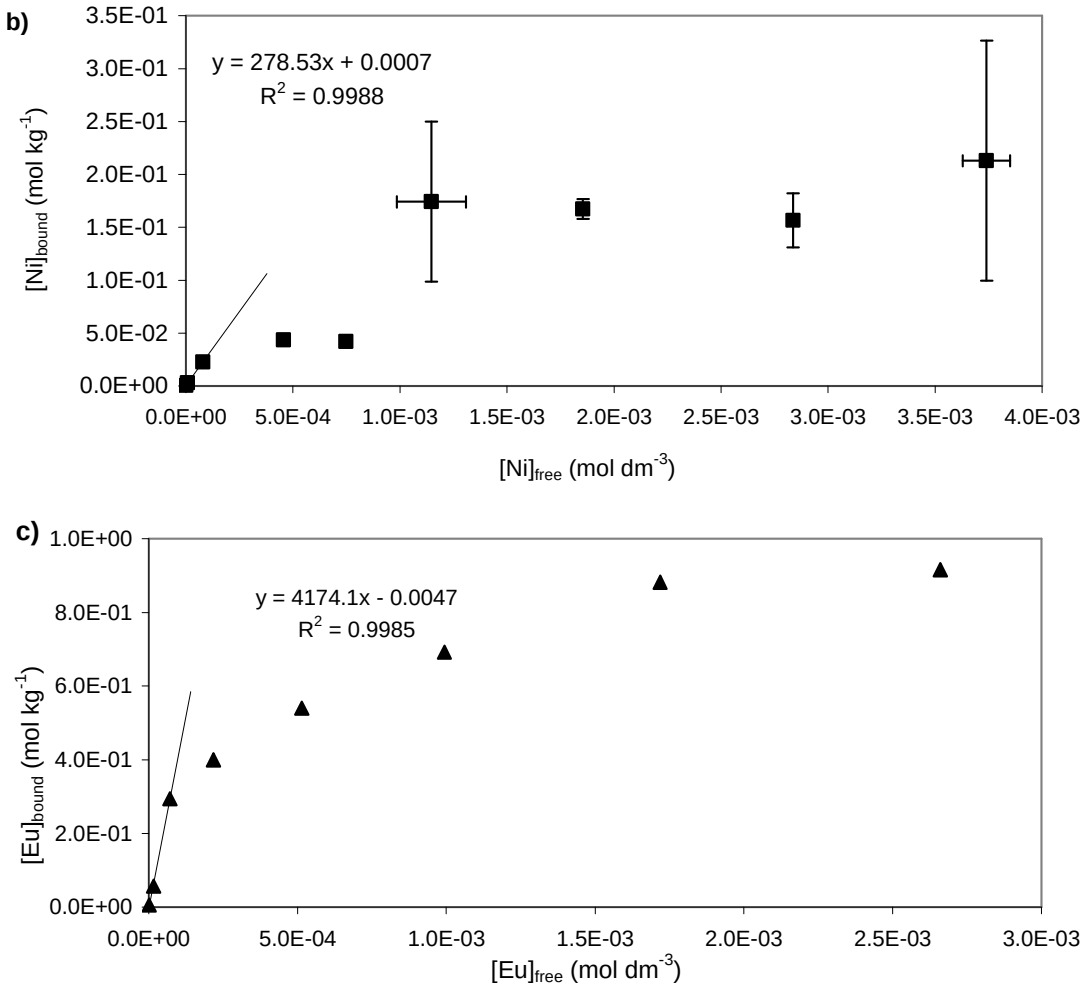

Figure 21. Sorption isotherms for (a) Cs, (b) Ni and (c) Eu sorption onto montmorillonite colloids at pH 7 and ionic strength 0.05 mol dm^{-3}.

Figure 21 shows linear sorption for Cs throughout the range of concentrations studied. The distribution ratio, R_d, could be determined from the slope, and was 33.5 ± 0.7 dm^3 kg^{-1}. Sorption of Ni increased linearly at low Ni concentrations but curved at higher Ni concentrations, indicating saturation of montmorillonite colloids. The slope of linear range of the isotherm represents the R_d value, which calculated for the desired range yielded 278.53 ± 9.51 dm^3 kg^{-1}. Eu sorption onto montmorillonite colloids increased sharply at low concentrations and curved reaching a plateau at the range of concentrations studied. This plateau indicated the sorption capacity of montmorillonite colloids, since the colloids reached saturation with Eu^{3+} ions. The linear range of the isotherm corresponds to the distribution ratio value, R_d, which yielded 4174.1 ± 164.4 dm^3 kg^{-1}.

In general, the sorption of metals onto montmorillonite colloids increased as the valence of the metal increased, consistent with the general trend observed in earlier sections where an increase in the ionic charge led to an increase in sorption. Furthermore, saturation of the colloids occurred at lower metal concentrations as the valence of the metal increased.

The sorption of metals onto montmorillonite colloids was modelled with the Langmuir, Freundlich and D-R models (Figure 22). The results are summarised in Table 15. The maximum amount of metal sorbed (Q_{max}) is in mol kg^{-1} and the free energy of sorption (E) in kJ mol^{-1}.

a) Langmuir fit for sorption on montmorillonite colloids

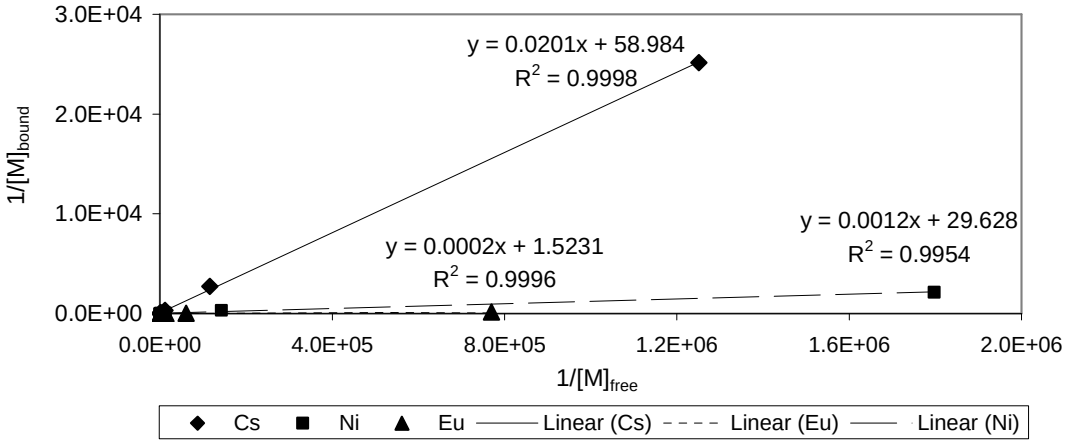

b) Freundlich fit for sorption on montmorillonite colloids

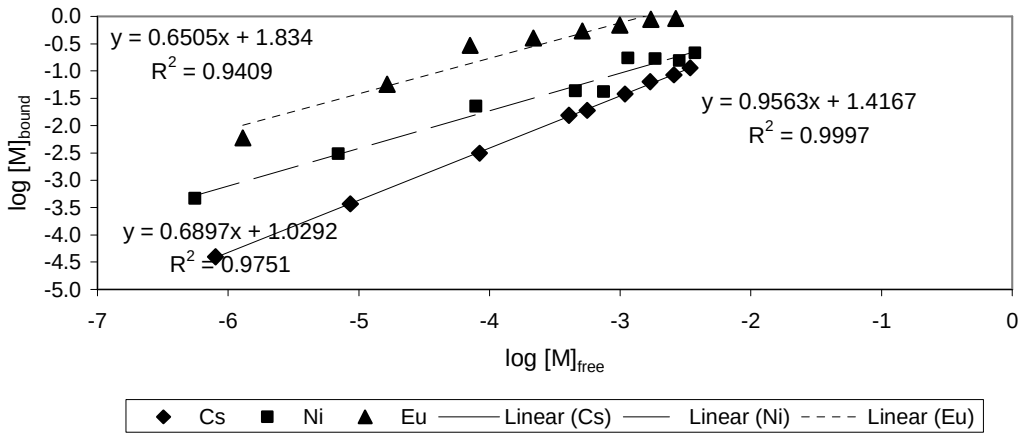

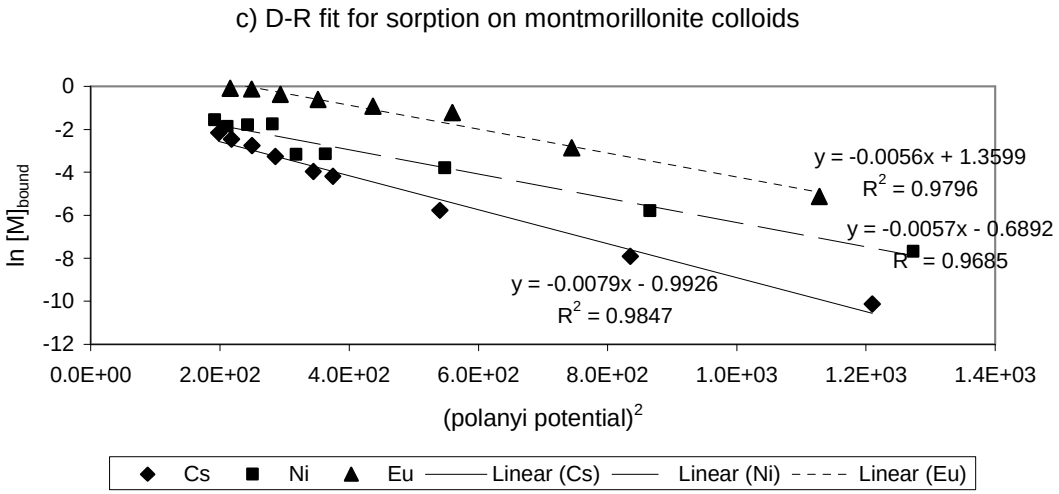

Figure 22. Modelling metal sorption on montmorillonite colloids at pH 7 and ionic strength 0.05 mol dm^{-3}.

Table 15. Modelling parameters for metal sorption on montmorillonite colloids.

	Langmuir		Freundlich		D-R		
	R^2	Q_{max} ($x10^{-2}$)	R^2	n	R^2	Q_{max} ($x10^{-2}$)	E
Cs	0.9998	1.695	0.9997	0.95 ± 0.01	0.9847	37.1	7.95
Ni	0.9954	3.375	0.9865	0.71 ± 0.03	0.9685	50.2	9.37
Eu	0.9996	65.656	0.9409	0.65 ± 0.07	0.9796	389.6	9.45

In general, the three models fit the experimental data yielding high values of R^2 (most of them above 0.98). The values of Q_{max} predicted by the Langmuir and by the D-R model observed in Table 15 were an order of magnitude lower for the Langmuir model. The sorption isotherm in Figure 21 indicated that the Q_{max} for Ni and Eu were approximately 20 and 80 x 10^{-2} mol kg^{-1}, respectively. The Langmuir model underpredicted these values for both Cs and Ni; however, the value predicted for Eu was close to that observed. Thus, the Langmuir model fitted better the experimental behaviour for Eu. The linearity shown in the sorption isotherm for Cs is reflected in the high value of the Freundlich constant, *n*.

Finally, the D-R model overpredicted the values of sorption capacity (not for Cs). The mean energy predicted for the three metals suggested an ion exchange mechanism of sorption.

2.3.2.1.6. Sorption on solid montmorillonite

The sorption of Cs, Ni and Eu to solid montmorillonite was investigated in the same way as that used for the colloidal phase. The mass of montmorillonite solid added to each vial was 50 mg for the Cs, 10 mg for the Ni batches and 16 mg for the Eu batch.

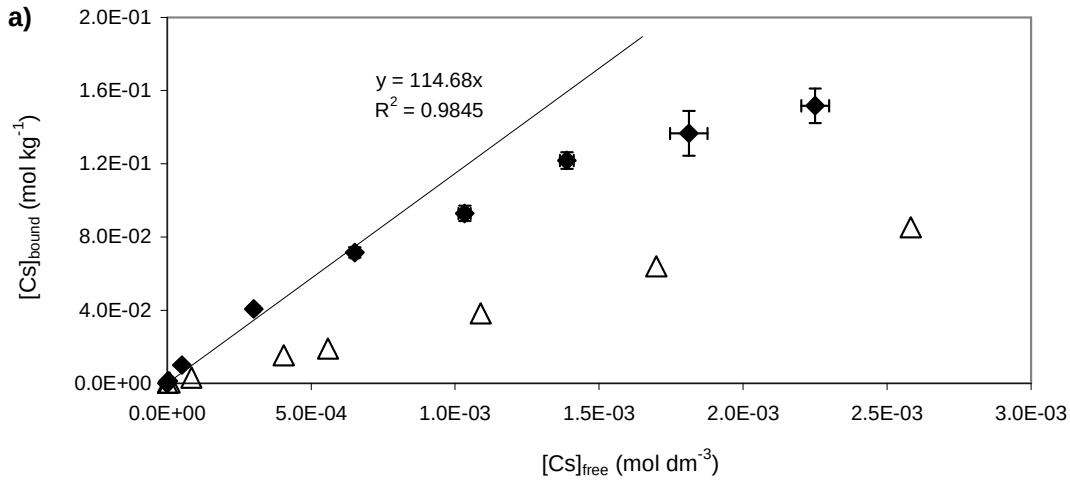

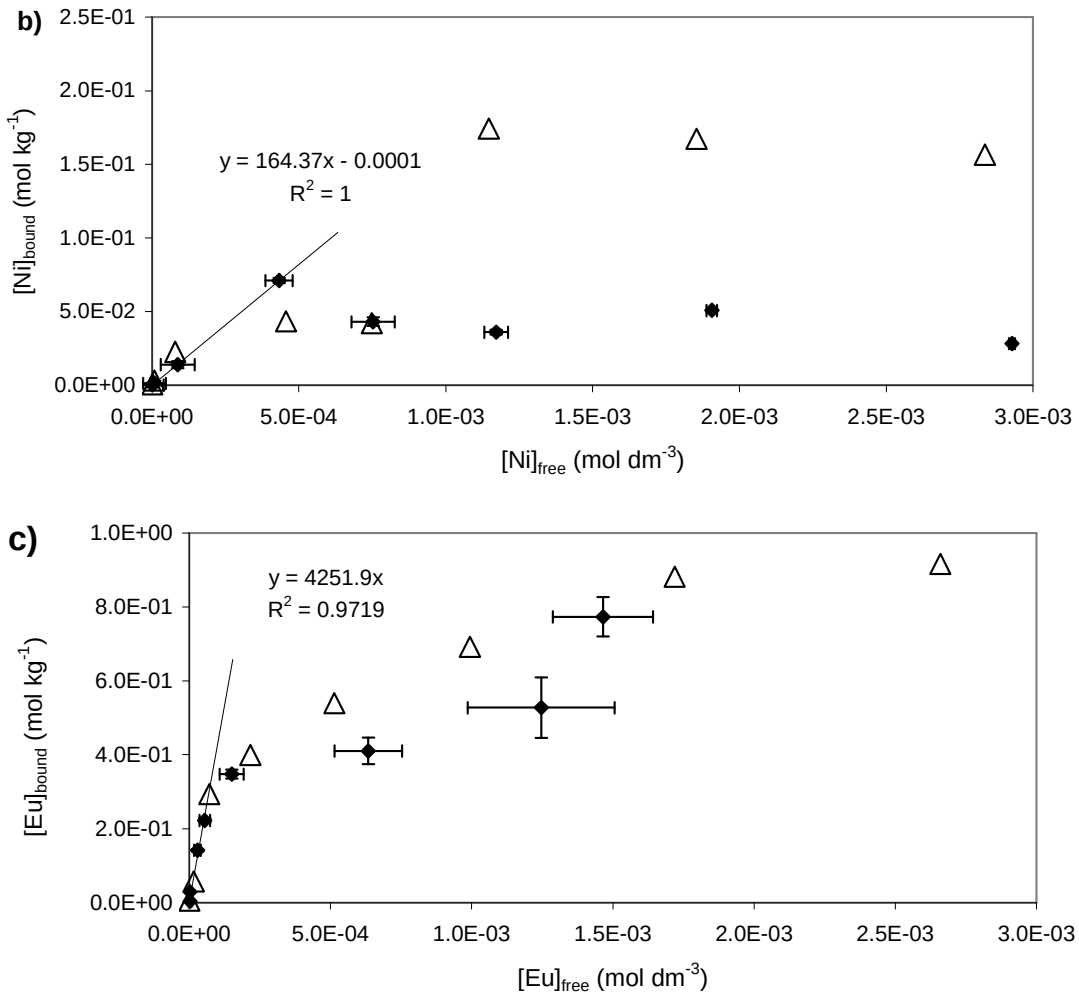

Figure 23. Sorption isotherms for (a) Cs, (b) Ni and (c) Eu sorption onto solid montmorillonite (black squares) and onto colloid (white triangles).

Figure 23 shows the isotherms for metal sorption onto solid montmorillonite. For ease of comparison, the sorption isotherms using the colloidal phase are also shown. Cs sorption onto solid montmorillonite showed a curved isotherm, suggesting a tendency to saturation. The slope of the linear range represented the distribution ratio, R_d, which was measured as 114.7 ± 6.0 dm^3 kg^{-1}. Ni sorption onto solid montmorillonite showed a tendency to saturation at higher Ni concentrations, which also occurred in the sorption to the colloidal phase. The R_d value yielded 51.5 ± 1.7 dm^3 kg^{-1}. Finally, sorption of Eu onto the solid phase of montmorillonite showed a steep increase at low metal concentrations, followed by a plateau and increased again at higher metal concentrations. The increase shown by the last data point could be due to either experimental error, or due to precipitation of a hydroxide form of Eu.

The R_d value was calculated as 4251.9 ± 427.8 dm^3 kg^{-1}. The sorption of metals on montmorillonite increased in the order Ni < Cs < Eu.

The sorption of metals onto montmorillonite was modelled using the Langmuir, Freundlich and D-R isotherms (Figure 24). The relevant parameters are shown in Table 16. The values of Q_{max} are mol kg^{-1} and the free energy kJ mol^{-1}.

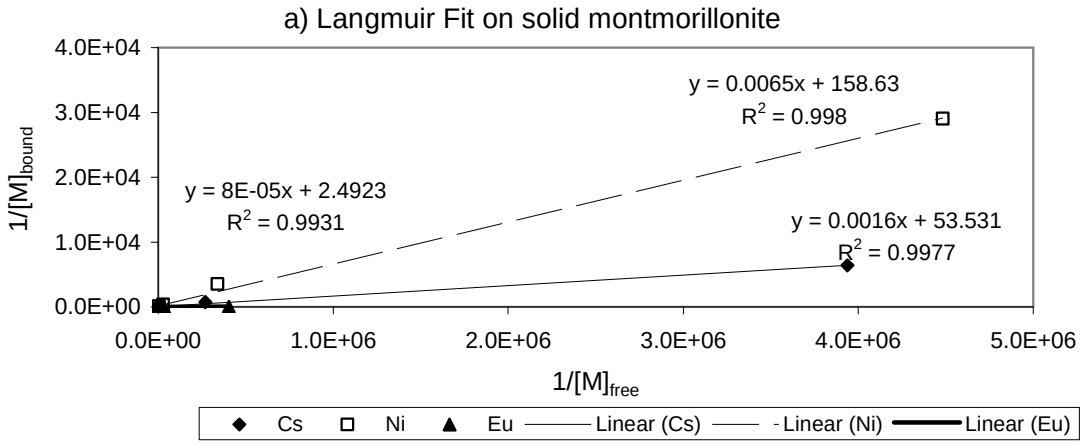

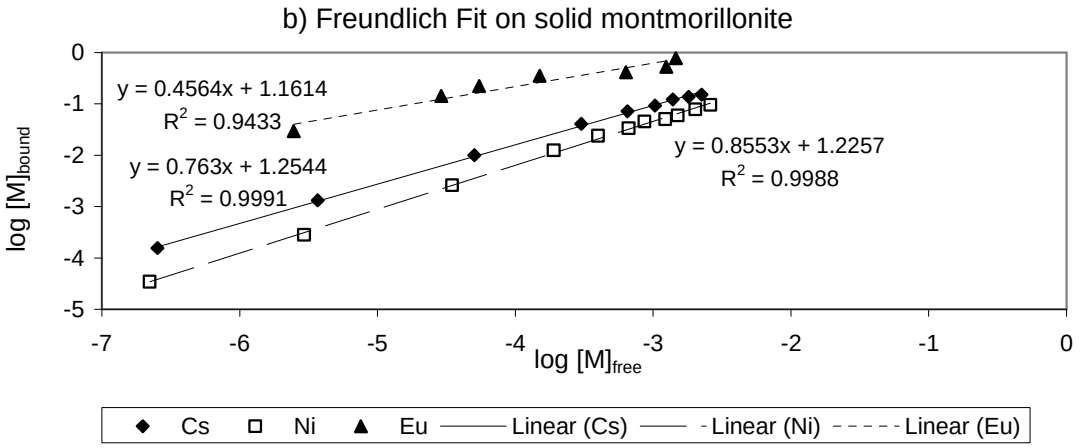

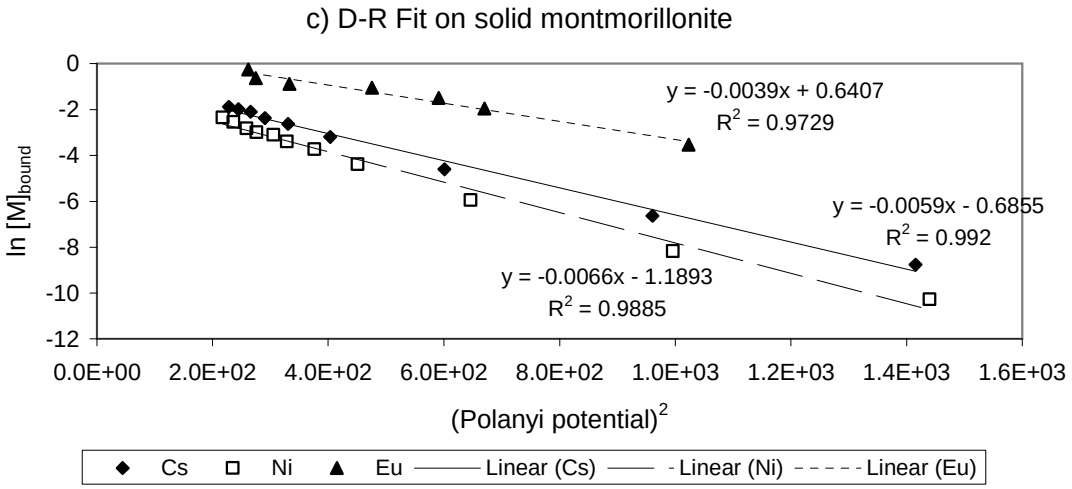

Figure 24. Modelling metal sorption on solid montmorillonite at pH 7 and ionic strength 0.05 mol dm^{-3}.

Table 16. Modelling parameters for metal sorption on solid montmorillonite.

	Langmuir		Freundlich		D-R		
	R^2	Q_{max} x10^{-2}	R^2	n	R^2	Q_{max} x10^{-2}	E
Cs	0.9977	18.7	0.9991	0.763 ± 0.01	0.992	50.4	8.70
Ni	0.998	6.30	0.9988	0.855 ± 0.01	0.9885	30.4	9.21
Eu	0.9931	401	0.9433	0.456 ± 0.05	0.9729	189.8	11.32

The sorption capacity of the solid, Q_{max}, is expressed as mol kg^{-1} and the mean energy as kJ mol^{-1}. From the results in Table 16, the Langmuir model underpredicted the sorption capacity of the solid for each of the metals, thus failing to explain appropiately the experimental observations. The D-R model predicted, for all of the metals, mean free energy values above 8 kJ mol^{-1} suggesting sorption took place via an ion exchange mechanism. The values found for the Freundlich constant, *n*, are in agreement with those found in the literature for sorption experiments under similar experimental conditions [94,95].

Influence of the solid to liquid ratio

The amount of montmorillonite used in the colloidal phase during the investigations of Ni was of approximately 11 mg. A separate batch experiment was carried out where the amount of montmorillonite weighed in the vial was 10 mg. The rest of the

sorption experiments were carried out following the same procedure as described for all the sorption experiments performed.

Series “10 mg linear” and “50 mg linear” in Figure 25 overlapped with “10 mg montmorillonite” and “50 mg montmorillonite”, respectively.

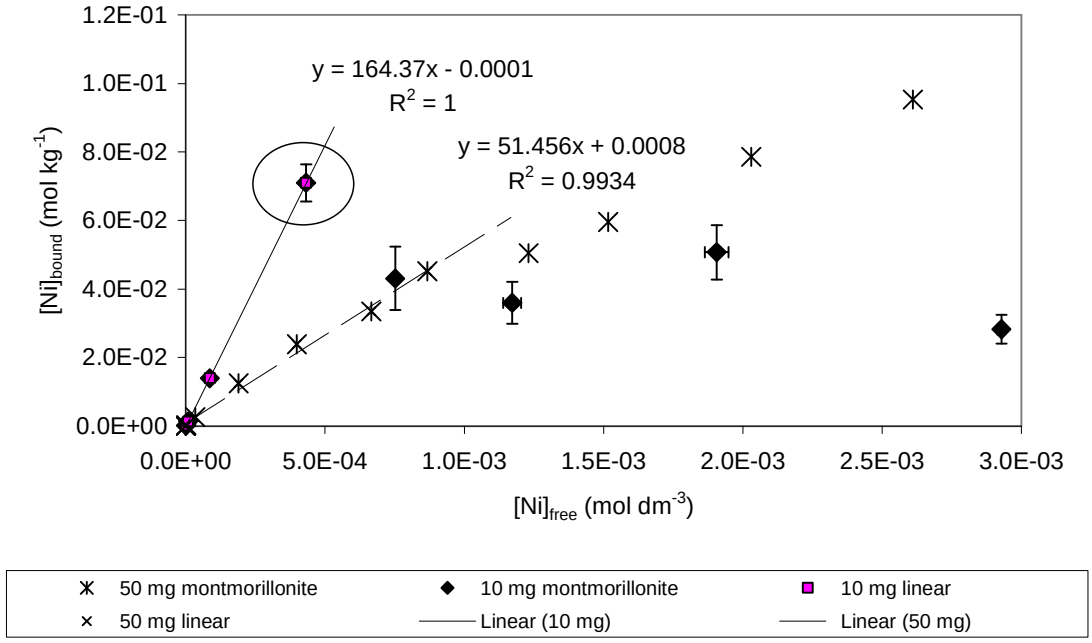

Figure 25. Sorption isotherm for Ni sorption on solid montmorillonite at different solid to liquid ratio, pH 7 and ionic strength 0.05 mol dm^{-3}.

Figure 25 shows the sorption of Ni onto solid montmorillonite at two different concentrations of montmorillonite in suspension, 10 and 50 mg in 10 cm^3. The lower concentration was chosen to compare the sorption of Ni on solid mineral to that on the colloidal phase. The isotherm shows two clearly distinct behaviours in the sorption of Ni on montmorillonite depending on the solid to liquid ratio. The series in black represents the sorption on 10 mg solid mineral and is characterised by a linear region, followed by a slight decrease in sorption leading to saturation. The data point highlighted by the circle was chosen to be accounted in the linear region, despite its slightly higher value. Not taking this point into consideration when calculating the distribution ratio from the linear region, would yield an R_d value of 159.79 dm^3 kg^{-1}, which is a value close to that reported earlier. The R_d value for the sorption of Ni on 10 mg of solid montmorillonite yielded 164.37 ± 0.63 dm^3 kg^{-1}, which was

significantly higher than the resulting value when the amount of solid increased to 50 mg, 51.46 ± 1.71 dm^3 kg^{-1}.

Solid vs colloid

Table 17 compares the R_d values for the sorption to the colloidal and solid phases of montmorillonite. Together with the distribution ratios, the mass of montmorillonite in each batch is also shown, as well as the type of isotherm observed in the range of concentrations studied, either linear or curved.

Table 17. Sorption parameters for metal sorption on montmorillonite (colloidal and solid phase).

	phase	mass (mg)	R_d (dm^3 kg^{-1})	isotherm
Cs	colloid	60	33.5 ± 0.7	linear
	solid	50	114.7 ± 6.0	curved
Ni	colloid	16	99.9 ± 19.4	curved
	solid	10	164.4 ± 0.6	curved
	solid	50	51.5 ± 1.7	curved
Eu	colloid	11	4174.1 ± 164.4	curved
	solid	16	4251.9 ± 427.8	curved

The general trend observed in section 3.2.1.2. in which changing the mineral phase of the boehmite led to an increase of the R_d value was not observed in the case of montmorillonite. Analysing the possible reasons, the sorption experiments were carried out in the same way and the amounts of montmorillonite are similar in the colloidal and the solid phase. However, the solid montmorillonite was not pre-conditioned prior to the sorption experiments. During the extraction of colloids, montmorillonite was saturated with Na^+ ions, thereby introducing a competitive element during the sorption experiment.

In addition to the R_d value, differences in the modelling of the sorption of metals on montmorillonite were also assessed.

Table 18. Modelling parameters for metal sorption onto colloidal and solid montmorillonite.

		Langmuir		Freundlich		D-R		
		R^2	Q_{max} ($x10^{-2}$)	R^2	n	R^2	Q_{max} ($x10^{-2}$)	E
Cs	Coll	0.9998	1.70	0.9997	0.956	0.9847	37.1	7.95
	Solid	0.9977	1.87	0.9991	0.763	0.9920	50.4	8.70
Ni	Coll	0.9953	3.54	0.9865	0.708	0.9792	58.9	9.28
	Solid	0.9980	0.63	0.9988	0.855	0.9885	30.4	9.21
Eu	Coll	0.9996	65.66	0.9409	0.650	0.9796	389.6	9.45
	Solid	0.9931	40.12	0.9433	0.456	0.9729	189.8	11.32

Coll : Colloid

The R^2 values obtained for most of the fits were above 0.99, indicating good fits. Eu sorption onto solid montmorillonite was best fitted by the Langmuir isotherm. In addition, the predicted sorption capacities agree with those observed experimentally in the sorption isotherms. The D-R fits exhibited lower R^2 values for the three metals, but suggested ion exchange mechanism for the sorption of the metals on montmorillonite. Eu was the metal to present higher values of mean energy of sorption. Finally, the Freundlich isotherm predicted the linear sorption of Cs on colloids and the non-linear behaviour of the metals on montmorillonite.

2.3.2.2. Desorption experiments

Following the sorption experiments, a series of three consecutive desorptions were carried out to study the extent of the reversibility of the sorption. To this purpose, an aliquot of fresh electrolyte solution was added to restore the initial volume. The activities obtained from the desorbed metal were transformed by mathematical operations into metal concentrations. The plot of the desorbed metal concentration versus the concentration of bound metal (from sorption) resulted in the desorption isotherm. For ease of interpretation desorption is shown as desorption percentages. This was possible when the desorption isotherms were linear in the range of concentrations studied. As a result, the desorption percentage was derived from the slope.

2.3.2.2.1. Desorption from boehmite colloids

Figure 26 shows the desorption percentages for the three consecutive desorptions (white, lined and dotted columns in figure) carried out following the sorption of Cs, Ni and Eu onto boehmite colloid. The total desorptions calculated for each metal after the three steps were: 19.75 ± 7.12, 63.33 ± 7.17 and 30.01 ± 1.24 % for Cs, Ni and Eu, respectively. Ni was the metal which showed the highest desorption percentage, followed by Eu and Cs. All the metals showed the same general trend: the first desorption was the one in which the greater amount of metal was desorbed, especially for Cs, which did not show significant desorption percentage beyond the first desorption. Overall, the results indicated that sorption was reversible to a greater or a lesser extent. The desorption isotherms from which the desorption percentages were calculated are shown in Figure 27 to Figure 29.

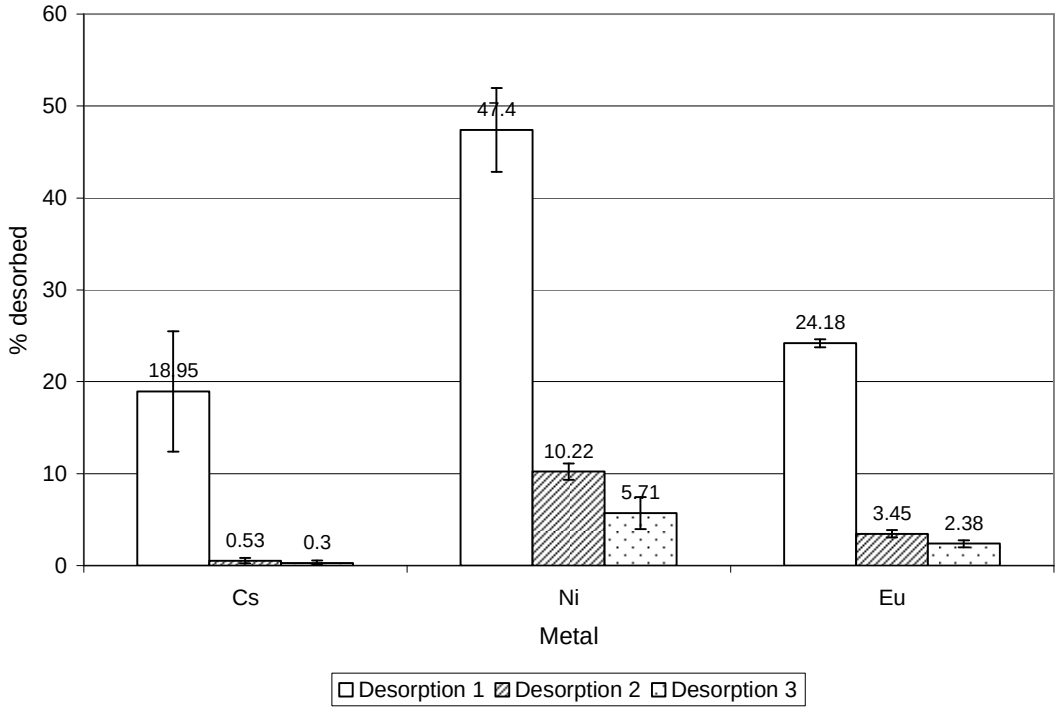

Figure 26. Desorption percentages for three consecutive desorptions of metals from boehmite colloids (30 mg) at pH 7 and ionic strength 0.05 mol dm^{-3}.

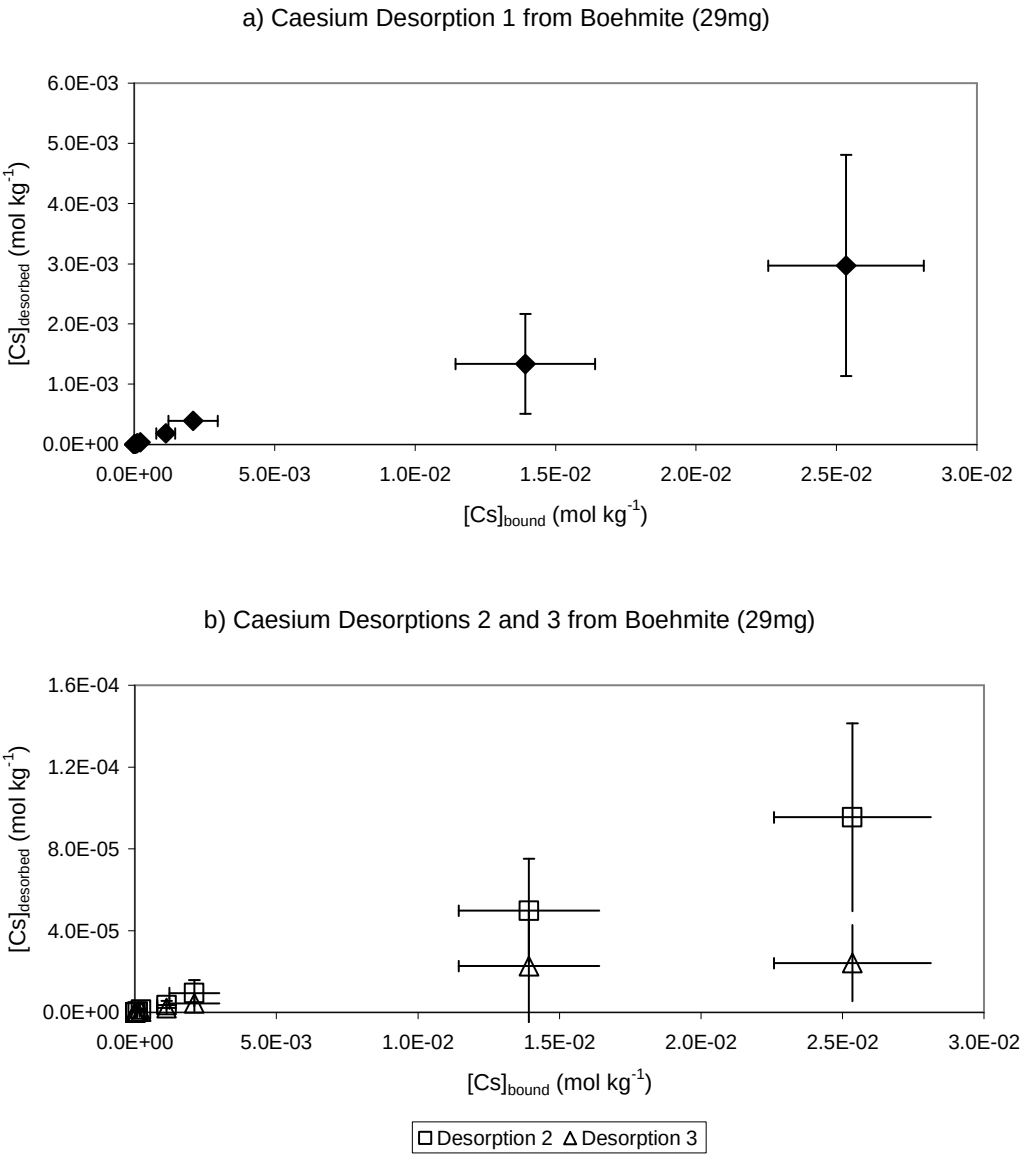

Figure 27. (a) First and (b) second and third desorptions of Cs from boehmite colloids at pH 7 and ionic strength 0.05 mol dm^{-3}.

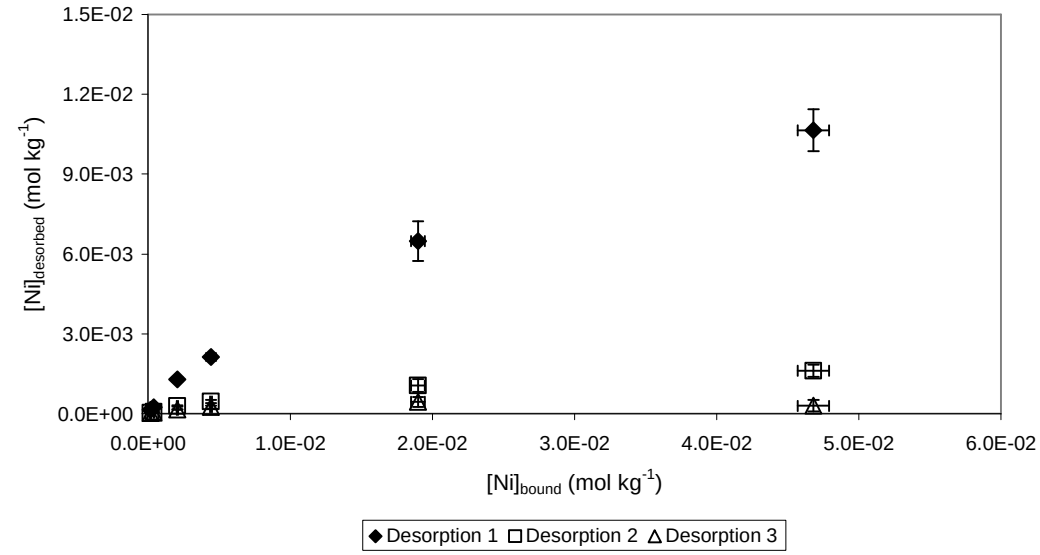

Figure 28. First, second and third desorption of Ni from boehmite colloids.

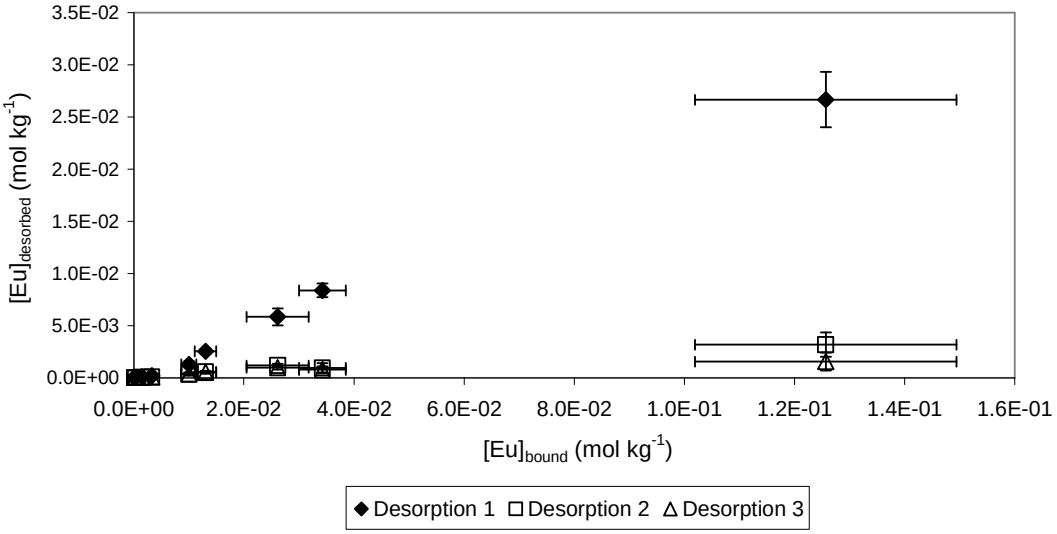

Figure 29. First, second and third desorption of Eu from boehmite colloids.

2.3.2.2.1.1. Influence of colloid concentration

The reversibility of the sorption of metals onto boehmite colloids in the presence of different concentrations of colloids was studied by carrying out three consecutive desorption steps following the sorption experiments.

As a reminder, two different concentrations of colloids were used in the sorption experiments. The masses of boehmite colloids in each experiment are summarised in Table 8.

Figure 30 shows three different illustrations, one for each of the metals; furthermore, each illustration represents the three desorption results for the two different masses of colloid, indicated in the x-axis.

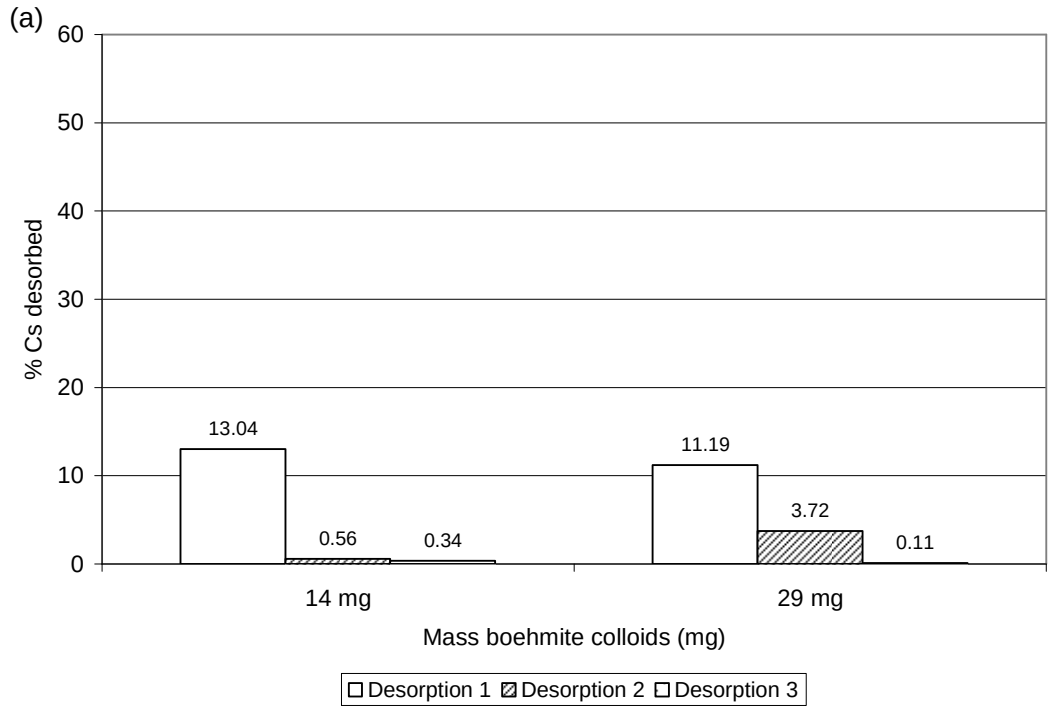

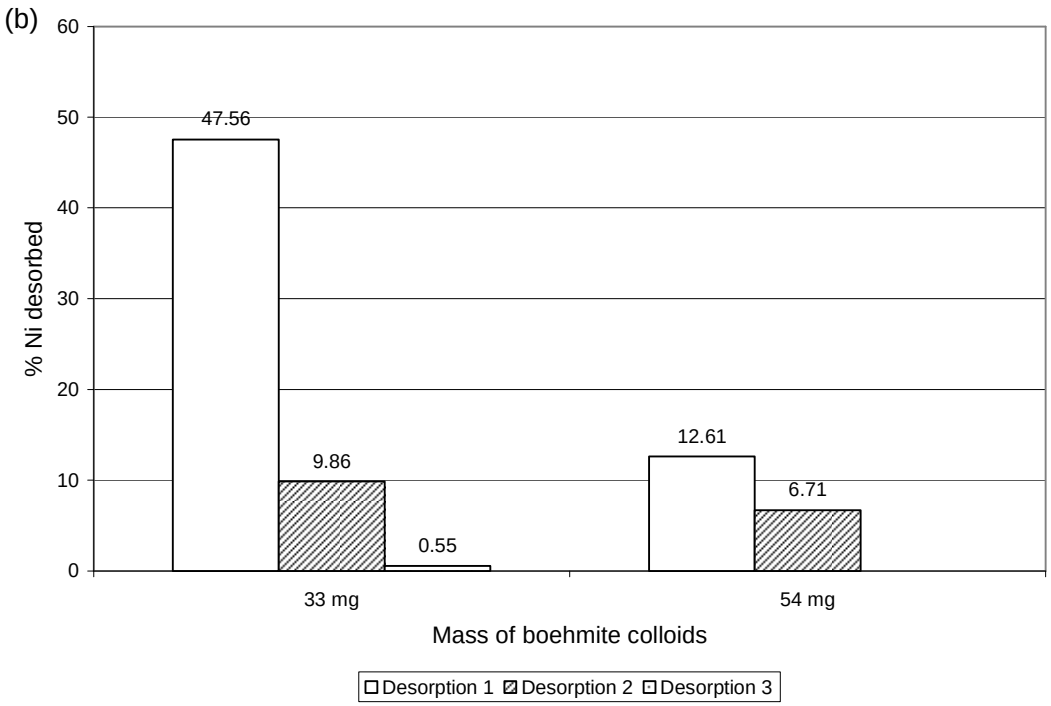

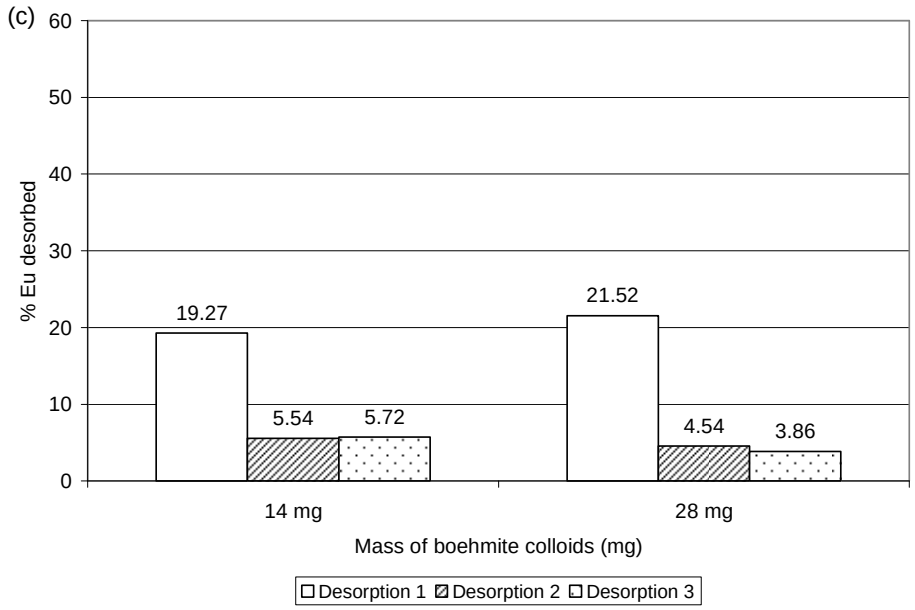

Figure 30. Influence of solid to liquid ratio on the desorption of (a) Cs, (b) Ni and (c) Eu from boehmite colloids.

A number of conclusions can be drawn from Figure 30:

- Ni was the metal to show higher overall desorption percentage, followed by Eu and Cs, which was the metal to exhibit larger irreversibility.
- The concentration of boehmite did not influence significantly the desorption behaviour of Cs or Eu. However, the desorption percentages of Ni decreased with an increase of the amount of boehmite in suspension.
- In all cases, the first desorption showed higher values than the second or third.

2.3.2.2.2. Desorption from solid boehmite

The desorption percentages for the three consecutive desorptions, determined from the desorption isotherms are shown in Figure 31. The desorption isotherms are shown in Figure 32. In the case of Cs, the second desorption yielded low values, constant for all concentrations used; thus, the average value was used as the desorption percentage.

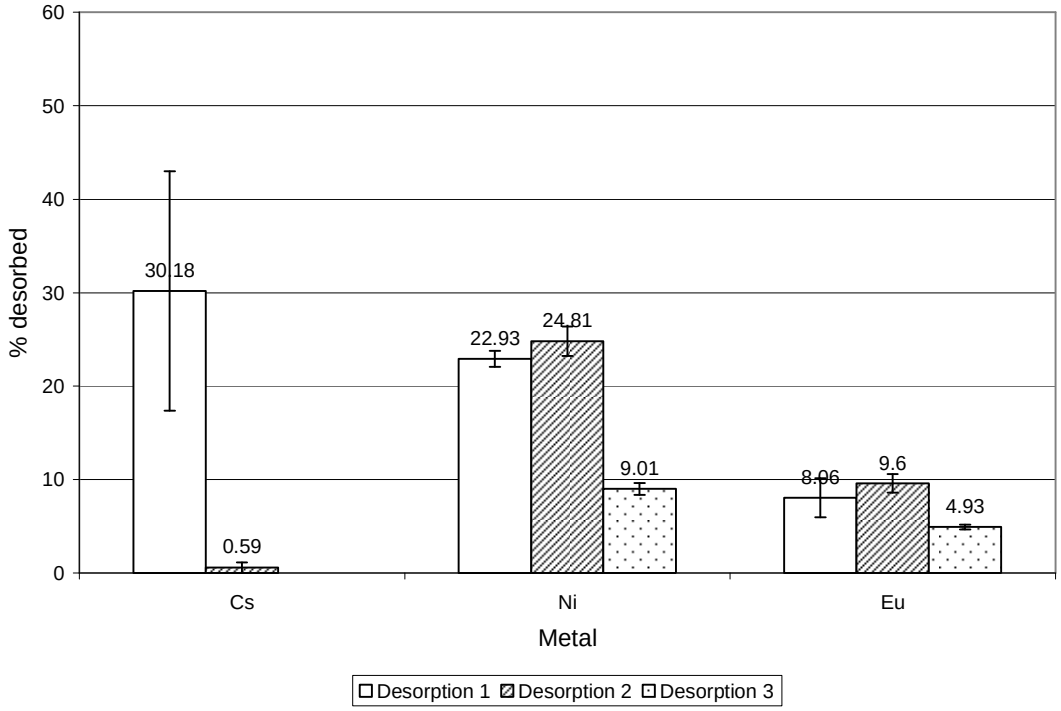

Figure 31. Desorption percentages for three consecutive desorptions of metals from solid boehmite at pH 7 and ionic strength 0.05 mol dm^{-3}.

The total desorption percentages shown in Figure 31 were 30.77 ± 13.37% for Cs, 56.75 ± 3.06% for Ni and 22.59 ± 3.34% for Eu. The order of desorption for the metals was Eu < Cs < Ni. No significant desorption of Cs took place after the first step, whereas Ni and Eu displayed similar desorption percentages for the first and second washes. The results for Cs suggested that 70% of Cs interacted with boehmite through formation of chemical strong bonds which were not altered by electrolyte washes; whereas the 30% desorbed was only physically bound through electrostatic interactions. On introduction of electrolyte solution, the Na^+ cations replaced the Cs^+ cations, releasing them into solution. The results observed for Ni and Eu suggested that ion exchange also took place between the Na^+ ions in the electrolyte solution and the metal ions on the surface.

Solid vs colloid

The desorption percentages determined for the solid and the colloidal phase were not significantly different, only slight differences could be observed (Table 19), except for Cs, which desorbed in a greater percentage from the solid phase.

Table 19. Desorption percentages for metal desorption from boehmite (colloidal and solid phase).

	Overall desorption percentage	
Metal	Colloid	Solid
Cs	19.75 ± 7.12	30.77 ± 13.37
Ni	63.33 ± 7.17	56.75 ± 3.06
Eu	30.01 ± 1.24	22.59 ± 3.34

a) Cs desorption from solid boehmite

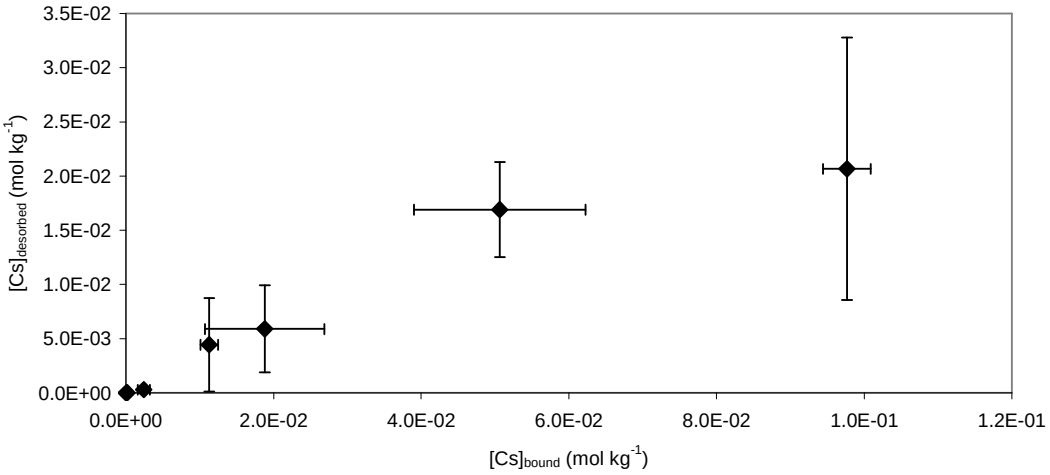

b) Ni desorption from solid boehmite

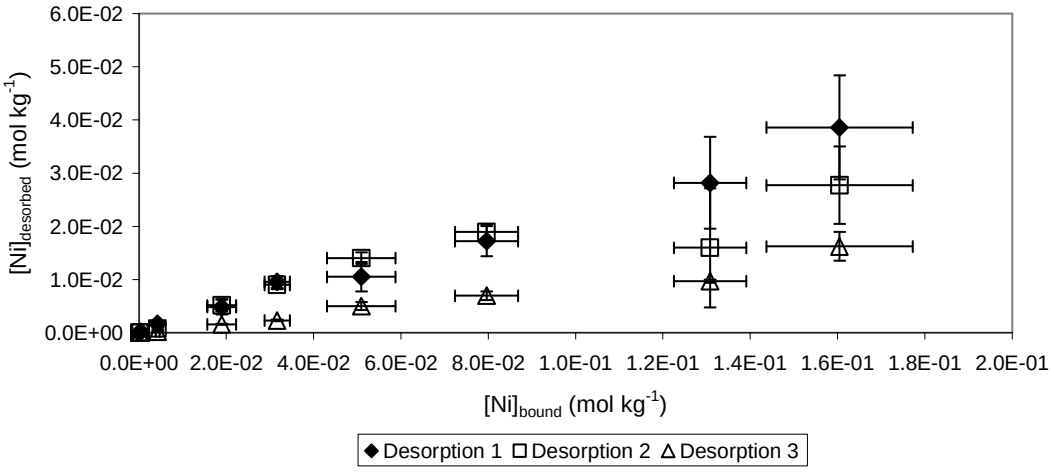

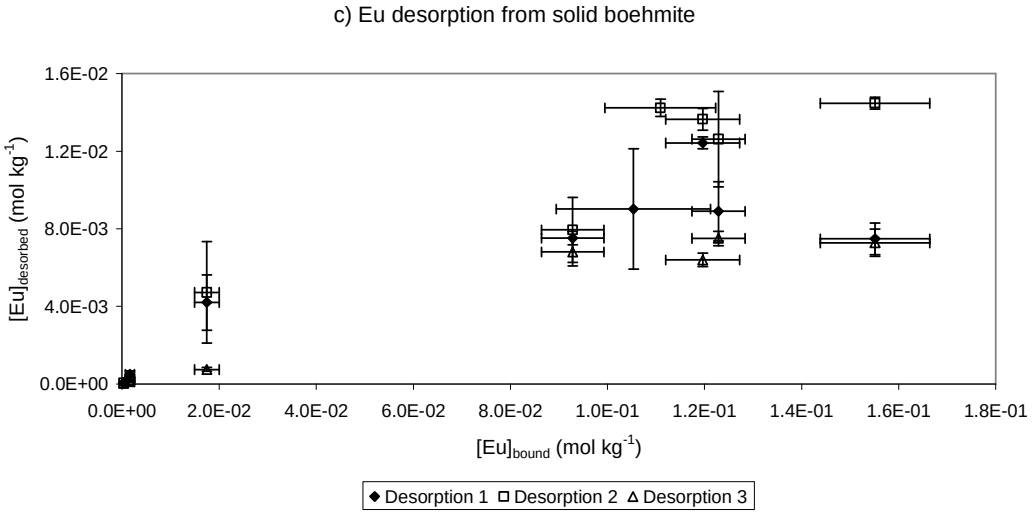

Figure 32. Metal desorption from solid boehmite at pH 7 and ionic strength 0.05 mol dm^{-3}.

2.3.2.2.3. Desorption from montmorillonite colloids

Figure 33 shows the desorption percentages for Cs, Ni and Eu desorption from montmorillonite colloids in three consecutive desorption steps. The total desorption percentages observed for each metal were 16.70 ± 1.71% for Cs, 43.51 ± 6.24% for Ni and 4.75 ± 2.62% for Eu. The highest desorption percentage was that from Ni, followed by Cs and then Eu. The general trend for all the metals was that the first desorption was the main desorption. The desorption isotherms from which the desorption data was derived are shown in Figure 34.

The results from the sorption experiment (Figure 21) showed that sorption increased in the order Cs < Ni < Eu. Figure 33 showed that the order of desorption was Eu < Cs < Ni. These results suggested that Eu was the metal which sorbed more strongly to montmorillonite colloids, as it sorbed to a greater extent and desorbed the least from the colloids.

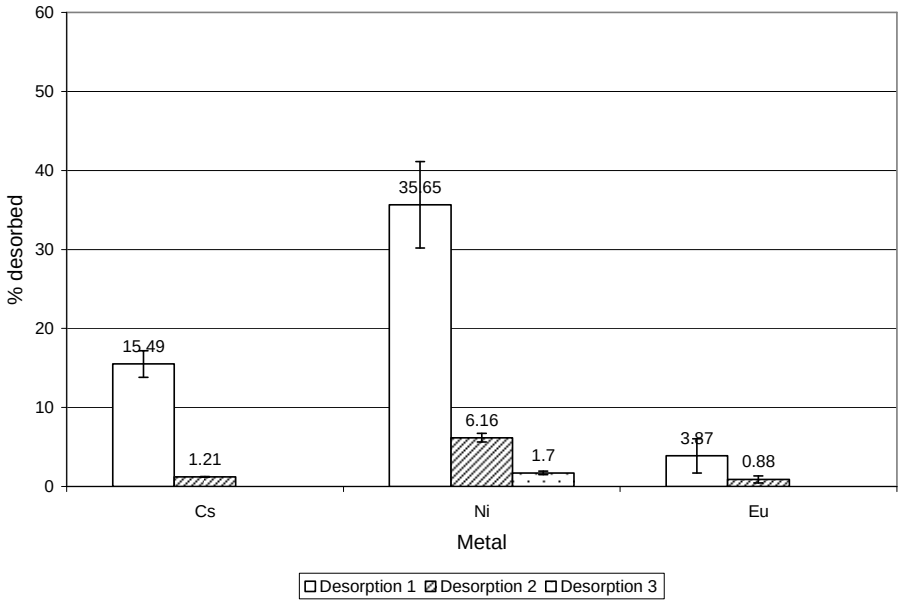

Figure 33. Desorption percentages for three consecutive desorption steps of metals from montmorillonite colloids at pH 7 and ionic strength 0.05 mol dm^{-3}.

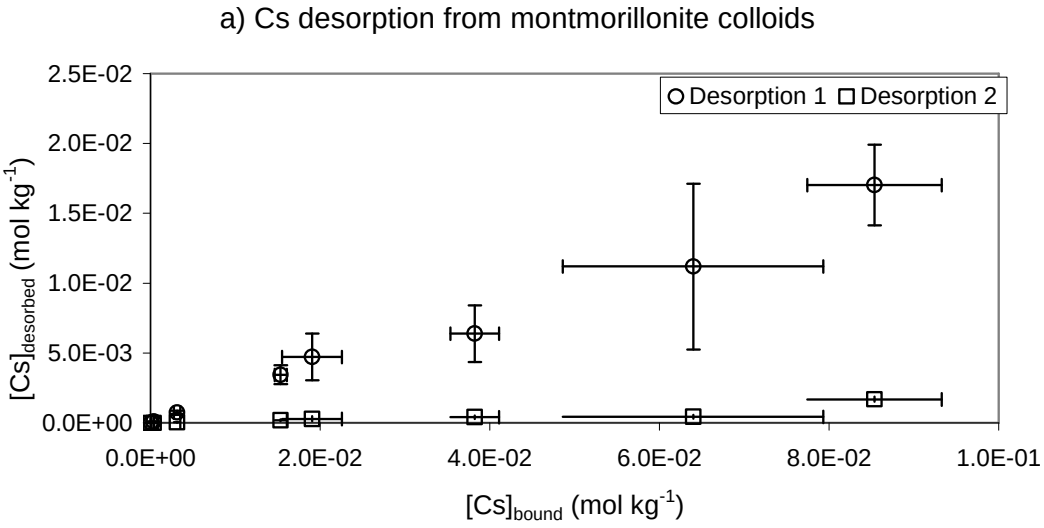

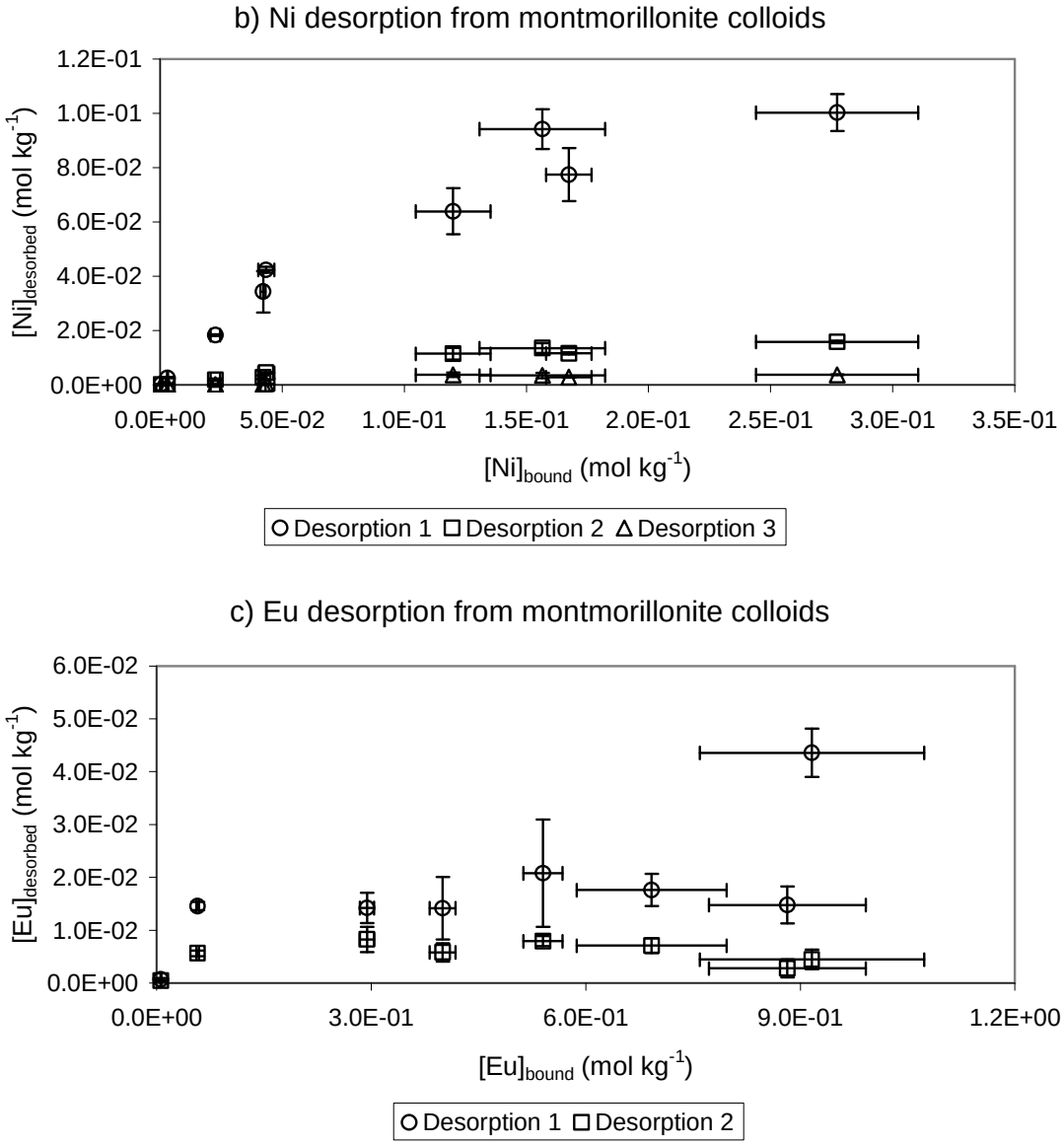

Figure 34. Metal desorption from montmorillonite colloids at pH 7 and ionic strength 0.05 mol dm^{-3}.

2.3.2.2.4. Desorption from solid montmorillonite

Figure 35 shows the desorption percentages for Cs, Ni and Eu from solid montmorillonite. The total desorption percentages after three consecutive steps were: 69.49 ± 1.80, 42.99 ± 1.18 and 2.59 ± 0.02% for Cs, Ni and Eu, respectively. Desorption occurred in a greater extent in the case of Cs, followed by Ni and then Eu. The desorption of Cs contrasted with previous experiments where little desorption took place beyond the first wash.

As indicated from the desorption experiments, sorption of Cs and Ni onto solid montmorillonite was reversible, as almost 70 and 50%, respectively, of the metal sorbed onto the solid was afterwards removed by washing with electrolyte. On the contrary, Eu exhibited low reversibility, with 3% desorption. The desorption of Eu from the colloidal phase of the mineral also suggested low reversibility.

The desorption percentages calculated for the solid phase of montmorillonite are similar to those calculated for the colloidal phase (see Figure 33), except for Cs, which desorbed four times more from the solid phase than from the colloid.

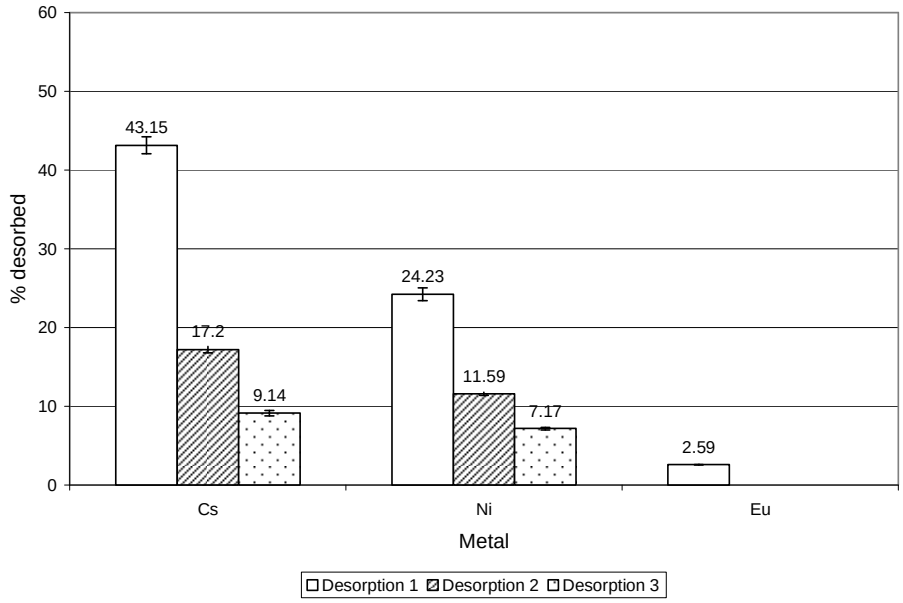

Figure 35. Desorption percentages for three consecutive desorption steps of metals from solid montmorillonite at pH 7 and ionic strength 0.05 mol dm^{-3}.

a) Cs desorption from solid montmorillonite

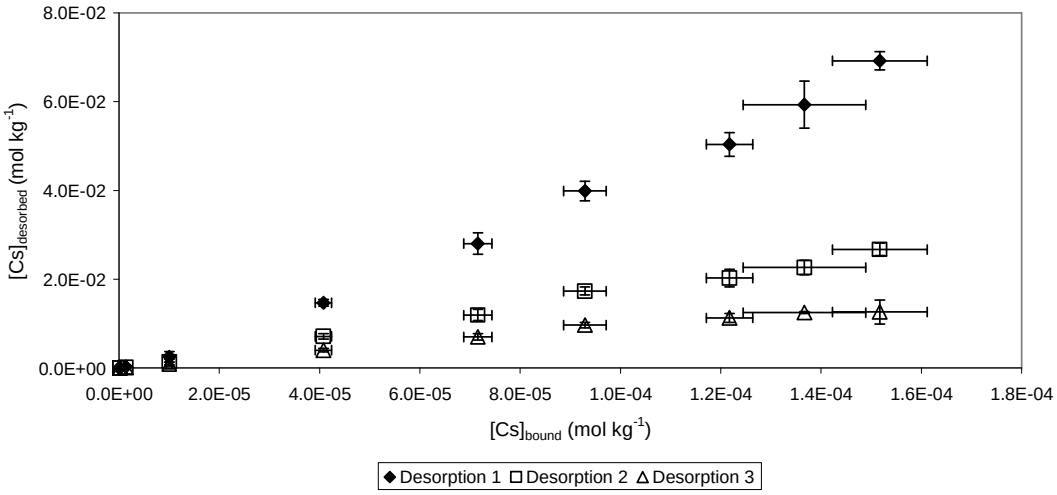

b) Ni desorption from solid montmorillonite

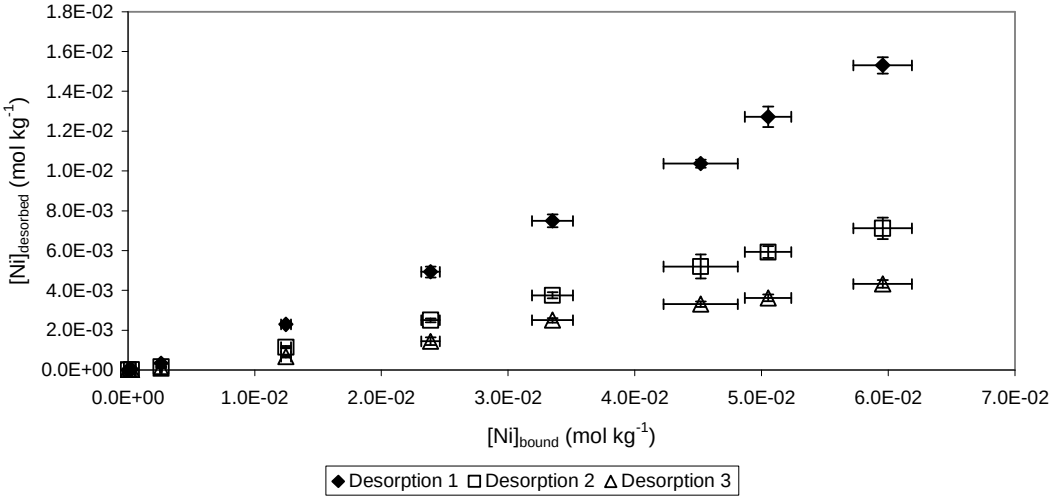

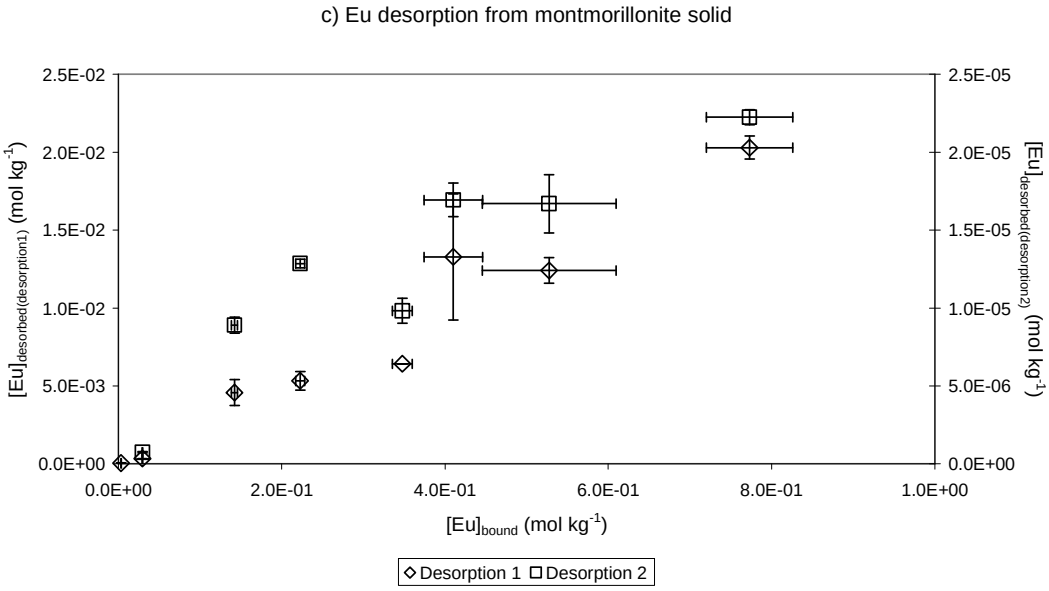

Figure 36. First, second and third desorption for (a) Cs, (b) Ni and (c) Eu from solid montmorillonite at pH 7 and ionic strength 0.05 mol dm^{-3}.

2.3.3. Surface area of boehmite

The specific surface area of boehmite colloids was measured by N_2-BET adsorption. PEC and CEC were also measured for the colloidal and the solid phase of boehmite. However, the CEC and PEC increases are not proportional to the increase in surface area. Table 20 shows the difference in surface parameters between the colloidal and the solid phase of boehmite. The average size was approximately 70 times higher for the solid phase (considering the average size as 7000 nm; data provided by manufacturer). Consequently, some characteristic parameters of the surface were significantly smaller for the solid phase: the specific surface area measured by BET was 50 times bigger for the colloid, the difference in the CEC was 3 times more for the colloid and finally an order of magnitude was the difference in the PEC, greater for the colloid. The results show that the larger surface area of the colloid results in a higher CEC and PEC. However, the CEC and PEC increases are not proportional to the increase in surface area.

Table 20. Surface parameters of colloidal and solid boehmite.

Boehmite	Average size (nm)	Surface Area ($m^2\ g^{-1}$)	CEC (meq g^{-1})	PEC (mol $H^+\ g^{-1}$ boehmite)
Colloid	122.4 ± 3.9	114.2797 ± 0.9035	21.57 ± 1.05	$2.6 \times 10^{-4} \pm 6.2 \times 10^{-6}$
Solid	*	2.4673 ± 0.0018	7.12 ± 0.10	$1.3 \times 10^{-5} \pm 3.0 \times 10^{-6}$

*Diameter (μm) as provided by manufacturer: d10 = 1.2; d50 = 7; d90 = 17
d10 indicates that 10% of the particles have a smaller diameter than 1.2 μm, being the remainder 90% larger than that size. d50 and d90 indicate same parameters.

The BET method involves the solidification of the colloids, a process which may affect the structure or surface properties of the colloids. Therefore, other methods have been developed to measure the surface area of colloids. These methods involve the adsorption of an appropiate dye to the colloids [79]. The method was described in section 2.2.4.1.

For ease of use, the method was first applied to the solid. As boehmite is positively charged in the range of pHs studied, the method required the selection of a suitable dye. Unfortunately, none of the dyes tried herein were suitable for the measurement of the surface area of boehmite. The following table summarises the problems encountered when using the dyes, as well as the conditions tried. The third column shows, in most of the cases, the absorbance observed for the dye solution (named blank) and the absorbance for the dye-solid sample. When the absorbance measured for the sample was similar to that measured for the blank, no sorption took place.

Table 21. Attempt to measure surface area of boehmite by adsorption of organic dyes.

Dye	Conditions	Problems
DPSO	[DPSO] = $5x10^{-4}$, $8.3x10^{-6}$ mol dm^{-3}	UV too concentrated for higher concentration and not measurable for lower concentration. Range too narrow.
NBA	[NBA] = 10^{-4} mol dm^{-3} m boe = 0.955 g	Blank A = 0.9788 A = 1.1500 No sorption observed
3NP	[3NP] = 10^{-2} mol dm^{-3} m boe = 0.0999 g m boe = 0.2020 g m boe = 0.3015 g	Blank A = 0.7189 A = 0.7330 A = 0.7743 A = 0.7450 No sorption observed
	[3NP] = 10^{-3} mol dm^{-3} m boe = 0.1042 g	No sorption observed.
	[3NP] = 10^{-4} mol dm^{-3} m boe = 0.2023 g	No sorption observed.
Ponceau S	[Ponceau S] = 1% v/v m boe = 0.3064 g m boe = 0.3001 g m boe = 0.3013 g	Colour of dye disappeared. Apparent sorption. However, UV showed sorption. Possible reason could be decomposition of dye.
	[Ponceau S] = 1% v/v m boe = 0.2998 g m boe = 0.3056 g m boe = 0.3023 g	This time equilibration time was changed to 5 minutes. Just after the solid and dye were added together, a red solid started to precipitate. pH was 1.37.
	[Ponceau S] = $7.5x10^{-3}$, $5x10^{-3}$, $2.5x10^{-3}$ % v/v m boe ≈ 0.2 g	pH was taken to 9 with NH_3OH. The three solutions studied turned white immediately after adding the boehmite. After centrifuging the solution was still cloudy. After filtering the solution was still cloudy. UV could not be measured.

The last dye used, Ponceau S, seemed to be decomposing in the presence of boehmite, since the resulting colourless solution after the equilibration time showed

high absorbance in the UV. In case the aluminium was having a chemical effect on the dye, an experiment was carried out where the same concentration of dye (1 % v/v) was contacted with 0.3 g of $AlCl_3$ and $Al(OH)_3$. However, no changes were observed. Hence, apparently only boehmite had an effect on the dye at this concentration. Also, the calibration curve for this dye could only be acquired between 2.5 x 10^{-3} and 7.5 x 10^{-3} % v/v, since higher concentrations were too concentrated for UV and lower concentrations gave absorbance below 0.1 (background range).

Although a wide range of dyes were used, under different conditions, the measurement of the surface area of boehmite by using a dye was unsuccesful.

2.3.3.1. Surface imaging

SEM and XRD measurements were carried out on boehmite colloids, solid and on those metal-bound colloidal samples. SEM images were taken expecting to observe differences in the surfaces between colloidal and solid boehmite. Furthermore, SEM images were taken on metal-bound, radiotracer-free boehmite samples aiming to observe any changes induced by the sorption of metals onto the colloids.

XRD measurements were used initially to compare both colloidal and solid boehmite, expecting to observe similar or identical diffractograms. XRD was further used to observe whether the sorption of metals and HA had altered the structure of boehmite.

XRD measurements for boehmite, both the colloidal and the solid phase, showed identical diffractions for both phases (Figure 37). Further, the programme verified the presence of boehmite by positive match with the reference boehmite (Figure 38). The width of the peaks is inversely proportional to the size of the particles. Hence, the broader peaks observed for colloidal boehmite is consistent with a smaller size of the particles. The Scherrer equation [96] is defined as follows:

$$L = \frac{0.9 \cdot \lambda}{B \cdot \cos\theta}$$ **Equation 2.16**

Where L represents the size of the particle, in Å, λ is the wavelength (λ = 1.5418 Å), B is the full width at half maximum intensity of the peak, in radians and θ is the angle. L could be calculated in nm by multiplying the original value by 10, as 1 nm = 10 Å.

The Scherrer equation was used to calculate the size of boehmite particles for the first three peaks from Figure 37. The results are shown in Table 22.

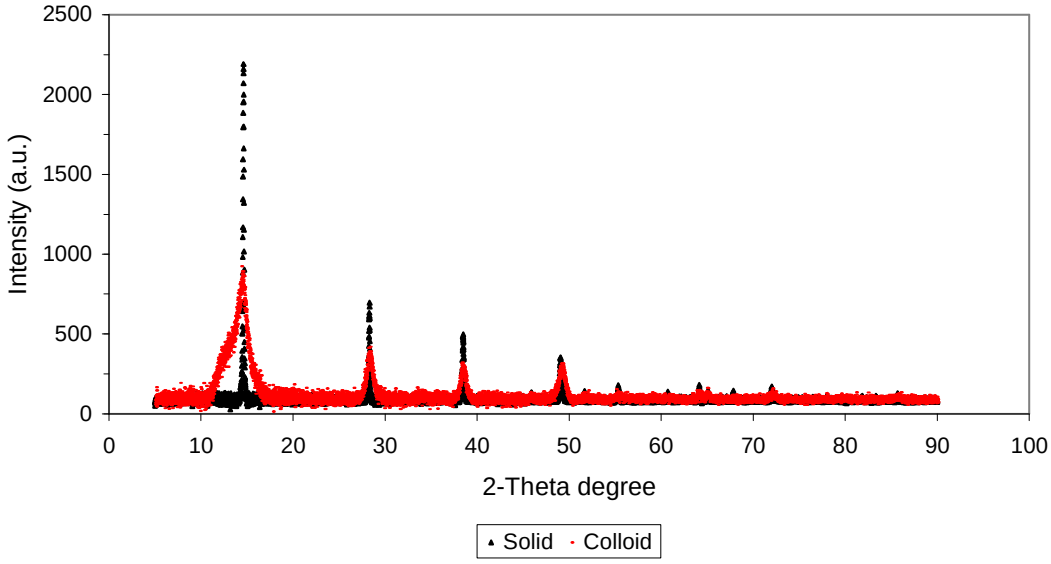

Figure 37. XRD diffractograms of solid and colloidal boehmite.

Table 22. Size of colloidal and solid boehmite calculated by the Scherrer equation.

	Colloid	Solid
Size (nm)	417.5	10146.4

The size of colloidal boehmite, as calculated by the Scherrer equation is orders of magnitude lower than the size observed for the solid particles of boehmite, in agreement with average size measurements carried out by DLS. However, the size measured for the colloidal boehmite is slightly higher than that measured in suspension by DLS (approximately 124 nm, Table 3). The increase in size is most probably due to aggregation of particles which took place during the evaporation process prior to the XRD measurement.

Two important conclusions could be drawn from the XRD measurements: (a) the size of colloidal particles was indeed significantly lower than the size of solid particles and that the solidification process affected the colloidal suspension by forming aggregates which altered the surface characteristics of the colloids, *i.e.* their size.

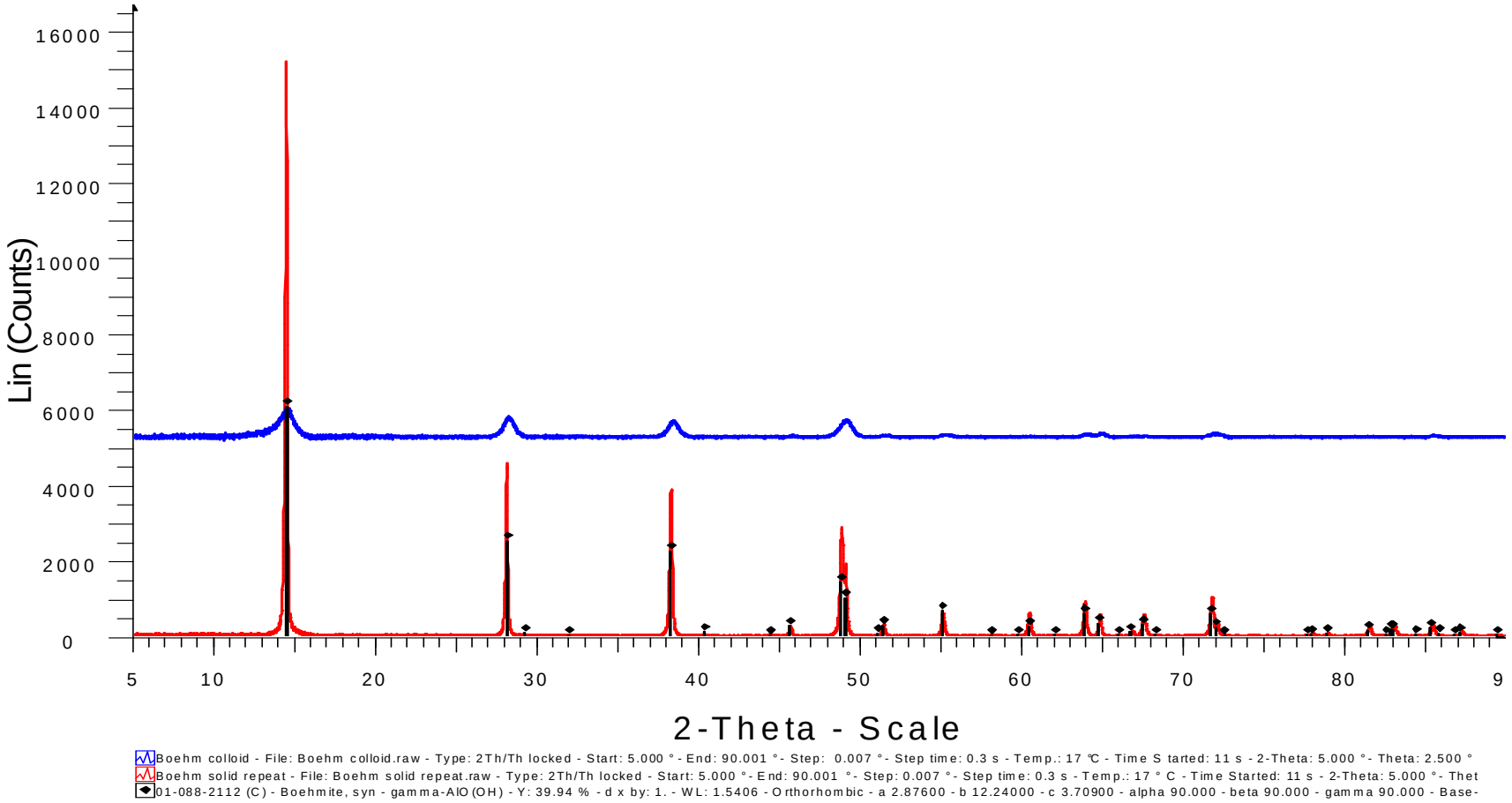

Figure 38. XRD Powder diffraction for boehmite (colloidal and solid samples) compared to reference boehmite.

The powder diffractions observed in Figure 37 show the presence of peaks at the same 2-theta degree, indicating that the same mineral was being analysed. The broader peak for the colloidal boehmite sample, together with the smaller (lower intensity) peaks, are probably due to the smaller amount of sample introduced in the instrument.

XRD measurements for boehmite colloids and metal-bound-boehmite colloids showed no significant differences, suggesting that the metals did not cause any alteration in the structure of boehmite (Figure 39).

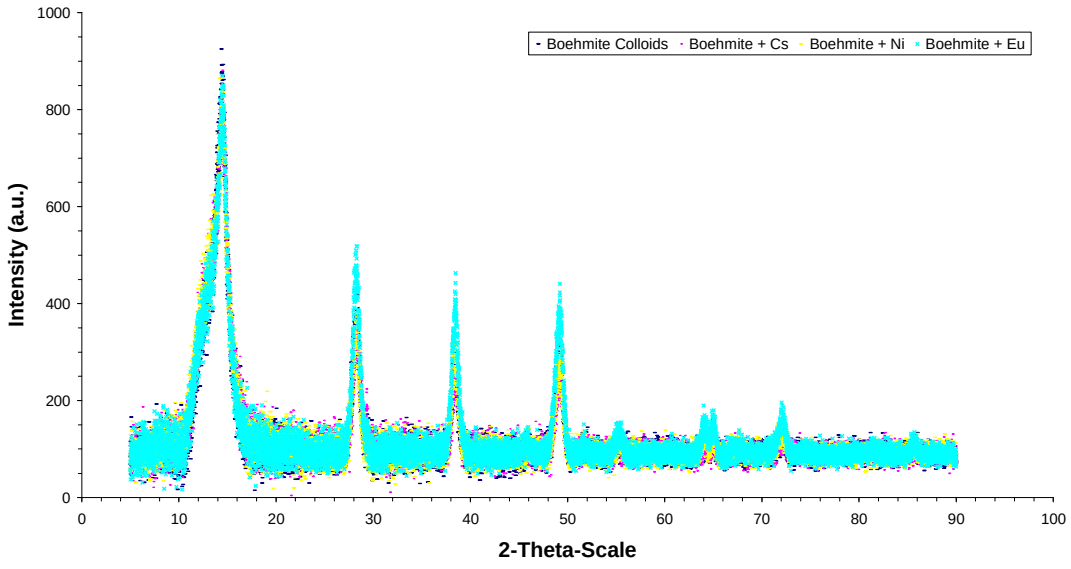

Figure 39. Effect of metal binding on boehmite colloids.

The SEM images were combined with EDAX mapping. The latter confirmed Al and O were dominant in boehmite. The images for boehmite colloids and solid are shown in Figure 40.

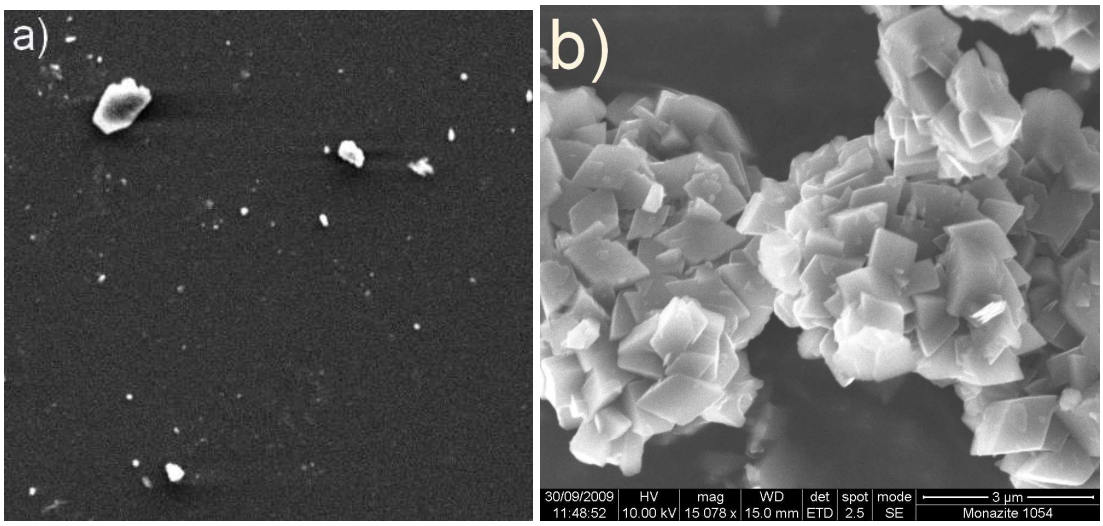

Figure 40. SEM images for boehmite (a) colloids and (b) solid.

The boehmite colloids were oven-dried prior to the measurement, resulting in a needle-like structure. Figure 40(a) shows the edge of that structure, which exhibited a rough surface with cavities. Instead, solid boehmite particles (Figure 40(b)) showed aggregation of pellets of smooth surface.

Samples of the radiotracer-free sorption batch experiments were also oven-dried prior to the surface imaging on SEM. EDAX mapping showed no metal on the surface, most probably due to the low concentrations of metal present. Due to the evaporation process, the SEM showed the samples to be mechanically broken. SEM images of Cs-, Ni- and Eu-sorbed boehmite colloids are shown in Figure 41 to Figure 43. All the SEM images show aggregates of particles, which probably originated during the evaporation process. For ease of understanding and interpretation, different expansions are shown, where a variety of sizes of the aggregates can be observed.

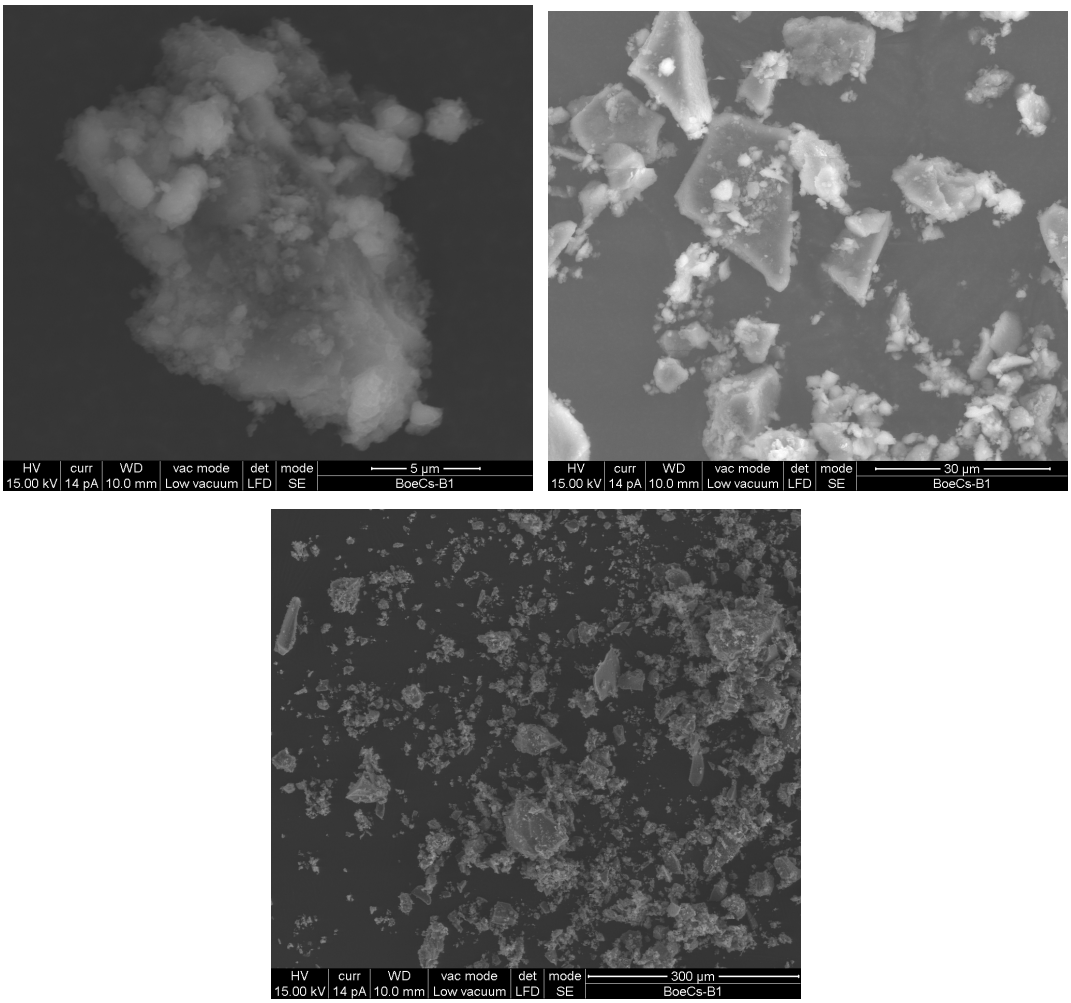

Figure 41. SEM images for Cs-bound boehmite colloids.

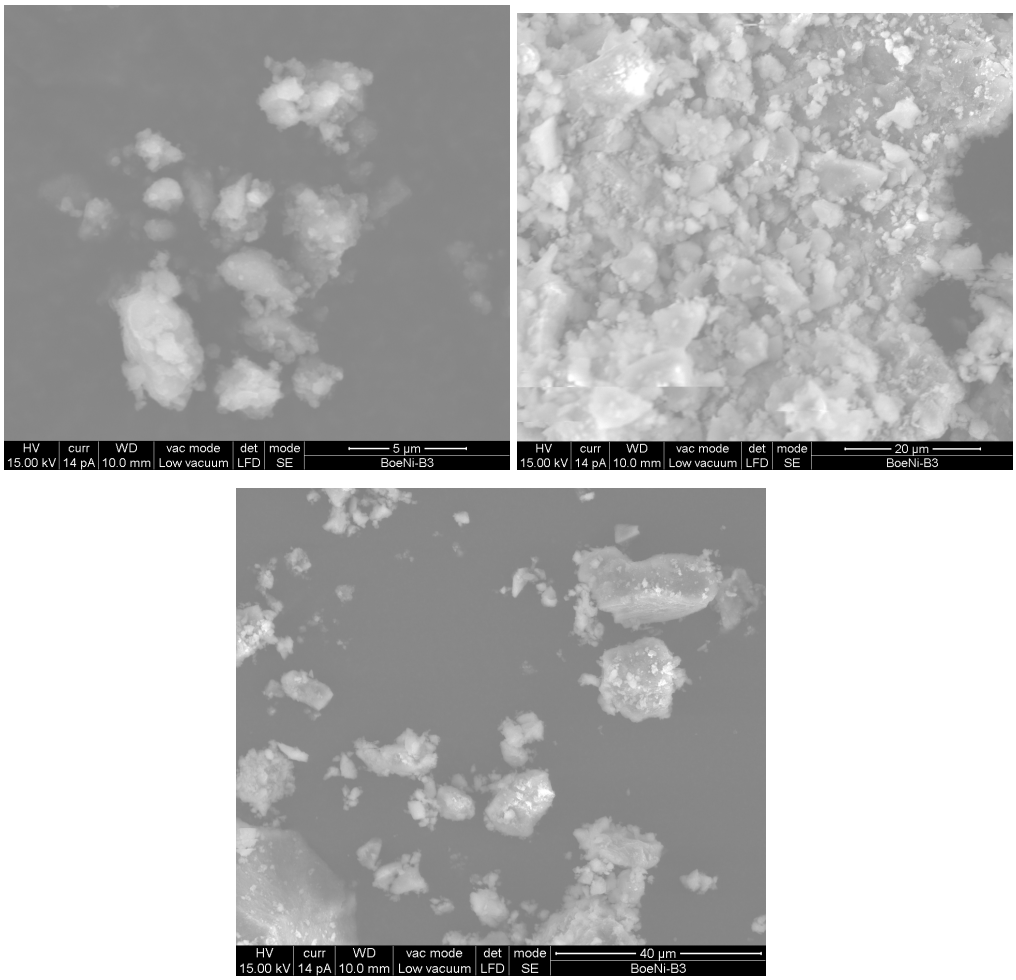

Figure 42. SEM images for Ni-bound boehmite colloids.

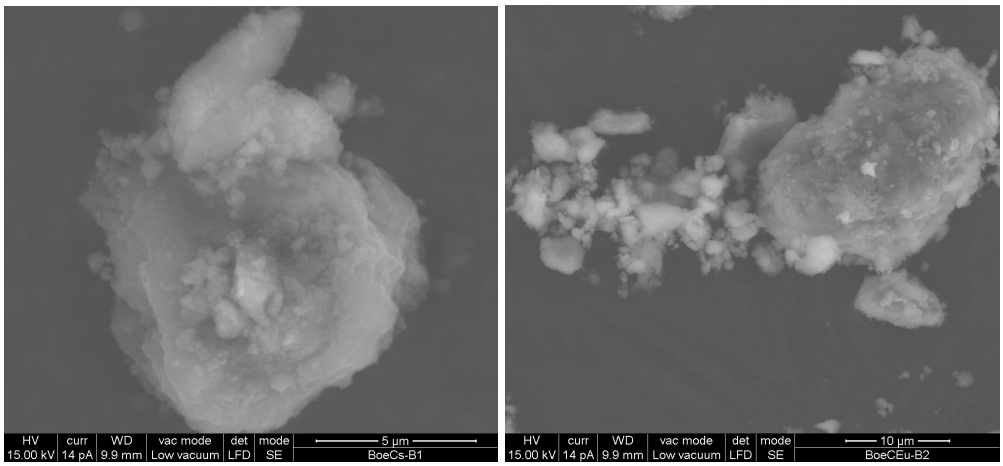

Figure 43. SEM images for Eu-bound boehmite colloids.

2.4. Discussions

Other studies reported in the literature have shown that metal sorption has generally been studied on solid surfaces rather than colloidal surfaces. The investigations herein have shown sorption isotherms and interpretations on both phases of minerals.

2.4.1. Metals and Boehmite

Sorption of Cs, Ni and Eu studied in this work, together with other investigations have shown that boehmite, despite being positively charged, can act as an adsorbent of cations through the OH^- groups. Spectroscopic studies have shown the mechanisms of interaction of multivalent metals with boehmite colloids. In this manner, Cu(II) was found to coordinate to the oxygens in the AlOOH [97], thereby forming inner-sphere complexes. As(V) associated to boehmite by forming bidentate binuclear structures, where As coordinated to two oxygens in a tetrahedral coordination [98]. Hiemstra *et al.* [99] concluded that the sorption of Fe(II) to boehmite could be explained in the same manner. Meng *et al.* [100] studied the sorption of Eu onto pseudo-boehmite and found that the chemical adsorption was due to electrostatic attraction. Phosphorous covered 20% of the boehmite surface at pH 4 [101]. Liu *et al.* [102] observed the reversibility of the sorption of Cd(II) to boehmite by means of column experiments. Finally, the reversibility of the sorption of metals onto boehmite colloids has also been observed in the case of Cr(VI) [59] and Rh(VII) [53].

To summarise the experimental observations, the sorption of metals onto boehmite (colloids and solid) increased with the ionic charge of the metal, and the R_d values were higher for the sorption onto the colloidal phase compared to those on the solid phase, due to the higher surface area of the colloid. Desorption experiments showed that Ni was the metal to desorb the most after three consecutive washes and that Cs desorption took place mainly after the first desorption. In the case of this metal, further washes did not exctract more metal from the surface of either colloidal or solid boehmite.

Na^+ ions, present in solution, compete succesfully with Cs^+ ions for outer-sphere sites [103], leading to a reversible sorption of Cs on boehmite, as observed

experimentally. However, this reversibility was only partial, as a significant amount of Cs remained sorbed after the first desorption. Hence, not only ion exchange mechanism, but also inner-sphere complexation can be assumed from the irreversible sorption observed. Although ion exchange is the main mechanism for Cs uptake on minerals [104], Kim et al. [103] proposed as well stronger bonds via inner-sphere complexation , which takes place by the proximity of Cs to the Stern layer.

Ni sorption on boehmite was linear and showed the highest reversibility on boehmite. The D-R model predicted ion exchange as the main mechanism for the sorption of Ni on boehmite, which would explain the high desorption observed. The presence of weak and strong binding surface sites were assumed by Villaseñor Nano [105] when investigating the sorption of Fe(II) onto oxides, and may also apply to the sorption of Ni onto boehmite colloids.

Batch sorption experiments indicated that Eu sorbed almost completely to boehmite at low concentrations, but soon saturated the surface of boehmite. Kraemer *et al.* [67] reported sorption percentages above 98% at metal concentrations 3 μmol dm^{-3} at pH 6.3, in agreement with the experimental observations. The high sorption of the metal to the boehmite surface might be due to the bonding of hydrated Eu to the aluminol groups [47,106]. Naveau *et al.* [107] modelled succesfully the sorption of Eu on goethite by introducing into the surface complexation model the ternary complexes $\equiv XOHEuCl^{2+}$ and $\equiv XOHEu(OH)_2$. These weak and electrostatic bonding lead to dettachment of the metal and thus reversible sorption may be expected.

Sorption of metals on boehmite, both solid and colloids, increased in the order:

$$Cs < Ni < Eu$$

Which agrees with the general trend that an increase in ionic charge leads to an increase in sorption [91]. Desorption increased in the order:

$$Cs \leq Eu < Ni$$

The desorption percentages observed for Cs from boehmite colloids were lower than those for Eu in the colloidal phase, but was in the same order (considering error) in the solid phase. The divalent metal was the one to desorb to a greater extent from boehmite in both phases, therefore, ionic charge is not the dominant factor to determine the extent of desorption. From the three metals studied, Ni is the metal to

exhibit the highest electronegativity and the lowest size (see Table 23). According to the hard-soft-acid-base rule, a hard acid is that Lewis acid (electron acceptor) which has high electronegativity and low ionic size [108,109]. Further, the rule states that hard acids tend to react or complex with hard bases and soft acids will tend to complex with soft bases [108]. Oxygen donors, like OH^-, are considered to be hard bases [110]. According to this, boehmite could be classified as a hard donor, which would tend to complex with Ni^{2+}, considered a hard acid, rather than Cs^+ or Eu^{3+} cations, which are softer in acidity. However, the experimental results of desorption suggest rather the opposite behaviour, since the higher reversibility observed suggests that boehmite tends to interact stronger with Cs^+ or Eu^{3+} ions. Moreover, Na^+ cations, classified as hard acids, would be expected to replace softer cations complexed to the surface of boehmite. The experimental findings that desorption of Ni from boehmite occurred to a greater extent than the other two metals could be explained by the HSAB theory assuming a soft-base character for boehmite.

Table 23. Ionic sizes and electronegativities of metals studied.

Cation	Ionic Size (pm)	Electronegativity (Pauling) [111]
Na^+	113	0.9
Cs^+	169 [93]	0.7
Ni^{2+}	69 [112]	1.8
Eu^{3+}	108.7 [113]	1.15

2.4.2. Metals and Montmorillonite

Due to the abundance of montmorillonite in natural soils [118], the sorptive behaviour of metals with this clay has been studied, and K_d values have been provided for sorption experiments under specific experimental conditions [114,115,116,117]. The number of investigations on sorption and desorption studies of metals onto colloidal montmorillonite is more limited.

Examples found in literature include Bouby *et al.* [118], who found that Eu(III) and Th(IV) bound to clay colloids, whereas, under the same conditions, Cs(I) and U(VI) would remain mainly dissolved. Czímerová *et al.* [119] found that Cs bound to

montmorillonite colloids directly to the oxygens in the siloxane groups. ^{85}Sr was found to adsorb quickly onto montmorillonite colloids present in natural groundwaters [120]. Baik and Cho [121] studied the sorption of U(VI) onto natural soil, constituted mainly by montmorillonite colloids, under different experimental conditions. Sorption was found to be greatest at pH 6.5.

As a summary of the results found for metal sorption and desorption onto montmorillonite colloids and solid phase, the sorption of metals onto montmorillonite colloids increased in the order Cs < Ni < Eu. The sorption of Eu showed a low reversibility, as only a 5% of the Eu sorbed was desorbed after three washes. Desorption increased in the case of Cs and was highest for Ni, but in all cases was below 50%. The sorption behaviour was different in the solid phase, as the order of sorption increased Ni < Cs < Eu. The reversibility was also low in the case of Eu, as less than 3% of the sorbed Eu was desorbed after three washes. Ni exhibited similar desorption percentages in the solid phase, as it did on the colloidal phase. Finally, Cs showed the largest reversibility, as 69% of the sorbed Cs was desorbed after three washes.

Ion exchange was the main sorption mechanism to explain the adsorption of Cs on solid montmorillonite, based on the mean free energy predicted by the D-R model, in agreement with previous reports found in the literature [94,122,95,104]. The model fitted succesfully the experimental observations in the work presented herein, predicting similar values of mean free energy to those found in literature.

Partial reversibility of Cs sorption on montmorillonite has been reported in literature. In this manner, Bellenger *et al.* [123] and Dyer *et al.* [124] reported preferential retention of Cs ions by solid montmorillonite; Bostick *et al.* [125] reported 31% desorption of Cs from solid montmorillonite after two washes with electrolyte. The author suggested two types of sorption mechanisms, inner sphere complexes, in which Cs would be more immobilised, and outer sphere complexes, where Cs would be easily exchanged by other cations present in solution. Significant desorption of Cs from clays containing montmorillonite was observed as well by Lujanienė *et al.* [126] and Krumhansl *et al.* [64].

A desorption percentage of approximately 43% in both the colloidal and the solid phase was determined for Ni. These results are in agreement with other authors who reported remobilisation of Ni on addition of other cations in solution [127]. Two different sorption sites have been described to account for the partial reversibility observed for sorption of Ni on montmorillonite: weak sites, and strong sites which would lead to retention of the metal on the surface [63,104].

Eu sorption to montmorillonite and similar clays is generally described by surface complexation [104]. This mechanistic explanation supports the findings herein in which low reversibility was found for Eu, suggesting strong bonding took place at the interface of montmorillonite.

The sorption of the metals increased as the ionic charge of the metals increased, in agreement with Adeleye *et al.* [91]. Both Cs and Ni were found to exhibit reversibility of the sorption, however, Eu desorption was low. The order of desorption increased in the order Eu < Ni < Cs.

Some R_d values reported in literature for sorption of metals on montmorillonite are shown in Table 24. All the values listed in the table correspond to batch experiments carried out at pH 7. The ionic strengths and solid to liquid ratios, however, varied from one reference to another, hence the differences in distribution ratio values.

Although few R_d values are referenced in Table 24 compared to the many more available in literature, the aim was to show the large range of values depending on the conditions of the batch experiments. A database was provided by Wold [128], where a large number of R_d values can be found for the sorption of different metals onto Ca^{2+} and Na^{+} montmorillonite, under different experimental conditions. In the same report, Wold highlighted the concerns in comparing the sorption of metals onto colloids when the experiments were carried out under different experimental conditions, mainly due to the influence of size distribution. Because the R_d value is normalised to the mass of colloid and not to the surface area, the smaller the colloids, the larger the surface sites available for sorption, and thus, the larger the R_d value. Hence, studying the sorption of metals onto colloids is not just influenced by the solid to liquid ratio, but also by the size distribution of the colloids.

Table 24. R_d values for metal sorption on solid montmorillonite at pH 7.

Reference	Metal	R_d value ($dm^3\ kg^{-1}$)	S/L ratio ($mg:cm^3$)
	Cs	115	60 : 10
Bostick *et al.* [125]	Cs	399	1 : 25
Bellenger *et al.* [123]	Cs	4514	
	Ni	164	10 : 10
Boonfueng *et al.* [65]	Ni	3900	1 : 1000
	Eu	4250	16 : 10
Bradbury *et al.* [129]	Eu	10^5	1.5
Rabung *et al.* [130]	Eu	2500	5 : 20

Note that the cells in grey are the values reported herein.

2.4.3. Solid to liquid ratio

Findings reported herein are in agreement with those of Granados Correa [59], in which the solid to liquid ratio influences, to a significant extent, the sorption of metals on boehmite. The effect is an observed increase of sorption of the metal with the amount of sorbent present in suspension. Sorption of Cs increased by 30% when the amount of boehmite in suspension doubled. For the same change, the distribution ratio for Eu increased by twelve-fold.

Ni, however, exhibited a decrease in the sorption upon increase of the solid to liquid ratio. When the concentration of boehmite colloids increased from 33.5 to 54 mg in suspension, the distribution ratio decreased by 26%, whereas an increase of five-fold in the concentration of solid montmorillonite led to a 70% reduction in the distribution ratio.

Another example of the influence of the solid to liquid ratio on the sorption of Cs on solid montmorillonite can be found in literature. Table 25 compares the differences in the Freundlich constants found for different solid to liquid ratios. The experimental values reported herein are also listed in the table (shaded area). All

experiments from literature summarised in the table were carried out at pH 7 and similar ionic strengths.

Table 25. References on Freundlich fit of Cs sorption to solid montmorillonite.

Reference	Solid to liquid ratio (mg : cm^3)	Freundlich constant *F*	Freundlich constant *n*
Adeleye *et al.* [91]	500 : 20	3.17×10^{-2}	0.755
Akyuz *et al.* [94]	50 : 50	3.64×10^{-3}	0.67
Atun *et al.* [95]	20 : 5	23.40	0.90
Filipovic *et al.* [69]	10 : 1	3.63	0.91
	60 : 10	17.96	0.76

Table 25 is an example of how sorption behaviour of Cs varies under varying conditions of solid to liquid ratios. The values observed in this work are consistent with those reported by Atun *et al.* [95], due to the similarity in the solid to liquid ratios.

2.4.4. Sorption onto solid vs colloid

The sorption of metals on boehmite and montmorillonite, solid and colloidal phases, has been described by means of the distribution ratio in the linear range of the sorption isotherm.

The linearity of the sorption isotherm observed for Cs sorption on colloidal boehmite turned into non-linearity (at the same range of concentrations) when the sorption was carried out on the solid phase of boehmite. XRD diffractograms showed the same pattern for both phases, confirming that the mineral analysed was boehmite. Also, equal chemistries could be assumed in both colloidal and solid phases.

Assuming equal chemistries, one can expect differences in the sorptive behaviour to be due to differences in the surface area of the mineral. These differences are mainly the size; the specific surface area of the colloids is larger than that of the solid phase thereby increasing the number of surface sites and hence, increasing the sorption. In addition, saturation would be reached at higher concentrations of metal in solution. The same explanation would apply for Ni and Eu.

This qualitative description could be improved by a quantitative approximation. The R_d values for the sorption of metals on colloidal and solid surfaces studied herein are summarised below (Table 26). A scaling factor based on the ratio of specific surface areas was proposed by Wieland [14] and succesfully applied on the sorption of Cs, Sr and Th onto cementitious colloids. A similar approach is used herein, where not only the ratios of SSA are considered, but also the ratios of CEC and PEC. Due to the limited available data, further studies and deeper insight is necessary to persue a mathematical equation.

Table 26. Sorption of metals on boehmite and montmorillonite, solid and colloidal phase.

	R_d ($dm^3\ kg^{-1}$)		
Metal-Mineral	Colloid	Solid	Boehmite
Cs – boehmite	99.3 ± 9.1	26.4 ± 0.3	$\frac{SSA_{col}}{SSA_{sol}} = 46.33$
Ni – boehmite	298.9 ± 15.3	47.7 ± 1.1	
Eu – boehmite	13851	448.4 ± 8.6	$\frac{CEC_{col}}{CEC_{sol}} = 3.03$
Cs – montmorillonite	33.5 ± 0.7	114.7 ± 6.0	
Ni – montmorillonite	99.9 ± 19.4	164.4 ± 0.6	$\frac{PEC_{col}}{PEC_{sol}} = 20$
Eu – montmorillonite	4174.1 ± 164.4	4251.9 ± 427.8	

The increase of R_d value when the phase changes from solid to colloidal has already been stated. In addition, the increase was sharper as the cation charge increased. Thus, not only the surface area plays a role on the enhancement factor, but also the cation charge. Table 26 shows the values of the ratios between specific surface area (SSA), the PEC and the CEC of boehmite for the two phases studied, which are considered to play a key role in the relation between the distribution ratios of the two phases.

A first mathematical approach to the relationship of the distribution ratios could consist of a linear relationship between the R_d on the solid ($R_{d,sol}$) and the enhancement factor, which could be a direct proportion between the charge and a parameter related to either the ratio of surface areas, the ratio of CECs or the ratio of PECs. In equation 2.12, the charge of the metal is represented by *z* and *Y* represents the ratio of one of the properties of the surface. The results are shown in Table 27.

$$R_{d,col} = R_{d,sol} \times z \times Y$$ **Equation 2.13**

Table 27. Estimated values of R_d values for metal sorption on boehmite.

Experimental R_d ($dm^3\ kg^{-1}$)		Predicted $R_{d,colloid}$ ($dm^3\ kg^{-1}$)		
		$Y = \frac{SSA_{col}}{SSA_{sol}}$	$Y = \frac{PEC_{col}}{PEC_{sol}}$	$Y = \frac{CEC_{col}}{CEC_{sol}}$
99.3 ± 9.1	Cs	1223.1	528	80
298.9 ± 15.3	Ni	4419.8	1908	289
13851	Eu	62323.1	26904	4076

The first approach used consisted on using the ratios of SSA as the proportional factor relating both distribution ratios. This function of *Y* resulted in an overestimation of the $R_{d,col}$. A second function of *Y* was used by taking the ratios of the PEC, which also led to an overestimation of the $R_{d,col}$. Finally, taking the ratios of CEC as the proportional factor *Y*, yielded values of $R_{d,col}$ slighly lower than those observed experimentally.

2.5. Conclusions

Briefly in this chapter, reversibility studies were performed by batch experiments where desorption tests followed those of sorption. These studies were carried out using stable colloidal suspensions. Preliminary investigations showed the conditions in which stability of the colloidal suspensions was ensured. Parallel sorption and desorption studies were carried out on the solid phase of the mineral with the aim of obtaining a mathematical expression which would relate the sorption behaviour on colloid phases to that on solid phases.

The stability of boehmite and montmorillonite colloids was assessed as a function of pH and ionic strength. The results concluded that pH 7 and ionic strength 0.05 mol dm^{-3} were appropiate for sorption experiments.

The sorbents used for the sorption experiments were boehmite and montmorillonite colloids, and boehmite and montmorillonite solids. Boehmite (colloidal and solid

form) and solid montmorillonite were used as provided by the manufacturer, whereas montmorillonite colloids were extracted by repeated washes with electrolyte from the solid form. The sorption of Cs (mono-), Ni (di-) and Eu (tri-valent) on these minerals was investigated. Generally, the findings agreed with an increase of sorption with ionic charge. Sorption isotherms and later modelling showed a general linear behaviour of Cs, general non-linear behaviour of Eu and a linear sorption of Ni on boehmite (both phases), followed by a non-linear sorption on montmorillonite (both phases).

The three sorption isotherms used in modelling were the empirical models Langmuir, Freundlich and D-R models, which provided estimates of sorption capacity of the minerals and energy of sorption. In general, the results proved unsuccesful for the Langmuir model, due to an underprediction of the sorption capacities, but good fits for the Freundlich isotherm. The D-R isotherm predicted ion exchange as the sorption mechanism in general.

Desorption experiments showed that the sorption of metals on boehmite was partially reversible. The sorption of metals on montmorillonite was also partially reversible, although Eu exhibited low desorption values in both phases of montmorillonite. The reversibility did not depend on the ionic charge, as Ni showed the highest reversibility in most of the cases. The results from the desorption experiments carried out have been interpreted from a thermodynamic approach and these have shown the order of desorption of metals from colloids. However, the kinetics of desorption would be necessary for a thorough and complete knowledge of the desorption rates.

The partial reversibility may be explained by different sorption mechanisms, supported by many authors in literature; sorption by inner-sphere complexation, which leads to the formation of strong, chemical bonds; and sorption by outer-sphere complexation, which is described by weak, physical and electrostatic interactions between the metal and the mineral surface. On addition of the electrolyte, the metal ions bound via outer-sphere complexation were exchanged by the cations from the electrolyte, whereas the complexed metal ions remained bound to the mineral surface.

The R_d values were found to be dependent upon the solid to liquid ratio, increasing as this parameter increased, in agreement with other studies found in literature. Another influencing parameter was the background electrolyte. Changing the electrolyte from Na^+ to K^+ led to a decrease in sorption and an increase in desorption of Cs to boehmite colloids, thus concluding that the similarity in ionic size resulted in a greater competition for the sorption sites.

Measurements of the specific surface area, proton and cation exchange capacities indicated that the lower particle size of the colloids provided a higher specific surface area for colloids, explaining the higher sorption observed on colloidal particles.

An attempt to quantify the distribution ratio of the sorption of metals on colloids as a function of the R_d value on solids, charge and surface, was made. A simplistic, linear equation was proposed where the R_d value for the sorption of metals on colloids could be determined from the R_d value for the sorption of metals on solids, the ionic charge of the metal and the ratio of CEC between the colloidal and the solid particles of the mineral. However, this simplistic model could only be applied on the results obtained herein for boehmite. Thus, a single system is insufficient for testing a model and more measurements and mathematical processing is needed to continue this line of enquiry.

Chapter 3. COLLOID HUMATE TERNARY SYSTEMS

3.1. Introduction

Inorganic and organic colloids are ubiquitous components of the subsurface and are likely to affect the mobility of radionuclides through the Geosphere. The interactions of metals with two inorganic colloids have been investigated in the previous chapter. Humic acids (HA) play an important role in the migration of contaminant metals through the Geosphere, as they may also influence the binary interactions of metals with minerals.

The effect of HA on the sorption of metals onto solid surfaces has been widely investigated, and some examples can be found in Chapter 1. In general, the presence of HA in a ternary system constituted by the metal, HA and a surface, has been found to increase the sorption of the metal onto the given surface at low pHs but to hinder it at high pHs. Examples apply for mono-valent, as well as for multi-valent cations: Tl(I) sorption decreased on pyrolusite in the presence of HA [131]; fulvic acids (FA) decreased the sorption of Am(III) on silica, but increased it on alumina [132]. The influence of HA on Th(IV) sorption onto silica [133] and alumina [134] was found to increase at low pHs and decrease at intermediate and high pHs. Sorption of U(VI) on attapulgite increased at all pHs in the presence of HA [135]. Cruz-Guzman [136] found that HA enhanced the sorption of Pb(II) and Hg(II) on montmorillonite, but hindered it on ferryhydrite, due to the high affinity of HA for the mineral and consequent blocking of sites.

Fewer studies, however, have been carried out to investigate the influence of HA on the sorption of metals onto colloidal surfaces. As an example, the sorption of Cm(III) onto silica colloids was enhanced by HA at low pHs due to complexation of Cm to HA, but decreased at pHs between 6.5 and 8 due to competition of HA and sorption sites of silica for the metal. At higher pH Soumitra Kar *et al.*[137] reported an increase in the sorption of Cm(III) onto silica colloids. Singh *et al.* [138] reported as negligible the effect of HA on the sorption of metals onto magnetite colloids. Jain *et al.* [139], observed an enhancement in the sorption of neptunium onto hematite colloids in the

presence of HA at acidic pHs. These studies provide evidence that the effect of HA on metal sorption to colloids does not always follow the general trend observed for most of the solids.

Following the investigation of the interaction of colloids with contaminant metals, this chapter studies the influence of HA on the sorption of metals (Cs, Ni and Eu) onto boehmite colloids and focuses further on the applicability of the linear additive model (LAM) to the experimental results.

3.1.1. Linear additive model

The LAM is a mathematical model used to predict the sorption of metals onto surfaces in the presence of HA. The ternary system is the system in which metal cations, HA and the solid or colloid surface coexist. The different interactions are shown in Figure 44, where, for simplicity, HA molecules have been given a spherical shape. This example uses a solid surface.

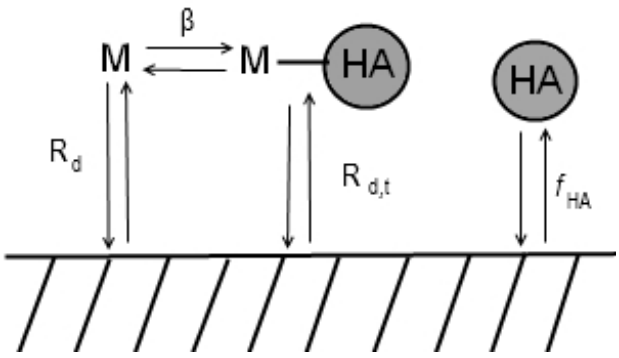

Figure 44. Interactions between metal cations (M), HA molecules and the surface of the solid.

The LAM assumes that the distribution coefficient for the ternary system ($R_{d,t}$) results as a combination of the distribution coefficients of the separate binary systems (β, f_{HA} and R_d). Several expressions have been proposed to determine $R_{d,t}$ values in ternary systems. For instance, Samadfam *et al.* [140] proposed the following expression for the LAM (as applied for solids):

$$R_{d,t} = \frac{R_d + \left(V/W\right) f_{HA} \beta [HA]}{1 + (1 - f_{HA}) \beta [HA]}$$ **Equation 3.1**

Where $R_{d,t}$ and R_d, in $dm^3\ kg^{-1}$, are the distribution coefficients for the ternary and binary metal-solid system, respectively, f_{HA} is the fractional sorption of HA onto the surface, β is the metal-humate stability constant, in mol dm^{-3}, V, in dm^3, and W, in kg, are the volume of sample and weight of solid, respectively, and *[HA]* is the concentration of HA, in mol dm^{-3}.

A slightly simpler model was proposed by Lippold *et al.* [141]:

$$R_{d,t} = \frac{R_d + f_{HA} \beta [HA]}{1 + \beta [HA]}$$ **Equation 3.2**

A series of assumptions are considered in both mathematical formulations of the LAM: [142,143,140,144]

- The individual sorption coefficients are independent of the metal concentration;
- The sorption properties or characteristics of the mineral are not affected by the presence of HA;
- Different molecular weight fractions of HA are neglected and sorption of HA is considered as a whole;
- Affinity of metals for mineral-bound HA and for dissolved HA are considered identical;
- The mass of mineral is much higher than the mass of mineral-bound HA;
- Electrostatic interactions at the mineral-water interface are neglected.

Although the LAM has been generally applied to model the influence of HA on the sorption of metals onto solids, in principle, its application could be extended to colloidal systems. However, the examples found to date in the literature report, in general, the failure of the model when applied to colloidal systems: Kumar *et al.*[145] observed an increase of Cs sorption on silica colloids at acidic pHs in the presence of HA. Although at first the LAM could not describe succesfully the effect of HA, the

use of two different stability constants for metal-humate complexation led to the success of the model. The two stability constants corresponded to the complexation of metal with dissolved HA in suspension and that of metal with surface-bound HA. Like this, the sorption of Cs onto silica colloids [145] and that of Tc (VII) onto alumina [146] were modelled by the LAM. However, this modification of the LAM did not satisfy the modelling of Cm(III) sorption onto silica colloids in the presence of HA [147]. Christl *et al.* [142] found that the additivity assumption underestimated the sorption of copper onto hematite colloids in the presence of HA.

This chapter aimed to study the influence of HA on metal sorption onto boehmite colloids. Further, an attempt to model the sorption with the LAM was made. With the objective of comparing the behaviour of metals on the colloids in the presence and absence of HA, the experimental conditions were the same as those used for the batch sorption experiments in the previous chapter.

3.2. Experimental

Before the investigation of the influence of HA on the sorption of metals onto boehmite colloids was started, the sorption of HA onto boehmite colloids was studied (see section 3.2.4). Special attention was given to the stability of boehmite colloids in the presence of HA, since initial tests provided experimental evidence of flocculation of the colloids taking place on addition of HA at a wide range of concentrations. Therefore, a study was carried out in which the stability of the colloids was followed by DLS or UV-Vis spectroscopy. Once the stability conditions were established, sorption experiments were carried out.

3.2.1. Preparation of reagents

Purified humic acid (Aldrich) [148] was used to prepare solutions of concentrations ranging 1 to 500 mg kg^{-1}. All the samples used were adjusted to pH 7 and ionic strength 0.05 mol dm^{-3} with NaCl.

Boehmite colloids were provided by Feralco Ltd. as a concentrated suspension. Aliquots were taken from there to prepare the suspensions for experimental study.

Gravimetric and spectrophotometric measurements were carried out to characterise the colloids. pH was fixed to 7 prior to any experimental measurement.

Metal solutions were prepared by dissolving the corresponding chloride salts in DI water. The solids used for each metal were: CsCl (BDH Laboratories AnalaR®), $NiCl_2$ (Fisher Scientific) and $EuCl_3$ (Sigma-Aldrich).

The pH and ionic strength were fixed to 7 and 0.05 mol dm^{-3} with NaCl (Sigma-Aldrich chemicals), respectively.

3.2.2. Preparation for measurement

UV measurements were taken using a UV Type Varian Cary Series 50 Bio Spectrophotometer. A quartz cuvette was filled with approximately 1 cm^3 HA sample and the absorbance spectrum was recorded at several wavelengths (254, 300, 350 and 400 nm).

Average size of the colloids was measured by dynamic light scattering (DLS) and was carried out in a Zeta Master S. An average of ten measurements were taken for each sample, except in the kinetic studies, where each recording corresponded to one measurement. A plastic cuvette was filled with approximately 3 cm^3 of sample.

Powder X-ray measurements were performed using Cu-Kα radiation (λ = 1.5418 Å) on a Bruker D8 diffractometer in reflection geometry and a Braun position sensitive detector. The sample was loaded onto a silicon zero background substrate and the data were collected in the range $5 < 2\theta < 90°$ with a step time of 1 second and step width of 0.014°. SEM pictures were taken in a LEO (Zeiss) 435VP Variable Pressure Digital Scanning Electron Microscope (SEM) at BGS.

pH measurements were carried out in a Jenway 350 pH meter. The instruments were calibrated prior to their use with three standard solutions (pHs 4, 7 and 10).

Samples were centrifuged in a Hermle Z206A centrifuge at 6000 rpm for 30 minutes. When necessary, samples were mixed using a Labnet VX100 Vortex mixer. The

filters used in all sorption and desorption experiments were supplied by Elkay (0.45 μm in pore size) and the plastic syringes used (5 cm^3) were provided by BD Plastipak. When used, the plastic syringes were filled with sample, the filter fitted to the end and the first 5 cm^3 of the filtered sample were discarded, collecting the following 2 cm^3 for radiometric measurement. Control experiments showed that sorption of activity to the syringe filters or to the centrifuge tubes did not take place.

Radionuclide assays (to an error of two sigma or better) were performed using either a Tricarb 1900TR Liquid Scintillation Analyzer (Packard Ltd) or a Cobra II Auto-Gamma Counter (Packard). The activities measured were transformed by mathematical operations into concentrations.

3.2.3. Stability of HA

Control experiments were carried out to measure the effect of centrifugation and filtration on HA solutions of different concentrations, ranging from 10 to 450 mg kg^{-1}. The UV-Vis absorbance of the solutions was measured at several wavelengths (254, 300, 350 and 400 nm). As humic acids have a range of molecular masses, the absorbance at one unique wavelength would not provide information about whether an important fraction of humic acids were being sedimented by centrifugation. Hence, the ratios between wavelengths were calculated and differences observed between these ratios would indicate any changes [149].

3.2.4. Stability of colloids in the presence of HA

To study the influence of HA on the sorption of metals onto colloidal boehmite, a stable suspension of humate-colloid was needed. The influence of HA on the stability of boehmite colloids (approximately 67 mg in 30 cm^3) was studied by measuring kinetically the average size of the colloids at pH 7 in the presence of varying concentrations of HA, ranging from 0 to 5, and 200 to 450 mg kg^{-1}. At higher concentrations of HA, UV-Vis spectroscopy was needed to monitor the stability of the sols, whereas at lower HA concentrations the stability was measured by DLS with the Zeta Master. For intermediate HA concentrations no spectroscopic measurements were carried out.

The same kinetic measurements were performed in sols containing approximately 11.4 mg of boehmite colloids and varying concentrations of HA (1 to 40 mg kg^{-1}). In this case, DLS was the only technique used to monitor the stability. The average size was measured every 50 seconds for 50 minutes.

3.2.5. Sorption of HA to boehmite

The extent of the sorption of HA onto boehmite was studied by means of batch experiments. The sorption of HA to both the colloidal and solid phases of boehmite was measured. The concentration of HA was measured using UV-Visible spectrometry at 254 nm. For this purpose, in triplicate, 20 cm^3 of HA were added to 10 cm^3 of boehmite colloids (total mass of colloids 33.5 mg). In the case of the sorption onto the solid phase of boehmite, 30 cm^3 of HA were added to 0.1 g of boehmite. The concentrations of HA were prepared to give a final concentration of 2 to 80 mg kg^{-1}. The samples were pH adjusted to 7.0 ± 0.4 by adding small amounts of HCl or NaOH 0.1 mol dm^{-3} and ionic strength 0.05 mol dm^{-3} with NaCl, and left to equilibrate for 24 hours, after which time the samples were centrifuged for 30 minutes at 6000 rpm. 5 cm^3 of supernatant were collected with a syringe, to be filtered with a 0.45 μm syringe filter. The first 2 cm^3 were discarded and the following 3 cm^3 of filtered suspension were collected in a quartz cuvette for UV measurement.

The absorbance of HA is related to the concentration through the calibration curve (see section 3.3.1.). Hence, the concentration of HA adsorbed to boehmite could be calculated as the difference between the initial HA added and the HA measured in solution after the equilibration time.

3.2.6. Sorption of metals to boehmite in the presence of HA

The effect of HA on the sorption of different metals (*i.e.* Cs, Ni and Eu) onto colloidal boehmite was studied by performing batch experiments where 1 cm^3 of metal solution and 1 cm^3 of HA were added to 10 cm^3 of colloidal boehmite (33.5 mg). 0.1 cm^3 radioactive spike were added (0.83 kBq cm^{-3}) (see Table 1 in Chapter 2

for isotopes used). The metal solutions were prepared so that the final concentration of metal ranged from 10^{-6} to $4x10^{-3}$ mol dm^{-3}. In a similar manner, HA solutions were prepared so that the final concentrations in suspension would be 0, 1 and 2 mg kg^{-1}. The corresponding volumes of metal and HA solutions were added within one minute to the boehmite suspension, minimising the effect produced by the order of addition. Pre-equilibration of the colloids with HA has been shown to influence the sorption of metal onto colloids [150]; however, for a better comparison of the results with those found in Chapter 2, this factor was not assessed.

The pH was adjusted to 6.8 ± 0.1 and the ionic strength was adjusted with NaCl to 0.05 mol dm^{-3}. The samples were left to equilibrate for 24 hours, after which, the samples were centrifuged for 30 minutes at 6000 rpm. An aliquot from the supernatant was filtered through a 0.45 μm filter and 2 cm^3 were measured for activity. The collected data were related to the concentration of metal left in solution by the following equation:

$$[M]_{soltn} = \frac{A_{sample}}{A_{spike}}[M]_i \qquad \textbf{Equation 3.3}$$

Where $[M]_{soltn}$ is the concentration of metal left in solution after the sorption experiment, A_{sample} is the activity of the sample, A_{spike} is the activity of a reference sample where no sorption process took place; and $[M]_i$ is the initial concentration of metal introduced in the ternary system. The concentration of metal bound was calculated as the difference between the initial concentration of metal and the concentration left in solution after the sorption experiment,

$$[M]_{bound} = [M]_i - [M]_{soltn} \qquad \textbf{Equation 3.4}$$

Note that the $[M]_{bound}$ considers not only the metal bound to the colloid but also the metal-humate complexes bound to the colloid. In a similar manner, the $[M]_{soltn}$ includes both the concentration of free metal cations in solution and metal-humate complexes, also in solution.

3.3. Results and discussions

3.3.1. Calibration curve of HA

The concentration of HA was measured by UV-Vis spectroscopy in all the experiments. The calibration curve was plotted for wavelengths varying from 254 to 400 nm, for HA concentrations ranging from 10 to 200 mg kg^{-1} (Figure 45). The calibration curve showed the values of corrected absorbance. Due to the high absorbance recorded at high concentrations of HA, dilution was necessary from HA concentrations above 80 mg kg^{-1}. The absorbances for samples of HA concentrations above 80 mg kg^{-1} were corrected for the dilution factor and data appear like "corrected absorbances" in the calibration curves. All the calibration curves were fitted by linear regression method and the R^2 of the fit was above 0.99 in all the cases.

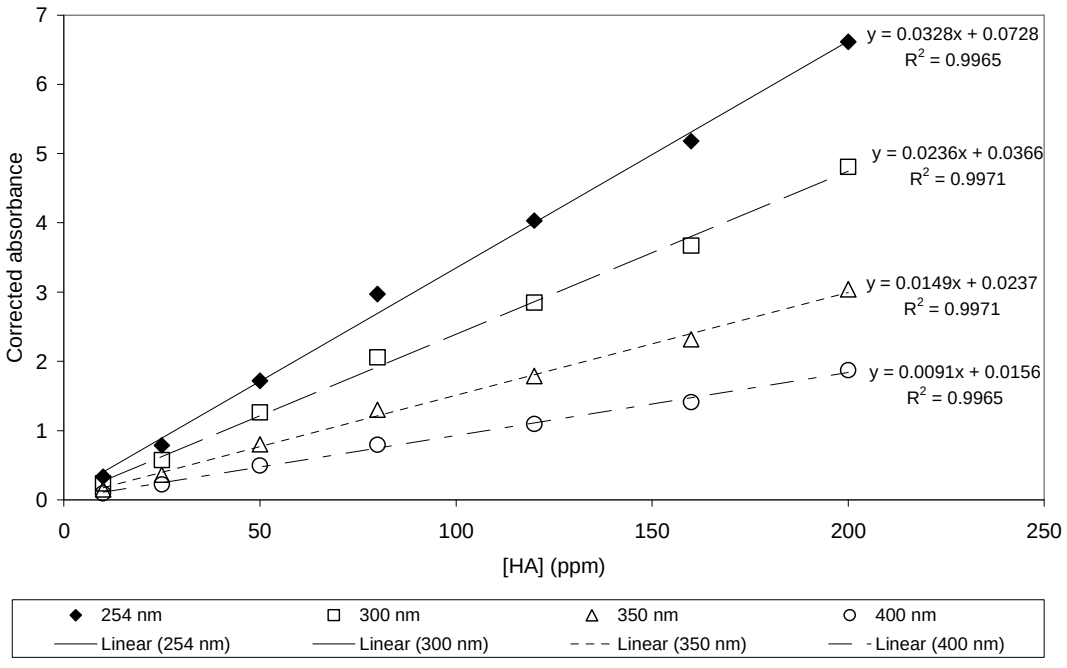

Figure 45. HA UV calibration curves

The limit of detection (LOD) and limit of quantification (LOQ) could be calculated as $LOD = \frac{3 \cdot SD}{m}$ and $LOQ = \frac{10 \cdot SD}{m}$ [151], where *SD* is the standard deviation of the blank solution, this being the background solution with no HA, and *m* the slope from

the calibration curves. The standard deviation of the blank solution was measured as $7x10^{-4}$ mg kg^{-1}. These values were calculated for the calibration curve measured at 254 nm; the LOD and LOQ were 0.0640 and 0.2134 mg kg^{-1} HA, respectively.

3.3.2. Stability of HA

The UV-Vis absorbance of several HA solutions was measured at 254, 300, 350 and 400 nm. The effects of centrifugation and filtration were studied by comparing the ratios of the absorbances at 300, 350 and 400 nm divided by the absorbance at 254 nm. The results for the effect of the different treatments applied to the HA solutions at 254 nm are shown in Figure 46. The ratios of absorbances as a function of centrifugation and filtration are shown in Figure 47.

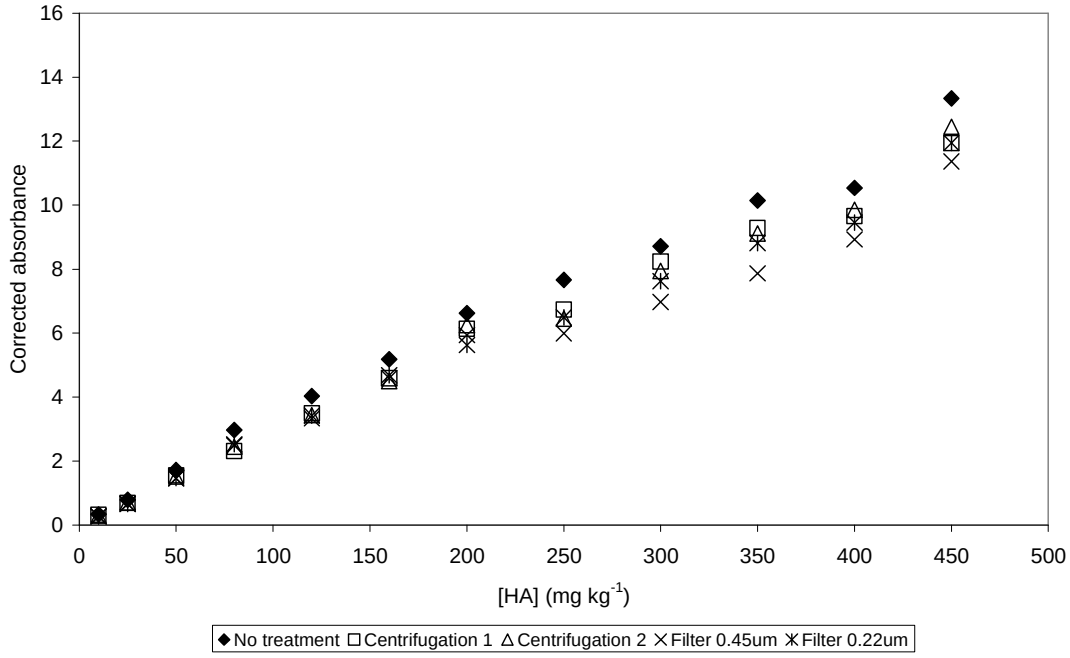

Figure 46. Effect of treatments on the absorbances of HA at 254 nm.

Figure 46 shows the corrected absorbances of HA measured at 254 nm after being centrifuged twice and filtered through 0.45 and 0.22 μm filters. The differences with the original absorbances (labelled as "no treatment" in Figure 46) were not significant at low HA concentrations, but increased slightly with HA concentration. The decrease of absorbance occurred after the first centrifugation process, suggesting that as the HA concentration increased, sedimentation was taking place. Further

centrifugation or filtration processes did not yield significant differences in the absorbance until a HA concentration of 250 mg kg^{-1}, when the absorbances decreased slightly with each process.

Due to the fractionation of HA, physical processes like centrifugation and filtration could affect the different molecular size fractions. The results observed in Figure 46 suggested sedimentation was taking place. This could be due to sedimentation of the bulk or due to fractionation of HA. In order to find out where the sedimentation originated, the ratios of absorbances were plotted against the HA concentration (Figure 47).

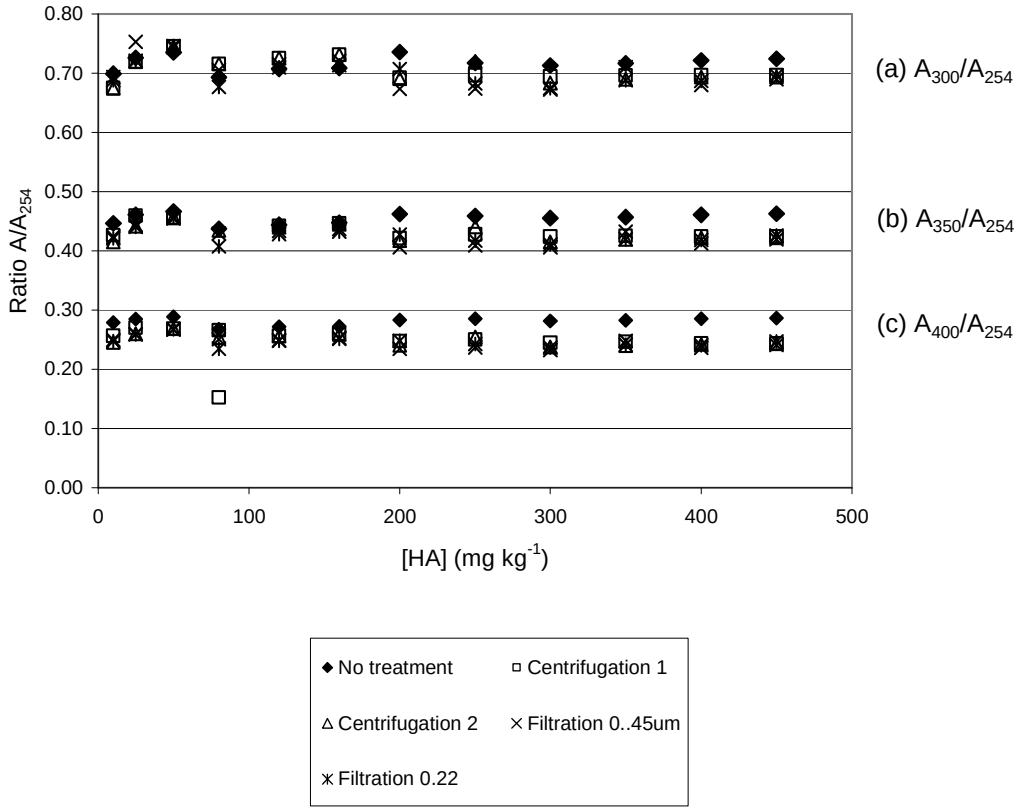

Figure 47. Effect of centrifugation and filtration on the ratios of UV-Vis absorbances for HA solutions at concentrations 10 to 450 mg kg^{-1}. (a) Ratio A_{300}/A_{254}, (b) Ratio A_{350}/A_{254} and (c) A_{400}/A_{254}.

The ratios between the absorbances at 300, 350, 400 nm and the absorbance at 254 nm decreased in value as the wavelength increased, as expected due to the decrease in the absorbance of HA with increasing wavelengths. A slight decrease in the ratios

was observed at higher HA concentrations after the different treatments, suggesting that fractionation of HA was taking place after centrifugation.

3.3.3. Stability of humate-boehmite suspensions

Stable humate-boehmite suspensions were needed to carry out the batch sorption experiments. This section reports the behaviour of colloidal boehmite when different concentrations of HA, ranging from 1 to 500 mg kg^{-1} were added. The stability of the humate-boehmite suspensions was measured by DLS as a function of time and HA concentration. Two different concentrations of boehmite colloids were used for the kinetic study: 67 and 11 mg per 10 cm^3. The total volume used for the stability experiments was 10 cm^3.

The colloidal suspension containing 67 mg of boehmite showed signs of destabilisation when concentrations of HA above 5 mg kg^{-1} were added. The increase in the average size with time, suggesting loss of stability, can be observed in Figure 48.

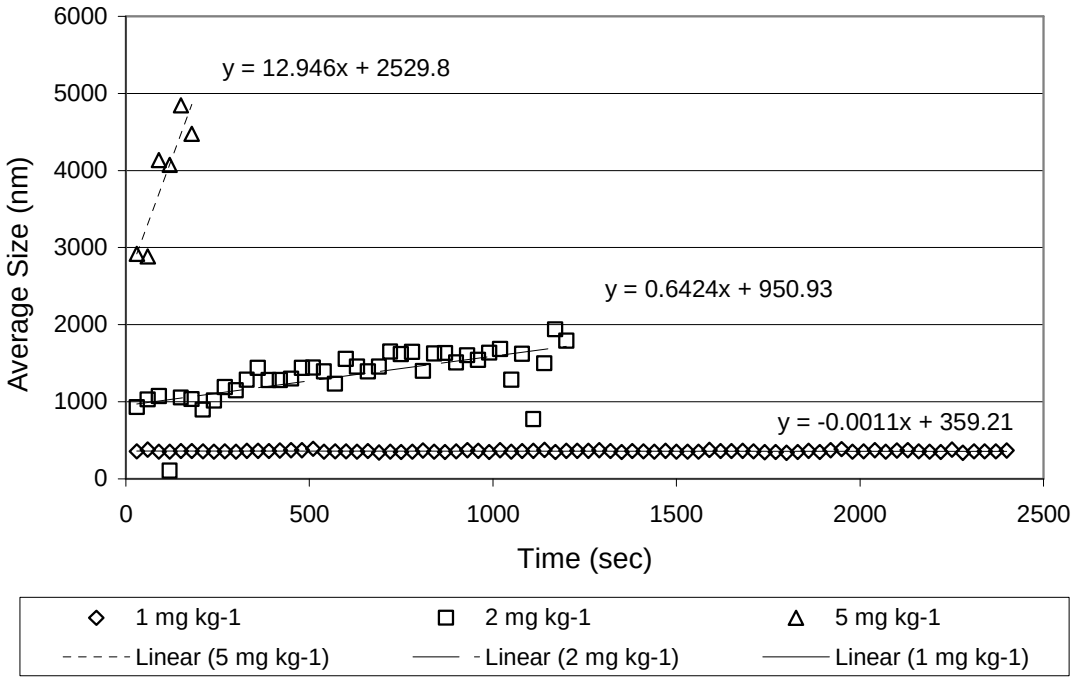

Figure 48. Stability of Boehmite (67 mg) HA suspensions followed by DLS measurements of average size.

Figure 48 shows the kinetic evolution of the average size with increasing concentrations of HA. The three different HA concentrations caused different responses on the colloidal suspension. In the presence of 1 mg kg^{-1} HA, the average size of boehmite was constant with time, suggesting stability of the suspension. In the presence of 2 mg kg^{-1} HA, the average size increased with time, suggesting flocculation was slowly taking place. When the HA concentration increased to 5 mg kg^{-1}, the average size quickly increased with time, indicating almost immediate flocculation of the colloids. Further addition of HA to boehmite colloids resulted in flocculation within five minutes. The average size could not be measured due to the high polydispersity. When HA was added in concentrations above 5 mg kg^{-1}, the scattering of the colloidal suspension was measured kinetically by UV spectroscopy. This technique recorded a constant high absorbance, which corresponded to scattering of the light rather than absorbance, until the particles flocculated, at which time no more scattering was detected. From the UV measurements, the time taken for the absorbance to fall to zero was used as an indication of stability.

As the added HA concentration increased, the time needed for flocculation to be detected also increased, as shown in Table 28. This suggested that the time for the binary humate-boehmite suspension to lose stability increased as the HA concentration increased, suggesting that at larger HA concentrations, the binary sol would remain stable. However, the HA concentration necessary for the system to be stable during 24 hours was not reached in these experiments.

Table 28. Time of flocculation for boehmite colloids (67 mg) in the presence of increasing concentrations of HA measured by UV-Vis spectroscopy.

[HA] mg kg^{-1}	Time of flocculation (min)
200	59.58
250	66.00
300	104.66
400	259.06

The kinetic stability of a humate-boehmite suspension containing 11 mg boehmite in 10 cm^3 was followed by DLS. Increasing concentrations of HA were added. The

average size of the colloids was recorded as a function of time and HA concentration (Figure 49).

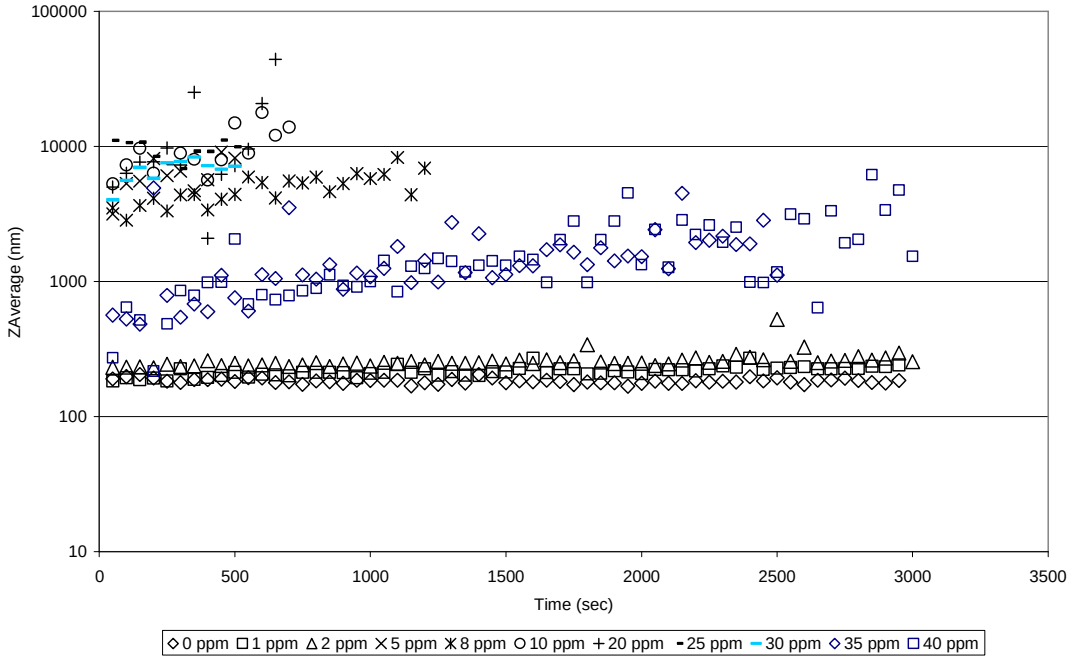

Figure 49. Kinetic stability of boehmite colloids (11 mg) in the presence of varying concentrations of HA at pH 7 and I 0.05 mol dm^{-3}.

Figure 49 shows three distinct regions:

- Beginning from the bottom, the first series of data show constant values of average size of 184 ± 8 nm. These data points corresponded to boehmite colloids in the presence of 0, 1 and 2 mg kg^{-1} HA.
- The top set of data points, rather scattered due to high polydispersity, corresponded to HA concentrations between 5 and 30 mg kg^{-1}. In this region, boehmite sols were unstable, suggested by the scattered values of data and the high values of average size. For some of the data, only a few points were shown, due to the high polydispersity of the samples.
- The middle set of data points, in blue, corresponded to higher concentrations of HA, *i.e.* 35 and 40 mg kg^{-1}. In this range of concentrations the average size decreased towards lower values and even though the results were slightly scattered, the data points showed a tendency to a more stable system.

A last kinetic experiment was performed on the binary system constituted by 30 mg boehmite in 10 cm^3 and 500 mg kg^{-1} HA. The suspension was followed kinetically by DLS for 10 hours. The average size and kcounts evolution are shown in Figure 50.

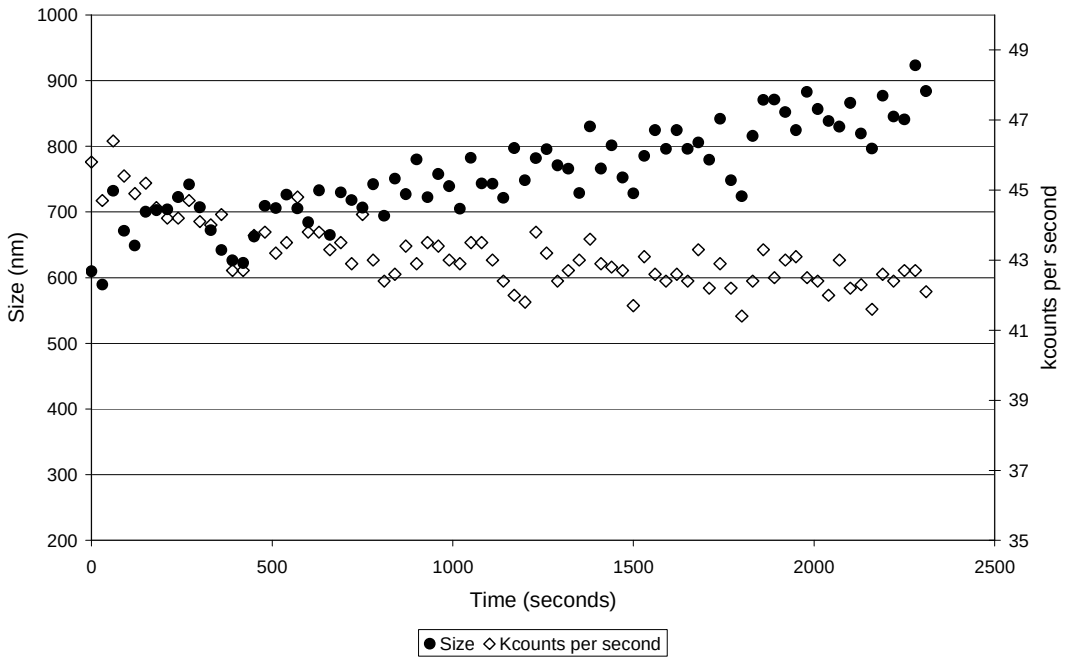

Figure 50. Kinetic stability of boehmite suspension in the presence of 500 mg kg^{-1} HA.

Figure 50 showed an increase in the average size, with the consequent decrease in counts per second, suggesting a slow decrease in the stability of the suspension. After 24 hours, the average size was 1338.9 ± 217.4 nm, the counts were 44.0 ± 1.0 and the suspension had a polydispersity index of 0.505 ± 0.087. The results suggested that coagulation had taken place. However, the remaining particles in suspension, despite being above the colloidal range, remained stable at that size.

The kinetic studies have shown a general trend for both suspensions: addition of low concentrations of HA did not alter the stability of the system, but as the HA concentration increased, the system lost stability and the colloids flocculated. However, further addition of HA resulted again in a stable system. As mentioned in Chapter 1, the stability of colloids was ensured as long as the repulsive forces were higher than the attractive forces. Applied to the binary system studied herein, boehmite colloids have a positively charged surface, which may readily interact with

HA, which possesses many negatively charged functional groups. This electrostatic attraction might have caused the particles to overcome the repulsive forces, leading to flocculation. The overall charge of boehmite colloids and HA, separately, were measured by zeta potential (Table 29).

Table 29. Zeta potential of boehmite colloids, HA and binary humate-boehmite suspension.

	HA concentration (mg kg^{-1})	Zeta potential (mV)
Boehmite 30 mg / 10cm^3	0	21.8 ± 2.9
HA	10	- 42.0 ± 3.6
Boehmite – HA	500	- 35.5 ± 3.4

In the absence of HA particles, boehmite colloids were stable in suspension due to the repulsive electrostatic interactions. As the HA concentration in suspension increased, electrostatic attractive interactions between the particles increased, lowering the zeta potential and leading to coagulation. Further increase in the HA concentration, above a certain threshold, perhaps resulted in electrostatic repulsion between HA particles and these were more abundant than the attractive forces. Table 29 shows the negative zeta potential of the binary humate-boehmite system, suggesting the dominance of electrostatic repulsions between negative charges.

The concentration of boehmite colloids used for the batch sorption experiments was 30 mg in 10 cm^3. Given the results observed in this section, the HA concentrations chosen to study the effects of HA on metal sorption onto boehmite colloids were 1 and 2 mg kg^{-1}, in order to ensure stability in the ternary system.

3.3.4. Sorption of HA to boehmite

The sorption of HA onto boehmite was studied by adding increasing concentrations of HA to colloidal (33.5 mg) and solid (100 mg) boehmite. After the equilibration time, the suspensions were centrifuged for 30 minutes at 6000 rpm and the supernatant was measured by UV-Vis spectroscopy to determine the HA in solution. The results are shown as a sorption isotherm in Figure 51. The sorption isotherm allowed the determination of f_{HA}, which is a parameter used in the LAM equation.

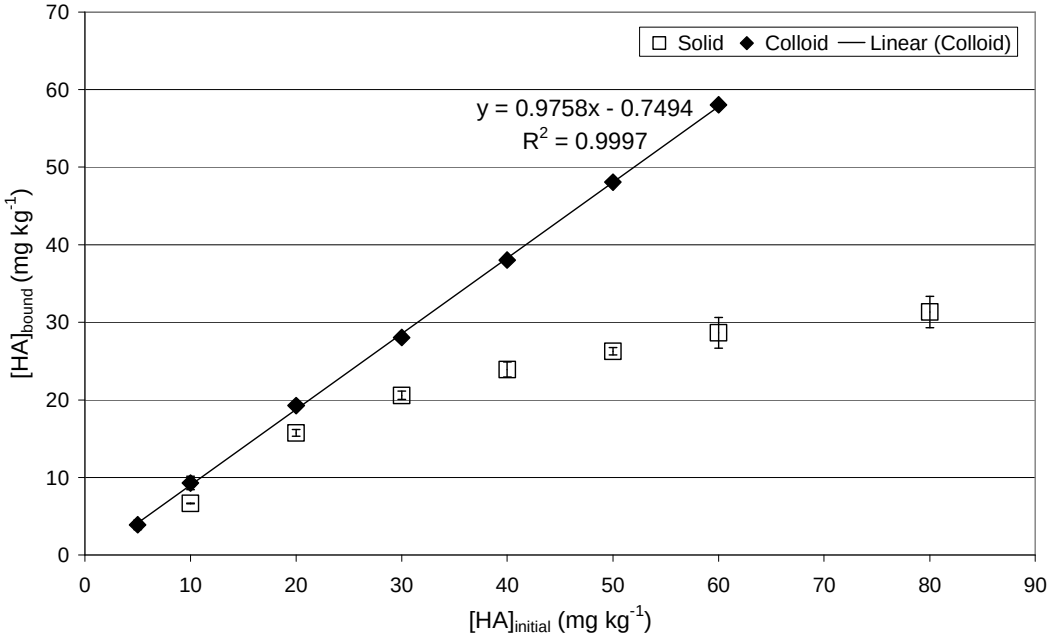

Figure 51. Sorption isotherm of HA to colloidal (30 mg) and solid (100 mg) boehmite measured by UV-Vis spectroscopy at 254 nm.

Figure 51 shows the difference in adsorption behaviour of HA to the colloidal and the solid phases of boehmite. The sorption isotherm shows the concentration of bound HA as a function of the initial concentration of HA added to suspension. As the concentration of HA increased, the solid phase of boehmite became saturated with HA, whereas the colloidal phase of boehmite continued to adsorb HA. This saturation was observed as the isotherm for the solid phase tended to curve at higher concentrations of HA (white), as opposed to the linear isotherm for sorption of HA onto colloidal boehmite (black).

The sorption isotherm also shows the higher adsorption capacity of colloids due to the higher surface area. When saturation occurred on the solid phase, the colloidal phase continued to adsorb HA molecules. Furthermore, no signs of saturation could be observed in the range of concentrations studied. The linear curve was fitted; the slope represented the fraction of HA bound to the colloids; moreover, multiplied by 100 it would yield the percentage of HA bound to the boehmite colloids. The experimental result showed high, almost complete sorption of HA to boehmite colloids, as f_{HA} = 0.976 ± 0.006, which could be explained by the overall positive charge of boehmite and the overall negative charge of HA (as shown by Table 29). This neutralisation of charge, however, led to the flocculation of colloids; section

3.3.3 discussed in more detail the HA concentrations at which the suspension lost stability. Therefore, the validity of the sorption isotherm and, hence f_{HA}, is limited to the stability of the suspension. Further discussions are made in section 3.3.6.1, where the applicability of the LAM is tested.

The binding mechanism of HA to boehmite surfaces is not yet clear. Several authors have proposed ligand exchange mechanism [88,144,152], as well as outer sphere complexation [153] and cation bridging [154]. Due to the positive overall charge of the boehmite surface and the negative charge of HA, under acidic and neutral conditions, electrostatic interactions can take place [88,152,155]. Varadachari *et al.* [154] confirmed by IR and crystallographic techniques the involvement of OH groups as a mode of binding of HA to boehmite, in the manner AlO – H^+/M^+ – HA, acting as bridges for HA. Carlsen *et al.* [156] found that HA bound to alumina surface via carboxilic groups present in the smaller molecular weight fractions in HA.

3.3.5. Sorption of metals onto boehmite in the presence of HA

The influence of HA (0, 1 and 2 mg kg^{-1}) in the sorption of three metals (Cs, Ni and Eu) onto colloidal boehmite (33.5 mg in 10 cm^3) was studied by batch experiments. The isotherms were calculated and the R_d values calculated and compared. The corresponding isotherms for sorption of metals onto 0, 1 and 2 mg kg^{-1} HA are shown together for each metal. Moreover, the linear curves were fitted by the least squares method and its parameters are shown in the figures.

3.3.5.1. Sorption of Cs

The influence of HA on the sorption of Cs onto boehmite colloids was studied by means of batch experiments. The sorption isotherms are shown in Figure 52.

Figure 52 shows the sorption isotherms for Cs sorption onto boehmite colloids in the presence of 0, 1 and 2 mg kg^{-1} HA. All sorption isotherms are linear in the range of concentrations studied, indicating that saturation was not reached. The R_d values correspond to the slopes of the linear curves and yielded 6.7 ± 2, 15.5 ± 0.8, and 5.2 ± 0.6 dm^3 kg^{-1} in the presence of 0, 1 and 2 mg kg^{-1} HA, respectively. Clearly, the R_d

values decreased as the concentration of HA increased, *i.e.* the higher the HA concentration, the lower the sorption of Cs to boehmite colloids.

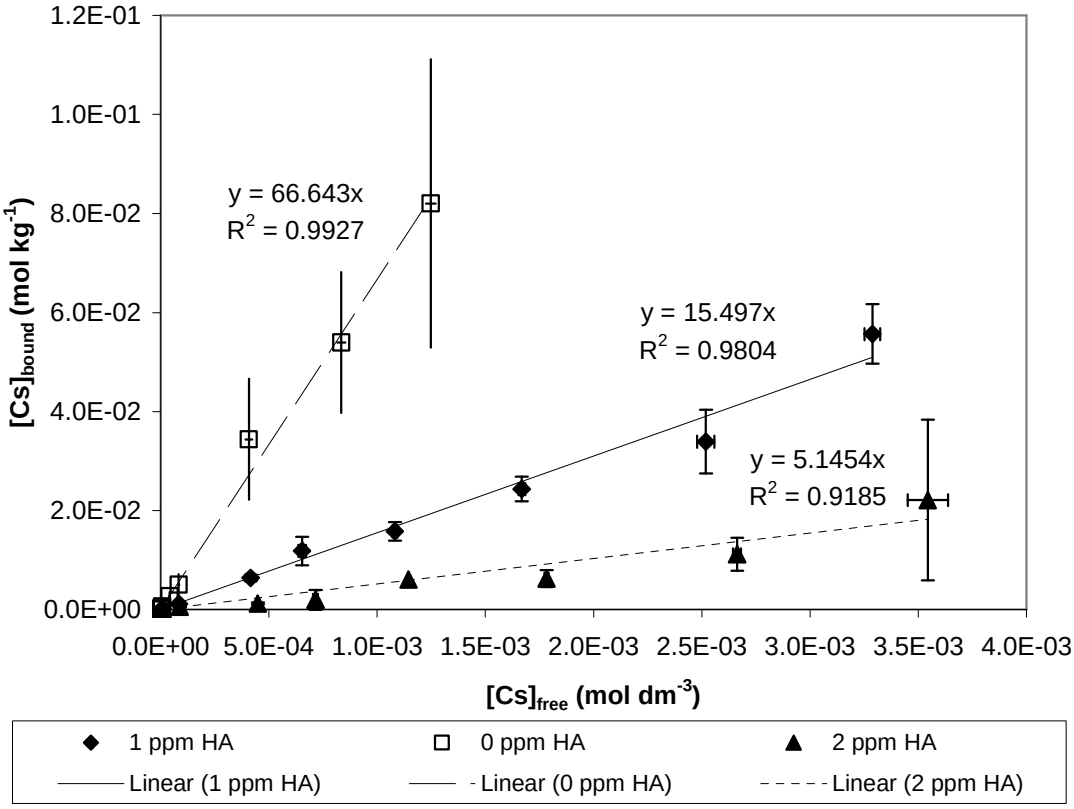

Figure 52. Sorption of Cs to boehmite colloids at pH 7 and ionic strength 0.05 mol dm^{-3} in the presence of 0, 1 and 2 mg kg^{-1} HA.

3.3.5.2. Sorption of Ni

The influence of HA on the sorption of Ni onto boehmite colloids in the presence of HA was studied.

Figure 53 shows the sorption isotherms for Ni sorption onto boehmite colloids in the presence of increasing concentrations of HA (0, 1 and 2 mg kg^{-1}). The sorption in the absence of HA was significantly higher than that in the presence of 1 and 2 mg kg^{-1} HA. A separate figure in the top left corner in Figure 53 shows the sorption isotherms for Ni in the presence of 1 and 2 mg kg^{-1} HA. The slopes of the linear isotherms for the three concentrations of HA yielded the R_d values, which were 292 ± 11, 58.1 ± 6.0 and 20.3 ± 0.9 dm^3 kg^{-1} for 0, 1 and 2 mg kg^{-1} HA, respectively. HA

decreased significantly the sorption of Ni onto the surface of boehmite colloids at pH 7, as observed by Strathmann *et al.* [150], who studied the effect of fulvic acids (FA) on the sorption of Ni onto boehmite.

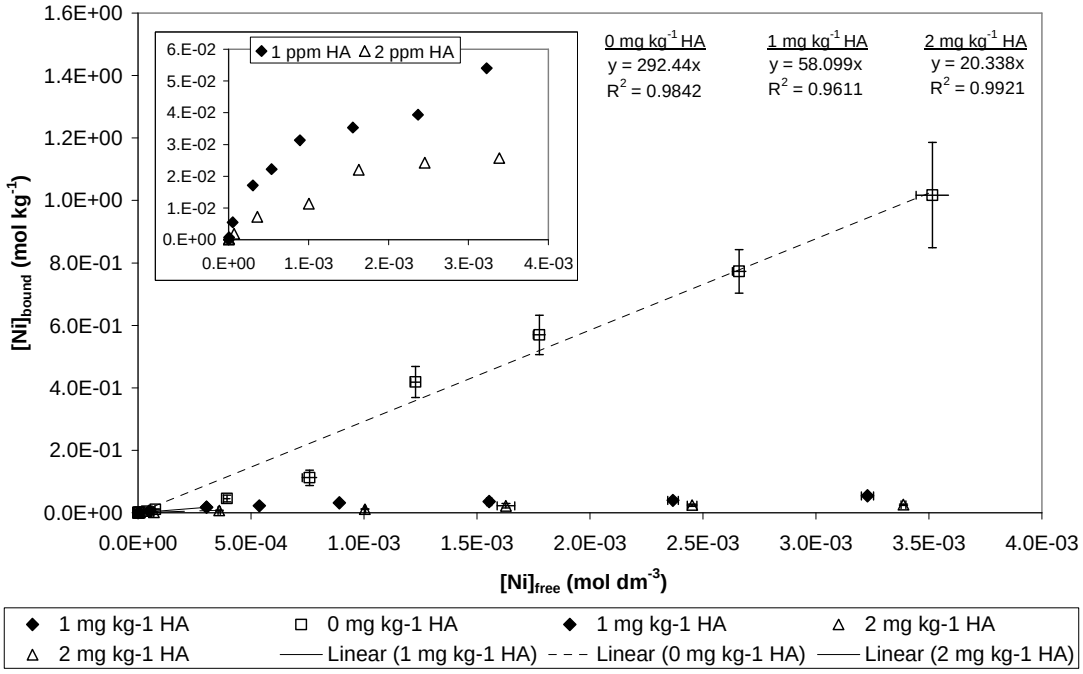

Figure 53. Sorption of Ni to boehmite colloids at pH 7 and ionic strength 0.05 mol dm^{-3} in the presence of 0, 1 and 2 mg kg^{-1} HA.

From Figure 53 it can be seen that the sorption isotherm for Ni in the absence of HA is linear, whereas in the presence of small concentrations of HA, boehmite colloids became saturated with Ni given the same range of concentrations. Both the decrease in the R_d values and the increase in saturation suggest that HA is hindering strongly the sorption of Ni onto boehmite colloids.

The tendency to saturation in the presence of HA could be due to a decrease on the available sites on the boehmite surface for Ni^{2+} ions, presumably due to blocking of the sites by HA. Given this assumption, the surface of boehmite colloids would become saturated by the metal ions at lower metal concentration.

3.3.5.3. Sorption of Eu

The effect of increasing concentrations of HA on the sorption of Eu onto boehmite colloids was studied. The sorption isotherms for the different HA concentrations are shown in Figure 54.

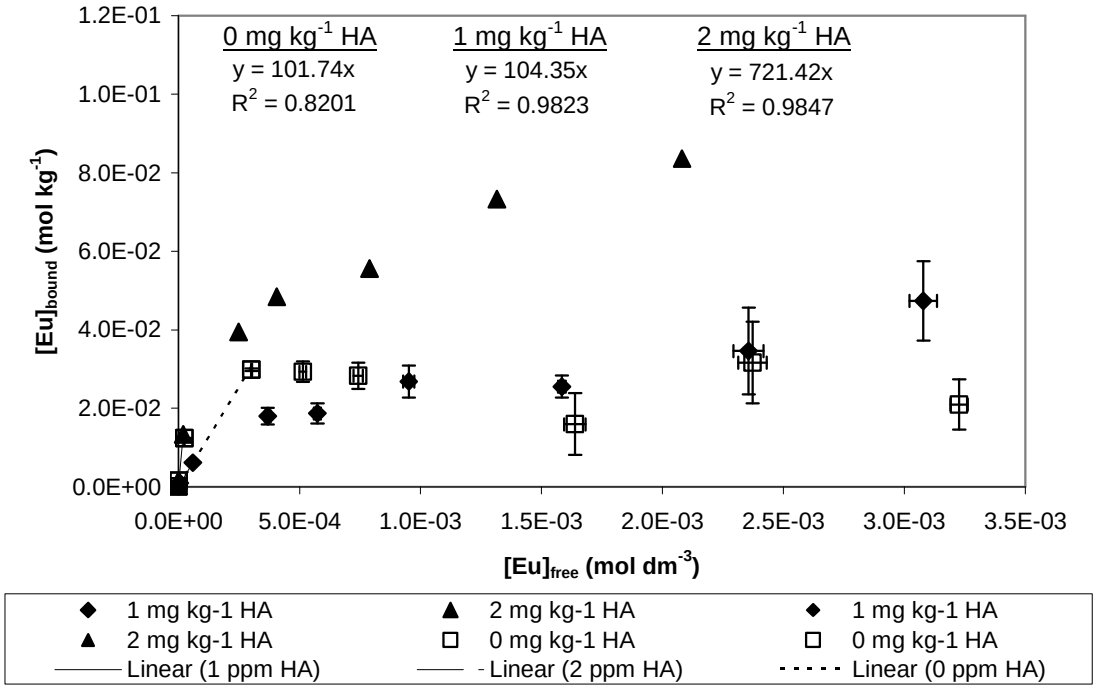

Figure 54. Sorption isotherm for Eu sorption on boehmite colloids in the presence of HA (0, 1 and 2 mg kg^{-1}) at pH 7 and ionic strength 0.05 mol dm^{-3}.

Figure 54 shows the influence of increasing concentration of HA on the sorption isotherms for Eu sorption on boehmite colloids. In the absence of HA the sorption isotherm shows a sharp increase but quickly reaches saturation, similarly to the sorption isotherm in the presence of 1 mg kg^{-1} HA. This analogy is reflected in the R_d value, as both yielded 102 ± 22 and 104 ± 8 dm^3 kg^{-1}, respectively. Further addition of HA (2 mg kg^{-1}) enhanced the sorption of Eu^{3+} to boehmite colloids, as reflected by the R_d value of 721 ± 53 dm^3 kg^{-1}.

3.3.5.4. Discussions

In the case of Cs and Ni the sorption isotherms showed a significant decrease of the R_d values in the presence of HA. In the case of Eu, the R_d values increased at higher

concentrations of HA studied. A table summarising data obtained from the sorption isotherms is shown below (Table 30).

Table 30. R_d values for Cs, Ni and Eu sorption in the presence of 0, 1 and 2 mg kg^{-1} of HA.

	0 mg kg^{-1} HA		1 mg kg^{-1} HA		2 mg kg^{-1} HA	
	R_d value	Regression Fit (R^2)	R_d value	Regression Fit (R^2)	R_d value	Regression Fit (R^2)
Cs	66 ± 2	0.9927	15.5 ± 0.8	0.9804	5.2 ± 0.6	0.9185
Ni	292 ± 11	0.9842	58 ± 6	0.9611	20.3 ± 0.9	0.9921
Eu	102 ± 22	0.9847	104 ± 8	0.9823	721 ± 53	0.9847

In general terms, the R_d value increased with the charge of the metal, even in the presence of HA. HA had a negative effect on the sorption of metals onto boehmite colloids, hindering the sorption, perhaps by blocking the sorption sites of the colloid. As the concentration of HA increased, this hinderence was stronger, except in the case of Eu, where the presence of 2 mg kg^{-1} HA enhanced the sorption of Eu onto boehmite colloids.

Organic coatings (humic and fulvic substances, organic polymers) have been shown to inhibit Cs sorption on reference clays like montmorillonite, illite or kaolinite (all solids) [157,123,158,159]. Rigol *et al.* [158] suggested the blocking of the specific sites of the mineral by organic compounds, limiting in this way the sorption of Cs. Wang *et al.* [160] explained the decrease in sorption of Cs onto γ-Al_2O_3 in the presence of HA due to complexation of Cs to free HA in solution.

The high sorption of HA to boehmite colloids observed in Figure 51 suggested that the concentration of free HA in solution would be limited. Therefore, the blocking of specific sites by HA seems a more plausible explanation, since interaction of Cs with HA has been reported as weak [159] and negligible at pH 8 [138]. These results would further suggest that HA sorbs onto boehmite colloids blocking the sorption sites for Cs^+ ions to sorb onto. Although the referenced investigations were carried out on solid surfaces, the same explanation could be applied to colloidal surfaces.

Ni has been reported [150] to bind to boehmite through inner-sphere complexation, binding directly to aluminol groups. In the presence of FA, Strathmann and Myneni [150] reported the formation of ternary complexes and binding of Ni where the organic ligand acted as a bridge between the metal and the solid surface. Assuming a similar behaviour from HA, this finding could suggest that HA blocked the sorption sites of boehmite, thereby reducing the sorption of Ni to boehmite colloids.

In the absence of any organic ligands, Eu was found to sorb onto alumina via the formation of hydroxo complexes with the surface [161]. In the presence of HA, Eu-humate complexes were formed that precipitated on the surface of compacted bentonite [162], being unable to diffuse into the bentonite structure.

The decreased sorption of metals onto boehmite colloids in the presence of HA could be mainly due to two reasons: the affinity of the metal for the humic was higher than that for the colloid, thereby forming metal-humate complexes that would remain in solution; or, due to the high electrostatic attraction, HA sorbed onto the boehmite sorption sites preventing the metals from sorbing onto them, hence remaining in solution as free metal ions. From previous studies found in the literature, it appears that the second reason would explain the experimental findings.

3.3.6. Surface imaging of boehmite colloids

Two different techniques, XRD Powder Diffraction and SEM, were used to analyse the surface of the boehmite in the presence and in the absence of HA to test for any surface changes induced by HA.

Figure 55 shows two XRD diffraction patterns, one for boehmite colloids and another for the humate-boehmite dried powders. The experimental preparation was identical for both samples, which were oven dried and kept in a dessicator. The results showed less intense peaks for the humate-boehmite colloids than for the colloids alone. This could be due to the smaller amount of sample from the humate-boehmite colloids available for the measurement, or due to surface changes caused by the HA. The ratios of the peaks were compared to distinguish amongst the two possible reasons (Table 31). The results showed an increase of the ratio with an

increase on the angle. The peaks from the humate-boehmite sample were weaker in signal as the angle increased. A linear increase in the ratios of the signals could suggest that HA induced changes in the structure of boehmite. However, these results are not conclusive.

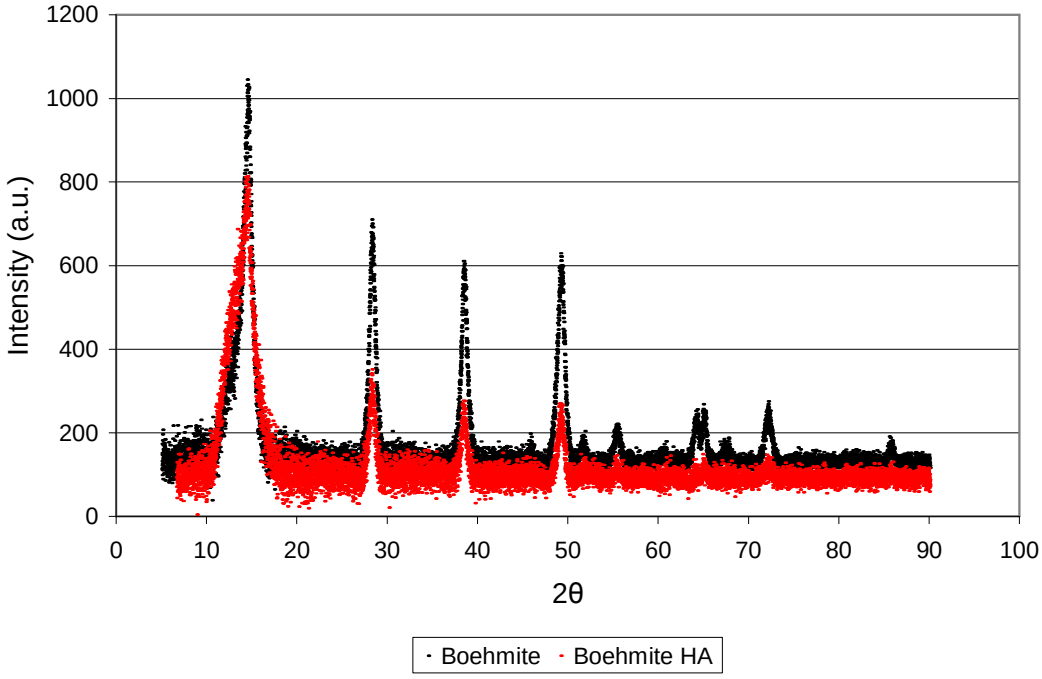

Figure 55. XRD pattern of colloidal boehmite and HA-bound boehmite.

Table 31. Intensity ratios for XRD peaks on boehmite and humate-boehmite colloids.

2 θ	Ratio	2 θ	Ratio
14.4	1.26	38.5	2.19
28.3	1.97	49.2	2.33

SEM images were taken from the boehmite colloids alone and the humate-boehmite colloids. The results are shown in Figure 55, where the presence of aggregates on the surface can be observed when HA was bound to the boehmite. These aggregates, however, could be due to the preparation process prior to the imaging. The SEM image for boehmite colloids showed a smoother surface. These results were not able to indicate whether significant changes on the surface of boehmite took place due to interaction with HA.

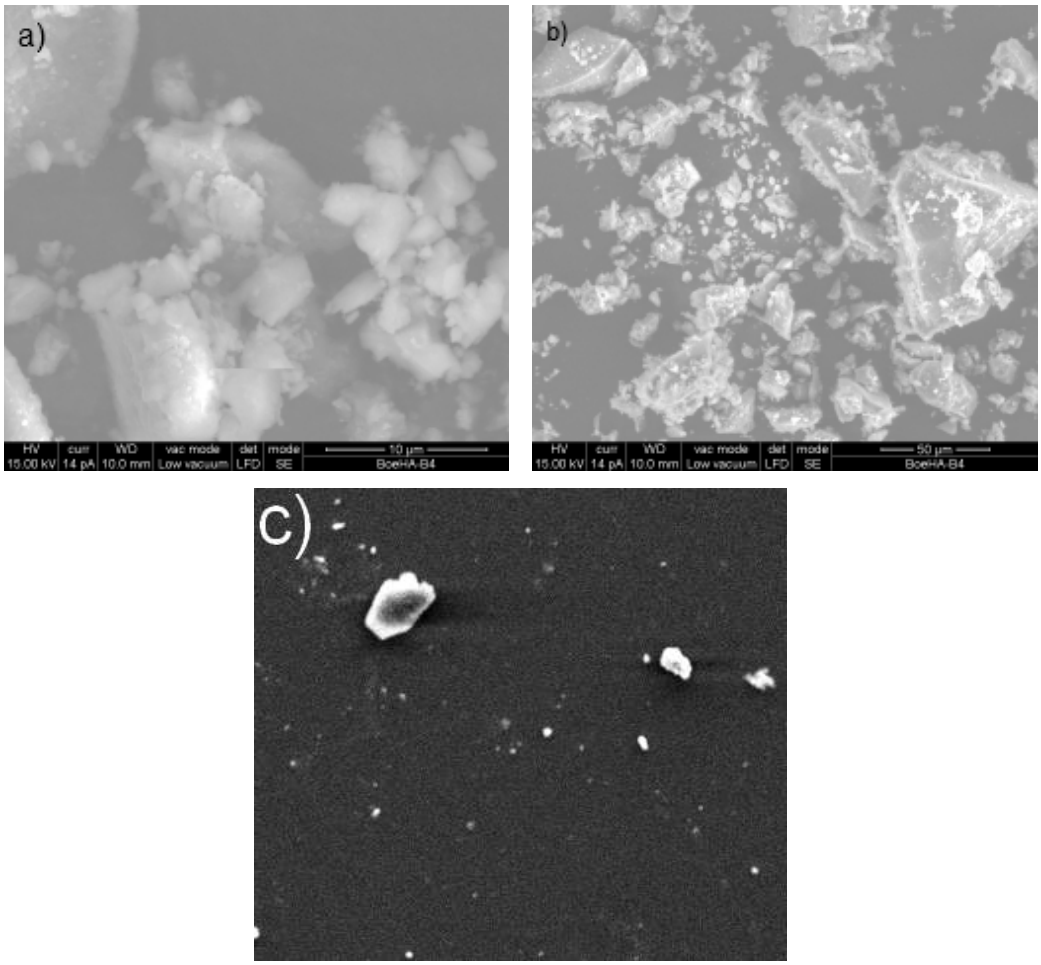

Figure 56. SEM images for (a) and (b) humate-boehmite and (c) boehmite colloids.

3.3.7. Modelling

Two different approaches were taken on modelling the sorption of metals onto boehmite colloids. Firstly, the LAM was applied to fit the effect of HA on the sorption of metals onto colloids, and secondly, sorption was modelled by the sorption isotherms previously described in Chapter 2, *i.e.* the Langmuir, Freundlich and D-R isotherms.

3.3.7.1. Linear Additive Model

The applicability of the linear additive model (LAM) was studied. The equation used for the LAM is the following [140]:

$$R_{d,T} = \frac{R_{d,1} + \left(V/W\right) f_{HA} \beta [HA]}{1 + (1 - f_{HA}) \beta [HA]}$$ **Equation 3.5**

Where $R_{d,T}$ is the R_d value for the ternary system ($dm^3\ kg^{-1}$), $R_{d,1}$ is the R_d value for the sorption of metal onto boehmite colloids ($dm^3\ kg^{-1}$), V is the volume of the suspension (dm^3), W is the mass of colloids (mg), f_{HA} is the fraction of HA bound to the colloid, β is the stability constant of the metal ion humate complex and $[HA]$ is the concentration of HA ($mg\ kg^{-1}$).

Binary sorption experiments (HA-boehmite colloids) showed that the relation between bound HA and the initial amount of HA added to the colloidal sols was $[HA]_{bound} = 0.9758\ [HA]_{initial} - 0.7494$ (Figure 51). With this equation, the $[HA]_{bound}$ when 1 or 2 mg kg^{-1} HA were added to the suspension could be calculated and yielded 0.2265 and 1.2022 mg kg^{-1}, which would correspond to a f_{HA} = 0.23 and 0.60, respectively. However, the experimental conditions under which the sorption isotherm was obtained were unfavourable for a stable suspension, as an increase in HA concentrations led to the flocculation of colloids due to charge neutralisation. These values of f_{HA}= 0.23 and 0.60 were used to estimate the $R_{d,t}$ predicted by the LAM, but the use of these values of f_{HA} is discussed further in this section.

The stability constants for the humate-metal complexes were calculated elsewhere [163]; the R_d values for the metal colloid suspensions were those calculated previously in Chapter 2. The $R_{d,T}$ values were calculated for a volume V = 12 x 10^{-3} dm^3 and a mass of colloids W = 33.5 mg. The results are shown in Table 32 and Table 33.

Table 32. Parameters for the application of the LAM for sorption of Cs, Ni and Eu onto boehmite colloids in the presence of 1 mg kg^{-1} HA. f_{HA} = 0.23.

	β (M – HA)	$R_{d,1}$ (M – Boehmite) (dm^3kg^{-1})	$R_{d,T,predicted}$ (dm^3kg^{-1})	$R_{d,t,observed}$ (dm^3kg^{-1})
Cs	9.33 x 10^2	66.4 ± 2.0	**9.24 x 10^{-2}**	*15.5 ± 0.8*
Ni	5.89 x 10^5	182.9 ± 3.6	**5.10 x 10^{-4}**	*58.1 ± 6.0*
Eu	1.78 x 10^6	101.7 ± 21.5	**1.81 x 10^{-4}**	*104.4 ± 7.8*

Table 33. Parameters for the application of the LAM for sorption of Cs, Ni and Eu onto boehmite colloids in the presence of 2 mg kg^{-1} HA. f_{HA} = 0.60.

	β (M – HA)	$R_{d,1}$ (M – Boehmite) (dm^{3}kg^{-1})	$R_{d,T,predicted}$ (dm^{3}kg^{-1})	$R_{d,t,observed}$ (dm^{3}kg^{-1})
Cs	9.33 x 10^2	66.4 ± 2.0	**8.93 x 10^{-2}**	*5.2 ± 0.6*
Ni	5.89 x 10^5	182.9 ± 3.6	**9.25 x 10^{-4}**	*20.3 ± 0.9*
Eu	1.78 x 10^6	101.7 ± 21.5	**6.09 x 10^{-4}**	*721.4 ± 52.8*

The LAM predicted a decrease in the sorption of metals to boehmite colloids in all cases. However, the R_d values predicted were orders of magnitude smaller than those observed. On a first attempt, the LAM could not be applied succesfully.

A simpler equation for the LAM was defined by Lippold *et al.* [141]:

$$R_{d,t} = \frac{R_d + f_{HA}\beta[HA]}{1+\beta[HA]} \qquad \textbf{Equation 3.6}$$

The application of this equation yielded the following values for the distribution ratio of the ternary system:

Table 34. Parameters observed from the application of the LAM [155] to the sorption of metals onto boehmite colloids in the presence of 1 and 2 mg kg^{-1} HA.

	1 mg kg^{-1} HA		2 mg kg^{-1} HA	
	$R_{d,t}$ predicted	$R_{d,t}$ observed	$R_{d,t}$ predicted	$R_{d,t}$ observed
Cs	3.01 x 10^{-1}	*15.5 ± 0.8*	6.36 x 10^{-1}	*5.2 ± 0.6*
Ni	2.30 x 10^{-1}	*58 ± 6*	6.01 x 10^{-1}	*20.3 ± 0.9*
Eu	2.30 x 10^{-1}	*104 ± 8*	6.01 x 10^{-1}	*721 ± 53*

This equation for the LAM predicts low distribution ratios, below 1 in all cases; values which are lower than those observed experimentally. Further, little differences in the $R_{d,T}$ are predicted between the three metals studied. This is due to the high value of β_M, which is is greater than 1 in all cases, and also greater than $R_{d,M}$. The terms of the equation (Equation 3.6) cancel out and the predicted $R_{d,t}$ becomes the f_{HA} multiplied by the HA concentration.

This model also failed to explain the sorption of metals in a ternary system formed by boehmite, HA and metals. Possible reasons for this are discussed in terms of modelling and methodology.

One of the assumptions of the LAM is a similar affinity of the metal for the humate-colloid and for the free HA in solution. If the affinity of the metal for the dissolved HA were higher than that for humate bound to the colloid, the $R_{d,T}$ would be lower than that predicted, in agreement with the results observed. Another assumption of the LAM is that the sorption properties of the mineral remain unaltered. Although the concentrations of HA and boehmite colloid were selected in order to achieve a stable system, HA might have induced some instability to the boehmite colloids, thereby affecting noticeably the sorption properties of the colloids. XRD and SEM measurements were not conclusive to whether the surface of boehmite colloids was altered by coating with HA.

Both equations used, Equations 3.5 and 3.6, depend mainly on three terms: $R_{d,M}$, f_{HA} and β_M, which are the distribution ratio for metal bound to colloids, the fraction of HA bound to the colloids and the stability constant of metal and HA, respectively. The $R_{d,M}$ values were obtained from the sorption of the metal to boehmite colloids under specific experimental conditions. As the distribution ratios are strongly dependent on the experimental conditions, the sorption of metals in the ternary system was carried out under the same experimental conditions as those used in the binary sorption studies to minimise errors due to differences in $R_{d,M}$. The values of β_M were calculated and used elsewhere [163].

However, the derivation of the fraction of HA bound to colloids may be a source of error due to the following reasons:
(1) The f_{HA} was calculated from the sorption isotherm (Figure 51) where increasing concentrations of HA were added to boehmite colloids. As the HA concentration increased, the stability of the suspension decreased, leading to coagulation of the colloids by charge neutralisation. f_{HA} was calculated for a non-stable binary system.

(2) On another hand, when HA concentrations below 3 mg kg^{-1} were added to a colloidal system containing 30 mg of boehmite, the dissolved HA in solution could

not be detected by UV-Vis, i.e. the signal corresponded to background levels (Figure 57). These results suggested that low amounts of HA, below limit of detection, remained in solution, in which case the value of f_{HA} would be close to 1, rather than the lower values predicted from the sorption isotherm.

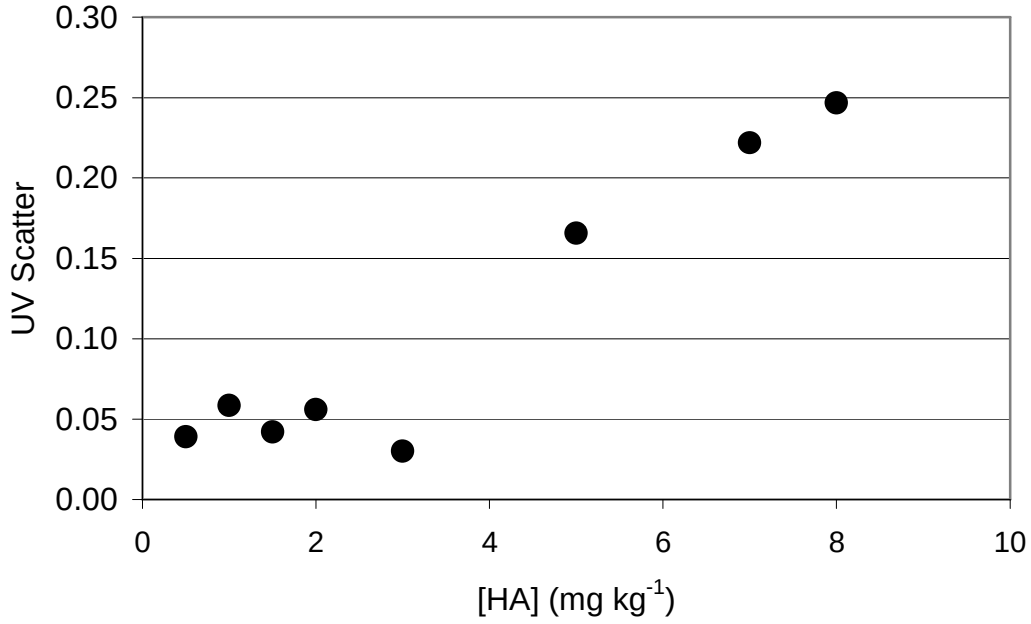

Figure 57. UV scatter of dissolved HA after equilibration with boehmite colloids at pH 7 and ionic strength 0.05 mol dm^{-3}.

Sensitivity Analysis

The application of equations 3.5 and 3.6 failed to reproduce the experimental observations. A sensitivity analysis was performed on the results obtained from modelling with Equations 3.5 and 3.6. The influence of each of $R_{d,1}$, f_{HA}, and β on Equations 3.5 and 3.6 was studied by doubling their values and observing the response of $R_{d,t}$. The results are summarised in Table 35 for Cs.

Table 35. Sensitivity analysis for Cs sorption onto boehmite colloids in the presence of (a) 1 and (b) 2 mg kg^{-1} HA.

a)	x2	$R_{d,t}$ Eq 3.5	$R_{d,t}$ Eq 3.6
$R_{d,Cs}$	66.4 → 132.8	$9.24 \times 10^{-2} \rightarrow 1.85 \times 10^{-1}$	0.3 → 0.37
f_{HA}	0.23 → 0.64	$9.24 \times 10^{-2} \rightarrow 1.32 \times 10^{-1}$	0.3 → 0.53
β_{Cs}	$9.33 \times 10^{2} \rightarrow 1.87 \times 10^{3}$	$9.24 \times 10^{-2} \rightarrow 4.63 \times 10^{-2}$	0.3 → 0.27

The values of Rd,t are those calculated by Equations 3.5 and 3.6, respectively

b)	x2	$R_{d,t}$ Eq 3.5	$R_{d,t}$ Eq 3.6
$R_{d,Cs}$	66.4 → 132.8	$8.94 \times 10^{-2} \rightarrow 1.78 \times 10^{-1}$	0.64 → 0.67
f_{HA}	0.6 → 1.0	$8.94 \times 10^{-2} \rightarrow 6.71 \times 10^{1}$	0.64 → 1.04
β_{Cs}	$9.33 \times 10^{2} \rightarrow 1.87 \times 10^{3}$	$8.94 \times 10^{-2} \rightarrow 4.50 \times 10^{-2}$	0.64 → 0.62

The values of Rd,t are those calculated by Equations 3.5 and 3.6, respectively

Table 35 shows the influence of doubling the three influencing parameters into Equations 3.5 and 3.6. When studying Equation 3.5, in general, when the values of $R_{d,Cs}$ and β_{Cs} were doubled, the expected $R_{d,t}$, was doubled and halfed, respectively. The sensitivity analysis of Equation 3.6 showed the clear dependence of the equation on f_{HA}, as the doubling of $R_{d,Cs}$ and β_{Cs} resulted in little changes on the expected $R_{d,t}$, but when the f_{HA} was doubled, the Rd,t was also doubled.

The sensitivity analysis showed similar results for Ni and Eu:

Table 36. Sensitivity analysis for Ni sorption onto boehmite colloids in the presence of (a) 1 and (b) 2 mg kg^{-1} HA.

a)	x2	$R_{d,t}$ Eq 3.5	$R_{d,t}$ Eq 3.6
$R_{d,Ni}$	182.9 → 365.8	5 x 10^{-4} → 9.13 x 10^{-4}	0.23 → 0.23
f_{HA}	0.23 → 0.64	5 x 10^{-4} → 8.80 x 10^{-4}	0.23 → 0.46
β_{Ni}	5.89 x 10^{5} → 1.18 x 10^{6}	5 x 10^{-4} → 3.09 x 10^{-4}	0.23 → 0.23

The values of Rd,t are those calculated by Equations 3.5 and 3.6, respectively

b)	x2	$R_{d,t}$ Eq 3.5	$R_{d,t}$ Eq 3.6
$R_{d,Ni}$	182.9 → 365.8	9.25 x 10^{-4} → 1.31 x 10^{-4}	0.64 → 0.67
f_{HA}	0.6 → 1	9.25 x 10^{-4} → 6.05 x 10^{+2}	0.64 → 1.04
β_{Ni}	5.89 x 10^{5} → 1.18 x 10^{6}	9.25 x 10^{-4} → 7.31 x 10^{-3}	0.64 → 0.62

The values of Rd,t are those calculated by Equations 3.5 and 3.6, respectively

Table 37. Sensitivity analysis for Eu sorption onto boehmite colloids in the presence of (a) 1 and (b) 2 mg kg^{-1} HA.

a)	x2	$R_{d,t}$ Eq 3.5	$R_{d,t}$ Eq 3.6
$R_{d,Eu}$	101.7 → 203.4	1.81 x 10^{-4} → 2.55 x 10^{-4}	0.23 → 0.23
f_{HA}	0.23 → 0.64	1.81 x 10^{-4} → 4.11 x 10^{-4}	0.23 → 0.46
β_{Eu}	1.78 x 10^{6} → 3.56 x 10^{6}	1.81 x 10^{-4} → 1.44 x 10^{-4}	0.23 → 0.23

The values of Rd,t are those calculated by Equations 3.5 and 3.6, respectively

b)	x2	$R_{d,t}$ Eq 3.5	$R_{d,t}$ Eq 3.6
$R_{d,Ni}$	182.9 → 365.8	6.08 x 10^{-4} → 6.80 x 10^{-4}	0.60 → 0.60

f_{HA}	0.6 → 1	$6.08 \times 10^{-4} \rightarrow 1.38 \times 10^{+3}$	0.60 → 1.00
β_{Ni}	$5.89 \times 10^{5} \rightarrow 1.18 \times 10^{6}$	$6.08 \times 10^{-4} \rightarrow 5.73 \times 10^{-4}$	0.60 → 0.60

The values of Rd,t are those calculated by Equations 3.5 and 3.6, respectively

The sensitivity analyses performed on modelling metal sorption onto boehmite colloids in presence of HA showed, for most of the systems, that changing the f_{HA} led to a change in the calculated $R_{d,t}$, whereas changing the other two parameters influenced to little extent the overall distribution ratio.

f_{HA} represents the fraction of bound HA to the surface of the colloid and has a maximum value of 1. Earlier in this section the errors implied in the calculation of this value were analysed. Further, a value of close to 1 was proposed as more appropiate.

As closure to the sensitivity analysis, an attempt was made to model the systems with values of f_{HA} close to 1, to find out whether the predicted $R_{d,t}$ could resemble those obtained experimentally. The following values of f_{HA} were adjusted manually in order to obtain a Rd,t value close to the experimental (Table 38).

Table 38. Values of fHA for similar values between $R_{d,t}$ predicted and experimental.

	f_{HA}	[HA] = 1		[HA] = 2	
		$R_{d,t}$ predicted	$R_{d,t}$ experim	$R_{d,t}$ predicted	$R_{d,t}$ experim
Cs	0.995	11.78	15.5	6.49	5.2
Ni	0.99999	57.17	58.1	47.33	20.3
Eu	0.999997	116.61	104.4	117.88	721.4

Table 38 shows the values of f_{HA} for which the LAM would yield similar results for the predicted distribution ratio and the experimental values. It can be seen that the number of decimal points needed increased with the cationic charge, and the values of $R_{d,t}$ predicted varied with the decimals used.

Table 38 confirms the errors in the derivation of f_{HA} via the sorption isotherm and further confirms the high sorption of HA to boehmite colloids. Moreover, assuming

these new values of f_{HA}, the LAM could be applied to the sorption of metals onto boehmite colloids in the presence of HA.

3.3.7.2. Langmuir, Freundlich and D-R modelling

In a similar manner as in Chapter 2, the experimental results for the sorption of metals to boehmite in the presence of HA were modelled using the Langmuir, Freundlich and Dubinin-Radushkevich (D-R) approximations. The linearised equations corresponding to each model are summarised below:

Langmuir $$\frac{1}{Q} = \frac{1}{q_m \cdot b}\frac{1}{C} + \frac{1}{q_m}$$ **Equation 3.7**

Freundlich $$\log Q = \log F + n \log C$$ **Equation 3.8**

D-R $$\ln Q = \ln q_m - k\varepsilon^2$$ **Equation 3.9**

$$\varepsilon = RT \ln\left(1 + {}^{1}\!/_{C}\right)$$ **Equation 3.10**

$$E = \left(2k\right)^{-{}^{1}\!/_{2}}$$ **Equation 3.11**

Where Q is the concentration of metal bound, R_d is the distribution coefficient, q_m is the maximum amount of metal sorbed on the colloid, C is the free concentration of metal in solution, F and n are constants, ε is the Polanyi potential, R is the gas constant, in kJ, T is the temperature, in K, and E is the mean free energy of sorption, in kJ mol^{-1}. A summary of the main parameters is detailed below:

Table 39. Parameters of the modelling of the sorption of Cs, Ni and Eu onto boehmite in the presence of HA (0, 1 and 2 mg kg^{-1}).

		Langmuir		Freundlich		D-R	
	[HA] (mgkg^{-1})	R^2	q_m (mol kg^{-1})	R^2	n	R^2	E (kJmol^{-1})
Cs	0	0.9807	9.8 x 10^{-3}	0.9991	1.01 ± 0.02	0.9875	8.22
	1	0.9996	5.5 x 10^{-2}	0.9979	1.03 ± 0.02	0.9894	7.37
	2	0.9968	-3.9 x 10^{-2}	0.9808	0.96 ± 0.05	0.9616	7.54
Ni	0	0.9948	-5.2 x 10^{-2}	0.9905	1.22 ± 0.04	0.9830	6.97
	1	0.9997	1.67 x 10^{-2}	0.9840	0.69 ± 0.03	0.9991	9.45

	2	0.9994	5.52×10^{-3}	0.9944	0.78 ± 0.02	0.9994	8.84
	0	0.9969	1.25×10^{-2}	0.8623	0.44 ± 0.06	0.9217	12.31
Eu	1	0.9952	9.12×10^{-3}	0.9891	0.60 ± 0.02	0.9958	10.31
	2	0.9955	1.48×10^{-2}	0.9876	0.53 ± 0.02	0.9994	11.63

Table 39 shows the parameters obtained from applying the three models to the experimental data obtained from the sorption of Cs, Ni and Eu onto boehmite colloids in the presence of HA. The R^2 represents the fit of the linear curve and q_m, n and E, respectively, represent the maximum concentration of metal adsorbed (mol kg^{-1}), the representative Freundlich constant and the mean free energy of sorption (kJ mol^{-1}).

The modelled data for Cs showed better fits for the Langmuir and the Freundlich models. Observing the sorption isotherm in Figure 52, the maximum concentration of Cs sorbed was above the value predicted by the equation. Therefore, this model did not fit the experimental data. The constant calculated by the Freundlich model had a value near unity, in agreement with the linear sorption observed experimentally.
In the case of Ni, the Langmuir model failed to explain the sorption of Ni onto boehmite colloids in the presence of HA as the predicted value of q_m was lower than that observed in Figure 53. The fits for both Freundlich and D-R models were acceptable. The mean free energy values calculated from the D-R equation and the n value from the Freundlich isotherm predicted a change in behaviour upon the presence of HA in the system, from linear sorption in the absence of HA to the saturation observed in the presence of HA.

Finally, the q_m values predicted by the Langmuir model for Eu sorption onto boehmite colloids in the presence of HA were just slightly lower that those observed in Figure 54. The fits for Eu were generally good for all the models. The Freundlich equation predicted a n value below one in all cases, showing a slight increase in the presence of HA. Finally, the mean free energy values were in all cases above 8 kJ mol^{-1}, suggesting ion exchange mechanisms of sorption [164].

The results of the models are shown below:

a) Langmuir fit for Cs sorption onto boehmite colloids in the presence of 0, 1 and 2 mg kg^{-1} HA.

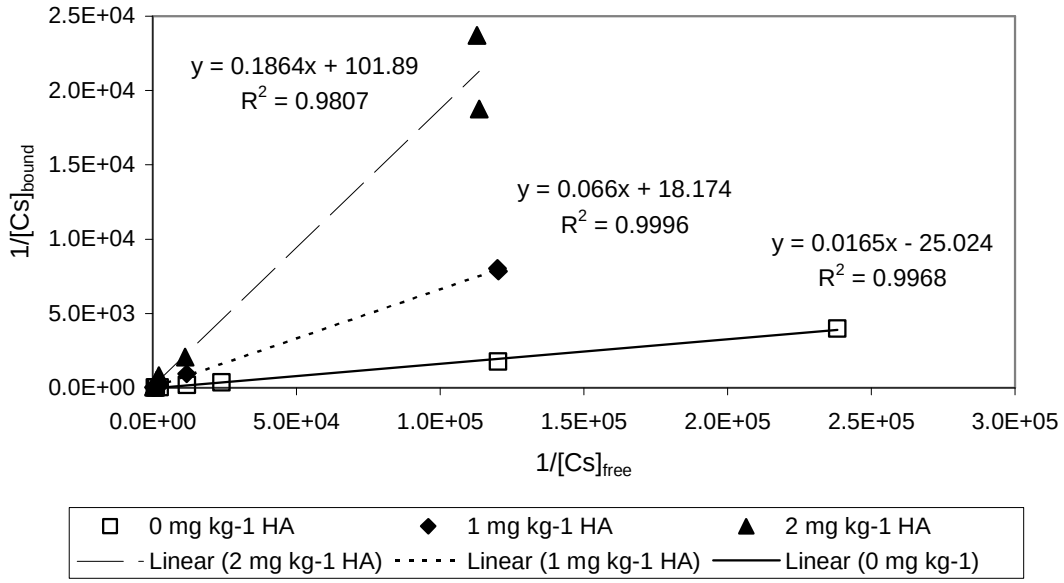

Freundlich fit for Cs sorption onto boehmite colloids in the presence of 0, 1 and 2 mg kg^{-1} HA.

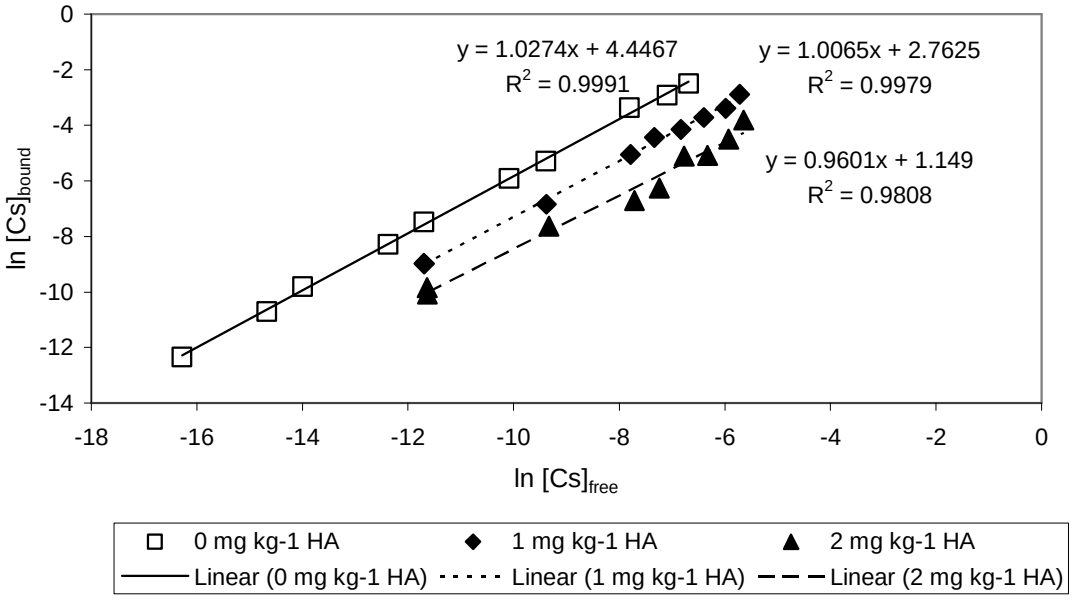

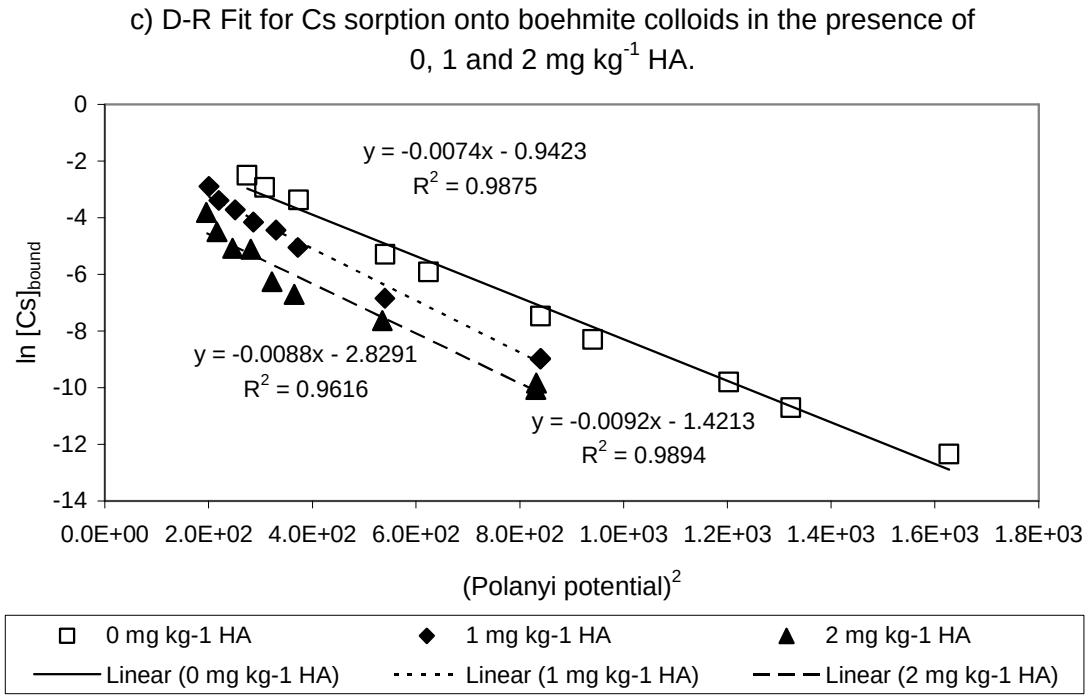

Figure 58. Modelling Cs sorption onto boehmite colloids in the presence of HA at pH 7 and ionic strength 0.05 mol dm^{-3}.

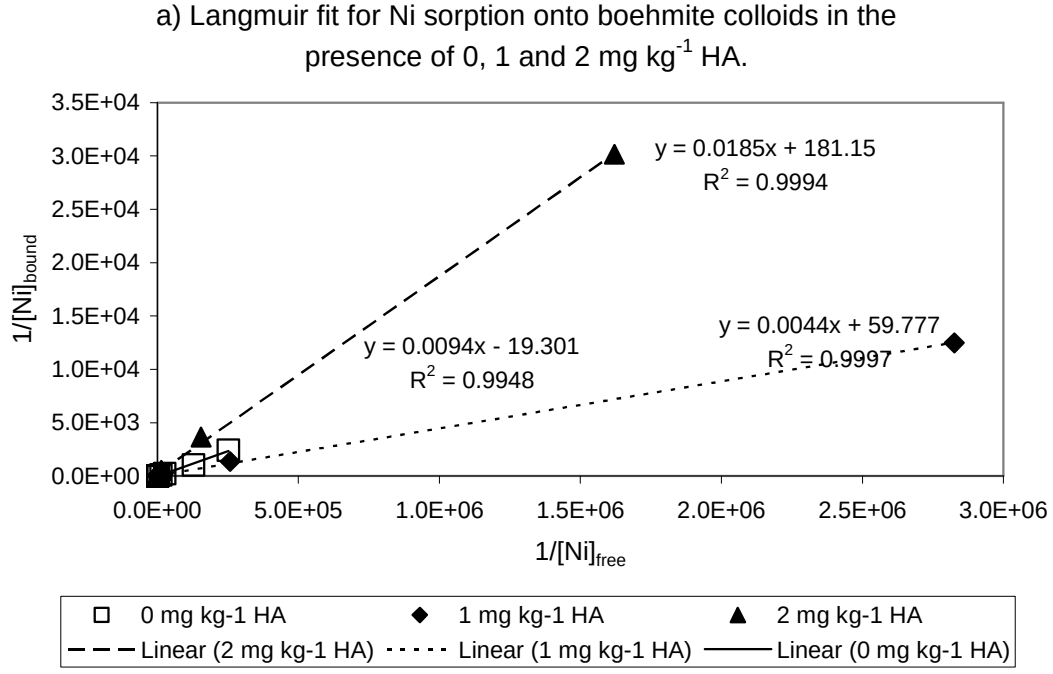

b) Freundlich fit for Ni sorption onto boehmite colloids in the presence of 0, 1 and 2 mg kg^{-1} HA.

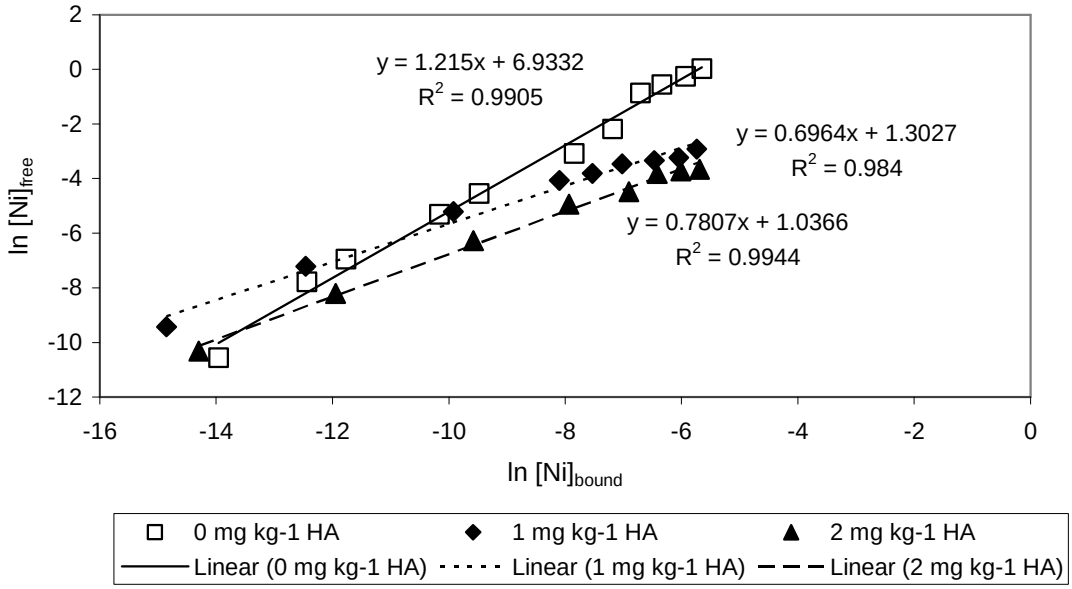

c) D-R Fit for Ni sorption onto boehmite colloids in the presence of 0, 1 and 2 mg kg^{-1} HA.

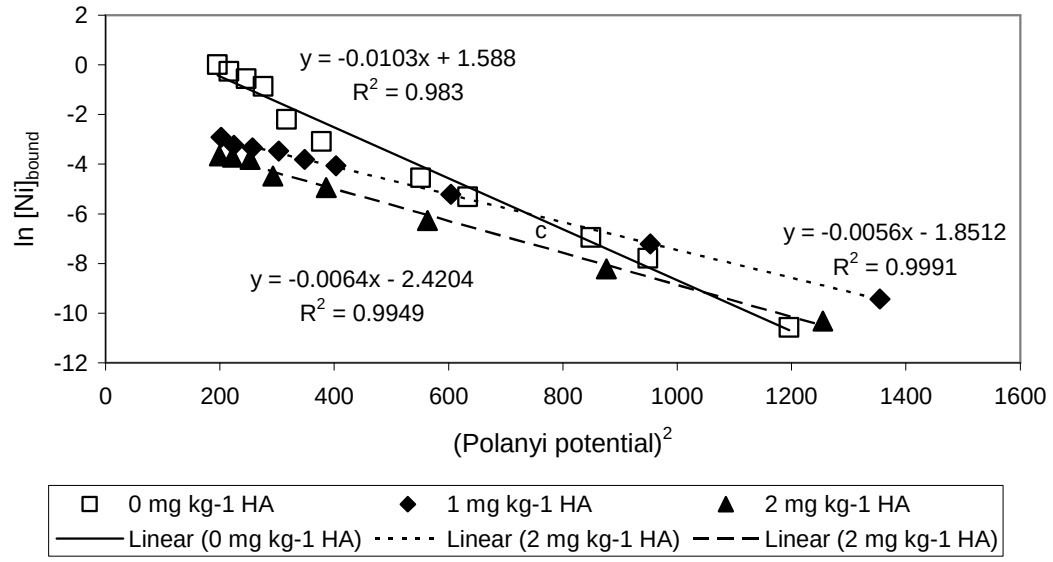

Figure 59. Modelling Ni sorption onto boehmite colloids in the presence of HA at pH 7 and ionic strength 0.05 mol dm^{-3}.

a) Langmuir fit for Eu sorption onto boehmite colloids in the presence of 0, 1 and 2 mg kg^{-1} HA.

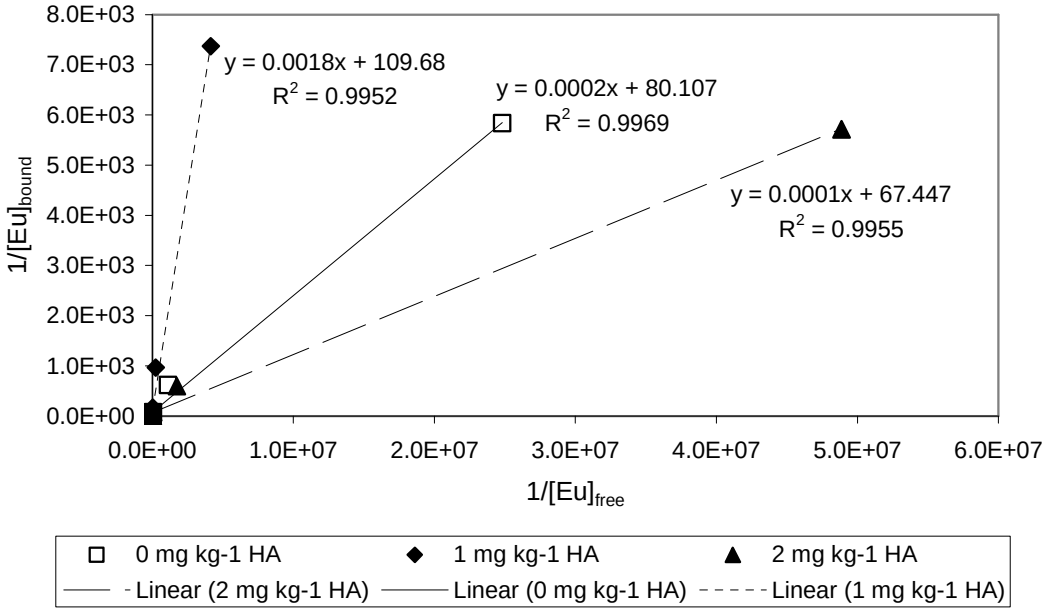

b) Freundlich fit for Eu sorption onto boehmite colloids in the presence of 0, 1 and 2 mg kg^{-1} HA.

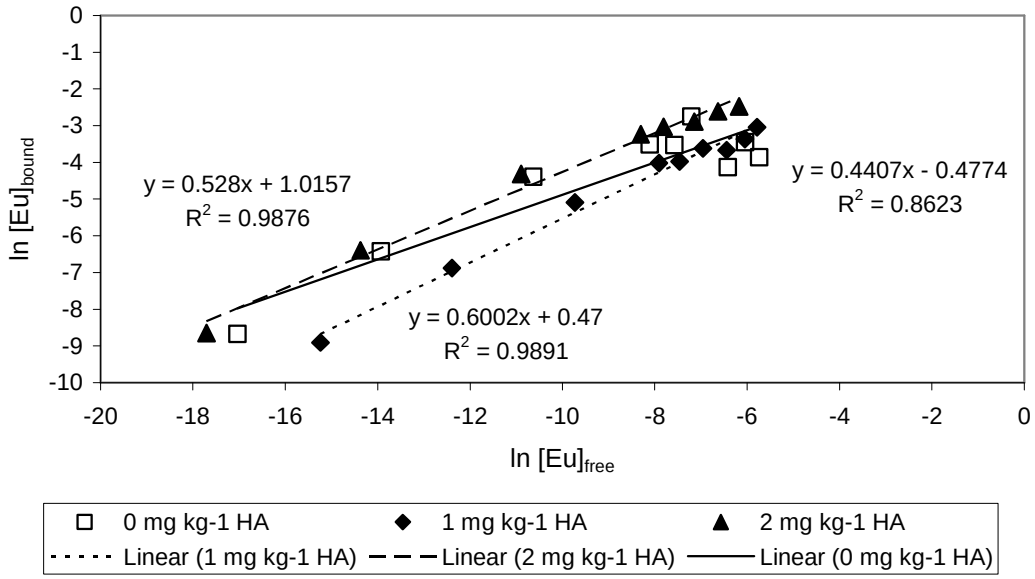

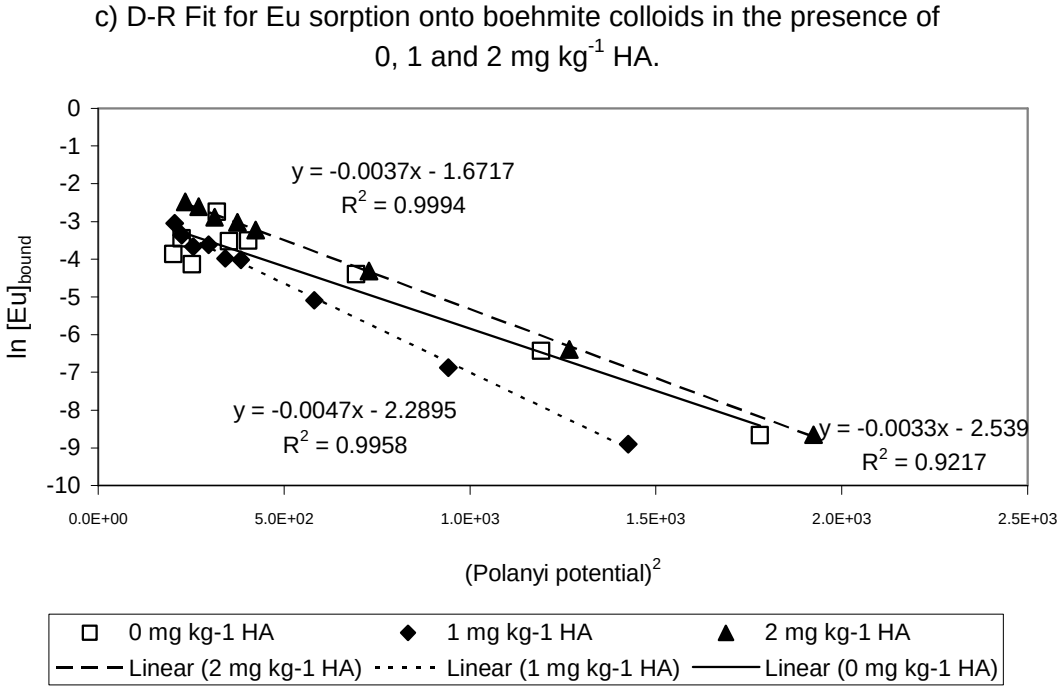

Figure 60. Modelling Eu sorption onto boehmite colloids in the presence of HA at pH 7 and ionic strength 0.05 mol dm^{-3}.

3.4. Conclusions

Organic substances have been shown to influence the sorption of radionuclides and other contaminants onto minerals. Although the studies with colloids are not as plentiful as on solid surfaces, some studies have been reported which show that HA enhances metal sorption at low pHs and hinders it at high pHs. This chapter has investigated the influence of humic acids on boehmite colloids as well as the effect of humics on the sorption of metals on boehmite colloids.

HA was found to destabilise boehmite colloids at fairly low concentrations. As the concentration of HA increased, boehmite colloids became stable. The experiments showed that the recovery of stability depended on the concentration of boehmite colloids, as lower concentrations of colloid recovered stability at lower concentrations of HA, whereas suspensions with higher concentration of colloids needed of higher concentrations of HA to become stable again.

Following the investigation carried out in Chapter 2, the conditions of pH, ionic strength and metal/colloid concentration were reproduced in this study, with the

inclusion of HA at different concentrations. In order to have a stable ternary system, either low concentrations of HA (below 5 mg kg^{-1}), or higher concentrations of HA were to be used. At high concentrations of HA, the surface coverage of boehmite by HA might have been too large as to allow sorption of metals onto colloids to be significant. Therefore, only 1 and 2 mg kg^{-1} HA could be used in this investigation. Further studies including higher concentrations of HA would be needed to better understand the mechanisms of sorption of metals onto boehmite colloids in the presence of HA, *i.e.* whether or not the metal in solution is present as free metal ions or as metal-humate complexes.

The investigation reported here revealed that HA, even at low concentrations, influenced greatly the sorption of metals onto boehmite colloids, hindering it in all cases. From previous literature, the most plausible explanation was the blocking of sorption sites by the HA.

Mathematical tools were used to model the sorption of metals onto boehmite colloids in the presence of HA. Two different equations of the linear additive model were used, but, in a first attempt, both failed to explain the effect of HA in the ternary system. A rigurous analysis of the possible sources of error was performed, from which a change in the value of f_{HA}, which represents the sorption of HA onto the boehmite colloids, was made. This modification led to the successful application of the LAM. Further, this modification highlighted the importance of considering a stable binary (colloid-HA) system.

Chapter 4. MOBILITY OF COLLOIDS AND COLLOID-FACILITATED TRANSPORT

4.1. Introduction

Migration of colloids has been widely studied using a large number of techniques, including fluorescence spectrophotometry [165,166167], UV-Vis spectrophotometry [168,169,170,171,172] turbidity [172], Rutherford backscattering spectrometry [173] and high sensitivity liquid in situ spectrometry [174]. The movement of colloids has been studied both in laboratory conditions [167,171] and in field experiments [175,165,176,177]. Factors affecting the retention of colloids through a column may be attachment, straining and filtering [167].

The influence that organic and inorganic colloids have on the mobility of contaminants through the Geosphere has also been assessed [174,176,177,178,179,180], and generally, the transport of contaminants was enhanced by the colloids.

Radiolabelling colloids can be used to track the colloid during a transport process, as it involves the incorporation of a radioactive spike in the structure of the colloid during its synthesis. It has been generally applied for medical purposes [181,182,183]. However, it could also be used to follow radiometrically the movement of colloids through a column.

The aims of this chapter were to synthesise stable radiolabelled colloids, study their migration through a sand column and assess the influence of colloids on the mobility of caesium through a sand column. Hence, this chapter may be divided into two parts, one concerning the synthesis and stability of radiolabelled silica colloids, and a second, concerning the migration of both silica colloids and caesium associated with the silica colloids through a sand column.

4.2. Experimental

A known method for synthesising silica colloids was used to generate radiolabelled silica colloids [184]. The stability of both the silica colloids and the radiolabel was studied by spectroscopic and radiometric techniques. Once the stability of colloids was assured, migration experiments were carried out by passing the radiolabelled silica colloids through a sand column.

4.2.1. Method development

2.1.1. Materials used

Silica colloids were synthesised from TEOS (tetraethyl orthosilicate), provided by Alfa Aesar. 0.88 mol dm^{-3} NH_4OH (Sigma Aldrich) and ethanol 99% were used in the synthesis. The dialysis bags used were Spectra/por Biotech Cellulose Ester (CE) Dialysis Membranes MWCO: 100-500 D. These were previously wetted in 0.1% NaN_3, from Alfa Aesar. The $NaClO_4$, 95%, was purchased from Sigma Aldrich.

BDH sand was used in the migration experiments.

^{152}Eu and ^{137}Cs are detailed in Table 1.

4.2.1.2. Preparation for measurements

Following those experiments carried out by Fairhust [198], characterisation of silica colloids took place by measuring the average size and zeta potential with a Zeta Master S (Malvern Instruments, UK). Approximately 3 cm^3 aliquots were used. UV measurements were carried out using a UV Type Varian Cary Series 50 Bio Spectrophotometer. A quartz cuvette was filled with approximately 1 cm^3 of sample and the absorbance spectra were recorded at 240.1 nm.

Migration studies were carried out by means of column experiments. A Pharmacia glass column with the following dimensions was used: 30 cm in length and 2.6 cm in diameter. 20 μm membranes were fitted at both ends of the column. A Pharmcia P1 pump was used. 1 cm^3 aliquots from the effluent were collected with a RediFRAC

fraction collector. The radioactive samples were measured by gamma counting (^{152}Eu and ^{137}Cs) using a Cobra II Auto-Gamma Counter (Packard Ltd), or by beta counting (tritiated water) using a Tricarb 1900TR Liquid Scintillation Analyzer (Packard Ltd). The activity along the length of the column was measured using a Na-I detector, Teledyne Brown Engineering Environmental Services – Scintillation Amplifier model 5010.

4.2.2. Synthesis and stability of radiolabelled silica colloids

4.2.2.1. Synthesis of silica colloids

Silica colloids were prepared by a method based on that detailed by Stöber *et al.* [184], where 50 cm^3 of ethanol 99% were added to 2 g of TEOS (tetraethyl orthosilicate). The sample was then placed in a sonicating bath whilst adding 2 cm^3 of 0.88 mol dm^{-3} NH_4OH. The samples were sonicated for a further 20 minutes and then placed in a shaker overnight. After this time, the samples were placed in dialysis bags previously wetted in 0.1 % NaN_3. 0.05 mol dm^{-3} $NaClO_4$ was used as the dialysis solution. This solution was changed every 12 hours until no ethanol was detected, usually 7 to 10 days (qualitative detection of ethanol was carried out by HPLC). The silica colloids were transferred to a previously dried beaker for gravimetric determination.

4.2.2.2. Synthesis of Eu-doped silica colloids

50 cm^3 of ethanol 99% were added to 2 g of TEOS. 1 cm^3 of ^{152}Eu (approximately 341.5 kBq dm^{-3}) was added. The sample was placed in a sonicating bath whilst adding 2 cm^3 of 0.88 mol dm^{-3} NH_4OH. The sample was left in the sonicating bath for a further 20 minutes and then placed in a shaker overnight. After this time the samples were transferred to a dialysis bag, previously wetted in NaN_3. 1 dm^3 0.05 mol dm^{-3} $NaClO_4$ solution was added to the measuring cylinder where the dialysis bag was placed. The sample was left in the dialysis bag for 10 days, changing the dialysis solution twice a day. After this time, the dialysis bag was emptied and the silica colloids were characterised.

4.2.2.3. Characterisation and stability of Eu-doped silica colloids

UV measurements at a wavelength of 240.1 nm were used to characterise the generated colloids. Gamma counting was used to monitor the stability of the radiolabel. Also, the average size and zeta potential of the synthesised colloids were measured using a Zeta Master S. A calibration curve was produced by plotting the measurements obtained by UV spectroscopy and gamma counting versus the dilution of Eu-doped silica colloids in water.

4.2.3. Migration experiments

Following the characterisation experiments, the synthesised silica colloids were used to assess the migration of silica colloids through a sand column, as well as the influence of silica colloids on the transport of a radioactive spike.

4.2.3.1. Migration of Eu-doped silica colloids through sand column

The migration of silica colloids was studied radiometrically by following the breakthrough of the synthesised Eu-doped silica colloids through a sand column. The overall dimensions of the column were 30 cm in length and 2.6 cm in diameter. The column was packed with approximately 250 g of sand (particle size diameter 100 – 300 μm [185,186,187]), previously wetted in DI water. To avoid the formation of air bubbles, water was preintroduced into the column from its bottom to a certain height; the sand was then poured slowly into the column while mechanical stirring took place with a glass rod. The top and the base of the column were fitted with 20 μm membranes. The eluants were flooded upwards through the column (see Figure 61).

The flow rate of the eluant used in all measurements was adjusted to approximately 0.25 cm^3 min^{-1}. Tritiated water (82 kBq dm^{-3}) was used as a conservative tracer to measure the porosity of the column. Following the porosity measurement, migration experiments were carried out by flooding 100 cm^3 suspension of the synthesised Eu doped silica colloids into the column until it was all added, at which point it was switched to deionised water, until no activity was detected in the outlet. A fraction collector was connected to the outlet at the top of the column. 1.25 cm^3 fractions of eluant were collected and measured in the gamma counter for activity.

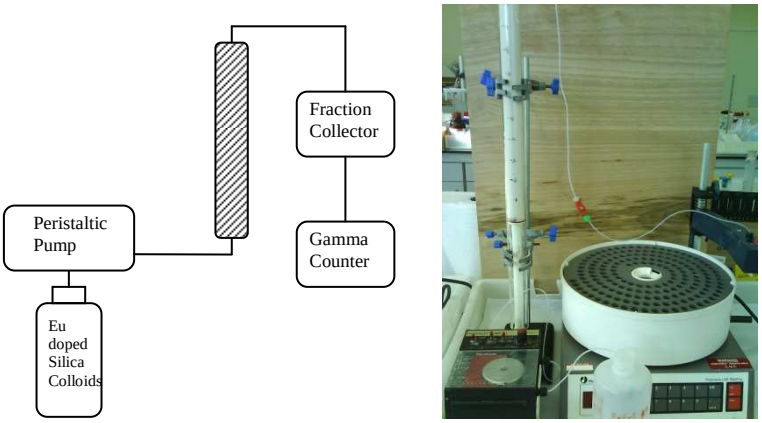

Figure 61. Experimental set up for the migration of radiolabelled silica colloids through a sand column.

On conclusion of the experiment, any retention of the radiolabelled colloids along the column was measured by gamma counting with a Na-I detector (see Figure 62 for two different angles of the experimental set up). The lead bricks were set so that a slit of 1.5 cm allowed the detector to measure the activity. The column was divided into 18 segments and each of the segments was measured for 40 minutes. The instrument was previously calibrated with ^{137}Cs, ^{22}Na and ^{57}Co standards. From the calibration, the channel numbers corresponding to the different photopeaks of ^{152}Eu were defined and consequently the regions of interest could be set.

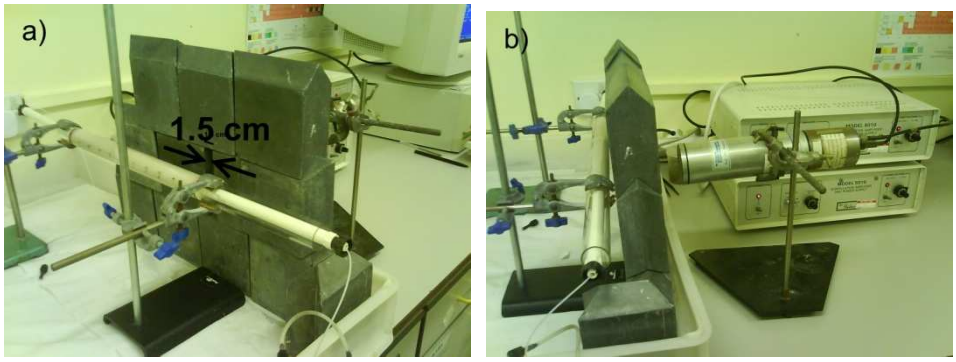

Figure 62. Experimental set up for the measurement of remaining gamma activity with NaI detector.

A control experiment was carried out to test the effectiveness of the lead bricks at shielding the detector from γ-activity. The control experiment consisted on measuring a standard sample of ^{152}Eu using the same set up as that used in the column experiment. The standard was measured in front of the detector and was

moved two centimeters to the left and right of the slit, when further recordings were taken (Figure 63).

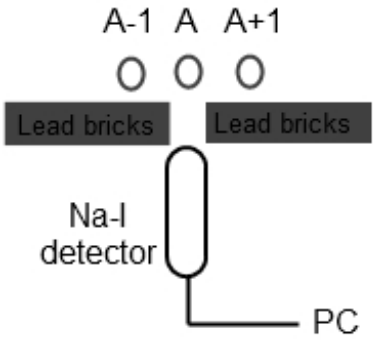

Figure 63. Diagram of the control experiment carried out for the detection of γ-activity through lead bricks with Na-I detector.

Briefly, the recordings decreased sharply when the standard was moved two centimeters away from the detector (Table 40), indicating that the lead bricks were effective at shielding the γ-activity coming from segments of the column at least two centimeters away from the segment in front of the detector.

Table 40. Control experiment proving the effectiveness of the lead bricks.

Position	A – 1	A	A + 1
Net counts	585 ± 121	19134 ± 367	384 ± 126

4.2.3.2. Migration of Cs associated to Eu-doped silica colloids through sand column

Column experiments were carried out to study the effect of colloids in the migration of Cs through a sand column. For this purpose, a batch of synthesised Eu doped silica colloids was contacted with a spike of ^{137}Cs (45 kBq cm^{-3}). After equilibration, 3.5 g of ion exchange resin were added to remove any Cs ions remaining in solution. Prior to investigating the migration of Cs, the interaction of the metal with silica colloids was assessed.

4.2.3.2.1. Sorption and desorption of Cs on silica colloids

Prior to the column experiment, the sorption and desorption of Cs to silica colloids were studied by means of batch experiments. The silica colloids were synthesised as described in section 4.2.2.1. In triplicate, 1 cm^3 of CsCl solution ($1x10^{-6}$ to $3x10^{-3}$ mol dm^{-3}) was added to 10 cm^3 of silica colloids. The suspension was spiked with ^{137}Cs (8.3 kBq dm^{-3}) and the pH adjusted to 7. The samples were left to equilibrate for 24 hours, after which separation took place by centrifugation (6000 rpm for 30 minutes), followed by filtration through 0.45 μm filters. The activity of a 2 cm^3 aliquot was measured by gamma counting.

Following the sorption experiments, desorption experiments were carried out by redispersing the Cs bound silica colloids in DI water. After a 24 hour period, the samples were centrifuged for 30 minutes at 6000 rpm. An aliquot of the supernatant was then filtered through a 0.45 μm filter and its activity was measured by gamma counting.

4.2.3.2.2. Column experiments

The procedure for the column experiments consisted of flooding 100 cm^3 of Cs – Eu doped silica colloids suspension into the column at a flow rate of 0.25 cm^3 min^{-1} until nearly all of the solution had entered to the column. After this, DI water was introduced into the column. Fractions of the eluant were collected until no more activity was detected in the outlet. On conclusion of the experiment, the column was measured with a Na-I detector to study the remaining activity along the column.

Both of the active elements present in suspension (^{137}Cs and ^{152}Eu) were gamma emitters. Detection and quantification of the activity coming from each element was possible due to the different energies of the photopeaks of the elements. ^{137}Cs has a single peak at 665 keV; ^{152}Eu has up to six different photopeaks, showing a more complex gamma spectrum [188]. The different values of energies made possible the separation of ^{137}Cs and ^{152}Eu in both the gamma counter and the Na-I detector.

A protocol was prepared in the gamma counter, where the channels were set to the following values:

Table 41. Selection of regions in gamma counter for ^{152}Eu and ^{137}Cs.

Channel	Lower Limit (channel number)	Upper Limit (channel number)
Region A	75	250
Region B	350	500
Region C	700	850

The selection of channels shown in the table above provided a good separation of the peaks for ^{152}Eu (Regions A and B) and for ^{137}Cs (Region C). In the case of the Na-I detector, the peak for ^{137}Cs could be clearly distinguished from those from ^{152}Eu. Two regions of interest were preset, the one for ^{152}Eu in channels 153 to 192 and the one for ^{137}Cs in channels 282 to 354. Figure 64 shows the spectra for the gamma counter of the (a) Cs – Eu doped silica colloids, (b) Eu doped silica colloids and (c) Cs spike on their own. Figure 65 shows the spectra for the Na-I detector for the Cs – Eu doped silica colloids.

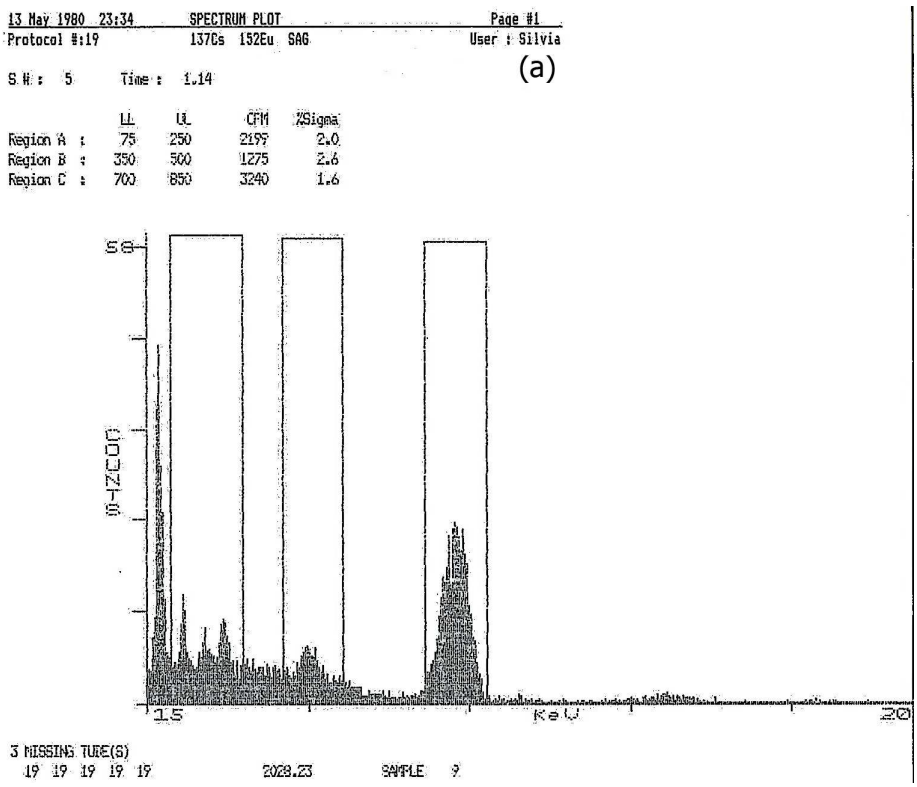

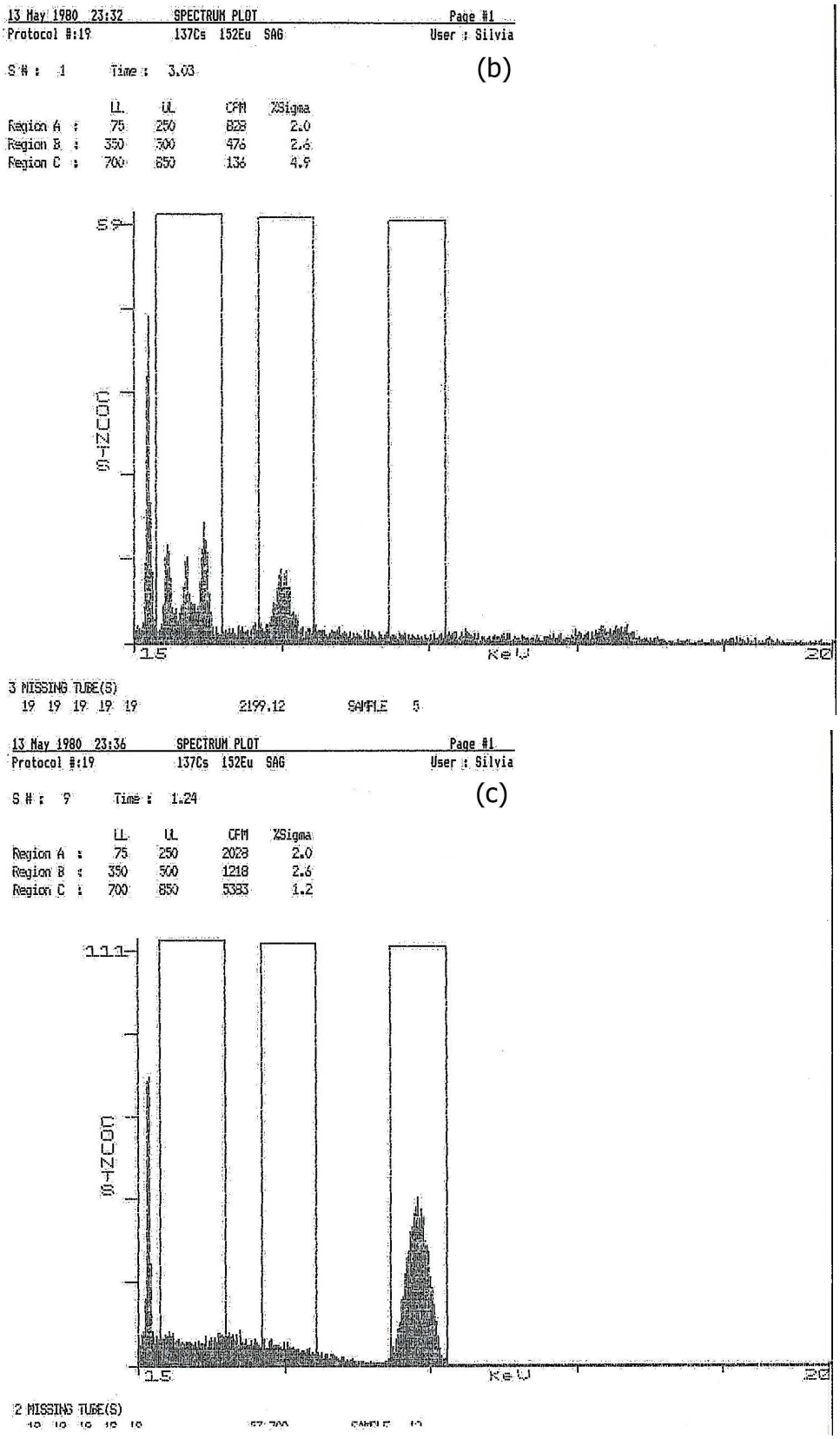

Figure 64. Gamma-counter scans for (a) Cs associated to Eu-doped silica colloids, (b) Eu-doped silica colloids and (c) Cs spike.

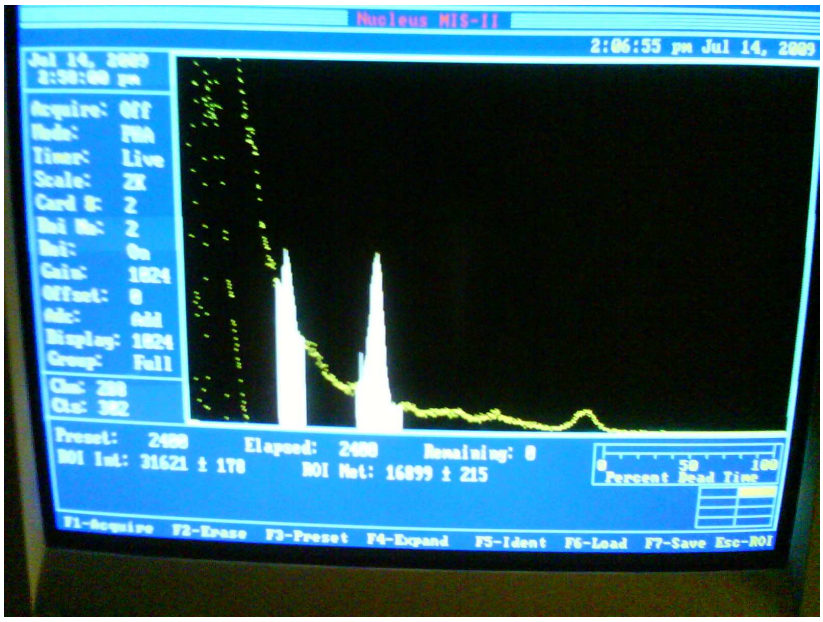

Figure 65. Spectra from NaI detector for Cs associated to Eu-doped silica colloids.

4.3. Results

4.3.1. Characterisation and stability of colloids

Various techniques including UV-Vis spectrometry, dynamic light scattering (DLS), zeta potential and gamma counting, were used to characterise the synthesised silica colloids and radiolabelled silica colloids. UV-Vis spectrometry (measurement at 254 nm) was used to study the stability of the colloids as a function of time and ionic strength. Gamma counting was used to study the stability of the radiolabel as a function of time.

4.3.1.1. Silica colloids

The average size of the (non-active) silica colloids was measured by DLS and showed an average size of 124.8 ± 4.0 nm. The zeta potential was measured by electrophoretic mobility and showed -55.3 ± 4.7 mV. These data are an average of ten measurements carried out in the Zeta Master. The values for the zeta potential of silica colloids found in literature vary greatly depending on the ionic strength of the suspension [189]. However, the experimental values are in agreement with the literature for the pH studied: -35 mV [190], -53.1 mV [191], -80 mV [192]. Both the average size and the zeta potential were measured in a Zeta Master S.

The surface area of the silica colloids was measured by the method described by Sears [193]. Briefly, 30 g of NaCl were added to 1.5 g of silica acidified to pH 3 to 3.5. The volume was made up to 150 cm^3 with DI water. After taking the pH to 4, the solution was titrated with 0.1 mol dm^{-3} NaOH to pH 9. The volume required to rise the pH from 4 to 9 is related to the surface area as described by the following relation:

$$S = 32V - 25 \qquad \textbf{Equation 4.1}$$

Where S is the surface area (m^2 g^{-1}) and V is the volume required for the titration (cm^3). This procedure yielded a surface area of 48.6 m^2 g^{-1}. Although this is a low result compared to values found in the literature, which are in the range of hundreds of m^2g^{-1} [194,195,196], Vasconcelos *et al.* [196] found that the specific surface area (as well as other physical properties), depend on the proportion of reactants, *i.e.* TEOS, NH_3OH, and ethanol, added to synthesise the silica colloids. In their experimental observations, the specific surface areas measured ranged from <1 to 900 m^2 g^{-1}.

The UV-vis scatter of the synthesised silica colloids was measured at 240.1 nm. The stability of the silica colloids was studied as a function of time and ionic strength (Figure 66).

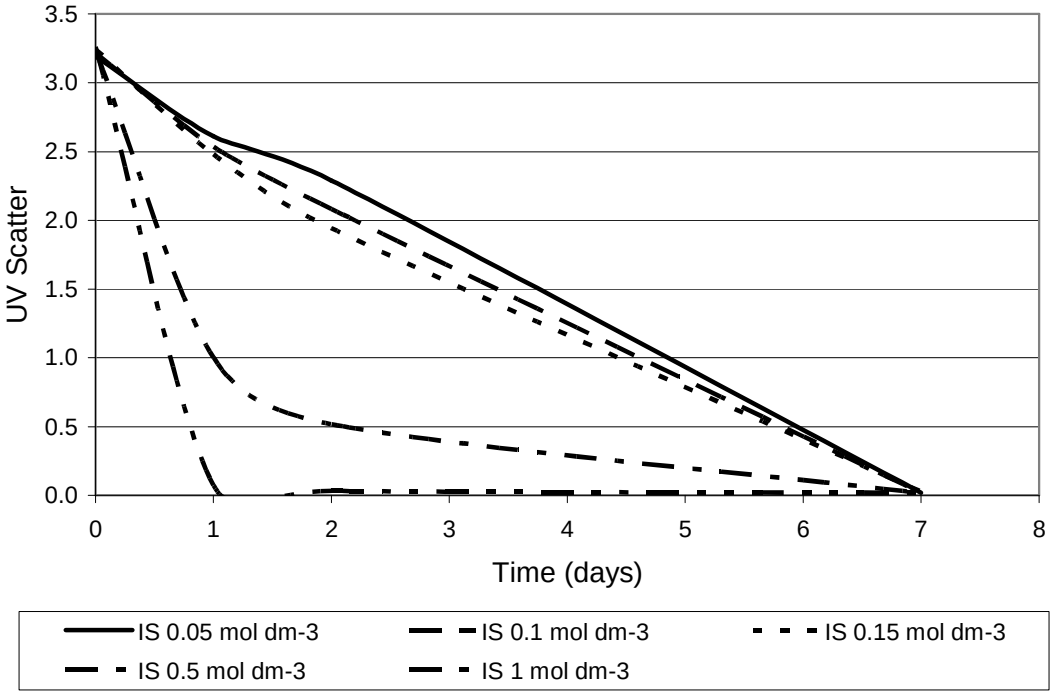

Figure 66. UV Scatter of silica colloids as a function of time and ionic strength (IS).

Figure 66 shows the kinetic stability of silica colloids at different ionic strengths over a period of seven days. The plots shown are the scattering of the colloid suspensions as synthesised, without further dilution. The high concentration of colloids in the synthesised suspension explains the high values of UV scattered light. Note that scatter decreased with time, more rapidly as the ionic strength increased. At the highest ionic strengths (0.5 and 1 mol dm^{-3}) the scatter of UV-Vis decreased drastically after one day. Thus, as the ionic strength increased, the stability of the colloids decreased. For ionic strenth 1 mol dm^{-3}, the colloids had flocculated after 24 hours. The ionic strength used in all experiments was 0.05 mol dm^{-3}. Also, for all migration experiments, the colloids were synthesised *in situ*, to avoid flocculation problems during storage.

4.3.1.2. Eu-doped silica colloids

The Eu doped silica colloids were characterised by measuring the average size, the zeta potential and the gamma activity. The reproducibility of the synthesis of Eu doped silica colloids is shown in Table 42, where the measured properties of three different sets of Eu doped silica colloids are summarised.

Table 42. Characterisation of Eu doped silica colloids.

	Set 1	Set 2	Set 3
Initial Activity (Bq cm^{-3})	385.17	316.78	322.44
Final Specific Activity (Bq cm^{-3})	310.84	152.93	194.09
Radiolabelling yield (%)	80.7	48.3	60.2
Average Size (nm)	167.8 ± 2.9	100.6 ± 15.8	253.7 ± 6.8
Zeta Potential (mV)	-56.7 ± 3.7	-50.6 ± 11.4	-46.8 ± 2.9

The initial activity refers to the activity of ^{152}Eu added at the beginning of the synthesis procedure, and the specific activity refers to the activity of the radiolabelled colloids measured at the end of the synthesis procedure. The radiolabelling yield varies in the three sets prepared. As the ratio of reactants added to each set of samples was equal in all three cases, the following experimental factors are discused:

- Prior to the average size and zeta potential measurements, the samples were diluted due to the high concentration of colloids. Dilution, however, should not affect the properties of the synthesised colloids.
- A different batch of dialysis bags were used for the synthesis of Set 3. This could be a reason for the slightly higher values of average size observed compared to the other two sets.
- The ionic strength is an important factor influencing the stability of colloids, but in this case, the ionic strength of the dialysis solution was kept constant at 0.05 mol dm^{-3}, as the solution was prepared *in situ*.
- The pH of the suspensions was adjusted on conclusion of the synthesis. Changes in pH could have occurred during the synthesis steps, explaining the differing properties of the colloids in the three different sets.

As previously mentioned, the synthesised Eu doped silica colloid suspensions were highly concentrated. To achieve a good UV-Vis measurement, the suspensions were diluted by taking different volumes of suspension into 10 cm^3 of deionised water. The scatter in UV-Vis light, as well as the specific activity, were measured and a calibration curve was plot (Figure 67).

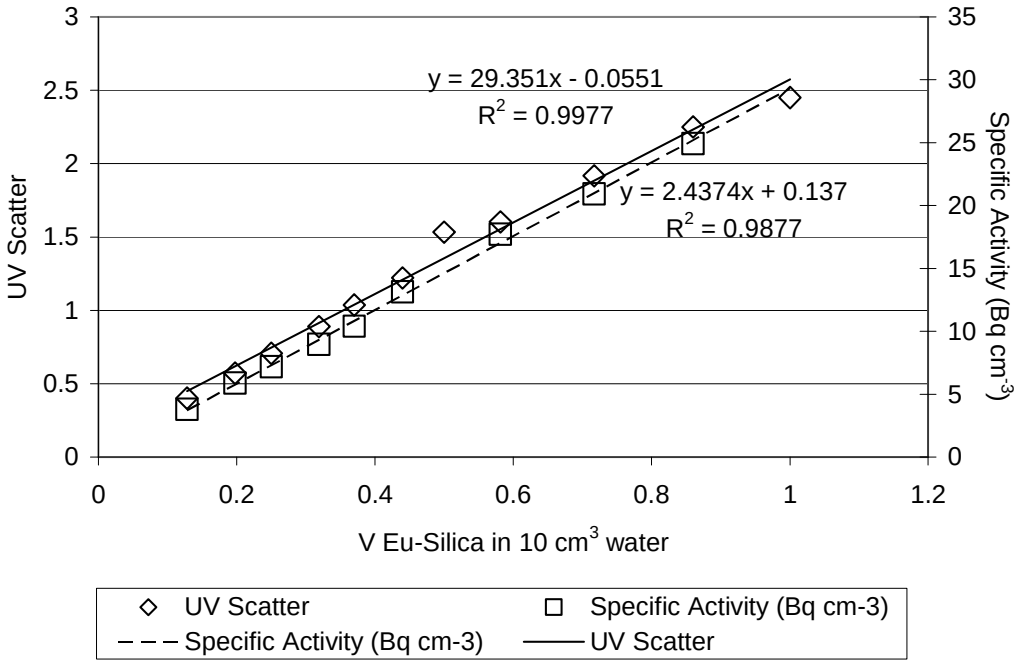

Figure 67. UV Scatter and specific activity of silica colloids in DI water.

Figure 67 shows a good correlation between both the UV scatter and the specific activity with the dilution of colloids in water. The calibration showed a linear relation between the volume of colloids and the UV light scattered or the specific activity. At higher concentrations of colloids in water, the UV scatter curved to a plateau (not shown), indicating that the light detected by the UV detector was originated by the scattering of the light to other surrounding colloidal particles, rather than being scattered directly by the particles.

Two experiments were carried out to study whether the ^{152}Eu label had been incorporated into the structure of the silica colloids. In one experiment, 10 cm^3 of Eu doped silica colloids (Set 2 in Table 42) were contacted with 4 g ion exchange resin (Amberlite IR-120). The activity of the supernatant was measured before and after equilibration (1 hour). A blank test was also carried out where the ion exchange resin was contacted with 10 cm^3 of aqueous Eu^{3+} (76.4 kBq dm^{-3}). The results for the blank test proved that the ion exchange resin sorbed effectively all the free Eu, as less than 1% of the initial activity was detected in the supernatant after the equilibration time. The results for the Eu doped silica colloids showed that approximately 70% of the initial activity remained in suspension after equilibration with the ion exchange resin.

A second experiment involved centrifuging a sample of Eu doped silica colloids (Set 2 in Table 42). The supernatant was measured for activity before and after centrifugation. After the process of centrifugation, the colloids were redispersed in the presence of different concentrations of NaCl. The samples were left to equilibrate and centrifuged again. The activity was measured before and after every treatment. The results are shown in Figure 68.

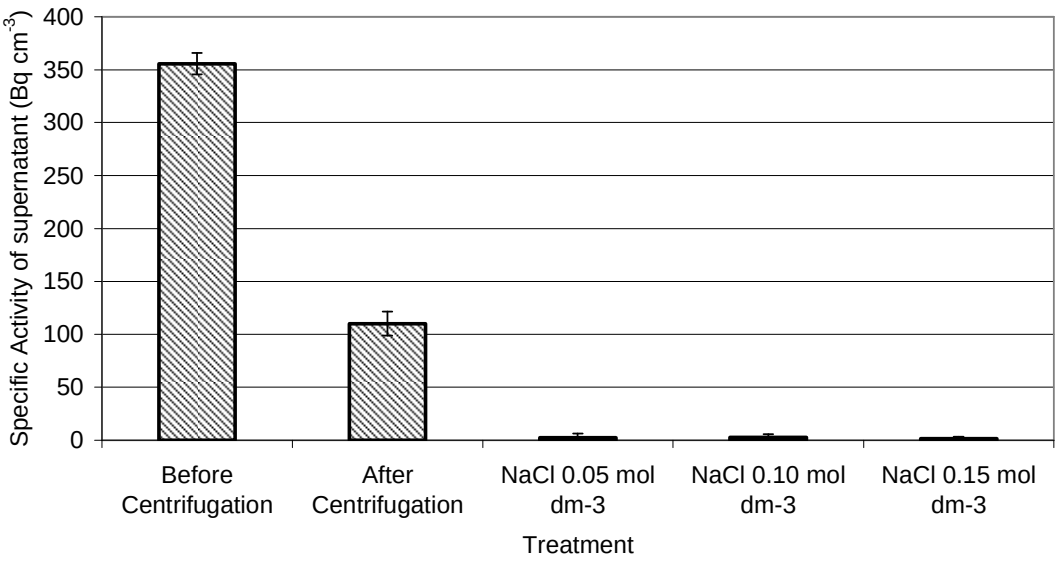

Figure 68. Specific activity of the supernatant of suspensions of silica colloids before and after centrifugation, and after redispersion in various concentrations of NaCl.

Figure 68 shows the specific activity (y-axis) of the supernatant in the samples described on the x-axis. The Eu doped silica colloids had an initial specific activity of approximately 350 Bq cm^{-3}. After centrifugation, the activity in the supernatant decreased by approximately 30% and, hence, 70% of the activity remained in the colloids. These results are in agreement with the findings from the experiments discussed earlier in this section. Furthermore, after redispersing the Eu doped silica colloids in various NaCl solutions and centrifuging these samples, the activity in the supernatant was negligible. These data show that the Eu^{3+} ions were not exchanged with the Na^{+} ions when sodium chloride solution was added.

Both experiments yielded the same results. Therefore, it can be assumed that after a treatment with ion exchange resin the $^{152}Eu^{3+}$ ions present in the sol are inside the

structure of the silica colloids. This treatment was applied prior to the use of the Eu doped silica colloids in the column experiments to ensure that no free Eu^{3+} ions were flooding the column.

4.3.2. Migration experiments

4.3.2.1. Migration of Eu-doped silica colloids through sand column

UV spectrophotometric techniques have been used in numerous studies to follow the transport, deposition and release of colloids [197,198,166,168]. In this work, the migration of silica colloids was studied radiometrically by radiolabelling the silica colloids with ^{152}Eu, which was incorporated in the structure of the colloids during its synthesis. The Eu doped silica colloids were introduced into the column as described in section 4.2.3.1 and the results are shown below. Table 43 shows the experimental parameters for the column experiment.

Table 43. Experimental parameters of column experiment carried out for the assessment of the migration of Eu doped silica colloids through sand column.

Colloid size (nm)	258.5 ± 5.0
Sand grain size (μm)	200
Column diameter (cm)	2.6
Column height (cm)	30
Porosity	0.39 ± 0.03
Dead/Pore volume (cm^3)	62.1 ± 4.5
pH	7.23
Colloid / water flow (cm^3 min^{-1})	0.260 ± 0.005

The elution of the conservative tracer and Eu doped silica colloids from the column as a function of total volume eluted is shown in Figure 69. Tritiated water was used as the conservative tracer, since it would not exhibit anion exclusion effects. The column porosity was calculated as the ratio between the volume filled with water (V_w) and the total volume of the column (V_T). The volume filled with water was measured as the volume at which tritium started to be detected in the outlet of the

column. The total volume and the porosity of the column were calculated by Equations 4.2 and 4.3, respectively [199].

$$V_T = \frac{\pi r^2}{4} l \qquad \textbf{Equation 4.2}$$

$$\phi = V_w / V_T \qquad \textbf{Equation 4.3}$$

Where r and h are the diameter and the height of the column, in cm, respectively, and ϕ is the porosity. The average porosity resulted in 39.0 ± 3.0%, which is in agreement with values reported by previous studies (between 37.7% and 47.7% [198,200,201]).

The breakthrough curve for both the tritiated water and the Eu doped silica colloids as a function of the total volume eluted can be seen in Figure 69(a). The breakthrough of the Eu doped silica colloids was followed by gamma counting since it was the ^{152}Eu radiolabel, rather than the silica colloids, the element measured.

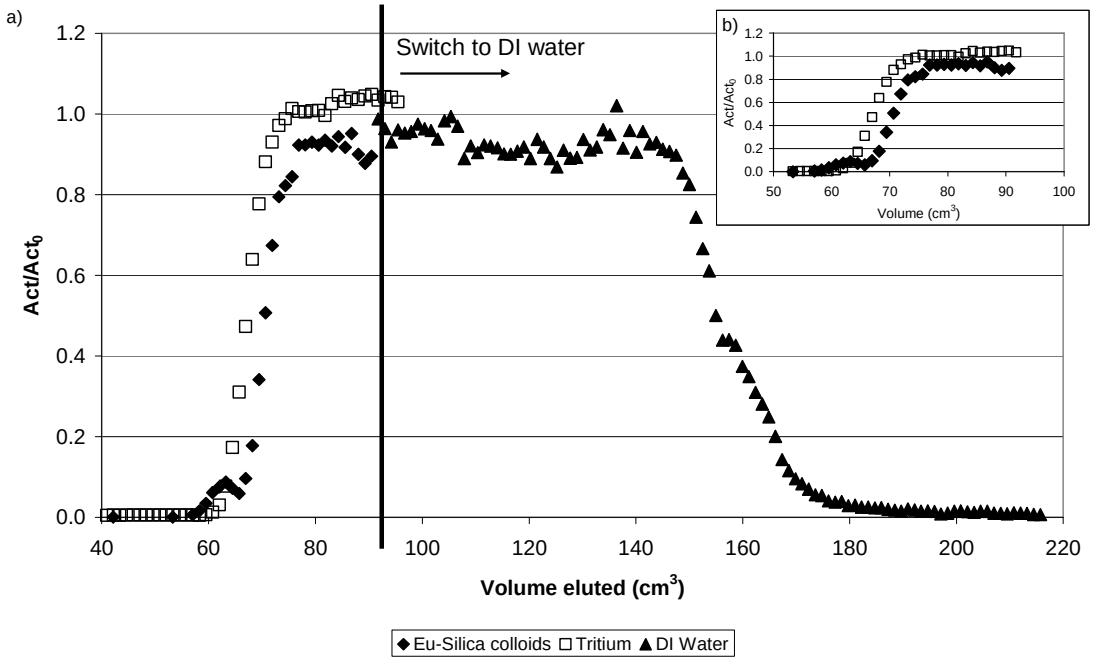

Figure 69. Recovery of Eu doped silica colloids and conservative tracer through sand column (pore volume = 60.75 cm^3). (a) Whole experiment and (b) Beginning of the breakthrough.

It can be seen that after starting the upflooding of Eu doped silica colloids, C/C_0 soon reached 0.90 and fluctuated between 0.87 and 0.98, indicating that little retention of colloids took place and almost full throughput was attained. On downflooding, the Eu doped silica colloids returned to zero with little tailing, indicating again slight interaction between the silica colloids and the column.

Figure 69 (b) shows the beginning of the elution curve, where it can be observed that the Eu doped silica colloids elute at a similar velocity as the conservative tracer. Previous studies have shown that breakthrough of silica colloids took place slightly faster or at the same time than tritiated water [198,165,174]. The slight retention observed in the experiment is most probably due to the electrostatic repulsion occurring between the negative surface charge of both silica colloids and the quartz sand bed in the column [174]. Several studies have observed little or no retention of negatively charged colloids passing through quartz sand columns [169,166,168,202].

The high recovery of Eu doped silica colloids suggests that the ^{152}Eu radiolabel was stable throughout the whole experiment. Studies investigating the elution of ^{152}Eu through a sand column in the absence and presence of colloids showed a 20% recovery of ^{152}Eu after approximately 20 pore volumes in the presence of colloids and no recovery in the absence of colloids [198]. Therefore, the detection of ^{152}Eu can be attributed solely to the ^{152}Eu doped silica colloids.

The total recovery of Eu doped silica colloids at the end of the experiment was calculated from the ratio of the overall activity measured from the outlet and the initial activity in the inlet, *i.e.* 3.38 kBq were recovered from the original 4.05 kBq in the suspension. These results yielded a 83.4% recovery of Eu doped silica colloids at the end of the downflood with DI water, indicating partial retention of the silica colloids in the sand column. A second wash with DI water was carried out, but no significant activity was detected in the outlet, suggesting the possibility that colloids were retained in the column in some manner that the colloids could not be released by further elution.

4.3.2.2. Migration of Cs associated to Eu-doped silica colloids

4.3.2.2.1. Sorption of Cs to silica colloids

The migration of ^{137}Cs contacted with Eu doped silica colloids was studied through a column of the same dimensions as the one described in the previous section. Prior to these experiments, the sorption of Cs onto silica colloids was investigated by means of batch experiments to study the extent of sorption of Cs onto silica colloids. The sorption isotherm as well as the percentages bound are shown in Figure 70 and Figure 71.

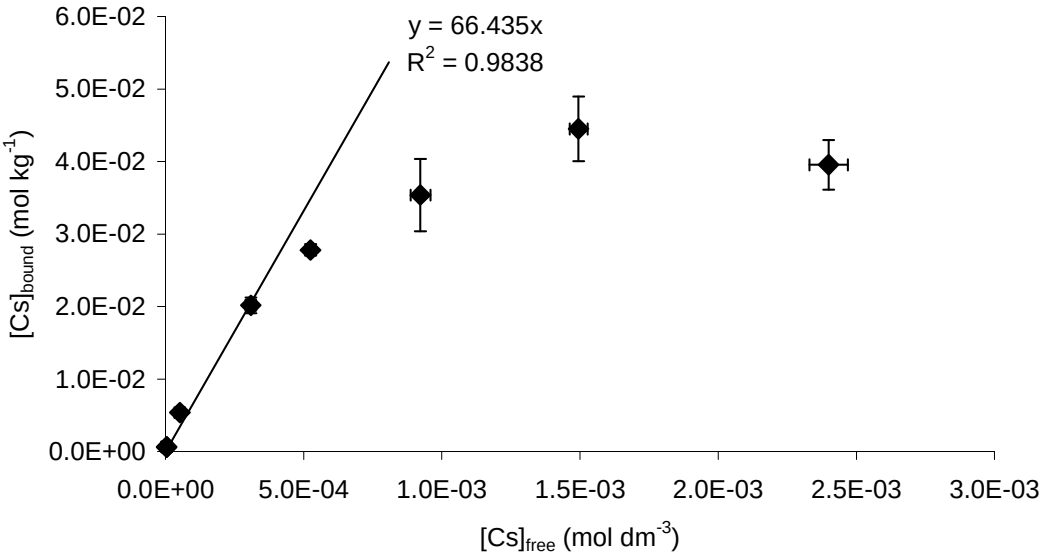

Figure 70. Sorption isotherm of Cs sorption onto silica colloids at pH 7.

The sorption isotherm shows a rapid increase of the amount of Cs bound with increasing Cs in solution, to a point where it curves and saturation begins. The slope of the linear part of the curve corresponds to the R_d value, which has a value of approximately 65.3 ± 4.1 dm^3 kg^{-1} under the conditions studied (pH 7 and ionic strength 0.05 mol dm^{-3}). This value is significantly higher than that observed by Flury *et al.* [203], who measured for 0.01 and 0.1 mol dm^{-3} ionic strength R_d values of 0.550 and 0.274 dm^3 kg^{-1}, respectively. The difference in R_d values are due to the different particle size of silica colloids used in this experiment, as opposed to non-colloidal particles used by Flury *et al.*[203]. Smaller particles provide a larger surface area where metals can bind to (discussion in Chapter 2).

The sorption percentages (Figure 71) show how, even at lower Cs concentrations, the sorption percentages show a maximum of 50% sorption. The findings are in agreement with Bascetin *et al.* [204], who observed a sorption of Cs onto silica gel (15 to 40 μm in particle size) lower than 40%. The slightly higher sorption percentage observed in Figure 71 is probably due to the smaller particle size (253.7 nm) used in the present experiment.

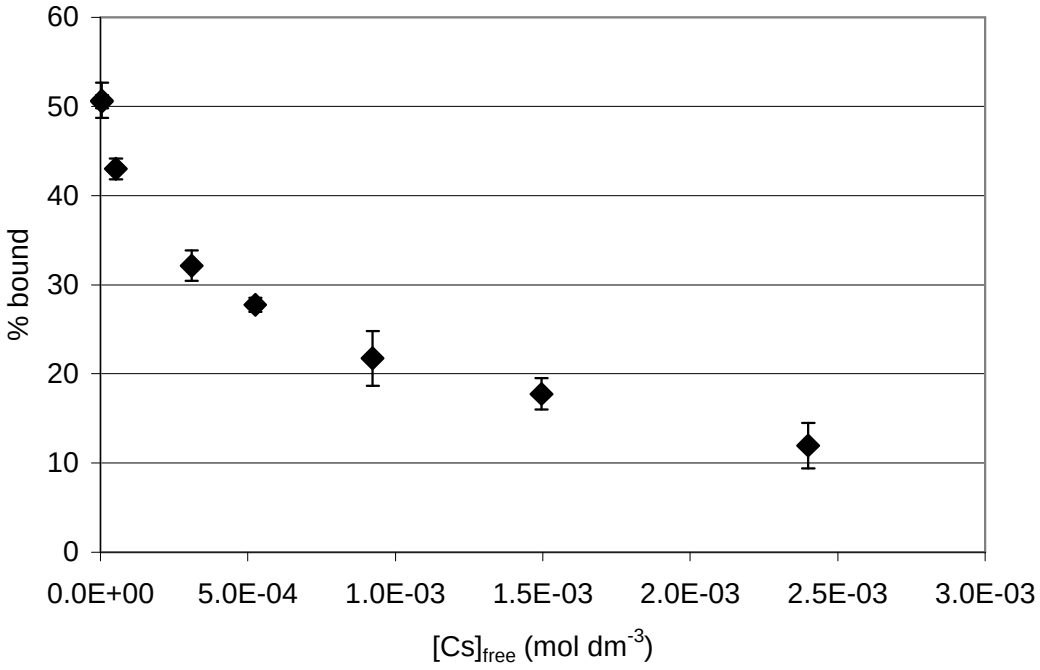

Figure 71. Sorption percentages for Cs sorption onto silica colloids at pH 7 and ionic strength 0.05 mol dm^{-3}.

Modelling

The sorption behaviour of Cs onto silica colloids was modelled by fitting the isotherms to the Langmuir, Freundlich and D-R isotherms.

The parameters obtained from each isotherm, as well as the fitting parameters are shown in Table 44. The Langmuir model did not fit the experimental values, as reflected by the low R^2 value observed. The Freundlich and D-R models could explain the sorption behaviour of Cs onto silica colloids.

Table 44. Modelling parameters for Cs sorption onto silica colloids.

R^2	Langmuir	0.9282
	Freundlich	0.9925
	D-R	0.9917
Freundlich parameters		F = 7.63 n = 0.76 ± 0.03 Q_{max} = 2.75 x 10^{-2} mol kg^{-1}
D-R parameters		K = (6.21 ± 0.03) x 10^{-3} E = 8.97 kJ mol^{-1}

The Q_{max} parameter calculated (2.75x10^{-2} mol kg^{-1}) corresponds to the maximum amount of Cs that would sorb onto the surface of the silica colloids. This value would correspond to the plateau which the curve tends to in the isotherm (Figure 70). It can be observed that although the predicted value is in the same order of magnitude as the experimental value, it is slightly lower than the observed value in the isotherm, which is approximately 4.5 x 10^{-2} mol kg^{-1}. The results from modelling shown in Table 44 are in good agreement with the findings reported by Bascetin *et al.* [205] and Pathak *et al.* [206] (see Table 45 for comparison). Noell *et al.* [174] reported a K_d value of 23.8 ± 1.2 dm^3 kg^{-1} and a Freundlich parameter n = 0.88 ± 0.01. The sorption energy (E) calculated from the D-R model resulted in 8.97 kJ mol^{-1}, which is also in agreement with the literature. This value of energy suggested an ion exchange sorption mechanism.

Table 45. Comparison of modelling parameters for Cs sorption onto silica colloids.

	Experimental	E. Bascetin [205]	P.Pathak [206]
n (Freundlich model)	**0.76 ± 0.03**	0.82	0.71 ± 0.02
K (D-R model) $x10^3$	**6.21 ± 0.23**	6.3	6.18 ± 0.14
E (D-R model) (kJ mol^{-1})	**8.97**	8.91	9.00 ± 0.09

Desorption

Desorption of Cs from silica colloids was studied by adding fresh deionised water to the previously sorbed Cs silica colloids. The desorption isotherm is shown in Figure 72, where the slope indicated that only 11.1 ± 1.2% of the Cs bound to the silica colloids was desorbed after a 24 hour period. However, the desorption of Cs from silica colloids was non-linear. The percentages of desorbed Cs increased with the Cs bound.

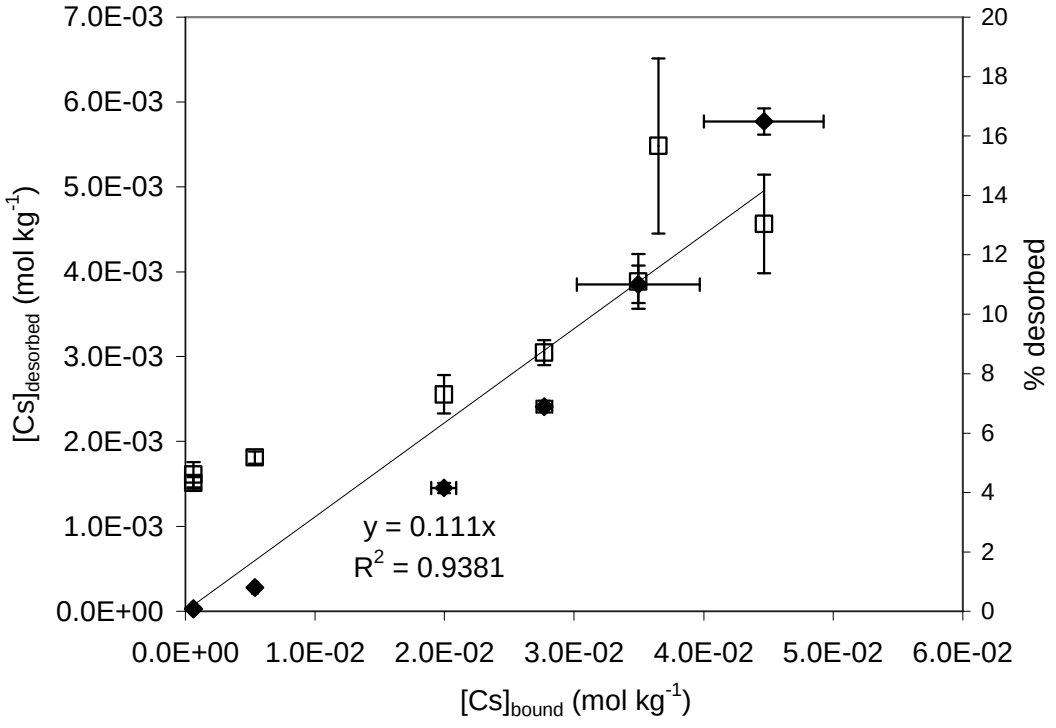

Figure 72. Desorption of Cs from silica colloids at pH 7 and ionic strength 0.05 mol dm^{-3}.

4.3.2.2.2. Migration of ^{137}Cs associated to Eu-doped silica colloids

The findings in the investigation of Cs sorption onto silica colloids suggested that Cs sorption to silica colloids took place via an ion exchange mechanism. A spike of Cs

was contacted with an aliquot of Eu doped silica colloids and left to equilibrate for 1 hour. Prior to flooding it through the column, an ion exchange resin was added to remove any excess Cs ions remaining in solution. The results for both Cs and Eu doped silica colloids breakthrough are shown in Figure 73.

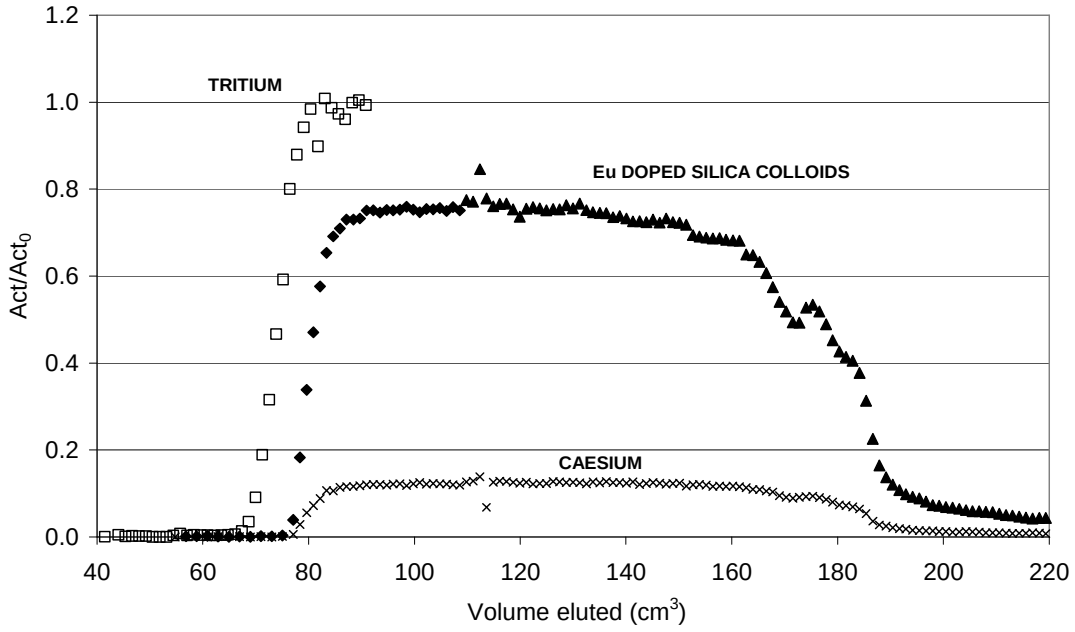

Figure 73. Cumulative recovery of Cs and Eu doped silica colloids through a sand column (Pore volume = 71.3 cm^3).

Figure 73 shows the breakthrough for the conservative tracer (tritiated water), superimposed onto the breakthrough of Cs associated to silica colloids and Eu doped silica colloids, as well as their elution with DI water. Four main aspects can be highlighted from the breakthrough curve, concerning both the migration of Eu doped silica colloids and Cs^+ ions:

(a) A slight delay on the breakthrough of both the colloids and the Cs can be observed with respect to the conservative tracer.

(b) Approximately 4.2 kBq of Eu (Eu doped silica colloids) were flooded in the column, from which 3.31 kBq were recovered by the end of the experiment, yielding a 78% recovery of Eu doped silica colloids.

(c) Less than 20% of Cs associated to silica colloids was recovered.

(d) Tailing appears upon downflood of both the Eu doped silica colloids and the Cs associated to the silica colloids.

The migration of silica colloids through the sand column was markedly different when the colloids were associated with Cs^+ ions. The experimental observations will be discussed in order to understand the effect of the introduction of positive charges in the system studied.

In the absence of Cs (Figure 69) the Eu doped silica colloids eluted similarly to the tritiated water, suggesting that the electrostatic repulsions between the sand and the silica colloids prevented the silica colloids from being retained in a significant extent. However, the presence of positive charges altered the system, introducing attractive van der Waals forces between the exchangeable Cs cations attached to the silica colloids interacting with the sand in the column. These interactions resulted in the retardation of the migration of the silica colloids, as well as in the retention of Eu-doped silica colloids.

The total retention of Eu doped silica colloids was calculated as the ratio between the activity measured in the effluent at the end of the experiment (3.15 kBq) and the activity in the inlet (4.25 kBq). These results showed a 74.3% recovery of the Eu doped silica colloids. Compared to the recovery obtained in the absence of Cs ions associated to the silica colloids (83.4%), the value calculated in this section is slightly lower, suggesting again that the presence of Cs altered the migration behaviour of the silica colloids.

The elution and downflood of Cs occurred at the same time as the silica colloids, indicating that the recovery of Cs is due to association with the colloids. Furthermore, the elution of Cs takes place after 1.2 pore volumes, whereas in the absence of colloids, Saiers *et al.* [207] observed elution of Cs after 10 pore volumes through a quartz sand column at pH 7.2 and ionic strength 0.01 mol dm^{-3}. Moreover, prior to flooding the column with Cs associated to silica colloids, cation exchange resin was added to the equilibrated suspension to remove any free Cs from suspension; therefore, any Cs passing through the column was bound to the silica colloids.

The total recovery observed for Cs was approximately 13% (0.58 kBq were measured in the effluent from the original 4.4 kBq in the inlet). Monitoring of the

activity along the column with a NaI detector took place at the end of the experiment. The monitoring showed that the majority of the Cs activity was removed within the first third of the column, followed by a plateau at the top of the column (Figure 74). No ^{152}Eu activity (associated to silica colloids) could be detected, as the NaI detector gave no readings, or backgroung readings in the region of interest corresponding to ^{152}Eu.

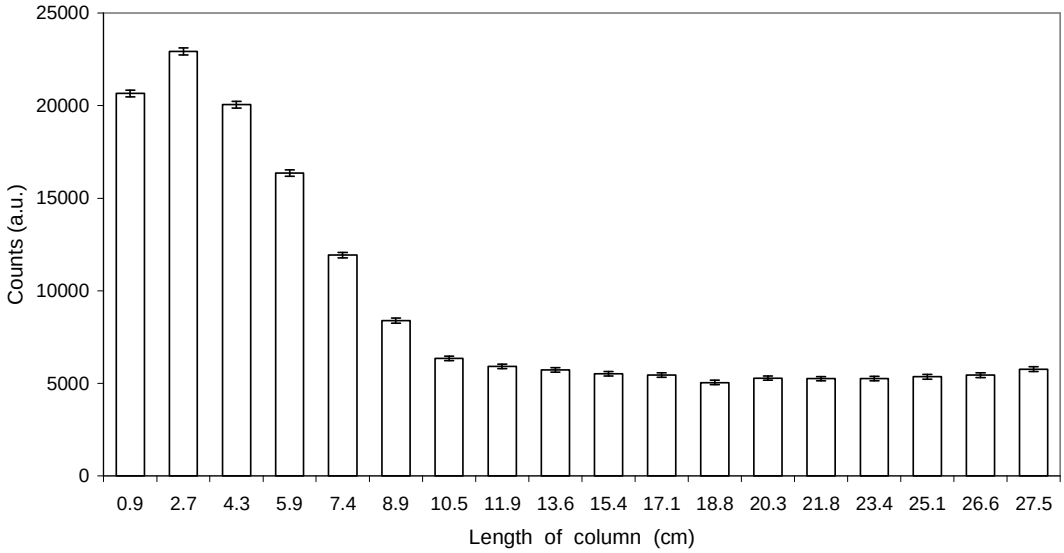

Figure 74. Measurement of ^{137}Cs activity (4.4 kBq) with NaI detector (ROI = 282 – 354) along column length after flooding of column with Cs associated to Eu doped silica colloids and DI water. Segments measured for 40 minutes.

Figure 74 shows the intensity of the activity in each segment of the column, represented by the counts measured by the NaI detector. The counts represented are the net counts recorded by the instrument, with the background counts substracted. The initial activity that was flooded in the column was measured as well prior to its flooding. The instrument recorded 144540 ± 228 net counts for this sample.

Two regions can be distinguished: during the first 10 cm of the column, strong retention of Cs onto the sand took place; Cs desorbed from the silica colloids and sorbed onto the sand, via an ion exchange mechanism. Beyond the first third of the column, a constant distribution of Cs along the column could be observed. Further injection of the column with DI water did not cause any significant extraction or

displacement along the column of Cs (Figure 76); moreover, the measurement with the NaI detector yielded a similar pattern as the one observed in Figure 74, indicating that Cs was not being transported any further by deionised water (Figure 77).

The results shown by the measurement of the γ-activity by the NaI detector appear contradictory with some of those shown by the measurements carried out in the γ-counter:

(1) The activities measured for each segment along the column added approximately 174557 counts, which are higher than the initial smple (approximately 144540). These results suggest that, not only that all the Cs which passed through the column was retained, but also that some extra activity was detected. These results are opposed to the approximate 87% retention found from the breakthrough curve.

The measurement of γ-activity along the column was carried out in such way that the end of one segment corresponded to the beginning of the following one. Although the lead bricks proved to be effective at shielding the detector from the rest of the column (control experiment detailed in Table 40), the extra γ-activity observed might be due to overlapping activities from the adjacent segments. Assuming this, an overlap factor (φ) may be defined as:

$$\varphi = \frac{A_{\exp ected}}{A_{observed}} = \frac{144540x0.87}{174557} = 0.72 \qquad \textbf{Equation 4.2}$$

Where the expected activity of Cs retained in the column at the end of the experiment ($A_{expected}$) would be approximately an 87% of the initial activity that entered the column. The $A_{observed}$ corresponds to the sum of the activities measured in each of the segments. Once the overlap factor is established, a new curve, more realistic of the Cs activity retained in each of the segments can be drawn (Figure 75). The shape of the diagram is the same as that prior to considering the overlap effect, but the net counts are smaller.

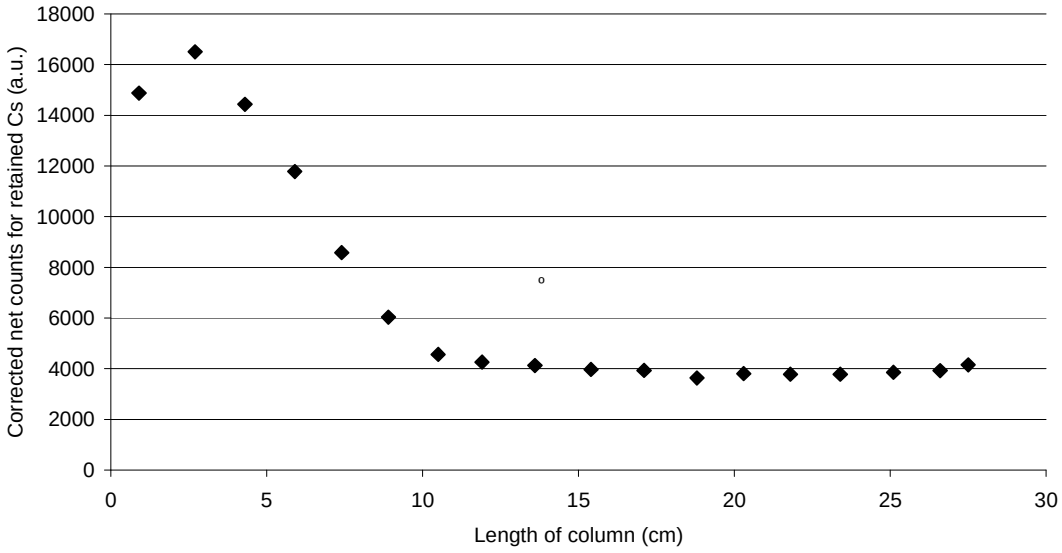

Figure 75. Corrected net counts for Cs retention along the column.

(2) The breakthrough curve showed that the levels of γ-activity from ^{137}Cs reached zero at the end of the experiment (Figure 76), suggesting that only ^{137}Cs associated to colloids were eluted from the column and free ^{137}Cs was retained in the column. When the NaI detector was used to find out the distribution of free ^{137}Cs along the column, constant values for the γ-activity of ^{137}Cs were recorded at the top of the column (Figure 74). Possible reasons for this findings include:

- The constant values of approximately 4000 net counts appear to be a baseline from the NaI detector. However, the background counts were substracted.
- Perhaps some movement of the suspension took place when the column was changed position for its measurement in the NaI detector, although maximum care was taken.
- The readings in the γ-counter for Eu-doped silica colloids showed that 25.7% of the colloids had been retained in the column. However, the NaI detector was unable to detect γ-activity coming from Eu. This could be due to a homogeneous distribution of the Eu-doped silica colloids along the column, which would result in a low γ-activity per segment. Assuming that these colloids were Cs-bound silica colloids, a baseline in ^{137}Cs activity could be explained by the homogeneous distribution of Cs-bound Eu-doped silica colloids along the column.

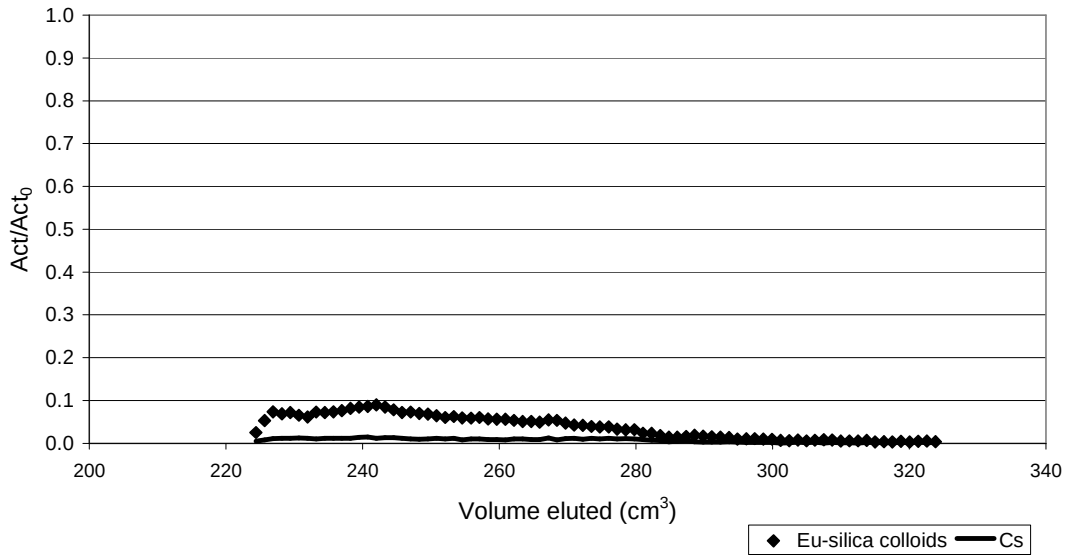

Figure 76. Breakthrough curve for second flush with DI water through Cs associated Eu-doped silica colloids - sand column

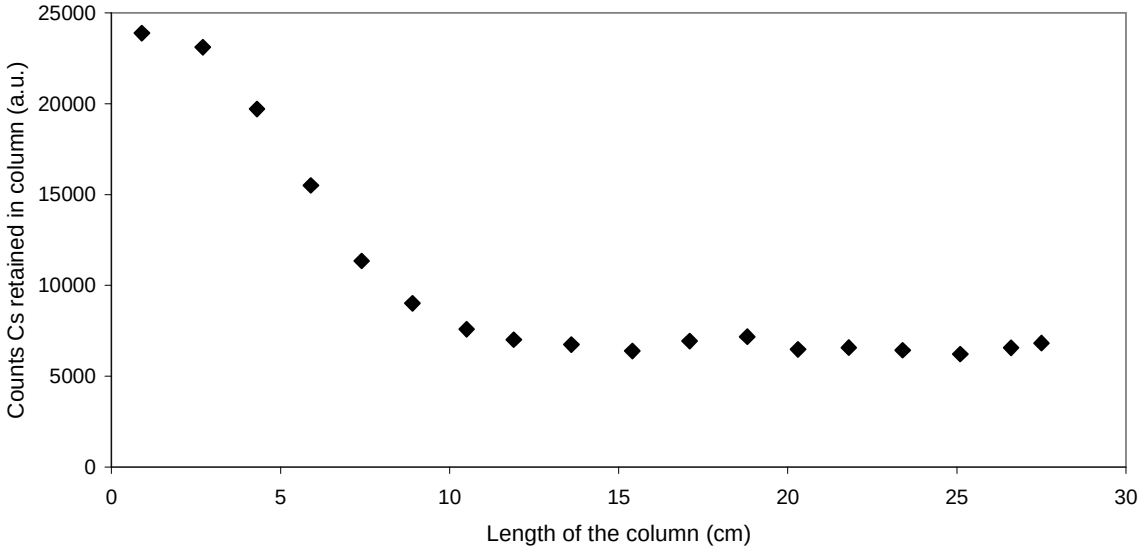

Figure 77. Na-I detector pattern for second flush of DI water through Cs associated Eu-doped silica colloids - sand column

Modelling

An attempt to model the retention of Cs associated to silica colloids was made by using some simple calculations, where the column was divided into 15 segments, 2 cm long each. The model assumed equal retention of Cs onto each segment. Previous measurements showed that the column retained approximately 86 – 87% of Cs, or, in other words, that the total recovery of Cs was 13.2%. With these data, the model

predicted 12.5% retention in each segment. A scheme of this can be seen in Figure 78. This model would allow to understand the distribution of the retained Cs along the column.

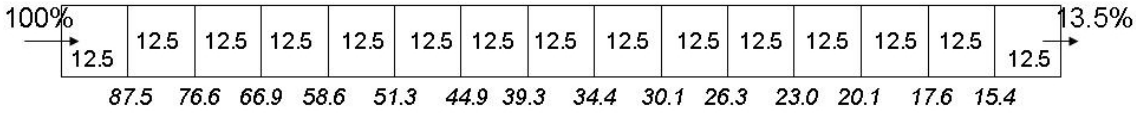

Figure 78. Modelling approach for Cs migration through sand column in the presence of silica colloids.

Figure 78 shows the breakthrough of Cs passing through the column in the case of equal retention in each segment of the column. A 12.5% retention in each segment was assumed for the modelling so that the total Cs recovered coincided with the experimental observation (approximately 13.5%). The numbers in italics show the percentage of Cs going through each segment. A plot of the expected retention predicted by the model and the measured retention is shown in Figure 79. The simple model failed to reproduce the experimental findings.

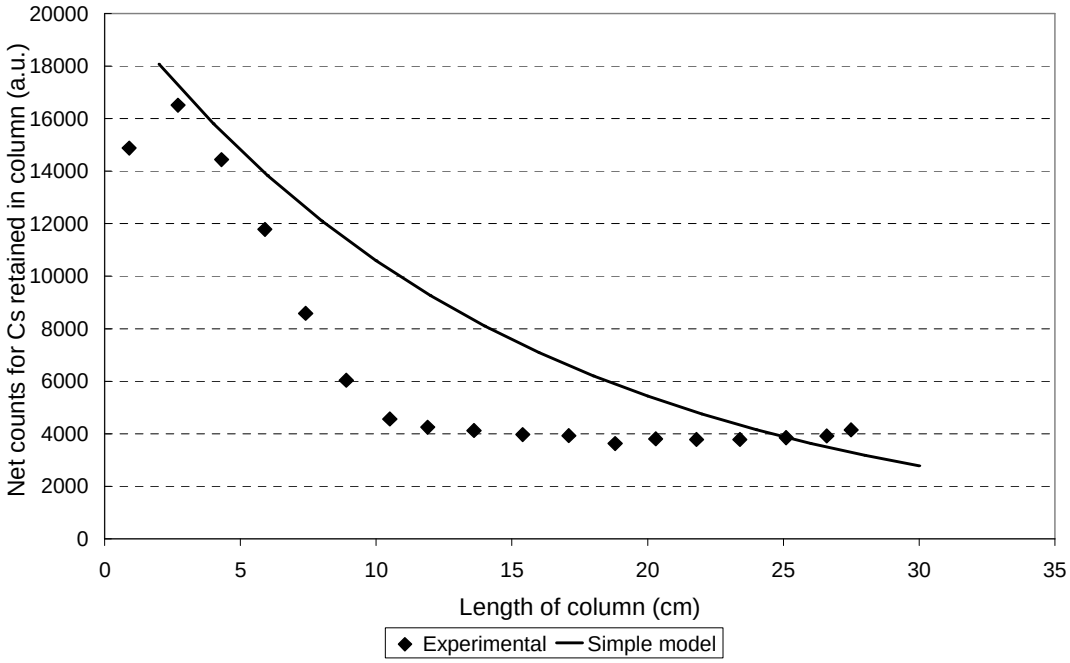

Figure 79. Modelling of Cs through sand column when associated with silica colloids.

4.4. Conclusions

The aims of this study were to synthesise stable Eu-doped silica colloids, and use these as a tool to investigate the migration of silica colloids through a sand column.

The Eu-doped silica colloids were succesfully synthesised by modification of a known method. Stability experiments were performed and indicated that the colloids were sufficiently stable to use them for migration experiments. Also, the stability of the radiolabel was such that the radiolabelled colloids could be detected and quantified by radiometric measurements.

The transport of Eu-doped silica colloids was thus studied radiometrically, showing near-complete recovery of silica colloids when passed through a sand column. The study also revealed low retention and little tailing of the silica colloids; results which were expected due to the similar nature of both silica colloids and sand, where the major interaction would be electrostatic repulsion, generating a rapid migration of the colloids through the column.

Using the same radiometric techniques, the migration of Cs ions when associated to Eu doped silica colloids was investigated. This experiment proved an enhancement of the transport of Cs by silica colloids, as approximately a 13% recovery was observed. The interaction of Cs^+ ions with the silica colloids and the surface of the sand in the column slightly retarded the transport of silica colloids through the column.

Chapter 5. CONCLUSIONS AND FURTHER WORK

The work presented in this thesis is divided into three parts: (i) the sorption of metals onto colloidal particles; (ii) the effect that organic colloids, HA, have on such sorption; and (iii) the effect that colloids may have on the migration of radionuclides.

The stability of colloidal particles is one of the necessary conditions for migration of colloids to occur, as non-stable colloids flocculate or coagulate leading to retention of the particles. The main parameters influencing stability are pH and ionic strength. Findings reported in this work have shown that stability of boehmite and montmorillonite colloids is achieved at low concentrations of ionic strength. The dependence of the stability of these colloids with pH was opposite for each of the colloids, due to the difference in overall positive charge for boehmite and negative charge for montmorillonite, which caused boehmite colloids to achieve stability at low to neutral pHs, whereas montmorillonite colloids would gain stability at neutral to high pHs. The stability of boehmite colloids was found to depend on the concentration of HA present; low and high concentrations promoted the stability of colloids whereas intermediate concentrations caused flocculation and coagulation.

Given stable colloidal suspensions in motion with groundwater flow, radionuclides found in the subsurface may interact with these suspensions, thereby enhancing the transport of contaminants. Chapter 2 focused on the sorption of metals onto two different colloidal minerals. Results showed that metal sorption onto the colloidal suspensions occurred and this sorption was quantified by the distribution ratio, R_d, which is the ratio between the surface-bound metal concentration and the concentration of dissolved metal in solution. Despite boehmite having an overall positive charge, the metals showed affinity for the hydroxyl groups on the surface and bound effectively to the colloids.

The sorption of metals was also measured on the solid phases of the same minerals. The general trend observed was that sorption was higher on the colloidal phase. A quantitative approach introduced an R_d relationship between colloids and solid surfaces by a proportionality factor, which for boehmite used the ratios between the cation exchange capacities of the colloid and the solid multiplied by the charge of the

metal. This approach however, was only examined for the experimental values obtained for boehmite. Further research includes the application of this mathematical approach to different colloidal systems, *i.e.* montmorillonite, bentonite, goethite. The success of such mathematical approach would be time-saving in the calculation of distribution ratios for binary systems with metals and colloids.

Knowledge of desorption processes is relevant in order to assess the transport of radionuclides through the Geosphere because the enhancement of the transport of contaminants is achieved if the association is irreversible. Results reported herein indicated that Ni desorbed by 50% from colloidal montmorillonite, whereas Eu only desorbed by 3%. The findings suggest that Eu could be transported by montmorillonite longer distances than Ni, due to the low desorption percentage exhibited by the former.

Both ion exchange and surface complexation were used to explain the partial reversibility observed in the sorption of the minerals. Ion exchange would account for the desorption of the metal by replacement by other metal ions present in solution; whereas surface complexation would explain the irreversible fraction of the sorption, i.e. chemical bonding of the metals onto surface sites led to their fixation to the surface. The mechanisms of sorption, however, were qualitative and based on findings reported in the literature.

The specific surface area of colloids was measured by the BET method, which involved the solidification of the colloidal suspension. During this process, the surface of the colloids was altered by the formation of aggregates. The sorption of dyes has been used to measure the specific surface area of colloids like montmorillonite. However, on an attempt to use the same method on boehmite colloids, the use of four different dyes yielded unsuccesful results. Further work in this field is strongly suggested, as measurement of this property by drying processes have shown to affect negatively the results obtained.

Humic acids are ubiquitous in all natural soils, thereby affecting the stability of colloids as well as the sorption of metals onto them. The findings reported herein were consistent with those found in the literature and suggested a decrease in the

sorption of metals onto boehmite colloids in the presence of HA, when compared to that observed in the absence of humics. Thus, transport of radionuclides by inorganic colloids would probably be hindered in the presence of HA.

An attempt to model the influence of HA, using the LAM was applied to the ternary system. The application of the LAM was successful assuming that the fraction of HA bound to the colloids was close to unity.

The stability of boehmite colloids was clearly influenced by HA concentration. The repulsive interactions introduced by HA at intermediate concentrations favoured flocculation and coagulation of the particles. As the boehmite concentration of colloids increased, HA concentration necessary to induce flocculation also increased. Hence, at higher colloidal concentrations, batch sorption experiments should be carried out to investigate whether the LAM could be applied. Due to comparison with the results carried out in Chapter 2, these experiments were not analysed.

As stated in the introductory chapter, for colloids to be of relevance in the migration of radionuclides, two of the factors to be met were (1) sorption of metals onto the colloids, which Chapter 2 investigated for two colloidal minerals; (2) and the mobility of colloids with groundwater flow. Chapter 4 investigated the mobility of silica colloids and also investigated the facilitation of Cs transport by silica colloids.

The migration of colloids was assessed by studying the mobility of silica colloids through a sand column. Rather than traditional spectroscopic techniques, a radiolabelling technique was used for radiometrically detecting the colloidal phase along the length of the column. For this experiment, stable silica colloids were labelled from early stages of the synthesis so that the radiolabel would be embedded in the structure of the silica at the end of the process. Migration experiments showed that silica colloids migrated through the sand column with little retention. Moreover, the mobility of Cs was enhanced by the presence of colloids.

Overall, the investigations carried out herein clarify the interactions of multi-valent metals with colloidal particles, the influence of HA on these and the influence colloids may have on the mobility of radionuclides. Considering the results observed,

it is suggested that colloidal phases present in the environment may significantly alter the retention of contaminants, particularly radionuclides by enhancing their transport, to a higher or lower extent, depending on the reversibility.

PERSONAL DEVELOPMENT TRAINING

Date & Location	Title	Training Type	Duration
6th – 7th November 2006, Loughborough University	Long Term Nuclear Waste Management: Next Steps	Conference attendance	2 Day
15th November 2006, Loughborough University	Induction Day	Orientational course	1 Day
29th November 2006, University of Leeds	RSC Annual Meeting		1 Day
11th December 2006, Louhborough University	Designing and Producing Conference Posters	Training course	½ Day
6th February 2007, London	A report of the Loughborough Workshop		1 Day
8th – 9th February 2007, Sellafield	Underpinning Assessment Sciences Programme Symposia	Tour and open day	2 ½ Day
8th March 2007, Loughborough University	Talks on Analytical Chemistry	Lecture series	½ Day
28th March 2007, Loughborough University	Report Writing	Training course	½ Day
17th – 19th April 2007, Loughborough University	COGER	Conference attendance and presentation of first year work	3 Day
25th April 2007, Leeds	Latest Developments in Particle & Material Characterisation Complimentary Seminars	Lecture series	1 ½ Day
30th May 2007,	AQUANET Colloids	Conference	2 Day

University of Birmingham	Workshop 2007	attendance	
25th – 30th August 2007, Münich, Germany	Migration Munich	Conference attendance	7 Day
January – September 2007, Loughborough	Malvern Instruments Webinars	Online lecture series	1 Day
23rd January 2008, BGS, Keyworth	Talk by Dr. Patrick Landais	Lecture attendance	½ Day
30th January 2008, Loughborough University	Teaching Skills Professional Development Course	Training course	1 Day
7th February 2008, Sheffield	Environmental Process Symposia (Nexia Solutions)	Conference attendance	1 Day
7th – 9th April 2008, University of Nottingham	COGER	Presentation of second year work	3 Day
16th April 2008, London	Young Researchers Meeting	Presentation	1 Day
23rd April 2008	PhD Research Training Programme: Plagiarism	Training course	½ Day
2007 – 2008	Physical Chemistry Foundation Year & First Year	Laboratory Demonstrating	+ 50 Hours
6th – 7th October 2008, Barcelona	3rd FUNMIG Training Course	Workshop attendance	2 Day
3rd – 6th August 2009, Glasgow	IUPAC Congress	Poster presentation and conference attendance	4 Day
21st – 24th September 2009, Kennewick,	Migration Seattle	Poster presentation and	4 Day

Seattle		conference attendance	
2006 – 2009, Loughborough University	Radiochemistry Group Meetings	Group meetings and presentations	Weekly

REFERENCES

[1] International Atomic Energy Agency. Use of Natural Analogues to Support Radionuclide transport Models for Deep Geological Repositories for Long Lived Radioactive Wastes. Vienna : IAEA, 1999. Technical Document. IAEA-TECHDOC-1109.

[2] NDA Radioactive Waste Management Directorate. Proposed research and development strategy. Nuclear Decomissioning Authority 2008.

[3] E. Tipping, J.J.W. Higgo. The role of colloids in the release and transport of radionuclides in the near and far field. British Geological Survey 1991. Fluid Processes Research Group Technical Report WE/91/16.

[4] D.J. Shaw. Introduction to colloid and surface chemistry. Butterworth-Heinemann. Fourth Edition

[5] M. Manciu, E. Ruckenstein. Role of the hydration force in the stability of colloids at high ionic strengths. Langmuir **17** (2001) 7061 – 7070.

[6] B. Sudhir, S. Kumar. Existence of a new force in colloidal systems – Hydrophobic attraction between macroscopic surfaces. Resonance April 2002 67 – 81.

[7] R. J. Hunter, *Foundations of Colloid Science*, Clarendon Press, Oxford, 2001.

[8] B.P. Singh, R. Menchavez, C. Takai, M. Fuji, M. Takahashi. Stability of dispersions of colloidal alumina particles in aqueous suspensions. Journal of Colloid and Interface Science **291** (2005) 181 – 186.

[9] J. Sun, B.V. Velamakanni, W.W. Gerberich, L.F. Francis. Aqueous latex/ceramic nanoparticle dispersions: colloidal stability and coating properties. Journal of Colloid and Interface Science **280** (2004) 387 – 399.

[10] P. Zhao, S.A. Steward. Literature review of intrinsic actinide colloids related to spent fuel waste package release rates. 1997. Lawrence Livermore National Laboratory, Contract W-7405-Eng-48.

[11] H.M. Beckhit, M.A. El-Kordy, A.E. Hassan. Contaminant transport in groundwater in the presence of colloids and bacteria: Model development and verification. Journal of Contaminant Hydrology **108** (2009) 152 – 167.

[12] T. Ilina, M. Panfilov, M. Buès, I. Panfilova. A pseudo two-phase model of colloid transport in porous media. Transport of Porous Media **71** (2008) 311 – 329.

[13] J.F. McCarthy, L.D. McKay. Colloid Transport in the Subsurface: Past, Present, and Future Challenges. Vadose Zone Journal **3** (2004) 326 – 337.

[14] E. Wieland, J. Tits, M.H. Bradbury. The potential effect of cementitious colloids on radionuclide mobilisation in a repository for radioactive waste. Applied Geochemistry **19** (2004) 119 – 135.

[15] A. Javaid, R. Bajwa, U. Shafique, J. Anwar. Removal of heavy metals by adsorption on *Pleurotus ostreatus*. Biomass and Bioenergy **35** (2011) 1675 – 1682.

[16] J. Maresova, M. Pipiska, M. Rozloznik, M. Horník. Cobalt and strontium sorption by moss biosorbent: Modeling of single and binary metal systems. Desalination **266** (2011) 134 – 141.

[17] J. Simunek, C. He, L. Pang, S.A. Bradford. Colloid-facilitated solute transport in variably saturated porous media: numerical model and experimental verification. Vadose Zone Journal **5** (2006) 1035 – 1047.

[18] R.A.A. Muzzarelli. Potential of chitin/chitosan-bearing materials for uranium recovery: An interdisciplinary review. Carbohydrate Polymers **84** (2011) 54 – 63.

[19] W.W. Wan Ngah, L.C. Teong, M.A.K.M. Hanafiah. Adsorption of dyes and heavy metal ions by chitosan composites: A review. Carbohydrate Polymers **83** (2011) 1446 – 1456.

[20] X. Yang, R. Flynn, F. von der Kammer, T. Hofmann. Quantifying the influence of humic acid adsorption on colloidal microsphere deposition onto iron-oxide-coated sand. Environmental Pollution **158** (2010) 3498 – 3506.

[21] A.B.M. Giasuddin, S.R. Kanel, H. Choi. Adsorption of HA onto nanoscale zerovalent iron and its effect on arsenic removal. Environmental Science and Technology **41** (2007) 2022 – 2027.

[22] A. Liu, R.D. Gonzalez. Adsorption/desorption in a system consisting of humic acid, heavy metals and clay minerals. Journal of Colloid and Interface Science **218** (1999) 225 – 232.

[23] T. Yoshida, M. Suzuki. Effects of humic acid on migration of montmorillonite and alumina colloid in a quartz sand column. Colloids and Surfaces A: Physicochemical and Engineering Aspects **325** (2008) 115 – 119.

[24] N. Evans, P. Warwick, T. Lewis, N. Bryan. Influence of humic acid on the sorption of U(IV) to kaolin. Environmental Chemistry Letters **9** (2011) 25 – 30.

[25] P.W. Warwick, A. Hall, V. Pashley, N.D. Bryan, D. Griffin. Modelling the effect of humic substances on the transport of europium through porous media: a comparison of equilibrium and equilibrium/kinetic models. Journal of Contaminant Hydrology **42** (2000) 19 – 34.

[26] T.S. Anirudhan, P.S. Suchithra. Heavy metals uptake from aqueous solutions and industrial wastewaters by humic acid-immobilized polymer/bentonite composite:

Kinetics and equilibrium modeling. Chemical Engineering Journal **156** (2010) 146 – 156.

[27] J.F. Boily, J.B. Fein. Proton binding to humic acids and sorption of P(II) and humic acid to the corundum surface. Chemical Geology **168** (2000) 239 – 253.

[28] D. Grolimund, M. Borkovec. Colloid-facilitated transport of strongly sorbing contaminants in natural porous media: mathematical modeling and laboratory column experiments. Environmental Science and Technology **39** (2005) 6378 – 6386.

[29] T. Kanti Sen, K.C. Khilar. Review on subsurface colloids and colloid-associated contaminant transport in saturated porous media. Advances in Colloid and Interface Science **119** (2006) 71 – 96.

[30] J.N. Ryan, M. Elimelech. Colloid mobilization and transport in groundwater. Colloids and Surfaces A: Physicochemical and Engineering Aspects **107** (1996) 1 – 56.

[31] T. Ilina, M. Panfilov, M. Buès, I. Panfilova. A pseudo two-phase model of colloid transport in porous media. Transport of Porous Media **71** (2008) 311 – 329.

[32] J.W. Bridge, S.A. Banwart, A.L. Heathwaite. Noninvasive quantitative measurement of colloid transport in mesoscale porous media using time lapse fluorescence imaging. Environmental Science and Technology **40** (2006) 5930 – 5936.

[33] O. Spalla, S. Desset. Direct evidence of lateral migration of mineral colloids adsorbed at a water-solid interface. Langmuir **16** (2000) 2133 – 2140.

[34] C. Hinz. Description of sorption data with isotherm equations. Geoderma **99** (2001) 225 – 243.

[35] A. Delos, C. Walther, T. Schäfer, S. Büchner. Size dispersion and colloid mediated radionuclide transport in a synthetic porous media. Journal of Colloid and Interface Science **324** (2008) 212 – 215.

[36] S. Kurosawa, S.C. James, M. Yui, M. Ibaraki. Model analysis of the colloid and radionuclide retardation experiment at the Grimsel Test Site. Journal of Colloid and Interface Science **298** (2006) 467 – 475.

[37] N. Albarran, T. Missana, M. García-Gutiérrez, U. Alonso, M. Mingarro. Strontium migration in a crystalline medium: effects of the presence of bentonite colloids. Hournal of Contaminant Hydrology **122** (2011) 76 – 85.

[38] D. Grolimund, M. Borkovec. Colloid-facilitated transport of strongly sorbing contaminants in natural porous media: mathematical modeling and laboratory column experiments. Environmental Science and Technology **39** (2005) 6378 – 6386.

[39] S. Nagasaki, S. Tanaka, A. Suzuki. Interfacial behavior of actinides with colloids in the geosphere. Journal of Nuclear Materials **248** (1997) 323 – 327.

[40] S. Kurosawa, M. Ibaraki, M. Yui, S. Ueta, H. Yoshikawa. Experimental and numerical studies on colloid-enhanced radionuclide transport - The effect of kinetic radionuclide sorption onto colloidal particles. Materials Research Society Symposium Proceedings **824** (2004) CC8.40.1 – 6.

[41] A.L. Noell, J.L. Thompson, M.Y. Corapcioglu, I. R. Triay. The role of silica colloids on facilitated cesium transport through glass bead columns and modeling. Journal of Contaminant Hydrology **31** (1998) 23 – 56.

[42] P. Vilks, M.H. Baik. Laboratory migration experiments with radionuclides and natural colloids in a granite fracture. Journal of Contaminant Hydrology **47** (2001)197 – 210.

[43] G. Limousin, J.P. Gaudet, L. Charlet, S. Szenknect, V. Barthès, M. Krimissa. Sorption isotherms: A review on physical bases, modeling and measurement. Applied Geochemistry **22** (2007) 249 – 275.

[44] S. Goldberg, L.J. Criscenti, D.R. Turner, J.A, Davis, K.J. Cantrell. Adsorption-desorption processes in subsurface reactive transport modeling. Vadose Zone Journal **6** (2007) 407 – 435.

[45] T. Missana, M. García-Gutiérrez, C. Maffiotte. Experimental and modelling study of the uranium (VI) sorption on goethite. Journal of Colloid and Interface Science **260** (2003) 291 – 301.

[46] A.M.L. Kraepiel, K. Keller, F.M.M. Morel. A model for metal adsorption on montmorillonite. Journal of Colloid and Interface Science **210** (1999) 43 – 54.

[47] J.M.A. Caiut, S.J.L. Ribeiro, Y. Messadeq, J. Dexpert-Ghys, M. Varelst, H. Dexpert. Synthesis and luminescence properties of water dispersible Eu^{3+}-doped boehmite nanoparticles. Nanotechnology **18** (2007) 455606 (8pp).

[48] J. Theo Kloprogge, L.V. Duong, B.J. Wood, R.L. Frost. XPS study of the major minerals in bauxite: gibbsite, bayerite and (pseudo-)boehmite. Journal of Colloid and Interface Science **296** (2006) 572 – 576.

[49] R. Frost, H. Ruan, T. Kloprogge. Comparison of the Raman spectra of bayerite, boehmite, diaspore and gibbsite. Journal of Raman Spectroscopy **32** (2001) 745 – 750.

[50] J. He, C.B. Ponton. Hydrothermal synthesis and morphology control of boehmite. High Pressure Research **20** (2001) 241 – 254.

[51] Y. Watanabe, H. Yamada, T. Kasama, J. Tanaka, Y. Komatsu, Y. Moriyoshi. Adsorption behaviour of phosphorus on synthetic boehmites. Proceedings of the 19th International Japan – Korea Seminar on Ceramics, 2002, pp 80 – 84.

[52] B.S. Gevert, Z-S. Ying. Formation of fibrillar boehmite. Journal of Porous Materials **6** (1999) 63 – 67.

[53] J. Zhang, S. Liu, J. Lin, H. Song, J. Luo, E.M. Elssfah, E. Ammar, Y. Huang, X. Ding, J. Gao, S. Qi, C. Tang. Self-assembly of flowerlike AlOOH (boehmite) 3D nanoarchitectures. Journal of Physical Chemsitry B **110** (2006) 14249 – 14252.

[54] Q. Liu, A. Wang, X. Wang, P. Gao, X. Wang, T. Zhang. Synthesis, characterisation and catalitic applications of mesoporous γ-alumina from boehmite sol. Microporous and Mesoporous Materials **111** (2008) 323 – 333.

[55] S. Music, D. Dragcevic, S. Popovic, N. Vdovic. Microstructural properties of boehmite formed under hydrothermal conditions. Materials Science and Engineering **B52** (1998) 145 – 153.

[56] P. Zhang, J.L. Krumhansl, P.V. Brady. Boehmite sorbs perrhenate and pertechnetate. Radiochimica Acta **88** (2000) 369 – 373.

[57] J. He, C.B. Ponton. Hydrothermal synthesis and morphology control of boehmite. High Pressure Research **20** (2001) 241 – 254.

[58] J. Subrt, V. Stengl, S. Bakardjieva, L. Szatmary. Synthesis of spherical metal oxide particles using homogeneous precipitation of aqueous solutions of metal sulfates with urea. Powder Technology **169** (2006) 33 – 40.

[59] F. Granados-Correa, J. Jiménez-Becerril. Chromium (VI) adsorption on boehmite. Journal of Hazardous Materials 162 (2009) 1178 – 1184.

[60] P. De Souza Santos, A.C. Vieira Coelho, H. De Souza Santos, P.K. Kiyohara. Hydrothermal synthesis of well-characterised boehmite crystals of various shapes. Materials Research **12** (2009) 437 – 445.

[61] R. Dähn, A.M. Scheidegger, A. Manceau, M.L. Schlegel, B. Baeyens, M.H. Bradbury, D. Chateigner. Structural evidence for the sorption of Ni(II) atoms on the edges of montmorillonite clay minerals: A polarized X-ray absorption fine structure study. Geochimica et Cosmochimica Acta **67** (2003) 1 – 15.

[62] C. Volzone, J.O. Rinaldi, J. Ortiga. N_2 and CO_2 adsorption by TMA- and HDP-montmorillonites. Materials Research **5** (2002) 475 – 479.

[63] B. Baeyens, M.H. Bradbury. A mechanistic description of Ni and Zn sorption on Na-montmorillonite. Part I: Titration and sorption measurements. Journal of Contaminant Hydrology **27** (1997) 199 – 222.

[64] J.L. Krumhansl, P.V. Brady, H.L. Anderson. Reactive barriers for ^{137}Cs retention. Journal of Contaminant Hydrology **47** (2001) 233 – 240.

[65] T. Boonfueng, L. Axe, Y. Xu, T.A. Tyson. Nickel and lead sequestration in manganese oxide-coated montmorillonite. Journal of Colloid and Interface Science **303** (2006) 87 – 98.

[66] D. Xu, X. Zhou, X. Wang. Adsorption and desorption of Ni^{2+} on Na-montmorillonite: effect of pH, ionic strength, fulvic acid, humic acid and addition sequences. Applied Clay Science **39** (2008) 133 – 141.

[67] S. Kraemer, J. Xu, K.N. Raymond, G. Sposito. Adsorption of Pb(II) and Eu(III) by oxide minerals in the presence of natural and synthetic hydroxamate siderophores. Environmental Science and Technology **36** (2002) 1287 – 1291.

[68] S. Goldberg, L.J. Criscenti, D.R. Turner, J.A. Davis, K.J. Cantrell. Adsorption-desorption processes in subsurface reactive transport modelling. Vadose Zone Journal **6** (2007) 407 – 435.

[69] N. Filipovic-Vincekovic, L. Brecevic, D. Krali. Interactions in clay/electrolyte systems. Journal of Radioanalytical and Nuclear Chemistry **130** (1989) 155 – 167.

[70] A. Agrawal, K. K. Sahu, B. D. Pandey. A comparative adsorption study of copper on various industrial solid wastes. American Institute of Chemical Engineers **50** (2004) 2430 – 2438.

[71] S. J. Allinson. Investigation of Inorganic Colloids in the Near-Field of a Waste Repository. PhD Thesis. Loughborough University, 2004.

[72] P. Klobes. Precision Measurement of the Specific Surface Area of Solids by Gas Adsorption. Federal Institute for Materials Research and Testing. BAM Reference Procedure, Chapter 4, 2011.

[73] J.J. Freeman, A.I. McLeod. Nitrogen BET surface area measurement as a fingerprint method for the estimation of pore volume in active carbons*. Fuel **62** (1983) 1090 – 1091.

[74] S.J. Kemp, G. Turner, D. Wagner. Initial testing and a laboratory manual for the Micromeritics Gemini VI physisorption system. British Geological Survey, Laboratory Operations Programme, Internal Report IR/08/086, 2009.

[75] M. Mazloumi, M. Attarchi, A. Lak, M.S. Mohajerani, A. Kajbafvala, S. Zanganeh, S.K. Sadrnezhaad. Boehmite nanopetals self assembled to form rosette-like nanostructures. Materials Letters **62** (2008) 4184 – 4186.

[76] S. Music, O. Dragcevic, S. Popovic. Hydrothermal crystallization of boehmite from freshly precipitated aluminium hydroxide. Materials Letters **40** (1999) 269 – 274.

[77] V. Pierre, D. Pierre, A.C. Pierre. Copper-alumina materials made by infiltration in boehmite. Journal of Materials Science **10** (1995) 2271 – 2276

[78] A.E. Blum and D.D. Eberl. Measurement of surface areas by polyvinylpyrrolidine sorption, G01N 30/96, U.S.A, 2003.

[79] M.J. Avena, L.E. Valenti, V. Pfaffen, C.P. De Pauli. Methylene blue dimerization does not interfere in surface-area measurements of kaolinite and soils. Clays and Clay Minerals **49** (2001) 168 – 173.

[80] B. A. Keiser and J. E. Whitten, Colloids Comprising Amorphous Borosilicate, C01B 35/00 (20060101); C01B 35/10 (20060101); D21H 21/10 (20060101); D21H 17/00 (20060101); D21H 17/68 (20060101); C01B 033/20 (); C01B 035/00 (), U.S., 2002.

[81] L.M. He, B.M. Tebo. Surface Charge Properties of and Cu(II) Adsorption by Spores of the Marine *Bacillus* sp. Strain SG-1. Applied Environmental Microbiology **64** (1998) 1123 – 1129.

[82] R. Dohrmann. Cation exchange capacity methodology I: An efficient model for the detection of incorrect cation exchange capacity and exchangeable cation results. Applied Clay Science **34** (2006) 31 – 37.

[83] K. Takazi. Transformations of Al-interlayered montmorillonite upon aging. Canadian Mineralogist **25** (1987) 347 – 352.

[84] H. Ciesielski, T. Sterckeman. A comparison between three methods for the determination of cation exchange capacity and exchangeable cations in soils. Agronomie **17** (1997) 9 – 16.

[85] D. Aran, A. Maul, J.F. Masfaraud. A spectrophotometric measurement of soil cation exchange capacity based on cobaltihexamine chloride absorbance. Comptes Rendus Geoscience **340** (2008) 865 – 871.

[86] R. Wood, D. Fornasiero, J. Ralston. Electrochemistry of the boehmite – water interface. Colloids and Surfaces **51** (1990) 389 – 403.

[87] M. Del Nero, C. Galindo, R. Barillon, E. Halter, B. Madé. Surface reactivity of α-Al_2O_3 and mechanisms of phosphate sorption: In situ ATR-FTIR spectroscopy and ζ potential studies. Journal of Colloid and Interface Science **342** (2010) 437 – 444.

[88] A.J. Fairhust, P. Warwick. The influence of humic acid on europium-mineral interactions. Colloids and Surfaces A: Physicochemical and Engineering Aspects **145** (1998) 229 – 234.

[89] A. Kaya, Y. Yukselen. Zeta potential of soils with surfactants and its relevance to electrokinetic remediation. Journal of Hazardous Materials **B120** (2005) 119 – 126.

[90] A.M.L. Kraepiel, K. Keller, F.M.M. Morel. A model for metal adsorption on montmorillonite. Journal of Colloid and Interface Science **210** (1999) 43 – 54.

[91] S.A. Adeleye, P.G. Clay, M.O.A. Oladipo. Sorption of caesium, strontium and europium ions on clay minerals. Journal of Materials Science **29** (1994) 954 – 958.

[92] P. Zhang, J.L. Krumhansl, P.V. Brady. Boehmite sorbs perrhenate and pertechnetate. Radiochimica Acta **88** (2000) 369 – 373.

[93] Y.Z. Wei, P. Chiang, S. Sridhar. Ion size effects on the dynamic and static dielectric properties of aqueous alkali solutions. Journal of Chemical Physics **96** (1992) 4569 – 4573.

[94] T. Akyüz, S. Akyüz, A. Bassari. The sorption of cesium and strontium ions onto red-clay from Sivrihisar-Eskisehir (Turkey). Journal of Inclusion Phenomena and Macrocyclic Chemistry **38** (2000) 337 – 344.

[95] G. Atun, B. Bilgin, A. Mardinli. Sorption of cesium on montmorillonite and effects of salt concentration. Journal of Radioanalytical and Nuclear Chemistry 211 (1996) 435 – 442.

[96] A.R. West. Solid state chemistry and its applications, Chapter 5. John Wiley & Sons 1985.

[97] M.B. McBride. Influence of glycine on Cu^{2+} adsorption by microcrystalline gibbsite and boehmite. Clays and Clay Minerals **33** (1985) 397 – 402.

[98] B.T. Beaulieu, K.S. Savage. Arsenate adsorption structures on aluminum oxide and phyllosilicate mineral surfaces in smelter-impacted soils. Environmental Science and Technology **39** (2005) 3571 – 3579.

[99] T. Hiemstra, W.H. van Riemsijk. Adsorption and surface oxidation of Fe(II) on metal (hydr)oxides. Geochimica et Cosmochimica Acta **71** (2007) 5913 – 5933.

[100] Y.S. Meng, D.J. Wang, J. Wu, H.J. Liu, S.H. Ju. Fluorescence studies of Eu ions adsorption on pseudo-boehmite colloidal particle surface. Guang Pu Xue Yu Guan Pu Fen Xi [Abstract] **29** (2009) 180 – 183.

[101] R.W. Taylor, W.F. Bleam, S.I. Tu. On the Langmuir phosphate adsorption maximum. Communications in Soil Science and Plant Analysis **27** (1996) [Abstract].

[102] G. Liu, P. Wang, Q. Liu, W. Han. Removal of Cd(II) by nanometer AlO(OH) loaded on fiberglass with activated carbon fiber felt as carrier. Chinese Journal of Chemical Engineering **16** (2008) 805 – 811.

[103] Y. Kim, R.J. Kirkpatrick. ^{23}Na and ^{133}Cs NMR study of cation adsorption on mineral surfaces: local environments, dynamics and effects of mixed cations. Geochimica et Cosmochimica Acta **61** (1997) 5199 – 5208.

[104] E. Tertre, G. Berger, S. Castet, M. Loubet, E. Giffaut. Experimental sorption of Ni2+, Cs+ and Ln3+ onto a montmorillonite up to 150ºC. Geochimica et Cosmochimica Acta **69** (2005) 4937 – 4948.

[105] G. Villaseñor-Nano, T.J. Strathmann. Ferrous iron sorption by hydrous metal oxides. Journal of Colloidal and Interface Science **297** (2006) 443 – 454.

[106] B. Piriou, M. Fedoroff, J. Jeanjean, L. Bercis. Characterization of the sorption of europium(III) on calcite by site-selective and time-resolved luminescence spectroscopy. Journal of Colloid and Interface Science **194** (1997) 440 – 447.

[107] A. Naveau, F. Monteil-Rivera, J. Dumonceau, S. Boudesocque. Sorption of europium on a goethite surface: influence of background electrolyte. Journal of Contaminant Hydrology **77** (2005) 1 – 16.

[108] R.W. Puls, H.L. Bohn. Sorption of cadmium, nickel and zinc by kaolinite and montmorillonite suspensions. Soil Science Society of America Journal **52** (1988) 1289 – 1292.

[109] A. Alfarra, E. Frackowiak, F. Bégouin. The HSAB concept as a means to interpret the adsorption of metal ions onto activated carbons. Applied Surface Science **228** (2004) 84 – 92.

[110] A. Beerbower, W.B. Jensen. The HSAB principle and extended solubility theory. Inorganica Chimica Acta **75** (1983) 193 – 197.

[111] R. Jayakrapash, J. Shanker. Correlation between electronegativity and high temperature superconductivity. Journal of Physics and Chemistry of Solids **54** (1993) 365 – 369.

[112] S. Trazzi Breviglieri, E.T. Gomes Cavalheiro, G.Orivaldo Chierice. Correlation between ionic radius and thermal decomposition of Fe(II), Co(II), Ni(II), Cu(II) and Zn(II) diethanoldithiocarbamates. Thermochimica Acta **356** (2000) 79 – 84.

[113] D. Phanon, A. Mosset, I. Gautier-Luneau. New iodate materials as potential laser matrices. Preparation and characterisation of α-$M(IO_3)_3$ (M = Y, Dy) and β-$M(IO_3)_3$ (M = Y, Ce, Pr, Nd, Eu, Gd, Tb, Dy, Ho, Er). Structural evolution as a function of the Ln^{3+} cationic radius. Solid State Sciences **9** (2007) 496 – 505.

[114] M. Cruz-Guzmán, R. Celis, M.C. Hermosín, W.C. Koskinen, E.A. Nater, J. Cornejo. Heavy metal adsorption by montmorillonites modified with natural organic cations. Soil Society of America Journal **70** (2006) 215 – 221.

[115] E. Morillo, C. Maqueda. Simultaneous adsorption of chlordimeform and zinc on montmorillonite. The Science of the Total Environment **123/124** (1992) 133 – 143.

[116] O. Ínel, F. Albayrak, A. Askin. Cu and Ph adsorption on some bentonitic clays. Turkish Journal of Chemistry **22** (1998) 243 – 252.

[117] M.M. Wahba, A.M. Zaghloul. Adsorption characteristics of some heavy metals by some soil minerals. Journal of Applied Sciences Research **3** (2007) 421 – 426.

[118] M. Bouby, H. Geckeis, J. Lützenkirchen, S. Mihai, T. Schäfer. Interaction of bentonite colloids with Cs, Eu, Th and U in presence of húmica acid: A flow field-flow fractionation study. Geochimica et Cosmochimica Acta **75** (2011) 3866 – 3880.

[119] A. Czímerová, L. Jankovic, J. Bujdák. Spectral properties of rhodamine 6G in smectite dispersions: Effect of the monovalent cations. Journal of Colloid and Interface Science **357** (2011) 322 – 330.

[120] N. Lu, C.F.V. Mason. Sorption-desorption behaviour of strontium-85 onto montmorillonite and silica colloids. Applied Geochemistry **16** (2001) 1653 – 1662.

[121] M-H. Baik, W-J. Cho. An experimental study on the sorption of Uranium (VI) onto a bentonite colloid. Journal of the Korean Radioactive Waste Society **4** (2006) 235 – 243.

[122] D. Karamanis, P.A. Assimakopoulos. Efficiency of aluminum-pillared montmorillonite on the removal of cesium and copper from aqueous solutions. Water Research **41** (2007) 1897 – 1906.

[123] J-P. Bellenger, S. Staunton. Adsorption and desorption of ^{85}Sr and ^{137}Cs on reference minerals, with and without inorganic and organic surface coatings. Journal of Environmental Radioactivity **99** (2008) 831 – 840.

[124] A. Dyer, J.K.K. Chow, I.M. Umar. The uptake of caesium and strontium radioisotopes onto clays. Journal of Materials Chemistry **10** (2000) 2734 – 2740.

[125] B.C. Bostick, M.A. Vairavamurthy, K.G. Karthikeyan, J. Chorover. Cesium Adsorption on Clay Minerals: An EXAFS Spectroscopic Investigation. Environmental Science Technology **36** (2002) 2670 – 2676.

[126] G. Lujanienė, S. Motiejünas, J. Sapolaité. Sorption of Cs, Pu and Am on clay minerals. Journal of Radioanalytical and Nuclear Chemistry **274** (2007) 345 – 353.

[127] B. Lotenbach, G. Furrer, R. Schulin. Immobilization of heavy metals by polynuclear aluminium and montmorillonite compounds. Environmental Science and Technology **31** (1997) 1452 – 1462.

[128] S. Wold. Sorption of prioritized elements on montmorillonite colloids and their potential to transport radionuclides. Technical Report TR-10-20. Swedish Nuclear Fuel and Waste Management Co, April 2010.

[129] M.H. Bradbury, B. Baeyens. Sorption of Eu on Na- and Ca-montmorillonites: Experimental investigations and modelling with cation exchange and surface complexation. Geochimica et Cosmochimica Acta **66** (2002) 2325 – 2334.

[130] Th. Rabung, M.C. Pierret, A. Bauer, H. Geckeis, M.H. Bradbury, B. Baeyens. Sorption of Eu(III)/Cm(III) on Ca-montmorillonite and Na-illite. Part 1: Batch sorption and time-resolved laser fluorescence spectroscopy experiments. Geochimica et Cosmochimica Acta **69** (2005) 5393 – 5402.

[131] J. Liu, H. Lippold, J. Wang, J. Lippmann-Pipke, Y. Chen. Sorption of thallium(I) onto geological materials: Influence of pH and humic matter. Chemosphere **82** (2011) 866 – 871.

[132] Z. Tao, W. Li, F. Zhang, Y. Ding, Z. Yu. Am(III) adsorption on oxides of aluminium and silicon: effects of humic substances, pH and ionic strength. Journal of Colloid and Interface **265** (2003) 221 – 226.

[133] C. Chen, X. Wang. Sorption of Th (IV) on silica as a function of pH, humic/fulvic acid, ionic strength, electrolyte type. Applied Radiation and Isotopes **65** (2007) 155 – 163.

[134] C. Chen, X. Wang. Influence of pH, soil humic/fulvic acid, ionic strength and foreign ions on sorption of Th (IV) onto γ-Al_2O_3. Applied Geochemistry **22** (2007) 436 – 445.

[135] N. Zhiwei, F. Qiaohui, W. Wenhua, X. Junzheng, C. Lei, W. Wangsuo. Effect of pH, ionic strength and humic acid on the sorption of uranium(VI) to attapulgite. Applied Radiation and Isotopes **67** (2009) 1582 – 1590.

[136] M. Cruz-Guzmán, R. Celis, M.C. Hermosín, P. Leone, M. Nègre, J. Cornejo. Sorption-desorption of lead (II) and Mercury (II) by model associations of soil colloids. Soil Science Society of America Journal **67** (2003) 1378 – 1387.

[137] A. Soumitra Kar, S. Kumar, B.S. Tomar, V.K. Manchanda. Sorption of curium by silica colloids: Effect of humic acid. Journal of Hazardous Materials 186 (2011) 1961 – 1965.

[138] B.K. Singh, A. Jain, S. Kumar, B.S. Tomar, R. Tomar, V.K. Manchanda, S. Ramanathan. Role of magnetite and humic acid in radionuclide migration in the environment. Journal of Contaminant Hydrology **106** (2009) 144 – 149.

[139] A. Jain, N. Rawat, S. Kumar, B.S. Tomar, V.K. Machanda, S. Ramanathan. Sorption of neptunium by hematite colloids. BARC Newsletter **297** (2008) 297 – 301.

[140] M. Samadfam, S. Sato, H. Ohashi. Effects of humic acid on the sorption of Eu(III) onto kaolinite. Radiochimica Acta **82** (1998) 361 – 365.

[141] H. Lippold, N. Müller, H. Kupsch. Effect of humic acid on the pH-dependent adsorption of terbium (III) onto geological materials. Applied geochemistry **20** (2005) 1209 – 1217.

[142] I. Christl, R. Kretzschmar. Interaction of copper and fulvic acid at the hematite-water interface. Geochimica et Cosmochimica Acta **65** (2001) 3435 – 3442.

[143] T. Sakuragi, S. Sato, T. Kozaki, T. Mitsugashira, M. Hara, Y. Suzuki. Am(III) and Eu(III) uptake on hematite in the presence of humic acid. Radiochimica Acta **92** (2004) 697 – 702.

[144] M. Samadfam, T. Jintoku, S. Sato, H. Ohashi, T. Mitsugashira, M. Hara, Y. Suzuki. Effects of humic acid on the sorption of Am(III) and Cm(III) on kaolinite. Radiochimica Acta **88** (2000) 717 – 721.

[145] S. Kumar, B.S. Tomar, S. Ramanathan, V.K. Manchanda. Effect of humic acid on cesium sorption on silica colloids. Radiochimica Acta **94** (2006) 369 – 373.

[146] S. Kumar, N. Rawat, A.S. Kar, B.S. Tomar, V.K. Manchanda. Effect of humic acid on sorption of technetium on alumina. Article in press Journal of Hazardous Materials (2011) doi:10.1016/j.jhazmat.2011.06.007

[147] A.S. Kar. S. Kumar, B.S. Tomar, V.K. Manchanda. Sorption of curium by silica colloids: Effect of humic acid. Journal of Hazardous Materials **186** (2011) 1961 – 1965.

[148] K.L. Titley. Fundamental studies on metal – humic acid interactions. Thesis (PhD.) Loughborough University 2009.

[149] A. Pitois, L. Abrahamsen, P. Ivanov, N.D. Bryan. Humic acid adsorption onto a quartz sand surface: A kinetic study and insight into fractionation. Journal of Colloid and Interface Science **325** (2008) 93 – 100.

[150] T. J. Strathmann, S.C.B. Myneni. Effect of soil fulvic acid on Nickel(II) sorption and bonding at the aqueous-boehmite (γ-AlOOH) interface. Environmental Science and Technology **39** (2005) 4027 – 4034.

[151] J.C. Miller, J.N. Miller. Statistics for Analytical Chemistry. New York : Ellis Horwood PTR Prentice Hall, 1993. 3rd Edition.

[152] E. Tombácz, Á. Dobos, M. Szekeres, H.D. Narres, E. Lumpp, I. Dékány. Effect of pH and ionic strength on the interaction of humic acid with aluminium oxide. Colloid Polymer Science **278** (2000) 337 – 345.

[153] T. Hyun Yoon, S. B. Johnson, G.E. Brown Jr. Adsorption of organic matter at mineral/water interfaces. IV. Adsorption of humic substances at boehmite/water interfaces and impact on boehmite dissolution. Langmuir **21** (2005) 5002 – 5012.

[154] C. Varadachari, T, Chattopadhyay, K. Ghosh. The crystallo-chemistry of oxide-humus complexes. Australian Journal of Soil Research **38** (2000) 789 – 806.

[155] H. Lippold, N. Müller, H. Kupsch. Effect of humic acid on the pH-dependent adsorption of terbium (III) onto geological materials. Applied geochemistry **20** (2005) 1209 – 1217.

[156] L. Carlsen, P. Lassen, P. Warwick, A. Randall. Interaction between europium ions and selected size fractions of humic acids. Chemosphere **33** (1996) 659 – 670.

[157] C. Dumat, H. Quiquampoix, S. Staunton. Adsorption of cesium by synthetic clay – organic matter complexes : Effect of the nature or organic polymers. Environmental Science and Technology **34** (2000) 2985 – 2989.

[158] A. Rigol, M. Vidal, G. Rauret. An overview of the effect of organic matter on soil–radiocaesium interaction: implications in root uptake. Journal of Environmental Radioactivity **58** (2002) 191 – 216.

[159] S. Staunton, C. Dumat, A. Zsolnay. Possible role of organic matter in radiocaesium adosption in soils. Journal of Environmental Radioactivity **58** (2002) 163 – 173.

[160] X. Wang, Th. Rabung, H. Geckeis. Effect of pH and humic acid on the adsorption of cesium onto γ-Al_2O_3. Journal of Radioanalytical and Nuclear Chemistry **258** (2003) 83 – 87.

[161] D. Wenming, W. Xiangke, B. Xiaoyan, W. Aixia, D. Jingzhou, T. Zuyi. Comparative study on sorption/desorption of radioeuropium on alumina, bentonite and red earth: effects of pH, ionic strength, fulvic acid and iron oxides in red earth. Applied Radiation and Isotopes **54** (2001) 603 – 610.

[162] X. Wang, Y. Chen, Y. Wu. Diffusion of Eu(III) in compacted bentonite – effect of pH, solution concentration and humic acid. Applied Radiation and Isotopes **60** (2004) 963 – 969.

[163] T. Lewis. Sorption of metals to clay minerals in the presence of organic complexing ligands. Thesis (PhD), Loughborough University, 2008.

[164] O. Gezici, H. Kara, M. Ersöz, Y. Abali- The sorption behaviour of a nickel-insolubilized humic acid system in a column arrangement. Journal of Colloid and Interface Science **292** (2005) 381 – 391.

[165] J.J.W. Higgo, G.M. Williams, I. Harrison, P. Warwick, M.P. Gardiner, G. Longworth. Colloid transport in a glacial sand aquifer. Laboratory and field studies. Colloids and Surfaces A: Physicochemical and Engineering Aspects **73** (1993) 179 – 200.

[166] C. Shani, N. Weisbrod, A. Yakirevich. Colloid transport through saturated sand columns: Influence of physical and chemical surface properties on deposition. Colloids and surfaces A: Physicochem. Eng. Aspects **316** (2008) 142 – 150.

[167] S. A. Bradford, M. Bettahar, J. Simunek, M. Th. van Genuchten. Straining and attachment of colloids in physically heterogeneous porous media. Vadose Zone Journal **3** (2004) 384 – 394.

[168] K. Shiratori, Y. Yamashita, Y. Adachi. Deposition and subsequent release of Na-kaolinite particles by adjusting pH in the column packed with Toyoura sand. Colloids and surfaces A: Physicochem. Eng. Aspects **306** (2007) 137 – 141.

[169] T. Yoshida, M. Suzuki. Effects of humic acid on migration of montmorillonite and alumina colloid in a quartz sand column. Colloids and Surfaces A: Physicochemical and Engineering Aspects **325** (2008) 115 – 119.

[170] J. Zhuang, Y. Jin, M. Flury. Comparison of Hanford colloids and kaolinite transport in porous media. Vadose Zone Journal **3** (2004) 395 – 402.

[171] F. Kuhnen, K. Barmettler, S. Bhattacharjee, M. Elimelech, R. Kretzschmar. Transport of iron oxide colloids in packed quartz sand media: monolayer and multilayer deposition. Journal of Colloid and Interface Science **231** (2000) 32 – 41.

[172] S. B. Roy, D. A. Dzombak. Colloid release and transport processes in natural and model porous media. Colloids and Surfaces A: Physicochemical and Engineering Aspects **107** (1996) 246 – 262.

[173] U. Alonso, T. Missana, A. Patelli, V. Rigato. Bentonite colloid diffusion through the host rock of a deep geological repository. Physics and Chemistry of the Earth **32** (2007) 469 – 476.

[174] A.L. Noell, J.L. Thompson, M.Y. Corapcioglu, I. R. Triay. The role of silica colloids on facilitated cesium transport through glass bead columns and modeling. Journal of Contaminant Hydrology **31** (1998) 23 – 56.

[175] P. Grindrod, M. S. Edwards, J. J. W. Higgo, G. M. Williams. Analysis of colloid and tracer breakthrough curves. Journal of Contaminant Hydrology **21** (1996) 243 – 253.

[176] R. Artinger, B. Kienzler, W. Schüβler, J. I. Kim. Effects of humic substances on the ^{241}Am migration on a sandy aquifer: column experiments with Gorleben groundwater/sediment systems.

[177] H. Geckeis, T. Schäfer, W. Hauser, Th. Rabung, T. Missana, C. Degueldre, A. Möri, J. Eikenberg, Th. Fierz, W.R. Alexander. Results of the colloid and radionuclide retention experiment (CRR) at the Grimsel Test Site (GTS), Switzerland – impact of reaction kinetics and speciation on radionuclide migration. Radiochimica Acta **92** (2004) 765 – 774.

[178] T.K. Sen, S.P. Mahajan, K.C. Khilar. Colloid-associated contaminant transport in porous media: 1. Experimental studies. AIChe Journal **48** (2002) 2366 – 2374.

[179] D. Read, D. Ross, R.J. Sims. The migration of uranium through Clashach Sandstone: the role of low molecular weight organics in enhancing radionuclide transport. Journal of Contaminant Hydrology **35** (1998) 235 – 248.

[180] X-Y. Tang, N. Weisbrod. Colloid-facilitated transport of lead in natural discrete fractures. Environmental Pollution **157** (2009) 2266 – 2274.

[181] S. Brandriss, G. Borchardt, J. Kreuter, S. Margel. Radiolabeled ^{75}Se-silica nanoparticles: synthesis, characterization and coating with ω-functionalized alkylsilane compounds. Reactive Polymers **25** (1995) 111 – 125.

[182] Y. Lin, X. Zhang, J. Li, D. Yin, Y. Wang. Preparation and radiolabelling of antimony sulfide nanocolloids with two different particle sizes. Applied Radiation and Isotopes **58** (2003) 347 – 352.

[183] C. Tsopelas. Understanding the radiolabelling mechanism of ^{99m}Tc-antimony sulphide colloid. Applied Radiation and Isotopes **59** (2003) 321 – 328.

[184] W. Stöber, A. Fink, E. Bohn. Controlled growth of monodisperse silica spheres in the micron range. Journal of Colloid and Interface Science, **26** (1968) 62 – 69.

[185] P. Warwick, A. Hall, V. Pashley, J. Van der Lee, A. Maes. Zinc and cadmium mobility in Podzol soils. Chemosphere, **38** (1999) 2357 – 2368.

[186] G. Bavestrello, A. Arillo, B. Calcinai, C. Cerrano, S. Lanza, M. Sara, R. Cattaneo-Vietti, E. Gaino. Siliceous particles incorporation in *Chondrosia reniformes* (Porifera, Demospongiae). Italian Journal of Zoology, **65** (1998) 343 – 348.

[187] Penna, M. Magnani, I. Fenoglio, B. Fubini, C. Cerrano, M. Giovine, G. Bavestrello. Marine diatom growth on different forms of particulate silica: evidence of cell/particle interaction. Aquatic Microbial Ecology, **32** (2003) 299 – 306.

[188] J.A. Barclay, B. Perczuk. Nuclear structure and the hyperfine interaction of oriented ^{152}Eu, ^{155}Eu and ^{153}Gd in gold. Hyperfine Interactions **1** (1975) 15 – 24.

[189] L. Peng, W. Qisui, L. Xi, Z. Chaocan. Zeta-potentials and enthalpy changes in the process of electrostatic self-assembly of cations on silica surface. Powder Technology **193** (2009) 46 – 49.

[190] M.S. Tsai, W-C. Wu. Aluminum modified colloidal silica via sodium silicate. Materials Letters **58** (2004) 1881 – 1884.

[191] C.E. McNamee, M. Matsumoto, P.G. Hartley, M. Nakahara. Adsorption of quaternised polyvinylpyridine and subsequent counterion binding of perfluorinated anionic surfactants on silica as a function of concentration and pH: a zeta potential study. Colloids and Surfaces A: Physicochemical and Engineering Aspects **193** (2001) 175 – 185.

[192] G. Xu, J. Zhang, G. Song. Effect of complexation on the zeta potential of silica powder. Powder Technology **134** (2003) 218 – 222.

[193] G.W. Sears. Determination of specific surface area of colloidal silica by titration with sodium hydroxide. Analytical Chemistry **28**(12) (1956) 1981 – 1983.

[194] A.A. Christy. Quantitative determination of surface area of silica gel particles by near infrared spectroscopy and chemometrics. Colloids and Surfaces A: Physicochemical and Engineering Aspects **322** (2008) 248 – 252.

[195] A. Karami. Study on modification of colloidal silica surface with magnesium ions. Journal of Colloid and Interface Science **331** (2009) 379 – 383.

[196] D.A. Vasconcelos, W.R. Campos, V. Vasconcelos, W.L. Vasconcelos. Influence of process parameters on the morphological evolution and fractal dimension of sol-gel colloidal silica particles. Materials Science and Engineering **A334** (2002) 53 – 58.

[197] E. Tipping, J.J.W. Higgo. The role of colloids in the release and transport of radionuclides in the near and far field. British Geological Survey 1991. Fluid Processes Research Group Technical Report WE/91/16.

[198] A. Fairhust. The Role of Inorganic Colloids in the Transport of Toxic Metals Through the Environment. Thesis (PhD). Loughborough University, 1996.

[199] R.P. Schwarzenbach, P.M. Gschwend, D. M. Imboden. Environmental Organic Chemistry – Illustrative examples, problems and case studies. John Wiley and Sons 1995.

[200] C. Curry, R, Bennet, M. Hulbert, K. Curry, R. Faas. Comparative study of sand porosity and a technique for determining porosity of undisturbed marine sediment. Marine Geosources and Geotechnology, **22**(4) (2004) 231 – 252.

[201] J. Mibus, S. Sachs, W. Pfingsten, C. Nebelung, G. Bernhardt. Migration of U(IV)/(VI) in the presence of humic acids in quartz sand: A laboratory column study. Journal of Contaminant Hydrology **89** (2007) 199 – 217.

[202] R.A. Akbour, J. Douch, M. Hamdani, P. Schmitz. Transport of kaolinite colloids through quartz sand: Influence of humic acid, Ca^{2+} and trace metals. Journal of Colloid and Interface Science **253** (2002) 1 – 8.

[203] M. Flury, S. Czigány, G. Chen, J.B. Harsh. Cesium migration in saturated silica sand and Hanford sediments as impacted by ionic strength. Journal of Contaminant Hydrology **71** (2004) 111 – 126.

[204] E. Bascetin, H. Haznedaroglu, A. Y. Erkol. The adsorption behavior of cesium on silica gel. Applied Radiation and Isotopes **59** (2003) 5 – 9.

[205] E. Bascetin, H. Haznedaroglu, A. Y. Erkol. The adsorption behavior of cesium on silica gel. Applied Radiation and Isotopes **59** (2003) 5 – 9.

[206] P.N. Pathak, G.R. Choppin. Kinetic and thermodynamic studies of cesium (I) sorption on hydrous silica. Journal of Radioanalytical and Nuclear Chemistry **270**(2) (2006) 299 – 305.

[207] J.E. Saiers, G.M. Hornberger. Migration of ^{137}Cs through quartz sand: experimental results and modeling approaches. Journal of Contaminant Hydrology **22** (1996) 255 – 270.